Occurrence and Transport of Pollutants from Spilled Oil and Microplastics in the Coastal Areas

Zheng Wang

A Thesis

In the Department of

Building, Civil, and Environmental Engineering

Presented in Partial Fulfillment of the Requirements
For the Degree of
Doctor of Philosophy (Civil Engineering)

at Concordia University
Montréal, Québec, Canada

September 2023

©Zheng Wang, 2023

CONCORDIA UNIVERSITY

SCHOOL OF GRADUATE STUDIES

This is to certify that the thesis prepared

By: Zheng Wang

Entitled: Occurrence and transport of pollutants from spilled oil and microplastics in the coastal areas

and submitted in partial fulfillment of the requirements for the degree of

DOCTOR OF PHILOSOPHY (Civil Engineering)

complies with the regulations of the University and meets the accepted standards with respect to originality and quality.

Signed by the final examining committee:

_____ Chair
Dr. Govind Gopakumar

_____ External Examiner
Dr. Subhasis Ghoshal

_____ Examiner
Dr. Zhi Chen

_____ Examiner
Dr. Catherine Mulligan

_____ Examiner
Dr. Youmin Zhang

_____ Thesis Co-supervisor
Dr. Kenneth Lee

_____ Thesis Supervisor
Dr. Chunjiang An

Approved by _____
Dr. Chunjiang An, Graduate Program Director

October 12, 2023 _____
Dr. Mourad Debbabi, Dean of faculty
Gina Cody School of Engineering and Computer Science

Abstract

Occurrence and transport of pollutants from spilled oil and microplastics in the coastal areas

Zheng Wang, Ph.D.

Concordia University, 2023

The coast is a complex environment that comprises seawater, underwater, soil, atmosphere, and other environmental factors. Traditional and new pollutants, represented by oil spills and microplastic (MPs), persist in posing a constant threat to the ecosystems and social-economic features of coastal regions. Besides, the shoreline is exposed to various environment conditions, which may significantly affect the behaviors of pollutants on beaches. An in-depth understanding of the occurrence and fate of pollutants in coastal areas is a prerequisite for the development of sound prevention and remediation strategies. Firstly, the physicochemical behavior of crude oil on various types of shorelines under different environmental conditions were reviewed. The penetration, remobilization, and retention of stranded oil on shorelines are affected by the beach topography and the natural environment. The attenuation and fate of oil on shorelines from laboratory and field experiments were discussed. In addition, the source, type, distribution, and factors of MPs in the coastal areas were summarized. What is more, the occurrence and environmental risk of emerging plastics waste—personal protective equipment (PPE)—in the coastal environment during and pandemic were discussed.

Then, the role of natural nanobubbles (NBs) in the fate and transport of spilled oil were investigated through laboratory experiments and model simulations. NBs significantly increased the concentration of dissolved oxygen as well as changed the pH, zeta potential, and surface tension of the water. With the assistance of external energy, the bulk NBs enhanced the efficiency in oil detachment from the surface of the substrate. At the same time, the surface NBs on the substrate obstructed the downward transport of oil colloids. Considering the behavior between the NBs in two different phases and the oil droplets, the oil droplets tended to bind to the NBs.

Next, the behavior and movement of various MPs in the presence of bulk NBs was explored. In the presence of NBs, the binding of MPs and NBs resulted in an increase in the measured average particle size and concentration. The velocity of motion of MPs driven by NBs varies under different salinity conditions. The increase in ionic strength reduced the energy barrier between particles and promoted their aggregation. Thus, the binding of NBs and MPs became more stable, which in turn affected the movement of MPs in the water. Polyethylene (PE1) with small particle size was mainly affected by Brownian motion and its rising was limited, therefore polyethylene (PE2) with large particle size rose faster than PE1 in suspension, especially in the presence of NBs.

The effect of nanobubbles on the mobilization of MPs in shorelines subject to seawater infiltration was further studied. The motion of MPs under continuous and transient conditions, as well as the upward transport induced with flood were considered. Salinity altered the energy barriers between particles, which in turn affected the movement of MPs within the matrix. In addition, hydrophilic MPs were more likely to infiltrate within the substrate and had different movement patterns under both continuous and transient conditions. The motion of the MPs within the substrate varied with flow rate, and NBs limited the vertical movement of MPs in the tidal zone. It was also observed that

NBs adsorbed readily onto substrates, altering the surface properties of substrates, particularly their ability to attach and detach from other substances.

Finally, the changing characteristics and environmental behaviors of PPE wastes when exposed to the shoreline environment were examined. The transformation of chain structure and chemical composition of masks and gloves as well as the decreased mechanical strength after UV weathering were observed. In addition, the physical abrasion caused by sand further exacerbated the release of MPs and leachable hazardous contaminates from masks and gloves.

In conclusion, the coastal zone is threatened by various pollutants, including traditional pollutants (like the oil spill) and emerging pollutants (like MPs). Due to the complexity of the coastal zone, the occurrence, transport and fate of pollutants can be controlled by many factors, and some factors that are ignored before can also alter the environmental behavior of pollutants in the coastal zone. Natural NBs can change the properties of the water environment and affect the surface properties of the substrate. Bulk NBs contribute to the oil detachment from the sand surface, and surface nanobubbles in the substrate obstruct the downward transport of oil colloids. The behavior and mobilization of MPs in the coastal `zone are subject to mutual forces between the substrate, MPs, NBs, and other factors. Coastal zones are not only the main receptor of pollutants from oceans and lands but also play a key role in their fate and transport.

Acknowledgements

More than four years of doctoral work are coming to an end. From 2019 to the present, it has been a winding but passionate journey that will forever reside in my memories. Despite going through tough times like the Pandemic during this period, I am grateful that I have been able to fight with a group of like-minded people. I would like to take this opportunity to express my sincere gratitude to all those who have helped and inspired me.

First and foremost, I would like to express my deepest appreciation to my supervisor, Dr. Chunjiang An. I am grateful to have been able to join his team and have been fully supported from start to finish. Dr. An's unwavering dedication to scientific research and relentless pursuit of excellence is exemplary. Positive, optimistic and approachable, he is a truly outstanding mentor and colleague. It is better to teach a man fishing than to give him fish. His unwavering presence and wealth of wisdom have been instrumental in shaping my academic growth.

I also want to express my heartily gratitude to my supervisor, Kenneth Lee, who has been instrumental in my success over the past four years. I feel incredibly fortunate to have had the guidance and mentorship, which was really influential in shaping my research methods and critiquing my results. He is not only a highly respected academic, but also a guide for young researchers in their career planning. His guidance and encouragement have been invaluable.

In addition to my supervisors, I am indebted to my exceptional lab mates, Mengfan Cai, Qi Feng, Zhikun Chen, Xuelin Tian, Huifang Bi, Rengyu Yue, Liuqing Yang, Rezvan Iravani, Azar

Vahabisani, Xinya Chen, Shuyan Wan, Xiaohan Yang, Siyuan Zhou, Linxiang Lyu, Zhaonian Qu, He Peng, Jiyao Sui, Xinyu Xu, whose support has been a constant source of motivation. Their generous help was essential to ensure my study went smoothly. I would also like to thank our great lab technicians, Hong Guan, Mazen Samara, Luc Demers and Dmytro Kevorkov, for their generosity and enthusiasm.

Furthermore, I would like to thank my thesis committee members, Dr. Subhasis Ghoshal, Dr. Catherine Mulligan, Dr. Youmin Zhang, Dr. Zhi Chen, Dr. Kenneth Lee, and Dr. Chunjiang An, for their time, valuable suggestions, and constructive comments.

Lastly, I want to express my deepest gratitude to my beloved, Qi Feng, for always knowing what to say to me and for being by my side whenever I need a guiding hand. For every challenge and every obstacle that faces us, I know we will get through it together. I would also like to sincerely thank my parents for always believing in me unwaveringly, encouraging me, and supporting me unconditionally.

As I conclude my PhD journey of over four years, I can wholeheartedly say that I am immensely proud of my achievements. This journey has not only shaped me as a researcher but has also given me a new perspective on the world. I am both proud of my contribution to the field of research and in awe of the vastness of human knowledge. Now, I am about to reach the summit, but the majestic mountains await me in the distance.

Table of Contents

List of Figures ..... **xii**

List of Tables ..... **iii**

List of Abbreviations ..... **iv**

Chapter 1. Introduction **1**

1.1 Problem statement 1

1.2 Research objectives 4

Chapter 2. Literature review **6**

2.1 Oil transport and fate on beaches 6

2.1.1 The transport of oil in the coastal areas 8

2.1.2 Fate of oil in the shoreline 13

2.2 Transport of MPs in coastal areas 19

2.2.1 Sources and types of MPs in the coastal environment 20

2.2.2 Distribution of MPs in the coastal environment 26

2.3 Occurrence and environmental risk of PPE waste in the natural environment 29

2.3.1 Occurrence of PPE waste in the environment 29

2.3.2 Environmental risk of PPE wastes 31

Chapter 3. Exploring the role of nanobubbles in the fate and transport of spilled oil on shorelines **34**

3.1 Background 34

3.2 Methods 37

3.2.1 Materials and chemicals 37

3.2.2 Experimental design 37
3.2.3 Analytical methods 39
3.3 Results and discussion 40
3.3.1 Physicochemical properties of NBs suspension 40
3.3.2 Factors influencing the properties of NBs solution 43
3.3.3 Detachment of stranded oil from sand surface in the presence of bulk NBs 48
3.3.4 Effect of surface NBs on oil transport in shoreline substrates 53
3.3.5 Environmental implications 57
Chapter 4. Overlooked role of bulk nanobubbles in the alteration and motion of microplastics in the coastal environment 60
4.1 Background 60
4.2 Methods 63
4.2.1 Materials and chemicals 63
4.2.2 Sample preparation and experimental design 63
4.2.3 Settling/rising motion analysis 66
4.2.4 Derjaguin−Landau−Verwey−Overbeek (DLVO) theory 68
4.3 Results and discussion 69
4.3.1 Vertical motion of MPs in the presence of NBs 69
4.3.2 Effect of salinity on MPs motion 75
4.3.3 Interaction of external energy on MPs and NBs 81
4.3.4 Analysis of the mechanism underlying behavior of MPs–NBs suspensions 86
4.3.5 Environmental implications 90
Chapter 5. Effect of nanobubbles on the mobilization of microplastics in shorelines subject to seawater infiltration 93

5.1 Background 93
5.2 Methods 96
5.2.1 Materials and chemicals 96
5.2.2 Samples preparation and characterization 97
5.2.3 Experiment design 98
5.2.4 Theoretical considerations and model simulation 101
5.3 Results and discussion 103
5.3.1 Mobilization of MPs under ebb tide in unsaturated substrate 103
5.3.2 Mobilization of MPs at transient flow under ebb tide condition 107
5.3.3 Mobilization of MPs under flood tide in saturated substrate 110
5.3.4 Theoretical analysis of MPs motion in the substrate 114
5.3.5 Environmental implications 120
Chapter 6. Disposable masks release microplastics to the aqueous environment with exacerbation by natural weathering 123
6.1 Background 123
6.2 Methods 125
6.2.1 Materials and chemicals 125
6.2.2 Characterization of physicochemical properties of disposable masks 128
6.3 Results and discussion 129
6.3.1 Changes in the chemical composition of the masks under UV weathering 129
6.3.2 Physicochemical characteristics of masks impacted by UV weathering 131
6.3.3 Plastic particles released from weathered masks in aqueous environment 140
6.3.4 Effect of sand on MPs release from masks in aqueous environment 145
6.3.5 Environmental implications 148

Chapter 7 Physicochemical change and microparticle release from disposable gloves in the aqueous environment impacted by accelerated weathering 151

7.1 Background 151

7.2 Methods 154

7.2.1 Sample preparation 154

7.2.2 Characterization of physical and chemical properties 155

7.2.3 Analysis of leachable components 156

7.3 Results and discussion 157

7.3.1 Characteristics of gloves impacted by weathering 157

7.3.2 MPs release from gloves into the aqueous environment 166

7.3.3 Release of MPs from gloves with exacerbation by physical abrasion 170

7.3.4 Leachable hazardous components released from gloves 174

7.3.5 Environmental implications 180

Chapter 8. Contributions and significance of thesis research, and suggestions for future work 182

8.1 Contributions and significance of thesis research 182

8.2 Suggestions for future work 183

Publications 184

References 188

List of Figures

Figure 2.1 The distribution and behavior of stranded oil on shorelines affected by the beach topography and environmental factors.....7

Figure 2.2 Schematic diagram of MPs transport in the coastal areas (Zhang, 2017).....27

Figure 2.3 The environmental fate and impacts of PPE waste.....31

Figure 3.1 (a) Changes in the physicochemical properties of NBs over time. (b) Changes in the physicochemical properties of control sample (DI water) over time. (c) Size distribution of fresh NBs suspensions. (d) Size distribution of NBs suspensions at day 7.....43

Figure 3.2 (a–d) Effect of salinity on the properties of the NBs suspension. (e–f) Effect of Tween 20 on the properties of the NBs suspension. DI represents DI water. NBs represent NBs suspension. 10 mM, 100 mM, 1 wt% and 3.5 wt% represent NBs suspension at a salinity of 10 mM, 100 mM, 1 wt% and 3.5 wt%, respectively. 100 ug/L, 200 ug/L, 300 ug/L and 400 ug/L represent NBs suspension at a Tween 20 concentration of 100, 200, 300 and 400 ug/L, respectively. 46

Figure 3.3 Size distribution of NBs under different conditions. (a–h) Effect of different salinities. (i–p) Effect of different concentration of Tween 20. 48

Figure 3.4 Oil detachment rate in the presence of NBs suspension under different conditions. (a) Shaking condition. (b) Resting condition. 51

Figure 3.5 (a–d) Experimental and simulative BTCs of oil colloids under different conditions. (a) DI solution, represented by DI. (b) Tween 20-only solution, represented by T. (c) Salt-only solution, represented by S. (d) Solution with both Tween 20 and salt, represented by ST. (e–j) Inverse simulation of the transport of oil colloids in the column. B means with NBs.....56

Figure 4.1 Particle size distribution of fresh NBs solution 65

Figure 4.2 Particle size distributions of different types of MPs suspension.....70
Figure 4.3 Changes in the average particle size and concentration of MPs suspensions. (a), (b), and (c) are average sizes of PE1, PE2, and PTFE, respectively. (d), (e) and (f) are concentrations of PE1, PE2 and PTFE, respectively. 74
Figure 4.4 The settling/rising ratios of MPs over time. (a), (b), and (c) are PE1, PE2, and PTFE, respectively.....75
Figure 4.5 Changes in the average particle size and concentration of MPs over time under different salinities in the presence of NBs. (a), (b), and (c) are average sizes of PE1, PE2 and PTFE in suspensions, respectively. (d), (e) and (f) are concentrations of PE1, PE2 and PTFE, respectively. 77
Figure 4.6 The changes of the average particle size and concentration of MPs over time under different salinities in the absence of NBs. (a), (b), and (c) are average particle size of PE1, PE2, and PTFE in MPs−DI solution, (d), (e), and (f) are concentrations of PE1, PE2, and PTFE in MPs−DI solution. 78
Figure 4.7 Reduction percent of the average size and concentration under different salinities. (a), (b), and (c) are average sizes, (d), (e), and (f) are concentrations.....81
Figure 4.8 Effect of external energy on the average size and concentration of MPs suspension.....84
Figure 4.9 Effect of shaking conditions on the MPs concentration. 85
Figure 4.10 Péclet numbers and velocity of MPs under different conditions. 87
Figure 4.11 Interaction energy versus surface-to-surface separation distance for MPs and NBs at various salinities. 90
Figure 5.1 Particle size distribution of different MPs suspension.....98
Figure 5.2 Apparatus of the column experiments. (a) and (b) are under ebb ride condition, (c) and (d) are under flood tide condition. 100

Figure 5.3 Standard curve of different MPs suspension 101
Figure 5.4 Mobilization of MPs under ebb tide in the unsaturated media 105
Figure 5.5 Effect of salinity on the mobilization of MPs under ebb tide in the unsaturated media 107
Figure 5.6 Mobilization of MPs at transient flow under ebb tide condition 109
Figure 5.7 Mobilization of MPs under flood tide in saturated media 112
Figure 5.8 Effect of salinity on the mobilization of MPs under flood tide in saturated media..... 114
Figure 5.9 Interaction energy between particles under different salinity conditions..... 117
Figure 5.10 The interaction energy between NBs and GB 118
Figure 5.11 The contributions of each parameter to the diffusion coefficient based on inversion simulation 119
Figure 6.1 The particle size distribution in the water with only sand using different particle size analyzers. (a) Zetasizer ZS; (b) LISST-200X. 127
Figure 6.2 Experimental procedure for studying the release of particles from masks 127
Figure 6.3 FTIR spectra of masks with different UV weathering durations. (a) The outer layer. (b) The middle layer. (c) The inner layer. 130
Figure 6.4 SEM images for the three layers of masks with different UV weathering durations: (a, d, g) Images at 1000 magnification of the outer layer of mask with UV irradiation for 0, 18 and 36 hours. (b, d, h) Images at 1000 magnification of the middle layer of mask with UV irradiation for 0, 18 and 36 hours. (c, f, i) Images at 1000 magnification of the inner layer of mask with UV irradiation for 0, 18 and 36 hours. 134
Figure 6.5 SEM images for the middle layer of masks with different UV weathering durations: (a, d, g) Images at 1000 magnification of the middle layer of mask with UV irradiation for 0, 18 and 36 hours. (b, d, h) Images at 2000 magnification of the middle layer of mask with UV irradiation for 0,

18 and 36 hours. (c, f, i) Images at 5000 magnification of the middle layer of mask with UV irradiation for 0, 18 and 36 hours.....135
Figure 6.6 Mechanical tension and AFM images for different mask layers. (a) The AFM image of the virgin outer layer. (b) The AFM image of the outer layer when weathered for 24 hours. (c) The AFM image of the virgin inner layer. (d) The AFM image of the inner layer when weathered for 24 hours. 137
Figure 6.7 Contact angels for mask layers with different UV weathering durations 138
Figure 6.8 Analysis of particles entering the water from masks. (a) The SEM image of particles released from the virgin mask. (b) The SEM image of particles released from the mask weathered for 18 h. (c) The SEM image of particles released from the mask weathered for 36 h. (d) The particle size distribution in the absence of sand. (e) The particle size distribution in the presence of sand. 142
Figure 6.9 Size distributions for particles released from three mask layers under different weathering conditions 147
Figure 7.1 FTIR spectra of disposable gloves (a–c). FTIR mapping of the C-H functional groups (3000–2800 cm^{-1}) of pristine gloves (d–i). FTIR mapping of the C=O functional groups (1780–1700 cm^{-1}) of gloves after 48 h of UV weathering (j–o). 159
Figure 7.2 SEM images for the disposable glove with different UV weathering durations. Images are at 500X magnification.....161
Figure 7.3 (a–i): The AFM image of the surface of disposable gloves after UV weathering. (a), (d) and (g) are pristine, weathered 24 and 48 h of latex gloves, respectively. (b), (e) and (h) are pristine, weathered 24 and 48 h of nitrile gloves, respectively. (c), (f) and (i) are pristine, weathered 24 and 48 h of vinyl gloves, respectively. (j) is the surface roughness of the gloves after UV weathering. 162

Figure 7.4 Mechanical strength of disposable gloves with different UV weathering durations.... 164
Figure 7.5 The changes of contact angle of disposable gloves with different UV weathering durations 165
Figure 7.6 (a–c): The particle size distribution of MPs released from latex, nitrile, and vinyl gloves in the absence of sand. (d–i): The particle size distribution of MPs released from latex, nitrile, and vinyl gloves in the presence of sand. (g–i): The volume percent of particle size of MPs. 169
Figure 7.7 The size distribution of particles released from glass beads 171
Figure 7.8 (a–c): Concentrations of elements released from disposable gloves before and after UV weathering. (d–f): The concentration percent of leachable elements by different gloves before and after UV weathering. 176

List of Tables

Table 2.1 Permeability for beaches with different size sediments (Humphrey et al., 1993) 9

Table 2.2 Weathering ratios or biomarkers used in previous studies 16

Table 2.3 Research on the MPs in the urban runoff 22

Table 2.4 Concentrations and removal efficiencies of MPs from WWTPs 25

Table 3.1 Physical properties of Hibernia oil 37

Table 3.2 n-alkanes of the stranded oil under different conditions 53

Table 3.3 Fitted partition coefficient and regression coefficient of predicted vs observed data. 57

Table 4.1 Characteristics of freshly generated NBs solution. 64

Table 4.2 ζ -potential of NBs solution and MPs suspension 66

Table 4.3 pH of NBs solution, MPs suspension, and MPs−NBs suspension in the absence of salt 66

Table 5.1 Properties of different MPs particles 96

Table 5.2 Properties of NBs solution and MPs suspension 97

Table 6.1 Changes in the surface fiber roughness of the mask after UV weathering 133

Table 7.1 The organic matters released from disposable gloves 177

List of Abbreviations

MPs	Microplastics
AFM	Atomic Force Microscope
ATR–FTIR	Attenuated Total Reflection–Fourier Transform Infrared Spectroscopy
BTCs	Breakthrough Curves
DI	Deionized Water
DLVO	Derjaguin-Landau-Verwey-Overbeek
DO	Dissolved Oxygen
GBs	Glass Beads
GC-MS	Gas Chromatography–Mass Spectrometry
ICP-MS	Inductively Coupled Plasma-Mass Spectrometry
LISST	laser In-Situ Scattering and Transmissometry Analyzer
NaCl	Sodium Chloride
NBs	Nanobubbles
NPs	Nano-plastics
PE	Polyethylene
PET	Polyethylene Terephthalate
PMMA	Polymethylmethacrylate
PP	Polypropylene
PPE	Personal Protective Equipment
PS	Polystyrene
PSD	Particle Size Distribution
PTFE	Polytetrafluoroethylene

PV	Pore Volume
PVC	Polyvinyl Chloride
SEM	Scanning Electron Microscope
SFT	Surface Tension
UV	Ultraviolent
WWPTs	Wastewater Treatment Plants

Chapter 1. Introduction

1.1 Problem statement

The coast is a complex environment that comprises seawater, underwater, soil, atmosphere, and other environmental factors (Wang et al., 2020c). The shoreline is exposed to various wave and tide conditions, which may significantly affect the behaviors of pollutants on beaches (Geng and Boufadel, 2015). Thus, shorelines are not only the main receptor of pollutants from oceans and lands, but also play host to further transformation of pollutants under weathering conditions (Wang et al., 2021c; Wang et al., 2022b).

Accidental oil spills in ocean may occur during exploitation, storage, transportation and use of oil (Badiozamani et al., 2019; Bi et al., 2020; Skaare et al., 2008). The spilled oil frequently reaches shoreline where it may harm the ecosystem and socioeconomic features (Owens et al., 2018; Wang et al., 2020b). To minimize the risk of shoreline contamination oil spills and for the development and selection of effective response methods (Chen et al., 2019; Pi et al., 2017; Zhu et al., 2016), it is necessary to understand the transport and fate of oil on shorelines. Once oil is released into the environment, it will undergo various physical, chemical and biological changes such as evaporation, spreading, drifting, dispersion, oxidation, and aggregation (Chen et al., 2021; Gong et al., 2014). Due to the chemical complexity and interaction with the surrounding environment, it is often difficult to accurately monitor the transport and transformation following release. Low molecular weight components are generally lost initially, leading to an increase in the density and viscosity of the residual oil. Most of the residues are heavy components which are resistant to weathering. At

the same time, the interaction of oil and particles exacerbates the uncertainty of oil fate. Oil degradation rates are determined by various factors, such as the type of oil and environmental conditions (Sun et al., 2018; Tarr et al., 2016). In addition, the geomorphic characteristics such as wave energy, slope, and substrate of beach also have influence on the persistence of stranded oil on shoreline. Nanobubbles (NBs) are nanoscopic gaseous bodies that are attached to the surface of the medium and/or surrounded by solutions (Alheshibri et al., 2016; Sun et al., 2022). It has been reported that due to the presence of natural surfactants in seawater, air bubbles with a size less than 1 μm generated by wave breaking and shearing can exist stably for about 22 h (Johnson and Cooke, 1981). However, few studies have focused on the role of NBs in the natural environment. In addition to the substantial stable NBs found in the marine environment, it is speculated that turbulence caused by rapids and waterfalls can also generate NBs within freshwater rich in organic matters (Alheshibri et al., 2016). This likely indicates that NBs play a role in the environment beyond what has been predicted. The shoreline, as the intersection of ocean and land, is one of the most concentrated areas of wave energy (Ahn et al., 2019). Bubbles produced by breaking waves are also found in offshore areas (Thorpe et al., 1982). As a traditional pollutant in the ocean, oil spills can seriously harm local ecosystems once stranded in the shoreline environment (Chen et al., 2019; Wang et al., 2020c). There have been many studies investigating the fate and transport of oil stranded on shorelines, but almost all have paid attention to only light irradiation, temperature, salinity, shoreline substrate, microbial degradation, and other conventional factors (Abou-Khalil et al., 2022; Aeppli et al., 2022; Cao et al., 2022; Cao et al., 2020; Ji et al., 2021). No studies have thus far focused on the potential effects of NBs in the shoreline environment. Therefore, it is necessary to explore the environmental effect of NBs on stranded oil on the shoreline.

The transport and fate of microplastics (MPs) as emerging pollutants in the natural environment, especially in the aquatic environment, has received significant attention (Galloway et al., 2017; Vethaak and Legler, 2021). The highest concentration of MPs was reported in the Pacific Ocean with 918 items/m^3, followed by the Atlantic, Arctic, Indian, and Southern Oceans with 7.68, 0.7, 0.32, and 0.022 items/m^3, respectively (Bakaraki Turan et al., 2021). MPs come from a wide range of sources, including primary sources as well as secondary sources, such as the release of microbeads from commercial products (Belzagui et al., 2020; Hernandez et al., 2017b), and the degradation of large plastic fragments due to physical, chemical and biological processes (Hernandez et al., 2019; Wang et al., 2021c), respectively. MPs can adsorb other environmental pollutants, which not only affects the migration and transformation of pollutants (Wang et al., 2021b), but also indirectly affects the physicochemical properties of environmental media (Guo et al., 2022). More seriously, MPs are not only widely distributed in environmental medias, but also accumulate in organisms through the food chain (de Sa et al., 2018; Guzzetti et al., 2018), ultimately affect human health (Mohamed Nor et al., 2021; Vethaak and Legler, 2021). Current research has found that MPs have been found in various types of organs in the human body (Ibrahim et al., 2021; Yang et al., 2023), and even affects the next generation through the placenta (Ragusa et al., 2021). As the most one of the important sinks for MPs, the coast plays a crucial role in the transmission and transport of MPs. Identifying the environmental behavior of MPs in the coastal zone is a prerequisite for understanding their fate and developing cleanup strategies.

Since early 2020, the spread of the pandemic has exerted a profound influence on normal production and life in cities around the world (Cai et al., 2021; Tian et al., 2021). To prevent the transmission of the coronavirus (SARS-CoV-2), the public is encouraged to wear personal protective equipment (PPE), according to recommendations from the World Health Organization (World Health

Organization, 2020). As the most convenient and effective means of protection, disposable masks and gloves are widely used in various scenarios (Anedda et al., 2020; Gereffi, 2020; Jedruchniewicz et al., 2021). More importantly, the growth in the number of people diagnosed and a corresponding increase in surgical procedures have also posed a challenge in the demand for PPE (Powell-Jackson et al., 2020). It is estimated that more than 129 billion face masks and 65 billion gloves are consumed globally every month (Prata et al., 2020).

However, the explosive growth in the use of masks and gloves has introduced numerous issues related to the disposal and management of PPE waste (Patricio Silva et al., 2021; Prata et al., 2020; Yang et al., 2021a). A large amount of PPE waste is discarded without any treatment, as a result of inappropriate waste management and the lack of environmental awareness (Cordova et al., 2021; Haque et al., 2021). Various types of PPE have been widely observed on shorelines, rivers, lakes and in the aqueous environment (Aragaw, 2020; Canning-Clode et al., 2020; Fadare and Okoffo, 2020). The masks themselves pose a direct threat to marine life (Guzzetti et al., 2018). Moreover, the plastic fragments or MPs derived from PPEs can further cause many other environmental problems. Therefore, it is necessary to investigate the potential release of MPs from PPE waste to determine the pollution risk and improve PPE waste management.

1.2 Research objectives

The study aims to in-depth investigate the occurrence as well as the environmental behavior of traditional and emerging pollutants, represented by oil spills and MPs, in the coastal environment, combining general and neglected environmental factors. Complex environmental factors can be distinguished by conducting controlled laboratory experiments. Theoretical calculations and numerical simulations were applied to explain experimental phenomena. In order to achieve these

objectives, novel experimental designs and methods were designed in this study. The detailed research objectives are as follows:

- Characterize the properties of NBs and to determine the influencing factors in a shoreline environment. On this basis, the environmental behavior of NBs and their role in the fate and transport of spilled oil were further investigated;
- Examine the behavior and motion of various MPs in the presence of bulk NBs under conditions that take into account various coastal factors;
- Evaluate the vertical motion of MPs under steady state and transient conditions in the coastal vadose zone in the presence of NBs;
- Investigate the characterization of changes in disposable masks when exposed to coastal environments and the environmental factors that influence the release of MPs;
- Explore the physicochemical changes, and the release of MPs and other contaminants of disposable glove wastes in the coastal environment.

Chapter 2. Literature review

The risk of pollution of marine and coastal ecosystems is increasing dramatically (Cole et al., 2011). This not only affects the ecosystem, but also indirectly harm the social-economic features of the coastal communities (Feng et al., 2021a). Coastal pollution comes mainly from point and non-point sources such as rivers, drains, submarine outfalls and coastal cities (Vikas and Dwarakish, 2015). Unknown sources of pollution from offshore areas due to the ocean current are also receiving increasing attention (Suneel et al., 2019). Traditional pollutants, represented by oil spills, have been the one of most significant hazards to jeopardizing the coastal environment. The most prominent examples in recent decades are the large-scale oil spills from the Exxon Valdez (Boufadel et al., 2010; Peterson et al., 2003) and the Deepwater Horizon (Beyer et al., 2016; Reddy et al., 2012). At the same time, an increase in the accumulation of plastics in the oceans has been documented from year to year, which poses new risks, particularly with regard to MPs (Law and Thompson, 2014; Ostle et al., 2019). An in-depth understanding of the occurrence, transport, transformation, and fate of these pollutants is a prerequisite for the development of sound prevention and treatment strategies.

2.1 Oil transport and fate on beaches[1]

When the spilled oil reaches the shoreline, they will be distributed in different areas due to different beach characteristics and environmental factors. Due to the variety of terminology regarding oil residues in different studies, oil residues were divided into three major categories according to the

[1] This work has been published as Wang, Z; An, C; Lee, K; Owens, Chen, Z; Boufadel, M; Taylor, E; Feng, Q. 2020. Factors influencing the fate of oil spilled on shorelines: a review. Environmental Chemistry Letters, 19, 1611–1628.

vertical distribution in this review. The distribution of oil residues in different beach scenarios are shown in Figure 2.1. (i) Surface oil residues which are distributed on beaches that are either removed or retained depending on the environmental factors and substrate type. (ii) Subsurface oil residue which are typically buried below the surface of beach which can be transported to the supratidal area by large waves where subsequent waves have little effect. In addition, over time some oil can become entrained below the surface. This weathered oil left in the sand or residues left after mechanical beach cleanup can still be affected by the tide. (iii) Submerged oil mats which exist in the inshore zone that may be difficult to locate, so their spatial extent is uncertain. In general, this kind of mat is similar to sediment-oil mats as mentioned above, which are subject to currents and wave energy. According to the different properties and residual sites of shoreline oil, the distribution and transport will be further explored from three aspects: penetration, retention, and remobilization.

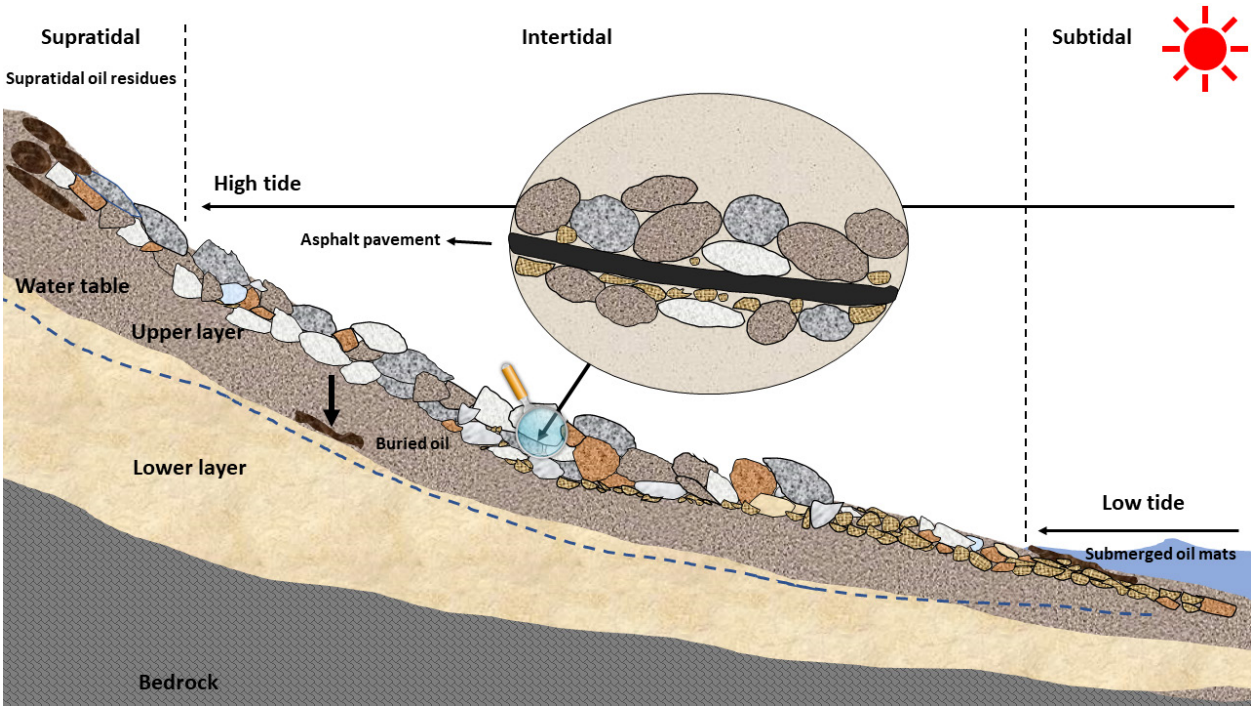


Figure 2.1 The distribution and behavior of stranded oil on shorelines affected by the beach topography and environmental factors

2.1.1 The transport of oil in the coastal areas

Shoreline substrate type and oil property are the key factors that influence the oil permeability (Lee et al., 2015). Generally, on beaches where very fine matrix particles are tightly packed together, the penetrating force will be small, while the penetrating force will be great on coarse matrices. Etkin et al. (2008) found that when the pores were large and interconnected, the substrate was more permeable, thus deeper penetration and horizontal motion of oil were carried out through capillarity. The permeability for coarse and fine sediments is summarized in Table 2.1. Bedrock shoreline is essentially impermeable to oil unless it can enter the interior through a crack on the rock surface. The interstices for gravel beaches are usually large and interconnected, which makes the oil easy to penetrate (Etkin et al., 2008). For coarse-grained beaches with boulder-armored structure, oil can penetrate into the finer deposits below the pebble or boulder layer. These surface armor effectively attenuates wave energy and prevents further weathering of the oil below (Irvine et al., 2006). In the case of fine-grained beaches, the oil will slowly penetrate into the fine gaps between the particles over time and may further reach the sediments in lower layer (Owens, 1978). Although sediment in sandy or muddy beaches has small pores and is not easily for oil to penetrate, it is still possible to permeate for some light oils. In some special cases, shoreline features that are not related with sediment or particle size, such as holes made by animals on mudflats, can affect oil penetration (Humphrey et al., 1993).

Table 2.1 Permeability for beaches with different size sediments (Humphrey et al., 1993)

	Coarse sediments	**Fine sediments**	**Very fine sediments**
Effective porosity	0.12-0.46	0.12-0.46	0.12-0.46
Permeability	High	Low	Low
Penetration	High	Low	Low
Residual loading	Low	High	Low

In addition to the properties of the shoreline substrate and oil, some natural environmental factors such as hydraulic conductivity of sediments and the height of groundwater table can also affect the permeability. Short et al. (2006) found that when the low tide was high, the time interval of groundwater penetration into the sediments was shortened. With the ebb tide, even if the oil viscosity is about 1000 cp, it can penetrate into the sand and gravel sediments in a few hours. Some beaches have two-layered structure with different hydraulic characteristics. The permeability of the upper layer is so high that the groundwater flows as fast as the ebb tide, and the permeability of the lower layer is so low that it is difficult for the groundwater to continue to fall (Li and Boufadel, 2010). The two-layered structure (Figure 2.1) greatly promotes the penetration of residual oil from the surface to the lower layer. When tide falls, the water table drops rapidly, and oil stranded on the beach surface can easily penetrate into the lower layers, protecting them from continued weathering (Li and Boufadel, 2010; Xia et al., 2010). Models can also be used to evaluate the oil burial depth. The calculation was performed by considering the depth difference between the initial and final beach at a representative level and oil type (Bernabeu et al., 2016). When large amounts of oil are deposited on shoreline, the feedback of oil to the beach should also be taken into consideration. Large deposits of oil act as a protective layer and prevent further penetration.

The redistribution of sediments in the coastal zone can result in a variety of morphological changes, which are different in scale and rate of change (Asif and Chen, 2016; Yuan et al., 2017). When assessing the remobilization of buried oil stranded in the intertidal zone, the periodic or aperiodic variations must be considered, such as seasonal beach processes or sand bar migration. Under storm conditions, coastal erosion changes quickly, usually within a few days. In addition to these shoreline material movements, the mobilization of sediments along the coast is also a phenomenon that cannot be ignored (Lee et al., 2015). By migrating oil to a beach microenvironment with more favorable properties, storm can promote the sensitivity of polycyclic aromatic hydrocarbons to biodegradation (Curtis et al., 2018). Some large waves with more momentum may help the floating oil penetrate into the lower layer of the beach. But sediment on the beach can counteract this trend (Boufadel et al., 2019).

The remobilization of sediments on beaches has different spatial and temporal scales. As long as there is enough mechanic energy, the beach sediment will continue to move, and the rate and extent of the movement will depend on the size of the sediment and the wave energy. The greater the energy is, the more significant the change in coastal morphology. In relatively low energy environments, the stranded oil can be changed by bonding to the sediment, thus forming the asphalt pavement (Owens, 1985). It has been proposed that in mudflat or marsh environments, washover can alter the location of oil residues. Observations after the storm show that oil residues on intertidal zone can be moved to the supratidal zone (Curtis et al., 2018). The morphology of the beach changes due to the wind and waves over time, and the oil may be exposed or reburied (Operational Science Advisory Team, 2011). Under storm conditions for Prestige oil spill, the upper part of the beach showed a tendency to be eroded and to move towards the subtidal zone. Some large fractures can

produce very strong turbulent motion, greatly facilitating the remobilization of sediments in the bottom (Bernabeu et al., 2006; Xia and Boufadel, 2011). In addition, the grinding between the particles greatly improves the fluidity of the oil attached to the particles. During a storm, if the energy is large enough, the oil attached to the particles has a chance to be removed (Humphrey et al., 1993). Simulation results showed that under general hydrodynamic and wave conditions, the sediment-oil agglomerates on the seabed were mobile about 60%, while the buried sediment-oil agglomerates were difficult to move (Gustitus and Clement, 2017). It should be noted that the formation of oil-mineral aggregates on shorelines plays an important role in natural oil removal, especially in low energy environment. Under the wave actions, the stranded oil interacts with minerals, and in turn reduce adhesion of the oil to substrate (Lee et al., 2002; Owens and Lee, 2003).

Within days to months, free flowing oil in the pore space may be naturally removed from the beach, and the movement of oil remaining on the beach will be restricted. If the remaining oil on the beach does not change significantly after several tides, it is considered to be retention (Boufadel et al., 2019). Shoreline type is a key factor in determining the persistence of stranded oil. Oil film can be formed when particles combine with oil, and it is associated with interfacial tension and surrounding buoyancy or gravity. The contact point of oil and particle is stable. As the particle size increases, the distance between the contact points increases, which means that oil is more likely to be affected by the environment (Lee et al., 2015). As shown in Figure 2.1, most buried oil residues are distributed in the middle and upper intertidal zones, and a few small sediment-oil mats deposits are distributed in the position of the lower intertidal zone (Boehm et al., 2008; Curtis et al., 2018; Operational Science Advisory Team, 2011). The retention of subsurface oil residues is affected by a variety of factors, including the protection from wave action by boulder-cobble armor, the presentation of water penetration and circulation in fine particle matrix, and the formation of asphalt pavement to

prevent further weathering. Sediment composition can also affect the retention of buried oil on beaches. Mixed carbonate sands facilitate oil degradation, and siliceous sands allow oil particles to penetrate freely into the sand phase and quickly reach the external environment. This trend may have important significance for the underground pollution treatment of oily beaches (Fernandez-Fernandez et al., 2014).

There have been some field surveys with respect to the retention of buried oil on beach from previous oil spill events. Boehm et al. (2014) reported that weathered buried oil residues in the Exxon Valdez oil spill could be trapped in intertidal sediments for decades, and the erosion, dissolution and groundwater flow required for degradation was low. Page et al. (2008) also conducted a long-term investigation into the underground oil in the Exxon Valdez spill. A survey in 2000 found that subsurface oil deposits were mainly under exposed boulders/cobble stones, while these cobblestones with the protection effect hold only a small portion of the original spill area. In 2007, some of buried oil was still scattered at these sites because they were isolated. The sediments had low porosity and were protected by boulder-cobble armor structure. By comparing the distribution of sediments in 2002 and 2007, it was found that the residues did not move in the tidal zone during this period and were all deeply degraded oils. This again demonstrates that spilled oil penetrating under boulders can be isolated by the protection of boulders and the formation of weathered asphalt layers on the exposed surface, thus protecting the inner layer of the residues from natural degradation. Guo et al. (2010) believed that oil retention was also related to the two-layered structure from the survey regarding the Exxon Valdez oil spill. When the tide and water table drop rapidly, oil stranded on the beach surface can penetrate down and remain there if it is not removed manually. Under certain storm conditions, these residues can be changed. In the case of Deepwater Horizon oil spill, the

remaining oil in the subtidal zone was in the form of submerged oil mats, and remaining oil in the subtidal zone was buried during the storms (Curtis et al., 2018).

2.1.2 Fate of oil in the shoreline

The amount and distribution of remaining oil along the shoreline are affected by the beach topography and wave action. At present, the main method to evaluate oil spill residue is to determine the amount of alkanes and polycyclic aromatic hydrocarbons in beach sediment samples. There are many factors such as total organic carbon content and sediment size that affect the physical and chemical behavior of polycyclic aromatic hydrocarbons in beach sediments (Ríos et al., 2009). The adsorption of polycyclic aromatic hydrocarbons to sediments increases with increment of salinity. At the same time, the solubility of some polycyclic aromatic hydrocarbons such as naphthalene and phenanthrene also decreases with increasing salinity. Organic coating of sediment particles enhances hydrocarbon adsorption. The sediments composed of carbonate rocks and organic matter affect the adsorption and desorption of low molecular weight polycyclic aromatic hydrocarbons (Soliman et al., 2019; Srogi, 2007).

There were few studies on simulating weathering in the laboratory, while most studies were based on field surveys of past oil spill events. In the case of the Exxon Valdez oil spill in 1989, 258,000 barrels of crude oil were released into the marine environment (Lindeberg et al., 2018; Short et al., 2004). It was estimated that around 40% of the spilled oil affected the coastline of Prince William Sound, and the western part of the Gulf of Alaska was also contaminated to varying degrees. Irvine et al. (2006) found that although the pebble protective beach continued to be contaminated by underground oil with reappeared contamination in 1999, the surface oil coverage at the study sites declined significantly. By 2001, almost no surface oil had been found, except for some newly formed

asphalt pavement. Some estimations showed that oil residues on shoreline fell to 25% in 2001. After 2001, the rate for the natural reduction of buried oil-sediments dropped to about 4% per year due to the exposure of the remaining oil to sunlight and rain (Boehm et al., 2008; Nixon and Michel, 2018). From 2001 to 2009, the amount of residual oil in beach sediments continued to decline. But as the bad weather continued, oil reappeared in parts of the site where there was no oil left (Boehm et al., 2014). By analyzing the chemical composition of residual oil, it was found that polycyclic aromatic hydrocarbons were the most difficult to degrade, and the degradation rate of other compounds was generally higher. However, light polycyclic aromatic hydrocarbons such as 4-, 5-, and 6-cyclic compounds can also degrade rapidly (Boehm et al., 2014). Boufadel et al. (2010) also found that more than 20 years later, the oil on sediments contained high concentrations of polycyclic aromatic hydrocarbons and these heavy polycyclic aromatic hydrocarbons were potentially harmful to marine and shoreline ecosystems. After 5 years of natural weathering of Deepwater Horizon oil spill, the total amount of n-alkanes in beach sediments accounts for about 50%, while the n-alkanes with medium molecular weight (C21-C30) account for 76.6% of the total n-alkanes (Du and Kessler, 2012; Duan et al., 2018; Wang and Roberts, 2013).

When an oil spill occurs, the oil residues stranded on the beach will gradually degrade through physical, chemical and biological processes, so the chemical change of oil composition is an important indicator to assess the degree of oil weathering. Chemical changes are impacted by a variety of factors, including oil properties, such as viscosity, solubility and adsorption capacity, shoreline morphology, and natural factors (Zhao et al., 2019). Although the weathering process varies in different oil spill event, the overall pattern is similar. In general, the most likely to occur is the physical and chemical degradation of some low-molecular-weight alkanes or polycyclic aromatic hydrocarbons (Hagemann et al., 2019). In addition, most studies suggest that

photooxidation plays an important role in the initial stage of oil spill. When oil retains on the beaches, the long-term photooxidation process should not be ignored, although some oils have been weathered (Prince et al., 2003). Garrett et al. (1998) analyzed the photooxidation of crude oil and identified the chemical change. They found that the sensitivity of some aromatic compounds to photooxidation increases with the increase of alkyl substitution. In contrast, biodegradation is slow but with a good degradation effect on the high-molecular-weight part of oil, and is considered to be the most efficient natural degradation process (Owens et al., 2018; Yin et al., 2015).

In order to evaluate the risk of spill accidents to animals, plants and the entire ecosystem, the changes of oil chemical composition in the sediments at different weathering periods should be well understood. Due to the variation in the amount of oil and the aggregation type of the sediments, the ratios of the compounds measured were used to detect the composition variation patterns driven by the weathering process (Table 2.2). In addition, the temporal changes of total petroleum hydrocarbons, alkanes, polycyclic aromatic hydrocarbons in the stranded oils can be used for estimating degradation rates and environmental half-lives of oil (Yim et al., 2011). Besides, the relative ratios of source-specific hopanes have been used to identify oil origins (Duan et al., 2018; Fang et al., 2019; Turner et al., 2014). It was found that surface oil residues were the most degraded oil, evidenced by nearly complete depletion of n-alkanes and isoprenoids and by complete loss of benzene, toluene, ethylbenzene, and xylenes compounds.

Table 2.2 Weathering ratios or biomarkers used in previous studies

Weathering ratios or biomarkers	**Description**	**Ref**
C2-Dibenzothiophenes/(C2-Phenanthrenes/Anthracenes), DBT3/PA3	Weathering identification for Deepwater Horizon oil spill	(Stout et al., 2016)
chrysene/benz(a)anthracene	Photodegradation	(Huba and Gardinali, 2016)
n-C18/phytane	Biodegradation	(Huba and Gardinali, 2016)
alkylated phenanthrenes/ dibenzothiophenes	Double ratio plots	(Yim et al., 2011)
17a(H)21b(H)hopane	Biomarker	(Prince et al., 2003; Prince et al., 2002; Radovic et al., 2014; Stout and Payne, 2016; Stout et al., 2016; Zakaria et al., 2018)
total naphthalenes ($C1\text{-}4_N$)/ total chrysenes ($C1\text{-}3_C$)	Weathering identification for Exxon Valdez Spill	(Boehm et al., 2008)
$(100\times\Sigma PHEN)/(\Sigma PHEN+\Sigma CHRYS)$*[1]	Weathering of biodegradation	(Curtis et al., 2018)
$(100\times\Sigma DBZ)/(\Sigma DBZ+\Sigma CHRYS)$*[1]	Weathering of biodegradation	(Curtis et al., 2018)

*Continuous

Weathering ratios or biomarkers	Description	Ref
17a(H), 21b(H)-30-norhopane (H29), 17a(H), 21b(H)-hopane (H30), C31-C34 (S, R)-17a(H), 21b(H)-homohopanes (C31-C34 (S/R))	Biomarker	(Yang et al., 2018)
14 carbon atoms (i-C14)/ phytane	Volatilization	(Esquinas et al., 2017)
Phenanthrene/ Benzo(a)pyrene	Weathering of biodegradation	(Esquinas et al., 2017)
Pyrene /hopane; C2-DBT /hopane; (C1-APh+ C2-APh) / hopane*[2]	Depletion ratios for Prestige oil spill	(Gallego et al., 2006)
shorter-chain (⩽C26) alkanes; longer-chain (⩾C16) and branched alkanes; polycyclic aromatic compounds (PACs)	Weathering of biodegradation or photo-oxidation	(Vergeynst et al., 2019)
total n-alkanes/ chrysenes; total PAH/ chrysenes	Weathering identification for Exxon Valdez Spill	(Short et al., 2007)
C2-DBTs/C2-PHENs, C3-DBTs/ C3-PHENs, DBT/MCHRY, CHRY/PHENs*[1, *2]	Weathering of biodegradation	(Wang et al., 2011)
$C_{30}\alpha\beta$-hopane	Biomarker	(Mulabagal et al., 2013; Yin et al., 2015)

*Continuous

Weathering ratios or biomarkers	Description	Ref
17α(H)-22,29,30-trisnorhopane/17α(H),21β(H)hopane; 17α(H),21β(H)-30-norhopane/17α(H),21β(H)-hopane	Biomarker	(Evans et al., 2017)
naphthalenes (2-rings); phenanthrene/anthracenes (3-rings); dibenzothiophenes (2-rings fused to a central thiophene ring)	Weathering identification for Deepwater Horizon oil spill	(Bejarano and Michel, 2010)
Σ (C_1, C_2, C_3-PHEN, C_1, C_2, C_3-CHRYS)/C30-hopane; 100×Σ (C_1, C_2, C_3-PHEN)/ (Σ (C_1, C_2, C_3-CHRYS)+ Σ (C_1, C_2, C_3-PHEN)) *[1, *2]	Weathering of biodegradation	(Pardue et al., 2014)

*[1] ΣPHEN=sum(C1-C4 phenanthrenes), ΣDBZ=sum(C1C3 dibenzothiophenes) and ΣCHRYS=sum(C1-C3 chrysenes); *[2] C1-APh: methyl anthracenes and phenanthrenes; C2-APh: dimethyl anthracenes and phenanthrenes; C2-DBT: dimethyldibenzothiophenes;

As a fundamental means of organic component characterization, mass spectrometric analysis plays a vital role in oil spill investigation. Based on gas chromatography–mass spectrometry (GC-MS) fingerprinting analysis of sediment samples from Cantabrian shoreline in Asturias, Esquinas et al. (2017) found that the saturated aromatic compounds were the first part to degrade, and then the degradation rate gradually decreased. However, degradation rates of heavy components such as resins and asphaltenes increased gradually. As time went on, the proportion of each component did not change greatly, indicating the synchronous degradation of each component. Although GS-MS

or GC- Flame Ionization Detector (FID) are widely used to analyze the oil and organic matters, these methods are more suitable for fresh crude oil samples. Because the weathered oil residues on the beach contain few biomarkers suitable for GC-MS analysis, most of which are heavy substances such as asphalt, new analytical methods are needed. In addition, the concentration and distribution of metals may also interact with the oil behaviors on beaches. Previous studies have shown that the concentration of trace metals is correlated with the content of short chain alkanes and polycyclic aromatic hydrocarbons (Liu et al., 2012). When the organic components with low molecular weight are degraded, the metals may combine with the heavy organic components in the oil and accumulate continuously, resulting in the negative correlation of their concentration. Secondly, some functional groups such as carboxyl and hydroxyl groups can also be coupled to metals. In addition, metals can be complexed with dissolved organic ligands, which may further promote metal enrichment (Botello et al., 2015).

2.2 Transport of MPs in coastal areas

MPs are typically characterized as plastic pellets with a particle size of less than 5 mm (Andrady, 2017). The primary sources of MPs include the direct release of plastic microbeads from certain commercial products (Hernandez et al., 2017b), while secondary sources encompass the generation of MPs through physical abrasion, as well as chemical and biological degradation of larger plastic fragments (Naji et al., 2017). As plastic production continues to increase, the oceans have become one of the most important sinks for plastic waste. It has been reported that about 80% of the plastic in the oceans comes from land-based sources, with the rest coming from human activities in the oceans (Li et al., 2023). Particularly in nearshore areas, the sources of MPs are closely linked to human production and living activities (Pedrotti et al., 2016; Zhou et al., 2018). MPs are affected by

waves (De Leo et al., 2021), surface currents and winds (Iwasaki et al., 2017), and air-water exchanges (Allen et al., 2020), and are transported to remote areas, even to the polar regions (Obbard, 2018). In addition, the vertical distribution of MPs in the aqueous phase varies depending on factors such as polymer types, salinity gradients, tides, temperature, and other suspended particulate matters (Feng et al., 2023a; Feng et al., 2022; Li et al., 2019). There is a pressing need to study the environmental behaviour of MPs in the coastal areas for better understanding their ecological risks and develop effective responses.

2.2.1 Sources and types of MPs in the coastal environment

The primary contributors of MPs to the coastal environment include urban and industrial runoff (Wang et al., 2022a), wastewater treatment plants (WWPTs) (Murphy et al., 2016), riverine discharge (Yakushev et al., 2021), atmospheric deposition (Szewc et al., 2021) and maritime activities (Avio et al., 2017; Napper et al., 2022). Urban and industrial areas are significant contributors to MP pollution. Large quantities of MPs from synthetic materials, such as packaging materials, synthetic textiles, and from industrial processes sink into coastal waters through runoff. Previous studies regarding the concentration, size, and type of MPs in urban runoff were summarized in Table 2.3. It can be found that MPs of PP, PE and PS are commonly found in urban runoff all over the world due to their wide range of applications, such as plastics bags, netting, rope, bottle caps (Wang et al., 2021a). In addition, MPs are mostly present in the environment in the form of fibers or fragments. Concentration is an important parameter in determining the environmental risk of MPs. Concentrations are highly variable from region to region, and even within the same region, the range of variation in concentrations is large. This is greatly affected by emissions from neighboring communities and industrial endeavors. WWTPs are recognized as a major source of MP contaminants in the aquatic environment.

Current water treatment technologies used at WWTPs do not completely remove MPs from wastewater. Blair et al. (2019) found that the overall abundance of MPs decreased by 6%, 68%, 92%, and 96% after preliminary, primary, secondary, and tertiary treatments, respectively, in a given WWTPs. Even though the removed MPs are mainly transferred to the sludge after treatment, a significant amount of MPs are still discharged into natural water bodies and eventually into the ocean (Ngo et al., 2019). It is estimated that an average of 7.2 billion MPs enter rivers from sewage treatment plants every day (Liu et al., 2021). Table 2.4 summarized the concentrations and removal efficiencies of MPs from WWTPs around the world. It can be seen that most of the WWTPs for MPs removal efficiency are greater than 80%, when there are still some removal efficiencies are less than 70%. Rivers are part of the freshwater system that holds and transports MPs to downstream lakes, coastal areas, and oceans. Michielssen et al. (2016) summarized the characteristics and source pathways of MPs in Chinese freshwater systems, and found that the main types of MPs were PE and PP, with fibers and fragments being the most common forms. Vermaire et al. (2017) evaluated the abundance and distribution of MPs in the Ottawa River in Canada and found that MPs were widespread in the Ottawa River and at higher concentrations than in many other freshwater systems, including the Great Lakes. Compared with river discharge, the plastic particles transported by the atmosphere are mainly smaller MPs (mostly less than 500 μm) or even nano-plastics (NPs) (Zhang et al., 2020). It is estimated that between 0.013 and 25 million metric tons of MPs and/or MPs may be deposited from the atmosphere into the oceans each year (Allen et al., 2022). Evangeliou et al. (2020) simulated the migration of MPs/NPs from road traffic and suggested that about 34% of tire brake wear particles and 30% of brake wear particles ended up in the ocean. In addition, processes such as bubble burst ejection and wave action in the ocean can lead to the release of MPs into the

atmosphere (Allen et al., 2020). Identifying the sources and types of MPs will help to provide effective methods to prevent their entry into the coastal environment.

Table 2.3 Research on the MPs in the urban runoff

Site	**Size (µm)**	**Type**	**Shape**	**Concentration (items/L)**	**Reference**
Tijuana, Mexico		PE, PS, PA, PET, PP	Fiber, granule, film, sphere	66-191	(Piñon-Colin et al., 2020)
Greater Paris, France	930-2920	PE, PP, PS, PVC, PA, polyester	Fiber	1.9 for MPs; 29 for microfiber	(Treilles et al., 2021)
Bushehr, Iran	500-1000		Fiber, fragment, film, round shape	1.86	(Hajiouni et al., 2022)

*Continuous

Site	Size (µm)	Type	Shape	Concentration (items/L)	Reference
Beijing, China	225-900 (38%); 1000-2000 (34%); 2000-3000 (20%); 3000-5000 (8%)	PP, PE, PAN, polyester, Rayon	Fiber, fragment, film, foam, granule	1.6-29.6	(Zhang et al., 2023)
San Francisco, USA	123-355	PE, PP, PS, PC, PVC, PU, PET, PVA	Fiber, fragment,	1.1-24.6	(Werbowski et al., 2021)
Toronto, Canada	125-5000	PE, PPE. PP, PET, PVA	Fiber, fiber bundle, film, foam, sphere, fragment, gel	13.3±15.5	(Grbić et al., 2020)

*Continuous

Site	Size (µm)	Type	Shape	Concentration (items/L)	Reference
Tokyo, Japan	10-5000	PE, PEP, PEPD, PET		81-292	(Sugiura et al., 2021)
Greater Kuala Lumpur, Malaysia		PS, PP, HDPE, LDPE	Fiber, fragment, film, bead	42.2±35.29	(Chen et al., 2022)
Newark, New Jersey, USA	Most of less than 125	PP, PE, PET, Ny	Fragment, fiber, film	12-213	(Parameswarappa Jayalakshmamma et al., 2023)

Table 2.4 Concentrations and removal efficiencies of MPs from WWTPs

Site	Concentration MPs/L	Removal efficiency	Reference
Italy	2.5 ± 0.3 (Inlet); 0.4 ± 0.1 (Outlet)	84%	(Magni et al., 2019)
Korea (50 representative WWTPs)	0.004 to 0.51	98.7–99.99%	(Park et al., 2020)
Paris, France	260-320 (Inlet); 14-50 (Outlet)	88.1%	(Dris et al., 2015)
Vancouver, Canada	31.1±6.7 (Inlet); 2.6 ± 1.4 (Outlet)	98%	(Gies et al., 2018)
Bangkok, Thailand	12.2 (Inlet); 2 (Outlet)	84%	(Hongprasith et al., 2020)
Hunter Region, New South Wales, Australia	11.8 ± 1.10 (Inlet); 2.7 ± 0.11 (Outlet)	76.6%	(Raju et al., 2020)
Wuhan, China	79.9±9.3 (Inlet); 28.4±7.0 (Outlet)	64.4%	(Liu et al., 2019a)
Agadir metropolis, (Moroccan)	188-519 (Inlet); 50-86 (Outlet)	74%-87%	(Hajji et al., 2023)
Glasgow, Scotland, United Kingdom	133 (Inlet); 5.9 (Outlet)	95.6%	(Michielssen et al., 2016)

2.2.2 Distribution of MPs in the coastal environment

Inputs of MPs from land, rivers, and oceans reach beaches and adjacent areas through stranding, drift, and sedimentation. The movement and distribution of MPs is controlled by hydrodynamic processes such as nearshore and cross-shore transport, tidal circulation, estuarine circulation, seawater intrusion, Stokes drift and bed-load transport (Zhang, 2017). Sampling and modeling in coastal waters revealed a significant decreasing relationship between water depth and MPs abundance (Dai et al., 2018; Reisser et al., 2015). Liu et al. (2020a) summarized the vertical distribution of MPs in the coastal areas and proposed that the abundance of MPs was higher in the surface and subsurface layers and continued to decrease with increasing water depth. The interaction of coastal groundwater with seawater also affects the distribution of MPs, and previous study have proved a higher abundance of MPs in groundwater, and believed the that the density stratification have a significance influence on the vertical distribution (Zobkov et al., 2019). Several studies have found higher abundance of MPs in surface water and water column in areas with high traffic activity or tourism (Carbery et al., 2022; Zhang et al., 2017). Plastics as well as MPs are highly susceptible to surface currents and winds, and are transported and stranded on the beach. At the same time, MPs stranded on shore are affected by the wave and tidal cycle, and can be constantly distributed between the solid and water phases.

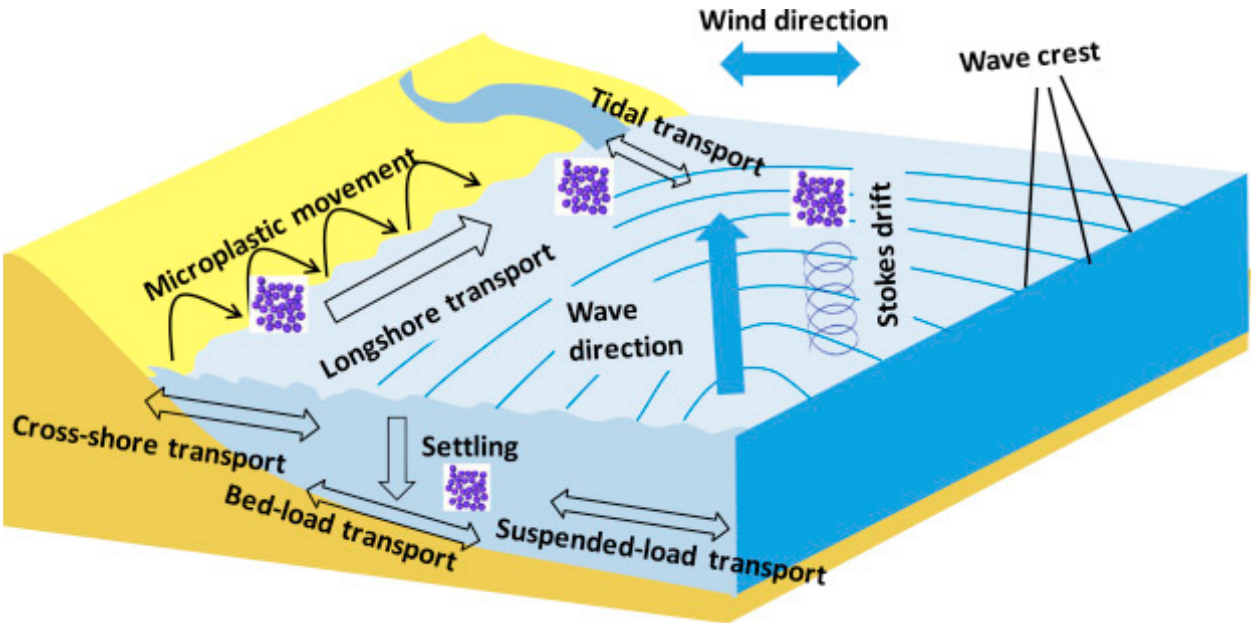


Figure 2.2 Schematic diagram of MPs transport in the coastal areas (Zhang, 2017)

The complexity of the coastal environment results in the transport and distribution of MPs being affected by a variety of factors. The physicochemical properties of MPs are important parameters that affect their movement, especially density, particle size, and shape, which affect their movement by controlling the hydrodynamic properties of MPs (Song et al., 2018). In addition, surface friction, hydrophilicity and other surface parameters are also factors that cannot be ignored that affect the transport of MPs (Feng et al., 2023a; Feng et al., 2022). The density difference between MPs and the aqueous phase is the first factor to consider when studying MP movement. In general, MPs with densities greater than seawater are easy to settle and enrich in seabed sediments, while particles with lower densities tend to float in the water column (Mountford and Morales Maqueda, 2019). However, the density of MPs can change due to weathering, biofilm growth, and other processes, resulting in some of the less dense MPs becoming negatively buoyant MPs, which in turn descend in the water column and eventually deposit to the seafloor. Van Melkebeke et al. (2020) found that marine biofouling not only increased the hydrophilicity of MPs, but was also a potential factor in the

downward deposition of low-density MPs. It is important to note that the density of seawater is not fixed, and salinity is the most significant factor affecting the density of seawater. Horizontal and vertical distribution of salinity is influenced by a variety of factors. For example, salinity increases with depth and there is a distinct zone called the halocline, where salinity increases abruptly. Salinity at the surface of the sea is decreased by the input of fresh waters or increased by the loss of water to ice or evaporation. As salinity increases, the settling rate of MPs decreases. When the salinity is constant, the temperature decreases and the density of seawater increases, which also affects the sedimentation of MPs (Uurasjärvi et al., 2021). The shape and size of MPs usually affects the drag and surface tension to influence the movement of MPs in the water. Van Melkebeke et al. (2020) quantitatively investigated the sinking behavior of MPs from different plastic waste samples by means of a resistance model, and proposed that particle shape was an important parameter that strongly influences the sinking behavior of MPs. Kowalski et al. (2016) argued that the irregularity in the shape of the MPs results in a larger specific surface area than that of a sphere with the same equivalent spherical diameter, resulting in a greater drag force that reduced the sinking rate. Previous studies on the effect of particle size on MPs movement were not uniformly. Kaiser et al. (2019) concluded that the settling velocity increased as the particle size increased. However, Zhang et al. (2021) showed that the abundance of MPs in sediments was higher for smaller MPs. The interaction of MPs with clay in the aqueous environment also affects their movement and sedimentation. The aggregation between MPs and clay was affected by repulsive energy barriers and external energy. Mild wave conditions favored aggregation, while strong and sustained high energies were detrimental to aggregation behavior (Yang et al., 2022b).

2.3 Occurrence and environmental risk of PPE waste in the natural environment[2]

2.3.1 Occurrence of PPE waste in the environment

The commonly used disposable masks are made from polymeric materials, especially PP. A standard disposable mask typically consists of 3 layers: the outer hydrophobic spun bond layer, a middle melt-blown layer, and an inner non-woven layer. The materials used and the performance of disposable gloves used vary widely for different applications. Three main types of disposable gloves used during the pandemic are latex, nitrile, and folic, accounting for almost 94.6% of all gloves (Jedruchniewicz et al., 2021). Latex or nitrile gloves are typically used in medical, manufacturing, laboratories, and domestic environments. Specifically, latex gloves are mainly made of natural rubber (cis-1,4-polyisoprene), which has good physical properties (Yew et al., 2019). However, natural rubber also contains small amounts of protein, fatty acids, wax, phospholipids, steroids, and other impurities, indicating that natural rubber can trigger allergic reactions among a small number of people (Rolere et al., 2015). Nitrile gloves are widely used as a better alternative to latex gloves in a variety of environments. Nitrile rubber is produced with butadiene and acetonitrile, and it is also called nitrile-butadiene rubber (NBR) (Yew et al., 2020). Metal ion crosslinkers, including Zn, Fe, and Al, can promote chain bonding of the polymer and enhance the dexterity of gloves (Yew et al., 2020; Zhang et al., 2019b). The main component of vinyl gloves is polyvinyl chloride (PVC), which can release chlorinated substances in degradation, leading to a high level of environmental risk (Chao et al., 2015; Jedruchniewicz et al., 2021; Yan et al., 2021).

[2] This work has been published as Wang, Z; Guy, C; Ng, KTW; An, C. 2021. A new challenge for the management and disposal of personal protective equipment waste during the COVID-19 pandemic. Sustainability, 13, 7034.

The wide use of PPE has brough a new challenge to municipal solid waste management and disposal. First, the fast growth of PPE waste has put enormous pressure on existing waste facilities, including transfer stations, material recovery facilities, incinerators, and landfills. In addition, unlike regular medical waste generated from clinics, hospitals, and nursing homes, PPE waste generated during COVID is often mixed with other municipal waste streams. It is difficult to sort and process PPE waste prior to disinfection and PPE waste will often end up in municipal waste streams (Ammendolia et al., 2021; Wang et al., 2021d). At present, the main methods of solid waste treatment are landfilling and incineration, accounting for 79% and 12% of the total treatments, respectively (Khoo et al., 2021). During the pandemic, incinerators and landfills are currently under significant pressure, despite the deployment of ancillary and additional treatment facilities in some countries.

Due to the lack of environmental awareness and regulations, a certain amount of PPE waste is discarded into the environment rather than going to landfills and incinerators (Figure 2.3) (Akhbarizadeh et al., 2021b; Ardusso et al., 2021; De-la-Torre et al., 2021). Since most PPE items are plastic products, these wastes can remain in the environment for a long time. Although much of PPE waste is generated in the urban area, this waste is found in the oceans through surface runoff, placing new environmental risk to oceans. As the mediator between the land and ocean, shorelines play a key role in the transport and transformation of pollutants (Gaylarde et al., 2020; Huang et al., 2021a; Kalogerakis et al., 2017). When subjected to the shoreline environment, the physicochemical characteristics of PPE wastes are altered by the effects of sun light, waves, and sand abrasion, and this, in turn, affects the surrounding environment (Kotek et al., 2004; Song et al., 2017).

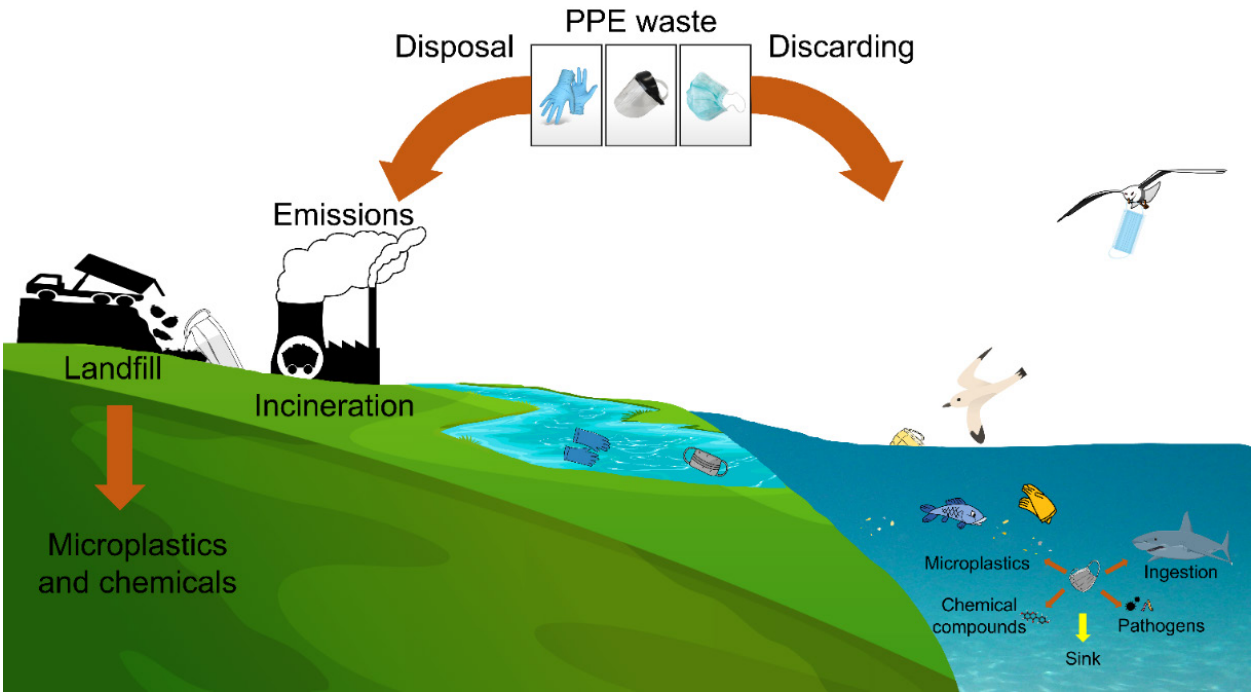


Figure 2.3 The environmental fate and impacts of PPE waste.

2.3.2 Environmental risk of PPE wastes

Studies have shown that PPE wastes can not only affect the marine ecosystem directly, but also indirectly threaten human health through various routes of exposure. On the one hand, the presence of PPE items in the marine environment will directly increase the potential risks to birds and marine fauna. For example, some marine animals can be entangled with the elastic ear loops of face masks, or trapped inside gloves, reducing their mobility, and may lead to starvation. In addition, PPE waste may be ingested by marine fauna, even endangering their lives. On the other hand, PPE waste will be another source of plastic fibers and MPs in the environment. MPs even nano-size plastic particles (less than 100 nm) are widely present in marine (Andrady, 2011), sediments (Lin et al., 2020), soil (Corradini et al., 2019; Yin et al., 2015), freshwater (Li et al., 2018), the atmosphere (Zhang et al., 2020), and other environmental matrices (Geilfus et al., 2019; Kanhai et al., 2019). Not surprisingly, evidence of MPs in living organisms is now being discovered. MPs can accumulate and transfer

within plankton, fish, and birds through the food chain (de Sa et al., 2018). What is more shocking is that MPs have been found in the human colon (Ibrahim et al., 2021), and even in the human placenta (Ragusa et al., 2021). PPE waste is the source and carrier of pathogens and chemical contaminants. Current evidence suggests that the virus can persist on the media surface for 72 h or longer when the conditions are favorable (Doremalen et al., 2020). The training on the handling, sorting, and processing PPE waste and preventive measures are still limited. This may put the waste management practitioners at a higher risk of infection. Along with weathering processes, discarded PPE can also release various chemical additives such as stabilizers, photosensitizers, and pigments. For example, to improve the glove performance, such as stretch, modulus of elasticity, sensitivity and tactility upon wearing, various additives are added during the manufacturing process (Aalto-Korte et al., 2007; Olson et al., 2019; Reichel, 2012). Along with weathering, these chemical additives can be released into the environment, which not only harms terrestrial and marine animals, but also ultimately affects humans via the food chain (Takdastan et al., 2021; Taylor et al., 2019). As the physicochemical properties of these plastic PPE products change after weathering, the surface is more likely to adsorb various organic compounds and heavy metals as well, leading to the enrichment of pollutants (Sun et al., 2020). In addition, the formation of biofilm is more conducive to microbial colonization. There may be significant differences between the microbial composition of the biofilm on masks and gloves and the microbial community in the surrounding aquatic environment, leading to some changes such as lower cell motility, higher xenobiotic degradation ability, and elevated antibiotic resistance (Sun et al., 2021). From a systematic view, energy and environmental issues related to the production and transportation of PPE products need to be further considered. The massive production of PPE results in a growing demand for raw plastic materials derived from fossil fuels. At the same time, the energy use associated with the transportation, distribution, and retail of PPE products contributes to the increasing emissions of greenhouse gases

(GHGs), volatile organic compounds (VOCs), nitrogen oxides (NO_X), etc. It is even worse when PPE waste is burnt inappropriately, emitting more GHGs as well as toxic compounds such as dioxins, polychlorinated biphenyl (PCBs), and furans. Landfilled PPE can also release MPs and chemical additives via leachate that may contaminate the soil and groundwater.

Although many efforts have been made to alleviate the environmental pressure caused by PPE waste, there is still a lack of effective approaches for managing the PPE production, transportation, retail, usage and treatment from a systematic view (Doustmohammadi and Babazadeh, 2020; Jones, 2020; Vu et al., 2021). Distinct waste disposal characteristics and recycling behaviors were observed during the first wave of COVID-19 (Richter et al., 2021a; b), and more research is needed on the subsequent waves with respect to PPE waste disposal and recycling.

Chapter 3. Exploring the role of nanobubbles in the fate and transport of spilled oil on shorelines[3]

3.1 Background

NBs are nanoscopic gaseous bodies that are attached to the surface of the medium and/or surrounded by solutions (Alheshibri et al., 2016; Sun et al., 2022). Although the theory regarding the generation and growth of bubbles has been proposed since 1950, the definitions for the size boundaries of the different bubble categories have not yet been standardized (Alheshibri et al., 2016; Sun et al., 2022). Based on bubble size and shared physicochemical properties, bubbles less than 1000 nm in diameter are considered as NBs or ultra-fine bubbles, and those larger than 10 μm are considered as microbubbles (Temesgen et al., 2017). The traditional Young–Laplace equation states that the pressure difference between inside and outside the bubble is inversely proportional to the bubble's radius. This suggests that the smaller the particle size, the higher the pressure on the bubble, and thus the more likely it is to break and dissolve (Epstein and Plesset, 1950). However, the observation of NBs breaks the inherent perception that bubbles with a particle size less than 1000 nm have a lifetime no longer than 0.02 s (Alheshibri et al., 2016). It has been reported that due to the presence of natural surfactants in seawater, air bubbles with a size less than 1 μm generated by wave breaking and shearing can exist stably for about 22 h (Johnson and Cooke, 1981). Experimental and theoretical results also prove that microbubbles could remain stable in electrolyte solutions (Bunkin et al., 1996). Although the existence and stability of NBs are still not fully understood, an increasing

[3] This work has been published as Wang, Z; An, C; Lee, K; Feng, Q; Zhang, B. 2023. Exploring the role of nanobubbles in the fate and transport of spilled oil on shorelines. ACS EST Water, 3 (1), 30-40.

amount of research has focused on the generation and application of NBs due to their extraordinary characteristics.

The principal mode of the generation and growth of NBs is cavitation, based on which can be divided into hydrodynamic, acoustic, and electrical methods (Agarwal et al., 2011). Among them, hydrodynamic methods are the one of most widely used, including venturi, spiral-liquid-flow, pressurized dissolution, multi fluid mixture, periodic pressure change, and porous (Parmar and Majumder, 2013; Ulatowski and Sobieszuk, 2020). Compared to large bubbles, NBs display some unique properties. Because the specific surface area is inversely proportional to the radius of the sphere, NBs have a large specific surface area, leading to the ability to remarkably adhere to other compounds on the surface (Yoshida et al., 2008). A high mass transfer efficiency is expected in NBs by a faster dissolved air increasing rate and higher dissolved oxygen peak value (Bai et al., 2021; Chu et al., 2007; Kawahara et al., 2009). Previous studies have shown that hydroxyl radicals are generated when bubbles collapse, which can enhance the oxidative capacity (Li et al., 2009; Takahashi et al., 2021). In addition, the negative ζ potential, rising velocity, high inertial pressure, and large gas–liquid interfacial area are also drivers of interest for NBs. Thus, NBs are currently employed in flotation (Fan et al., 2010a; b), surface cleaning (Jin et al., 2022; Li et al., 2022), irrigation (Liu et al., 2015; Liu et al., 2019b), water treatment (Fan et al., 2021; Hu and Xia, 2018), soil remediation (Kim and Han, 2020; Zhang et al., 2019a), drug delivery (Batchelor et al., 2020; Wang et al., 2010), oil recovery (Bera et al., 2013), and other fields.

Nevertheless, few studies have focused on the role of NBs in the natural environment. In addition to the substantial stable NBs found in the marine environment, turbulence caused by rapids and waterfalls can also generate NBs within freshwater rich in organic matters (Alheshibri et al., 2016).

This likely indicates that NBs play a role in the environment beyond what has been predicted. It is reported microbubble could affect the surface fluxes of carbon dioxide, methane and other sparingly soluble gases (McGinnis et al., 2015). Surface oxygen NBs could be beneficial for anoxia/hypoxia remediation and methane emission control (Shi et al., 2018). The shoreline, as the intersection of ocean and land, is one of the most concentrated areas of wave energy (Ahn et al., 2019). Bubbles produced by breaking waves are also found in offshore areas (Thorpe et al., 1982). More importantly, the shoreline is not only a sink for pollutants but also play host to further transport and transformation of pollutants (Feng et al., 2022; Wang et al., 2021c; Wang et al., 2022b). As a traditional pollutant in the ocean, oil spills seriously harm local ecosystems once stranded in the shoreline environment (Chen et al., 2019; Wang et al., 2020c). There have been many studies investigating the fate and transport of oil stranded on shorelines, but almost all have paid attention to only light irradiation, temperature, salinity, shoreline substrate, microbial degradation, and other conventional factors (Abou-Khalil et al., 2022; Aeppli et al., 2022; Cao et al., 2022; Cao et al., 2020; Ji et al., 2021). NBs affect not only the physical transport of pollutants, but also their chemical weathering, biodegradation, and adsorption with other environmental pollutants. While no studies have thus far focused on the potential effects of NBs on spilled oil in the shoreline environment. The complexity of oil behaviors can be exacerbated by various shoreline environmental conditions (Feng et al., 2021b; Yang et al., 2022a). In addition, as an environmentally friendly substance, nano bubbles also have potential applications in oil spill responses. Therefore, it is necessary to explore the environmental effect of NBs on stranded oil on the shoreline. In this context, the objective of the study described in this study was to characterize the properties of NBs and to determine the influencing factors in a shoreline environment. On this basis, the environmental behavior of bubbles and their role in the fate and transport of spilled oil were further investigated.

3.2 Methods

3.2.1 Materials and chemicals

Deionized water (Milli Q, Merck, German) was used as the solvent to generate NBs water. Sodium chloride (NaCl) was purchased form Sigma Aldrich (Ontario, Canada) to prepare the saline water. Tween 20, as the surrogate of natural surface active materials in the ocean, was obtained from VWR (Canada). Hibernia oil, as the light crude oil, was obtained from the Hibernia oil field southeast of St. John's, Newfoundland, Canada (Table 3.1). The Hibernia oil was pre-weathered in a fume hood at 20 ℃ for 7 days and stored in amber sealed glass bottles. Standard washed and high-temperature ignited sand (30–40 mesh) was purchased from Millipore (Ontario, Canada). The sand was rinsed with DI water five times to further eliminate impurities and then dried at 105 ℃ in an oven. n-Hexane (analytical grade) was obtained from Fisher Scientific (Ontario, Canada). Glass beads with a particle diameter of 1 mm were purchased from VWR (Canada).

Table 3.1 Physical properties of Hibernia oil

Name	**Type**	**Density (g/cm^3)**	**American petroleum institute (API) gravity (°)**	**Fresh viscosity (cP)**	**Weathered viscosity (cP)**
Hibernia	Light	0.87	34.1	15.66	25.50

3.2.2 Experimental design

DI water of 1 L and air were introduced into a NBs generator (OM4–MDG–O4S, Aura Tec, Japan) at room temperature of 20 ℃ and a pressure of 0.26 ± 0.01 Mpa for 30 min generation and

subsequently placed in Erlenmeyer flasks and kept sealed for further analysis. To investigate the effects of salinity and natural active materials on the properties of NBs, different concentrations of NaCl solutions (10 mM, 100 mM, 1 wt%, and 3.5 wt%) and Tween 20 solutions (100, 200, 300, and 400 μg/L) were prepared for bubble generation. Preparation of oiled sands (1 g-oil/kg-sand) using standard washed sand and weathered Hibernia oil for the batch experiments were used to investigate the effect of bulk NBs on stranded oil on the shoreline. The pre-weathered Hibernia oil was dissolved in hexane and subsequently mixed thoroughly with sand and placed in a fume hood at 20 ℃ for 48 h to allow the solvent to evaporate completely. The prepared oiled sands were transferred into an amber glass bottle and stored in the refrigerator. 1 g of oiled sand and 15 mL of NBs suspension or non- NBs solution were added to a 20 mL vial, sealed and placed in an incubator shaker (New Brunswick Innova 42R, Eppendorf, Germany) at 150 rpm at 20 ℃ for 6 h. To analyze the effects of coastal energy on oil detachment, the same samples were left resting for 6 h as the control samples. The liquid was then carefully removed from the vial with pipettes, and all vials were placed in a fume hood at 20 ℃ for 48 h for natural drying. The oil left on the sand was extracted by adding 15 mL of n-hexane and shaking in an incubator shaker at 300 rpm for 24 h. All batch experiments were conducted in quintuplicate at least, and the average values were reported. The impact of surface NBs on the penetration and retention of oil in shoreline substrates was determined by the column test. A glass column with a length of 15 cm and an inner diameter of 2 cm was used for this task. A total height of 10 cm of sand was dry-packed into the glass column to imitate the beach substrates, and 2 cm high of glass beads was added at the top of the sand for balance. The bottom of the glass column was sealed by a stainless steel woven wire in 120 mesh to support the substrates inside. The NBs solution was introduced to the glass column from the top through a peristaltic pump (Masterflex L/S, Cole–Parmer, USA) with a flow rate of 10 mL/min for 20 min to pre-equilibrate the system. The oil colloidal (1 g-oil/L-water) was homogenized through a high-speed dispenser (T 25 digital Ultra–

Turrax, IKA, UAS) and then was pumped into the glass column at a flow rate of 10 mL/min. The effluents were collected from the bottom of the column every 1 min for a total of 20 min. 2 mL of effluent was added to a glass vial and extracted by adding 15 mL of n-hexane and shaking in an incubator shaker at 300 rpm for 24 h.

3.2.3 Analytical methods

The dissolved oxygen (DO) of the NBs suspension was measured by an optical DO probe (Orion RDO, Thermo Scientific, USA) to indirectly characterize the concentration of NBs. The concentration range of the probe is 0–20.00 mg/L, and the accuracy is ± 0.1 mg/L. The pH value was obtained by a pH meter (AR15, Fisher Scientific, USA). The surface tension (SFT) was detected by a bubble pressure tensiometer (BP100, Kruss, German). The size distribution of NBs in solutions and the ζ potential were measured using a particle size analyzer (Zetasizer Nano ZS90, Malvern Panalytical, the UK). All parameters were measured once a day for 7 days. The oil concentration in n-hexane was measured by an ultraviolet-visible (UV–vis) spectrophotometer (Evolution 201, Thermo Scientific, USA). The variation of chemical components in the oil was identified by a gas chromatography mass spectrometry system (GC–MS; 7890/5977, Agilent Technologies, USA) with an HP–5MS capillary column. 2 mL of the hexane-extracted sample was filtered through a 0.2 μm PTFE membrane and stored in a standard autosampler vial for further analysis. The oven temperature was retained for 2 min at 50 °C and then ramped at 10 °C/min to 200 °C, retained 5 min, then ramped at 15 °C/min to 300 °C and held for 10 min. The helium carrier gas flow was 1mL/min, and the injection temperature and volume were 250 °C and 2 μL, respectively (Agyei-Tuffour et al., 2020; Juahir et al., 2017).

3.2.4 Model Simulation

HYDRUS-2D is a modelling system for analyzing water flow and solute transport in a porous medium with varying saturations. The Richards' equation for saturated–unsaturated water flow and the Fickian-based advection–dispersion equation for solute transport are both numerically solved by the program. Linear equilibrium adsorption, zero-order production, and first-order degradation are all included in the transport equation. A Galerkin type linear finite element scheme is used to solve the governing flow and transport equations (Li et al., 2021; Pang et al., 2000). The coefficient of determination (R^2) was used as a fitting criterion. The equilibrium sorption of solutes can be represented by the following equation (Feizi et al., 2021).

$$S = \frac{K_d C^{\beta}}{1 + \eta C^{\beta}} \quad 3.1$$

where K_d (cm^3/g) is the partition coefficient and β and η are empirical coefficients. The HYDRUS-2D inverse solution function was previously applied to evaluate the migration of oil water in the sand columns based on experimental data (Li et al., 2021; Mekala and Nambi, 2016).

3.3 Results and discussion

3.3.1 Physicochemical properties of NBs suspension

The physicochemical properties of a solution can be changed by NBs (Bui et al., 2019; Liu et al., 2013). The DO, pH, SFT, and ζ potential of the NBs suspension and the control sample (DI water) are shown in Figure 3.1 (a-b). After NBs generation, the concentration of DO was 11.76 mg/L, which was higher than DI water. This indicates that indeed, a large number of NBs were present in the solution. After one day, the DO concentration of NBs suspension decayed to 8.6 mg/L, which was basically consistent with the DO concentration of DI water. The DO concentration of the NBs suspension then remained stable over the next six days. For control DI water, the DO concentration

fluctuated between 8.5 and 8.8 mg/L. The initial pH value of the NBs suspension was slightly lower than that of DI water. Presumably, this was due to the large number of air NBs dissolving in the solution, resulting in an increase in the concentration of carbon dioxide in the system as well, which in turn increased the concentration of carbonic acid and ultimately altered the pH value. Although the absolute value of SFT varied less, the relative change in the SFT of the NBs suspension was also more significant compared to DI water. The SFT for DI water was roughly 72.4 mN/m, while the SFT of the fresh NBs suspension was 71.34 mN/m. As with DO, the SFT stabilized over time. The conventional view is that there is no physical sense of the existence of the ζ potential of pure water because water theoretically does not contain any substances, however, an increasing number of measurements shows that ζ potential can be measured in pure water with values ranging from a few to several tens mV. Researchers are attempting to explore the reasons that this phenomenon occurs. Some suggestions are being proposed, such as the possible presence of impurities or air bubbles in the sample, which are not fully resolved (Buch et al., 2007; Jungwirth, 2009; Maduar et al., 2015). Possible reasons for the measurement of ζ potential for DI water in this study can be attributed to unavoidable air bubbles or dissolved gases in the samples. The ζ potential of the fresh NBs suspension was -16.8 mV. After 4 days, the absolute value of ζ potential increased and reached -33.4 mV at 7 days. This means that the NBs solution was not stable until after 4 days. The size distribution of NBs in the solution is shown in Figure 3.1 (c-d). The dominant size of the fresh NBs ranged from 70 to 100 nm, which accounted for 99.5% of the total number. Only 0.5% of the bubbles were around 300 nm in size. After 7 days, the size of all NBs was distributed in the range of 140 to 250 nm. This implies that the bubbles with a small size gradually aggregated to shape larger bubbles. At the same time, some of the large bubbles further aggregated until busting. There was no signal for DI water in terms of the size distribution.

The size and concentration of bubbles are the decisive factors affecting the properties of NBs suspension. Recent studies have shown that the smaller the particle size of air bubbles, the larger their specific surface and the more likely they are to be stable in the solution, thus maintaining the a constant concentration (Hu and Xia, 2018). A small size and high concentration ensure efficient mass transfer efficiency. The bubble size was small, and the concentration was high in terms of fresh NBs solutions, which means that a large amount of gas was dissolved in the water, resulting in a high DO concentration. However, the ζ potential indicated that this property was not stable over time. After 1 day, the sharp drop in the DO concentration indicated a decrease in NBs concentration accompanied by an increase in the SFT and pH value. Nevertheless, the size distribution of NBs remained, although some large bubbles were reduced. Accordingly, it is believed that the NBs solution can keep its properties stable for at least one day.

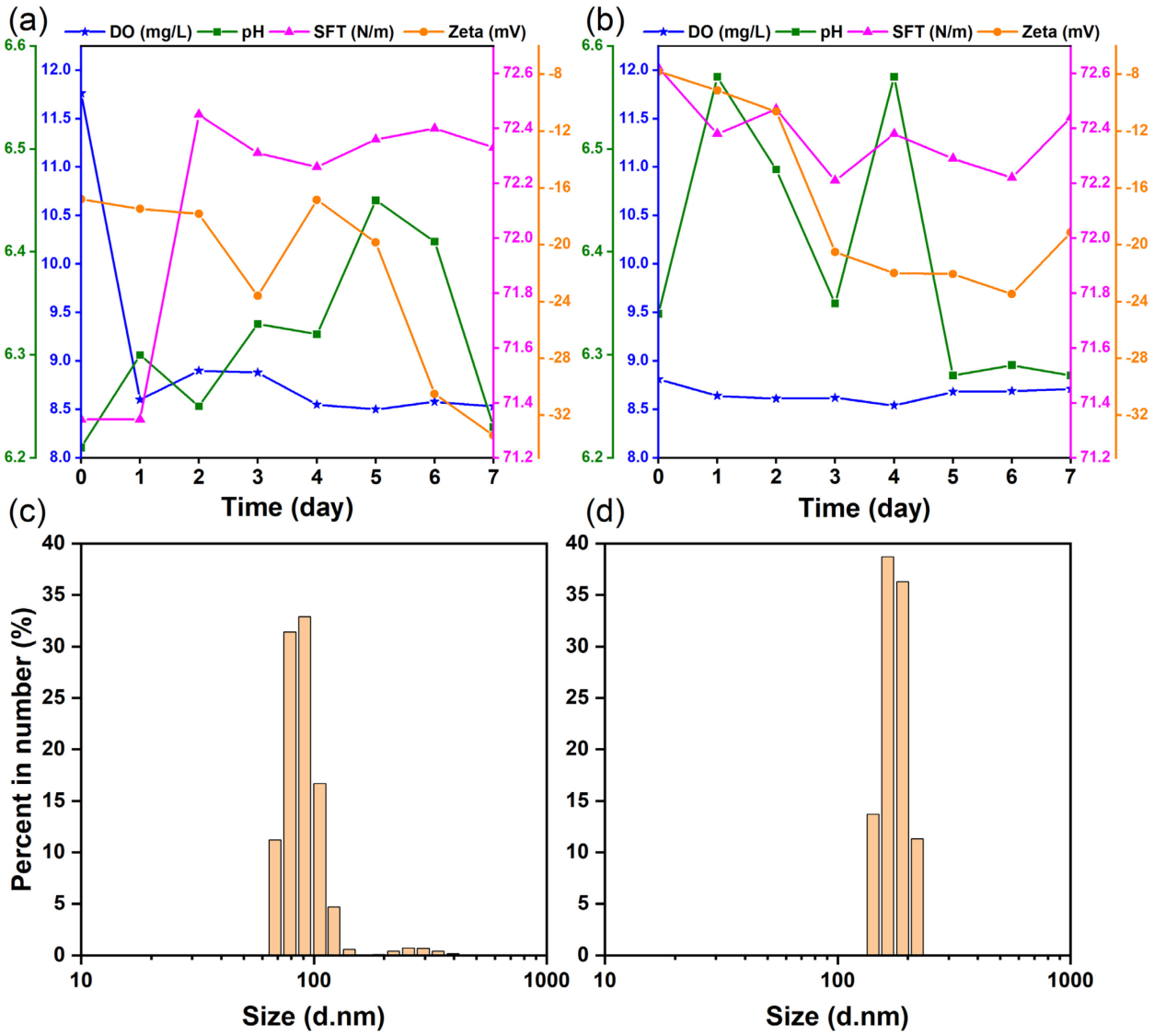


Figure 3.1 (a) Changes in the physicochemical properties of NBs over time. (b) Changes in the physicochemical properties of control sample (DI water) over time. (c) Size distribution of fresh NBs suspensions. (d) Size distribution of NBs suspensions at day 7.

3.3.2 Factors influencing the properties of NBs solution

The stability of NBs and the properties of the NBs solution are influenced by a number of factors. Excluding differences in generation methods, the salinity, pH, type of dissolved gases and additives in water should be considered. Given the uniqueness of the shoreline environment (Wang et al.,

2022b), the effects of salinity and natural surface active materials on the NBs suspension were taken into account. Figure 3.2 shows that the DO concentration in the NBs solution was influenced by the salinity and the concentration of Tween 20. The initial DO concentrations of the control NBs suspensions, and NB suspensions with salinities of 10 mM, 1 wt% and 3.5 wt%, respectively, were lower than 12 mg/L, while the concentrations were higher than 12 mg/L at a salinity of 100 mM. After one day, the DO concentration of all solutions decreased to less than 9.5 mg/L and was equal to DI water after the second day. In addition, the high salinity led to a lower pH of the initial NBs suspension. When the salinity exceeded 100 mM, the initial pH was less than 6, and the pH remained stable over time. The effect of salinity on SFT was insignificant except that when the salinity was 3.5 wt%; the SFT of the NBs suspension was around 72.5 N/m. The ζ potential was also influenced by salinity. During the experiment, the absolute values of the ζ potential were almost all less than 10 mV, indicating that salinity made the NBs suspension unstable. The effect of surface active materials on the DO concentration of the NBs solution was similar to that of salinity. The initial DO concentration was higher than DI water and the DO concentration decreased to the same level as DI water after one day. The initial pH values of the NBs suspension were less than 5.0 when Tween 20 was present, and these values changed little within 7 days. Although Tween 20 is generally a substance that regulates SFT, concentration is also an important factor. To match the actual seawater conditions, the concentrations of Tween 20 applied in this study were very low, so the SFT change influenced by Tween 20 was insignificant, as shown in Figure 3.2. Unlike the effect of salinity on ζ potential, when the concentration of Tween 20 was less than 200 μg/L, the values of the initial ζ potential were close to -30 mV and decreased in absolute value over time. If the concentration was greater than 300 μg/L, the ζ potential was greater than -15 mV. In particular, at a concentration of 400 μg/L, the initial ζ value was -5.22 mV. However, the ζ potential tended to fluctuate between -10 and -25 mV at different Tween 20 concentrations in more than 3 days. The size distribution of

NBs under different conditions is shown in Figure 3.3. For the fresh NBs solution with 10 mM, 100 mM, 1 wt%, and 3.5 wt% salinity, the bubbles with a size less than 100 nm accounted for 96.2%, 87.7%, 70.2%, and 83.0% of the total, respectively. Compared to fresh NBs in the absence of NaCl, the number of bubbles larger than 100 nm in size increased under salinity conditions. It was also clearly observed that the size of the NBs became larger after 7 days with different salinities. In addition, the size peaks of NBs were 224.7, 290.1, 332.8, and 479.9 nm under different salinities, which indicated that the average size of the NBs grew with increasing salinity after 7 days. The effect of surface materials on NBs size differed from that of salinity. The bubbles less than 100 nm in terms of the NBs solutions with Tween 20 at concentrations of 100, 200, 300, and 400 μg/L accounted for 75.7%, 78.5%, 61%, and 15% of the total, respectively. This showed that the proportion of bubbles less than 100 nm was not only smaller than that of the pure NBs solution, but also lower than that of the NBs solution with different salinities. Regardless, the bubbles were almost all between 70 and 600 nm, with a percentage of 99.9%, 100%, 99.4%, and 98.9%, respectively, for Tween 20 concentrations at 100, 200, 300, and 400 μg/L. In addition, the bubble size for the NBs solution with Tween 20 was notably smaller than that containing NaCl after 7 days. The results showed that 99.6%, 99.0%, 99.6%, and 98.1% of the total number of NBs had a size less than 100 nm, respectively.

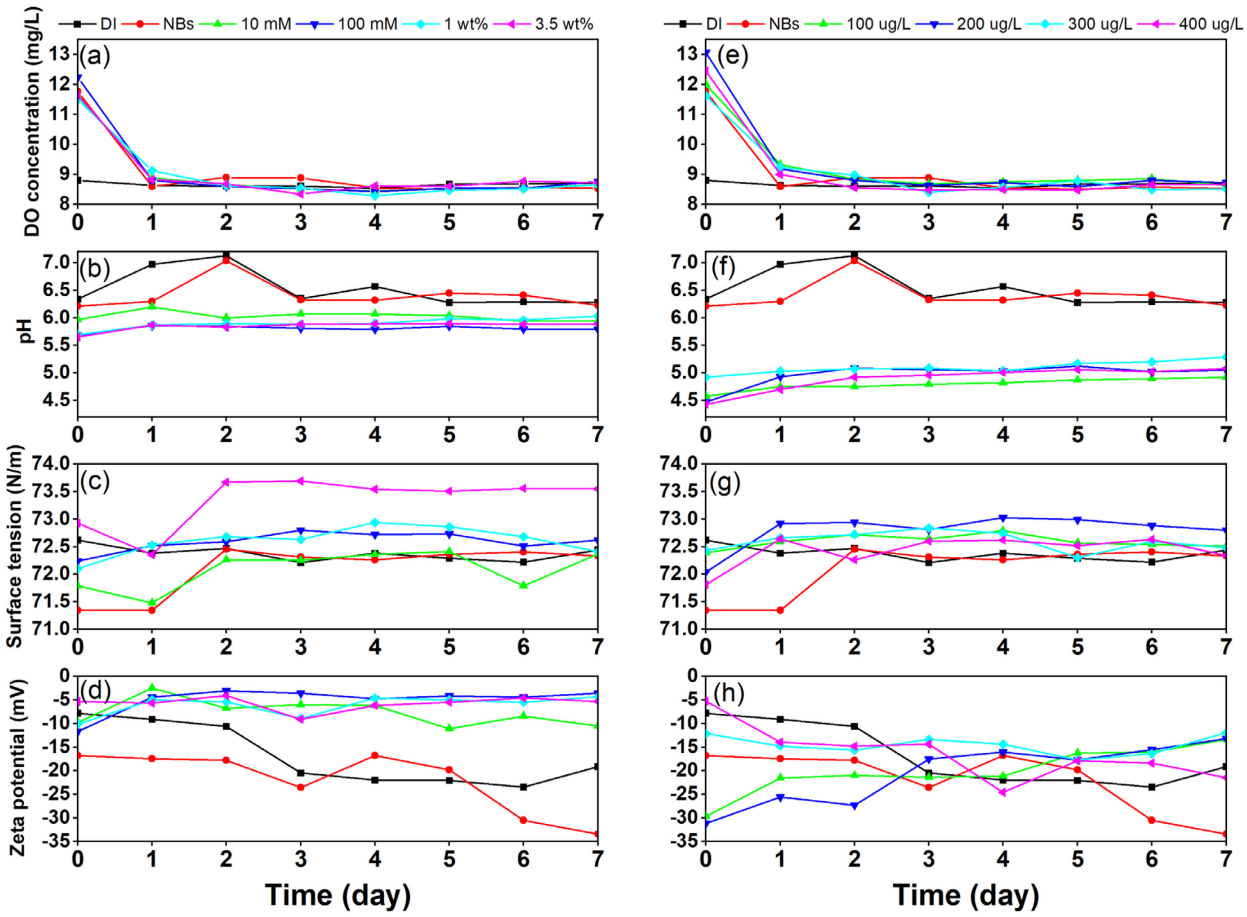


Figure 3.2 (a–d) Effect of salinity on the properties of the NBs suspension. (e–f) Effect of Tween 20 on the properties of the NBs suspension. DI represents DI water. NBs represent NBs suspension. 10 mM, 100 mM, 1 wt% and 3.5 wt% represent NBs suspension at a salinity of 10 mM, 100 mM, 1 wt% and 3.5 wt%, respectively. 100 ug/L, 200 ug/L, 300 ug/L and 400 ug/L represent NBs suspension at a Tween 20 concentration of 100, 200, 300 and 400 ug/L, respectively.

Generally, changes in DO, a key parameter reflecting NBs concentration, indicate that a low concentration of salinity is able to promote bubble production, while a high concentration inhibits the process. Previous studies have shown that micro and NBs remain for more than one week at low salinity due to the ion shielding effect, and the repulsive force between bubbles decreases at a high salinity, which in turn leads to a rapid disappearance of NBs (Uchida et al., 2016; Zhou et al., 2021).

At the same time, the reduced repulsive electrostatic forces drive the ζ potential to change from a negative value to zero, further causing the system to become unstable (Nirmalkar et al., 2018b). The size distribution of the bubbles is another parameter that reflects stability. The effect of salinity on the size of fresh generated NBs was low, but the size increased gradually with time. The higher the salinity, the larger the increase in size. This implies that the suspension became increasingly unstable with prolonged time and a higher salinity. Compared to NaCl, Tween 20 acted as a surfactant that promoted NBs generation and maintained the stability of the system, which is in line with the previous conclusions (Nguyen Hai Le et al., 2021; Nirmalkar et al., 2018a). It is generally believed that reducing SFT can promote NBs generation and maintain stability over time (Qiu et al., 2017; Sun et al., 2022). Although the variation of Tween 20 on surface tension was not considered in this experiment, it can be speculated from the size distribution and ζ potential that such surface active material did contribute to stabilizing the NBs. In addition, the effect of pH was in line with previous studies showing that average size increases with a decreasing pH value (Ke et al., 2019).

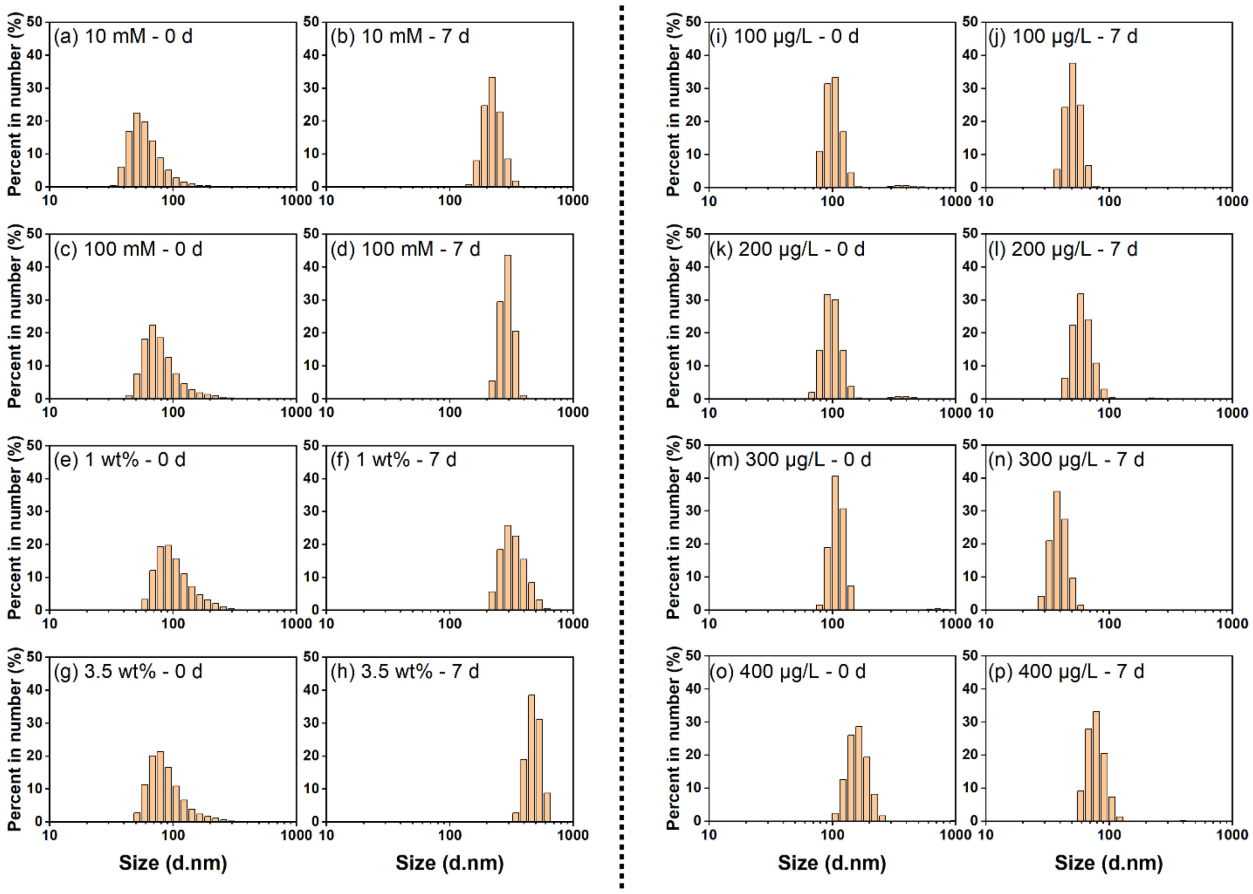


Figure 3.3 Size distribution of NBs under different conditions. (a–h) Effect of different salinities. (i–p) Effect of different concentration of Tween 20.

3.3.3 Detachment of stranded oil from sand surface in the presence of bulk NBs

After an oil spill occurs, the oil moves toward the near shore areas with waves. It is important to understand the behavior of stranded oil on shoreline substrate. Given the widespread presence of NBs in seawater, the role of NBs in oil transport was evaluated. Figure 3.4(a) and (b) present the oil detachment rate in the presence of NBs with and without the assistance of external energy, respectively. Under shaking conditions, the oil detachment rate of the NBs suspension produced by DI water was 9.7%, slightly higher than the 8.8% detachment rate of DI water without NBs. When Tween 20 was present and under shaking conditions, the oil detachment rate of the NBs suspension

increased to 25.7%, while without the NBs, the detachment rate was 21.3%. Compared to the detachment rate of DI water in the presence of NBs, the detachment rate of the NBs suspension containing Tween 20 increased by 1.6 times. Even without NBs, the detachment rate increased by 1.4 times. This indicates that Tween 20, as a nonionic surfactant, does have a significant improvement in oil detachment. Meanwhile, the presence of NBs further promoted detachment rate. When only NaCl was included, the oil detachment rate decreased significantly compared to that with Tween 20. The detachment rate was 15.3% washed by salt-only solutions with NBs, while the detachment rate was only 7.8% in the absence of NBs, which was comparable to the detachment rate of DI water. When both Tween 20 and NaCl were present, the oil detachment rate of the NBs suspension was 45.2% compared to 19.1% for the solution without NBs. Thus, for non-NBs solutions, regarding the presence of both Tween 20 and NaCl, it was Tween 20 that played a dominant role in oil detachment, while the presence of NaCl even slightly inhibited this process. Nevertheless, the NBs suspension performed differently in the detachment of stranded oil. Although the detachment rate of the NBs suspension with only NaCl was lower than that of the Tween 20-only NBs suspension, it was obviously higher than that of DI water. The NBs suspension with both present also had the highest detachment rate, indicating that it was the synergistic effect of the two that promoted oil detachment.

Oil detachment rate in the absence of external energy was also considered, and the results are shown in Figure 3.4(b). The detachment rates of DI water were 7.2% and 8.0% in the absence and presence of NBs, respectively. This was comparable to the detachment rate under shaking conditions and was slightly higher when NBs were present. For the Tween 20-only solution, the oil detachment rate was 18.2% without NBs and 22.1% with NBs. Obviously, although the detachment rate increased compared to DI water under the resting condition, the detachment rate reduced compared to the

shaking condition. For the salt-only solution, the detachment rates were 6.4% and 8.9% with and without NBs, respectively. The detachment rate of the salt-only solution was always less than that of the Tween 20-only solution, regardless of the shaking condition or the resting condition. Even the detachment rate of the salt-only solution was lower than that of DI water under the resting condition. The detachment rate was smaller than the shaking condition for the solution containing both NaCl and Tween 20 under the resting condition. The detachment rates were 10.1% and 11.5% for the suspensions without and with NBs, respectively, a reduction of 47% and 75% compared to the shaking condition. It is worth noting that the detachment rate of the solution with both Tween 20 and NaCl was not only lower than the case of Tween 20 only, but also almost close to the case of the salt-only condition.

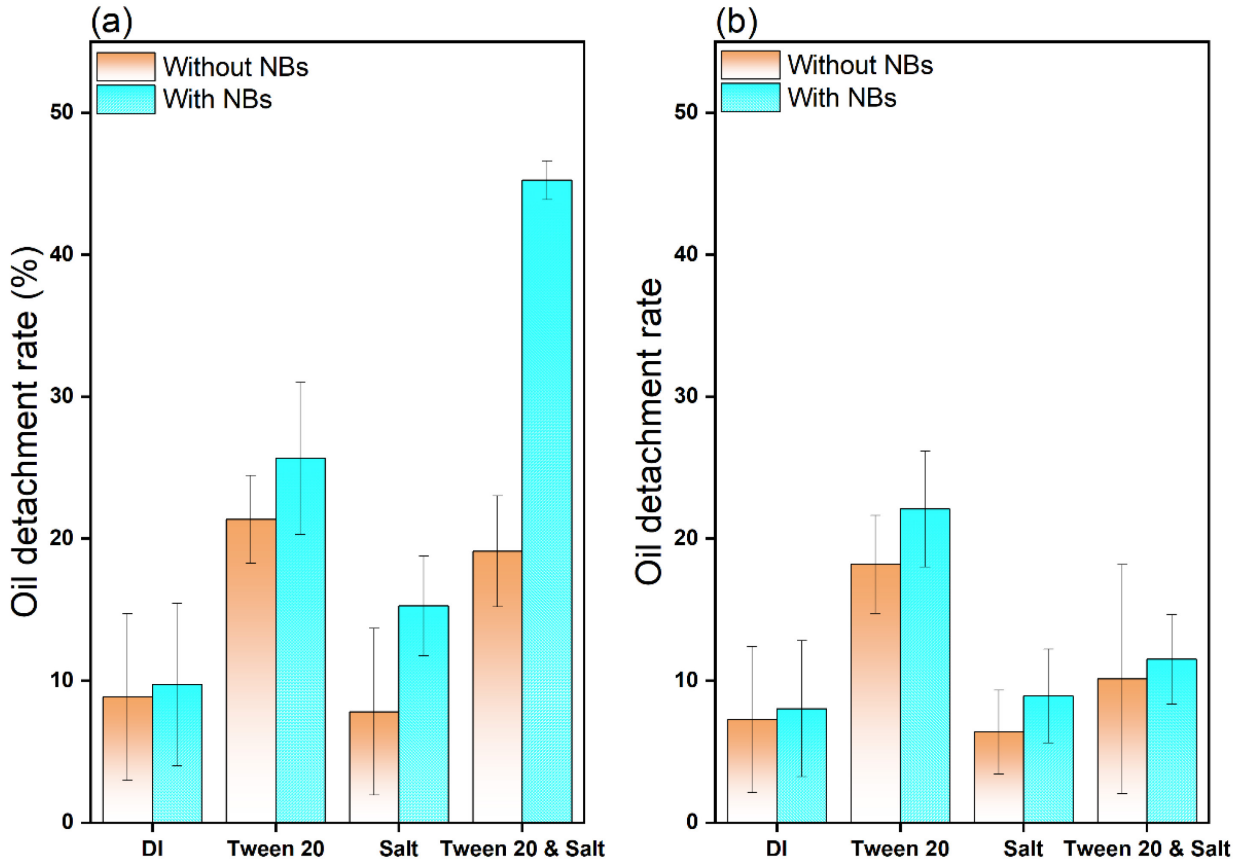


Figure 3.4 Oil detachment rate in the presence of NBs suspension under different conditions. (a) Shaking condition. (b) Resting condition.

The change in the n-alkanes of the stranded oil impacted by NBs was further characterized. It can be found in Table 3.2 that n-alkanes from C12 to C20 were detected from the blank samples. Whether under shaking or resting conditions, all n-alkanes were still detectable on the sand after washing with DI water without NBs, indicating no significant changes in the chemical components. For oily sand washed by DI water containing NBs under the shaking condition, some components (C12, C13, C15) were not observed, implying a high probability of decomposition during the cleaning process. In terms of the resting condition, only C13 was not found after the washing by DI water containing NBs. For the Tween 20-only solution, C12, C13, and C15 were observed in the

case of containing NBs, while C12 can be measured in the absence of NBs. Regarding salt-only solutions and solutions with both Tween 20 and salt, there was no uniform change in the chemical components. The results showed that DI water was inefficient for oil detachment, independent of the NBs. Tween 20 had a good capacity for oil detachment, especially under the shaking condition. In addition, the presence of NBs further facilitated this ability. Previous studies have shown that vibration can also produce NBs (Fang et al., 2020). Therefore, it is believed that in the presence of Tween 20, shaking also produced some NBs during the experiment. The presence of NaCl, however, had less of an effect on the improvement in oil detachment and even hindered the detachment under the resting conditions. It is speculated that under a high salinity, the sodium ions in the water and some of the unsaturated acids in the oil combined to form a structure that blocked further contact between the oil droplets and the solution. While when NBs were present, the NBs first bound to these positively charged sodium ions, and the energy provided by shaking caused the oil to detach from the surface of the sand. When both Tween 20 and salt were present, there was a synergistic effect between the two in the presence of NBs and the shaking condition, which greatly enhanced oil detachment rate. Previous studies have also reported that salt and surfactants in synergy can promote oil recovery (Bera et al., 2013).

Table 3.2 n-alkanes of the stranded oil under different conditions

	Control	DI-Sh	DI-B-Sh	DI-Re	NBs-Re	S-Sh	S-NBs-Sh	S-Re	S-NBs-Re	T-Sh	T-NBs-Sh	T-Re	T-NBs-Re	ST-Sh	ST-NBs-Sh	ST-Re	ST-NBs-Re
Dodecane	+	+		+	+	+				+		+					
Tridecane	+	+		+													
Tetradecane	+	+	+	+	+	+	+	+	+	+	+	+	+	+	+	+	+
Pentadecane	+	+		+	+				+					+	+	+	+
Hexadecane	+	+	+	+	+	+	+	+	+	+	+	+	+	+	+	+	+
Heptadecane	+	+	+	+	+	+	+	+	+	+	+	+	+	+	+	+	+
Octadecane	+	+	+	+	+	+	+	+	+	+	+	+	+	+	+	+	+
Nonadecane	+	+	+	+	+	+	+	+	+	+	+	+	+	+	+	+	+
Eicosane	+	+	+	+	+	+	+	+	+	+	+	+	+	+	+	+	+
Heneicosane	+	+	+	+	+	+	+	+	+	+	+	+	+	+	+	+	+
Docosane	+	+	+	+	+	+	+	+	+	+	+	+	+	+	+	+	+

DI means DI water, S means salt-only solution, T means Tween 20-only solution, ST means solution with salt and Tween 20 both, NBs means the solution contains nanobubbles, Sh means shaking condition, Re means resting condition, + means detected.

3.3.4 Effect of surface NBs on oil transport in shoreline substrates

Column experiments were conducted to evaluate the transport of oil colloids in the sand that contained different solutes. When the column was pre-equilibrated with a solution containing NBs, some NBs inevitably adhered to the surface of the sand particle, thus switching from bulk NBs to surface NBs. On the one hand, the surface NBs modified the surface of the sand, changing certain properties, such as wettability, which in turn affected the interaction with the oil droplets. On the other hand, the NBs filled within the column also changed the hydraulic conditions such as the porosity of the substrate, further altering the transport of oil colloids. The breakthrough curves (BTCs) and simulation fitting of the oil colloids are shown in Figure 5. The BTCs refer the concentration of the outflow component as a function of time when a multicomponent fluid flows through a fixed bed penetration column. The horizontal coordinate of the graph is usually time (t),

and the vertical coordinate is the effluent concentration (C) at time t. In general, when the effluent reaches a certain concentration, the corresponding time of the curve is called the breakthrough time. Breakthrough time was defined as the time corresponding to an effluent concentration of 10% of the original concentration in this study. The results indicated that the oil concentration was lower than the detect limit within 1 min and there was a significant outflow concentration at 2 min. Although the breakthrough times were within 1-2 min, the simulation results show that the breakthrough times in the presence of NBs were later than those without NBs. The fitted partition coefficient of the oil colloids in the column are shown in Table 3.3. It is shown that when pre-equilibrated with DI water, the partition of oil colloids in sand was faster in the presence of NBs. This implies that the longitudinal movement of the oil colloids was restricted, which in turn reduced the effluent concentration. This phenomenon is illustrated in Figure 3.5(e) and (f). Within 2 min, in the absence of NBs, the free oil colloid concentration was higher than that with NBs and was essentially equilibrated at 5 min. For the condition with NBs, the equilibrium was still not complete within 20 min. When pre-equilibrated by the Tween 20-only solution, the BTCs are shown in Figure 3.5(b). Similar to the case where there was only DI water, the partition coefficient of the oil colloids was greater when NBs were present than the condition without NBs. However, when Tween 20 was present, not only was the effluent concentration reduced but the time for the effluent concentration to reach stabilization was greatly delayed, especially for the condition with NBs. Figure 5(g) and (h) visually demonstrate that the concentration of free oil colloids within the system was low when NBs were present, indicating that some of the oil had been adsorbed by the sand with the assistance of Tween 20 and NBs. The situation was quite different when pre-equilibrated with the salt-only solution. Figure 3.5(c) shows that that the trend of the BTCs was similar for the case when pre-equilibrated by the salt-only solution. This was also confirmed by the transport of oil colloids within the column, as shown in Figure 3.5(h) and (i). After 10 min, the effluent concentration was almost

constant, and the maximum effluent concentration was also higher than the case of pre-equilibration with DI water. It is proposed that, on the one hand, when pre-equilibrated by the salt-only solution, part of the ions was adsorbed on the sand surface, blocking the direct contact of the oil with the rough surface of the sand. On the other hand, when the salinity of the solution was high, some of the free ions were combined to the oil droplets, thereby improving their fluidity. This concept is validated by the addition of salt to promote oil recovery efficiency during oil exploration (Song et al., 2020; Walter et al., 2019). When pre-equilibrated by the solution containing Tween 20 and NaCl, the BTCs of the oil colloid is shown in Figure 3.5(d). When NBs were present, the relative concentration was always lower than in the absence of NBs, and the maximum relative concentration was also smaller. Comparing the cases of being pre-equilibrated by Tween 20-only and salt-only solutions, Tween 20 inhibited the transport of oil, but salt facilitated this process, and this effect was neutralized when both were present.

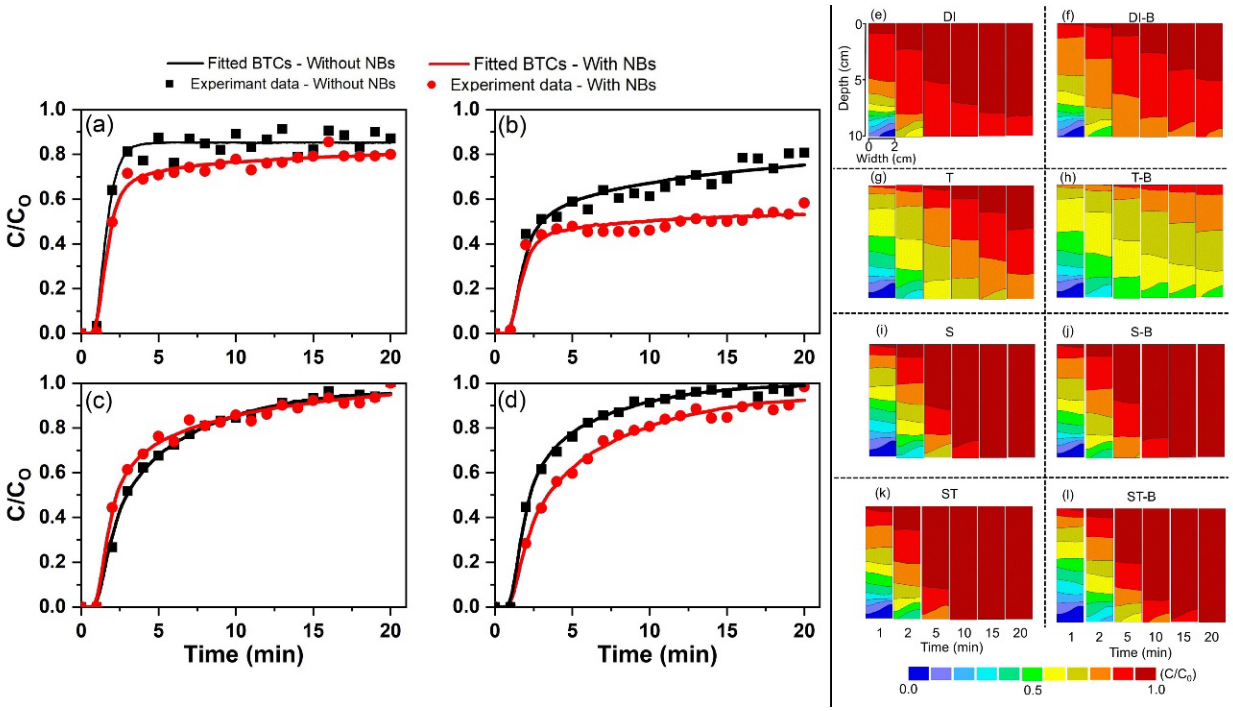


Figure 3.5 (a–d) Experimental and simulative BTCs of oil colloids under different conditions. (a) DI solution, represented by DI. (b) Tween 20-only solution, represented by T. (c) Salt-only solution, represented by S. (d) Solution with both Tween 20 and salt, represented by ST. (e–j) Inverse simulation of the transport of oil colloids in the column. B means with NBs.

Table 3.3 Fitted partition coefficient and regression coefficient of predicted vs observed data.

	DI	**NBs**	**S**	**S-NBs**	**T**	**T-NBs**	**ST**	**ST-NBs**
K_d (cm^3/g)	4.883	8.289	0.551	0.636	3.581	194.6	0.374	0.672
R^2	0.96	0.98	0.99	0.97	0.87	0.93	0.97	0.98

3.3.5 Environmental implications

The shoreline is the intersection of the ocean and the continent and is one of the most complex and frequent regions of material and energy transformation (Chen et al., 2019). Under the action of waves, a large number of stable bulk NBs exist in the seawater near the coast, and these NBs further diffuse into the substrate or even into the sediment and become surface NBs. The presence of NBs in the shoreline environment not only alters the physicochemical properties of the surrounding micro-environment, but also influences the transport of contaminants. Meanwhile, the changed micro-environment further determines the fate of the pollutants. When considering the behavior of contaminants in the shoreline environment, taking the oil spill as an example, the transport of oil is first tracked, including whether it is stranded in the environment and whether it is further transported to the underlying matrix. Subsequently, the fate and degradation of the oil in the environment need to be determined. Variable salinity and the presence of natural surface active materials are the crucial parameters contributing to the complexity of shoreline environments and must be considered when exploring the behavior of pollutants. First, a high salinity leads to an increase in the surface tension of water, which is not conducive to the formation of NBs. In contrast, the presence of natural organic matter reduces the surface tension of water, which in turn facilitates the generation and stabilization of NBs. Second, a high salinity has less of an effect on the spilled oil that is stranded on the surface

of the substrate in oil detachment, while organic substances can play a role similar to that of a surface active materials and greatly facilitate oil detachment. NBs contribute to oil detachment, especially when salinity and natural actives materials are present at the same time, which can be attributed to their synergistic effect (Bera et al., 2013). It should be noted that the breaking waves in the shoreline environment not only produce a constant stream of NBs but also provide a continuous physical energy for oil detachment. The detachment of stranded oil on the substrate by NBs is mainly physical detachment and supplemented by chemical degradation. It has been proven that hydroxyl radicals can be generated when NBs burst, and these reactive substances oxidize some of the low molecular weight components of crude oil, such as n-alkanes. It is further hypothesized that NBs could act as oxygen suppliers and thus modulate microbial metabolism to promote oil biodegradation, especially in substrates. With the exception of the stranded oil on the substrate surface, the transport of oil within the shoreline substrate is also hindered by NBs. As discussed, the hydraulic and substrate parameters are modified when NBs are present. In the presence of NBs, oil droplets prefer to be trapped by surface NBs on the sand particles, limiting their longitudinal transport under gravity. At the same time, the presence of natural active substances both increases the point of binding to the oil droplets and promotes the generation of NBs, further increasing the potential for oil retention within the substrate. However, under a high salinity condition, ions are more likely to adsorb to the sand surface, preventing NBs from attaching to the sand. This competitive adsorption leads to more bulk NBs downward transport after binding with oil.

There is an increasing interest in the use of NBs for environmental engineering applications such as surface cleaning, water treatment, and soil remediation. More attention has been paid to the benefits of NBs in the presence of human intervention, but little to the environmental implications of NBs in nature. The shoreline is both a sink for pollutants and a hotbed for their further fate and transport.

Therefore, the role played by NBs cannot be disregarded. The physicochemical properties, influencing factors, and the behavior of the NBs in the fate and transport of pollutants were investigated through batch tests and column experiments in this study. The results show that NBs significantly increased the concentration of dissolved oxygen as well as changed the pH, ζ potential, and surface tension of the solution. Low salinity favored the generation of NBs, while high salinity inhibited this process. The surface active materials played an positive role in the generation and stabilization of NBs. With the assistance of external energy, the bulk NBs enhanced the efficiency in oil detachment from the surface of the substrate. At the same time, the surface NBs in the substrate obstructed the downward transport of oil colloids. Considering the behavior between the NBs in two different phases and the oil droplets, it can be concluded that the oil droplets tended to bind to the NBs due to the hydrophobic nature. In addition to the ability of physical detachment, NBs also generated free radicals that promoted the chemical degradation of the spilled oil. Based on the current findings, NBs can not only influence the fate and transport of oil in the shoreline environment but can also be potentially used as a 'cleaning agent' for oil spill cleanup. Combined with other advanced oxidation technologies, such as ozone, the oxidation capacity can be further increased. Future research should also focus more systematically on the changes of NBs in the surrounding micro-environment and investigate their interrelationship with pollutants from microscopic perspective.

Chapter 4. Overlooked role of bulk nanobubbles in the alteration and motion of microplastics in the coastal environment[4]

4.1 Background

MPs are a significant environmental concern due to their widespread distribution and potential impacts on ecosystems (Xu et al., 2019; Zhang et al., 2020). MPs are defined as plastic particles less than 5 mm in size coming from a variety of sources, including decomposition of larger plastic debris (Cordova et al., 2021; Naji et al., 2017), microfiber shedding from synthetic fabrics (Hernandez et al., 2017a; Wang et al., 2021c), direct release of microbeads from personal care products (Hernandez et al., 2017b; Lei et al., 2017), and other pathways (Murphy et al., 2016; Wei et al., 2022). It is estimated that without effective remediation, MPs in the environment may reach 10 billion tons by 2040 (Lau et al., 2020). MPs have also been found to be ubiquitous in all of the world's oceans, and have been detected in a range of marine organisms, including fish (Le Bihanic et al., 2020), shellfish (Ding et al., 2020a), and birds (Carlin et al., 2020). Even more concerning is that MPs can enter human body through the food chain (Vethaak and Legler, 2021). Recent studies show that MPs have been identified in the human colon (Ibrahim et al., 2021), and even in the human placenta (Ragusa et al., 2021). On the one hand, organic pollutants and heavy metals in the natural environment can be adsorbed on the surface of MPs; on the other hand, MPs also release some chemicals, further increasing their environmental and health risks (Lin et al., 2022; Wang et al., 2022b; Zhang et al., 2022).

[4] This work has been published as Wang, Z; An, C; Lee, K; Feng, Q. 2023. Overlooked role of bulk nanobubbles in the alteration and motion of microplastics in the ocean environment. Environmental Science & Technology, 57(30), 11289-11299.

The shoreline is the intersection between the continent and the ocean, and it is also one of the most active areas for the migration and transformation of pollutants (Khadanga et al., 2022; Wang et al., 2021c). The environmental characteristics of shorelines can have a complex and dynamic impact on the fate and transport of pollutants, including MPs (Wang et al., 2020c). Variable salinity is one of the key characteristics of shorelines. In general, water becomes denser as the salinity increases, and the denser water may be more likely to sink and carry MPs, while less dense water may be more likely to rise to the surface (Vermeiren et al., 2016). Salinity can also affect the buoyancy of MPs, thereby influencing their behavior and movement (Jalon-Rojas et al., 2022; Zhang, 2017). In addition, the salinity of the shoreline environment can influence the rate of degradation of MPs. In general, the degradation of plastic tends to be slower in more saline environments, as the high salt content can inhibit the growth of certain types of bacteria and fungi that contribute to the breakdown of MPs (Pinheiro et al., 2022). Another important factor is the condition of currents and waves. Strong currents can transport MPs over long distances, carrying them from one part of the shoreline to another or out to sea (Chubarenko and Stepanova, 2017; Yang et al., 2022b). The vertical distribution of MPs is also influenced by the tides (Feng et al., 2023a; Feng et al., 2022).

There have been many studies examining the influence of polymer characteristics and traditional environmental parameters on the behavior of MPs in shoreline environments (Feng et al., 2021b). However, there are a number of substances present in the ocean that have yet to be investigated, and as such the impact of these substances on the marine environment and the fate and transport of pollutants is not yet well understood. Bulk NBs, for instance, can be generated in seawater containing natural surface-active materials under the action of wave breaking and sheering (Thorpe et al., 1982). NBs are gas-filled bubbles, usually less than 1 μm in diameter. NBs are characterized

by their small size and unique properties, including high specific surface areas, low density, and long lifetime (Alheshibri et al., 2016; Nirmalkar et al., 2018b). NBs have the ability to alter the pH, ζ potential, dissolved oxygen, surface tension, and other parameters of water, which in turn indirectly affect the fate and transport of pollutants in the aqueous phase (Li et al., 2013; Ushikubo et al., 2010; Xue et al., 2022). These extraordinary properties have led to the exploration of various applications of NBs in fields such as biology (Liu et al., 2015; Shi et al., 2018), materials science (Bao et al., 2015; Zhang, 2017), and environmental remediation (Atkinson et al., 2019; Yoo et al., 2021). In the context of MPs in shoreline environments, the presence of NBs may have significant impacts on the alteration and motion of these particles. Generally, the motion and transport of MPs in the shoreline environment are influenced by various physical and chemical factors, including salinity, waves, and surface tension (Borchers and Pieler, 2010; Pete et al., 2022; Zhang, 2017). NBs have been found to alter the surface tension of water, which may in turn affect the motion and behavior of MPs. The buoyancy of NBs may also influence the vertical distribution of MPs in the water column (Kooi et al., 2017; Waldschlager and Schuttrumpf, 2019).

Despite the potential effects of NBs on MPs in the shoreline environment, the mechanisms underlying these interactions are not clear. One of the challenges in studying the effects of bulk NBs on MPs is the difficulty in accurately measuring these small bubbles and particles, as well as in identifying their respective behaviors and characteristics from a microscopic perspective. With the increasing risk MPs pose to the shoreline environment, there is a pressing need for a deeper understanding of the movement of MPs under the effect of NBs. In this context, the main objective of this study was to examine the behavior and motion of various MPs in the presence of bulk NBs. As factors that affect the properties of both NBs and MPs, salinity and external energy—and

specifically their roles in the interactions between NBs and MPs—were evaluated. The mechanism underlying these interactions between NBs and MPs was then analyzed.

4.2 Methods

4.2.1 Materials and chemicals

PE1 with particle sizes of 8-10 μm and PE2 with particle sizes of 20-25 μm were purchased from Micro Powders Inc. (New York, NY, USA). The density of both PE1 and PE2 is 0.98 g/cm^3. PTFE with a particle size of 8-10 μm and a density of 2.2 g/cm^3 was purchased from Goodfellow (Pittsburgh, PA, USA). Artificial seawater of different salinities was prepared using Sodium chloride (NaCl) obtained from Sigma Aldrich (Ontario, Canada). Tween 20 was first diluted 10 times as the stock solution, and then added as a dispersant in the preparation of the MP suspensions.

4.2.2 Sample preparation and experimental design

An NB generator (OM4-MDG-045, Aura Tec, Fukuoka, Japan) was used to prepare bulk NBs solutions, by operating the generator for 20 min using deionized (DI) water and air at room temperature (20°C) and a pressure of 0.25 MPa. The pH, dissolved oxygen, ζ potential and surface tension of freshly generated NBs solution were examined via a pH meter (AR15, Fisher Scientific, USA), optical DO probe (Orion RDO, Thermo Scientific, USA), particle analyzer (Zetasizer Nano ZS90, Malvern Panalytical, the UK) and bubble pressure tensiometer (BP100, Kruss, German), respectively. The data are shown in Table 4.1. The size distribution of fresh NBs solution was examined by the Zetasizer Nano ZS90, and the result is shown in Figure 4.1. A well-dispersed MPs suspension with a Tween 20 concentration of 0.001%v/v was prepared by introducing 10 mg of PE and 1 L of DI water into a beaker and adding 100 μL of Tween 20 stock solution, then mixing at

13,000 rpm for 20 min using a homogenizer (Ultra-Turrax T25, IKA, USA). PTFE suspensions at a concentration of 0.1 g/L were prepared in a similar manner. To examine the effect of salinity on the behavior of NBs and MPs, different concentrations of NaCl were used when preparing the NBs and MPs solutions to achieve salinities of 5, 10, 15, 25 and 35 psu (0.085, 0.17, 0.26, 0.43 and 0.60 M), respectively. The cell was inserted into the Zetasizer Nano ZS90 to measure the ζ potential. Each sample was measured 3 times and each measurement scans 100 times. The data of ζ potential are shown in Table 4.3. Next, 100 mL of freshly generated MPs suspension and 100 mL of NBs solution were transferred to a glass bottle, and 20 mL of sample was slowly pipetted in the middle of the suspension at 15, 30, 60, 90, and 120 min and injected into a laser in-situ scattering and transmissometry analyzer (LISST-200X, Sequoia Scientific, Bellevue, USA) for the analysis of particle size distribution and total concentration of MPs in the suspension. Each sample was scanned for 1 min, and a total of 60 data points were collected in which 30 data points were selected for the calculation. The pH value of these suspensions was also measured by the pH meter (Table 4.2). To simulate the influence of wave energy on the MPs–NBs interactions, the mixed MPs and NBs solutions were shaken in an incubator shaker (New Brunswick Innova 42R, Eppendorf, Germany) at 100, 200 and 300 rpm for 0.5, 1, 6, 12, and 24 h, respectively. After shaking, the average size and concentration of MPs in the middle of the suspension were determined using the LISST. In addition, to comparatively analyze the effect of NBs on MPs, the same experiments were conducted concurrently with DI water substituted for the NBs solution.

Table 4.1 Characteristics of freshly generated NBs solution.

	Temperature (℃)	**pH**	**Dissolved oxygen (mg/L)**	**ζ potential (mV)**	**Surface tension (N/m)**
Fresh NBs solution	25	5.2-5.5	11.6-12.5	-16.8±3.3	71.3±0.1

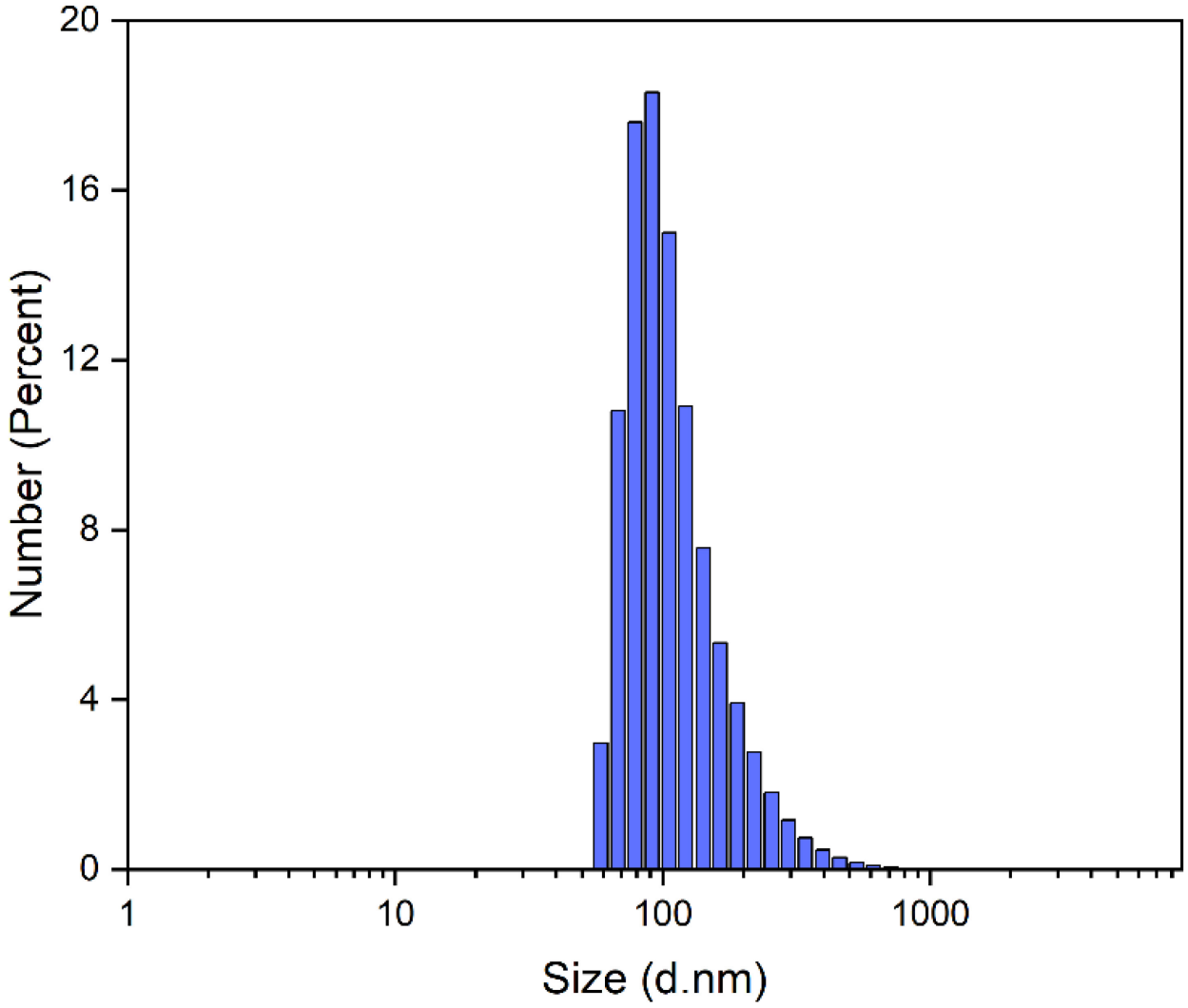


Figure 4.1 Particle size distribution of fresh NBs solution

Table 4.2 ζ -potential of NBs solution and MPs suspension

	Salinity (psu)	ζ potential (mV)*	pH
NBs	5	-12.3±0.9	5.5
	10	-11.7±1.2	5.5
	15	-9.7±1.3	5.5
	25	-7.9±1.8	5.5
	35	-5.4±1.1	5.5
PE1	5	-2.8±0.7	5.7
	10	-2.4±0.3	5.7
	15	-1.6±0.5	5.8
	25	-1.1±0.1	5.7
	35	-0.9±0.1	5.8
PE2	5	-1.7±0.2	5.6
	10	-1.3±0.5	5.6
	15	-1.2±0.3	5.7
	25	-0.7±1.1	5.8
	35	-0.5±0.1	5.7
PTFE	5	-2.2±0.4	5.7
	10	-1.6±0.4	5.8
	15	-0.9±0.2	5.8
	25	-0.8±0.1	5.8
	35	-0.3±0.6	5.8

* Smoluchowski model was applied in ζ potential measurement.

Table 4.3 pH of NBs solution, MPs suspension, and MPs−NBs suspension in the absence of salt

Time (min)	NBs	PE1	PE1−NBs	PE2	PE2−NBs	PTFE	PTFE−NBs
0	5.22	5.46	5.28	5.52	5.29	5.35	5.24
15	5.25	5.33	5.16	5.55	5.31	5.34	5.23
30	5.21	5.24	5.22	5.59	5.34	5.24	5.18
60	5.15	5.25	5.22	5.56	5.33	5.20	5.19
90	5.14	5.27	5.10	5.55	5.45	5.26	5.20
120	5.12	5.24	5.12	5.53	5.39	5.30	5.21

4.2.3 Settling/rising motion analysis

The concentration of MPs suspended in solutions changes with standing time. The ratio (R) of MPs settling to the bottom as well as that floating to the surface was calculated as follows:

$$R=\frac{C_0-C_t}{C_0}\times 100\% \quad (4.1)$$

where C_0 is the initial concentration of MPs in suspension (μL/L), and C_t is the concentration of MPs at time t (Li et al., 2019).

In this regard, previous research (Dietrich, 1982) showed the calculation of the settling velocity (V_s) from the equivalent spherical diameter based on the Stokes equation. This empirical equation has also shown to be applicable in the calculation of MPs settling (Kooi et al., 2017; Kowalski et al., 2016; Waldschlager and Schuttrumpf, 2019).

$$V_s=(|\frac{\rho_p-\rho_l}{\rho_l}|g\omega_*\upsilon)^{\frac{1}{3}} \quad 4.2$$

where ρ_p is the density of the MPs; ρ_l is the liquid density; g is the gravity constant (9.81 m/s^2); ω_* is the dimensionless velocity; and υ is the kinematic viscosity. The value of ω_* can be calculated using the following equation:

$$\omega_* = 1.71 \times 10^{-14} {D_*}^2 \ (D_* < 0.05) \quad 4.3$$

$$\log \omega_* = -3.76715+1.9294 \log D_* -0.09815(\log D_*)^2-0.00575(\log D_*)^3$$

$$+0.00056(\log D_*)^4 \ (0.05<D_* <5\times10^9) \quad 4.4$$

where D_* is the dimensionless diameter, which can be obtained from the spherical diameter *r* (m):

$$D_*=|\frac{\rho_p-\rho_l}{\rho_l\upsilon}|gr^3 \quad 4.5$$

The Péclet number (P_e) was calculated using the following equation to analyze the influence of Brownian motion and buoyancy on the behavior of MPs in suspension (Khaled Abdella Ahmed et al., 2018; Li et al., 2019).

$$P_e=\frac{2\pi g\left|\rho_p-\rho_l\right| r^4}{3k_BT} \quad 4.6$$

where k_B is the Boltzmann constant, and T is the absolute temperature.

4.2.4 Derjaguin−Landau−Verwey−Overbeek (DLVO) theory

DLVO theory was used to assess the interaction energies between MPs and MPs and between MPs and NBs in the suspension. The total interaction energy was obtained by the following equation:

$$U_{total}=U_{vdw}+U_{el} \tag{4.7}$$

where U_{total} is the total interaction energy; U_{vdw} is the Van der Waals interaction energy; U_{el} is the electrostatic interaction energy.

The interaction of MPs–MPs was treated as a particle–particle mode and was calculated as follows:

$$U_{vdw}=\frac{-Ar_1r_2}{6h(r_1+r_2)}\left(\frac{1}{1+\frac{11.12h}{\lambda_c}}\right) \tag{4.8}$$

$$U_{el}=4\pi\varepsilon\varepsilon_0\frac{r_1r_2}{r_1+r_2}[\xi_1\xi_2e^{-\kappa h}-\frac{1}{4}(\xi_1^2+\xi_2^2)e^{-2\kappa h}] \tag{4.9}$$

where A is the Hamaker constant; r_1 and r_2 are the radii of particles 1 and 2, respectively; h is the separation distance between two interacting particles; λ_c is the "characteristic wavelength" of the interaction; ε is the dielectric constant of DI water; ε_0 is dielectric permittivity of a vacuum; κ is the inverse Debye length; and ξ_1 and ξ_2 are the ζ potentials of particles 1 and 2, respectively.

Since the size of MPs was greatly larger than the NBs, a particle–plate mode was employed in the DLVO calculation of MPs–NBs interactions:

$$U_{vdw}=\frac{-A}{6}\left(\frac{r_3}{h}+\frac{r_3}{h+2r_3}+\ln\frac{h}{h+2r_3}\right) \tag{4.10}$$

$$U_{el}=\pi\varepsilon\varepsilon_0\left(\xi_1^2+\xi_2^2\right)\left[\frac{2\xi_1\xi_2}{\xi_1^2+\xi_2^2}\ln\frac{1+e^{-\kappa h}}{1-e^{-\kappa h}}+\ln\left(1-e^{-2\kappa h}\right)\right] \quad 4.11$$

where r_3 is the radius of NBs.

4.3 Results and discussion

4.3.1 Vertical motion of MPs in the presence of NBs

Different types of MPs vary in terms of their behavior in the environment. For example, the influence of gravitational, buoyancy, and drag forces on the movement of MPs in the aqueous environment will vary depending on the density of the MPs (Feng et al., 2022). In general, denser MPs are more likely to sink to the bottom and combine with sediments or flow off-shore with the return current; less dense MPs, on the other hand, are more likely to be transported on-shore via waves/wind (Chubarenko and Stepanova, 2017). In this study, the settling and aggregation of MPs of the same density but different particle sizes (PE1 and PE2) as well as MPs with the same particle size but different densities (PE1 and PTFE) were examined following their interaction with NBs. The particle size distributions of the MPs under investigation are shown in Figure 4.2. The average sizes of PE1, PE2, and PTFE were found to be 8.08 ± 0.53, 16.84 ± 1.29 and 9.02 ± 0.21 μm, respectively. It is worth noting that, although the concentration of the prepared PTFE suspension was 10 times higher than that of the PE solution, the two concentrations obtained by LISST-200X were in the same order of magnitude, this observation being in line with our expectation and with the design of the experiment.

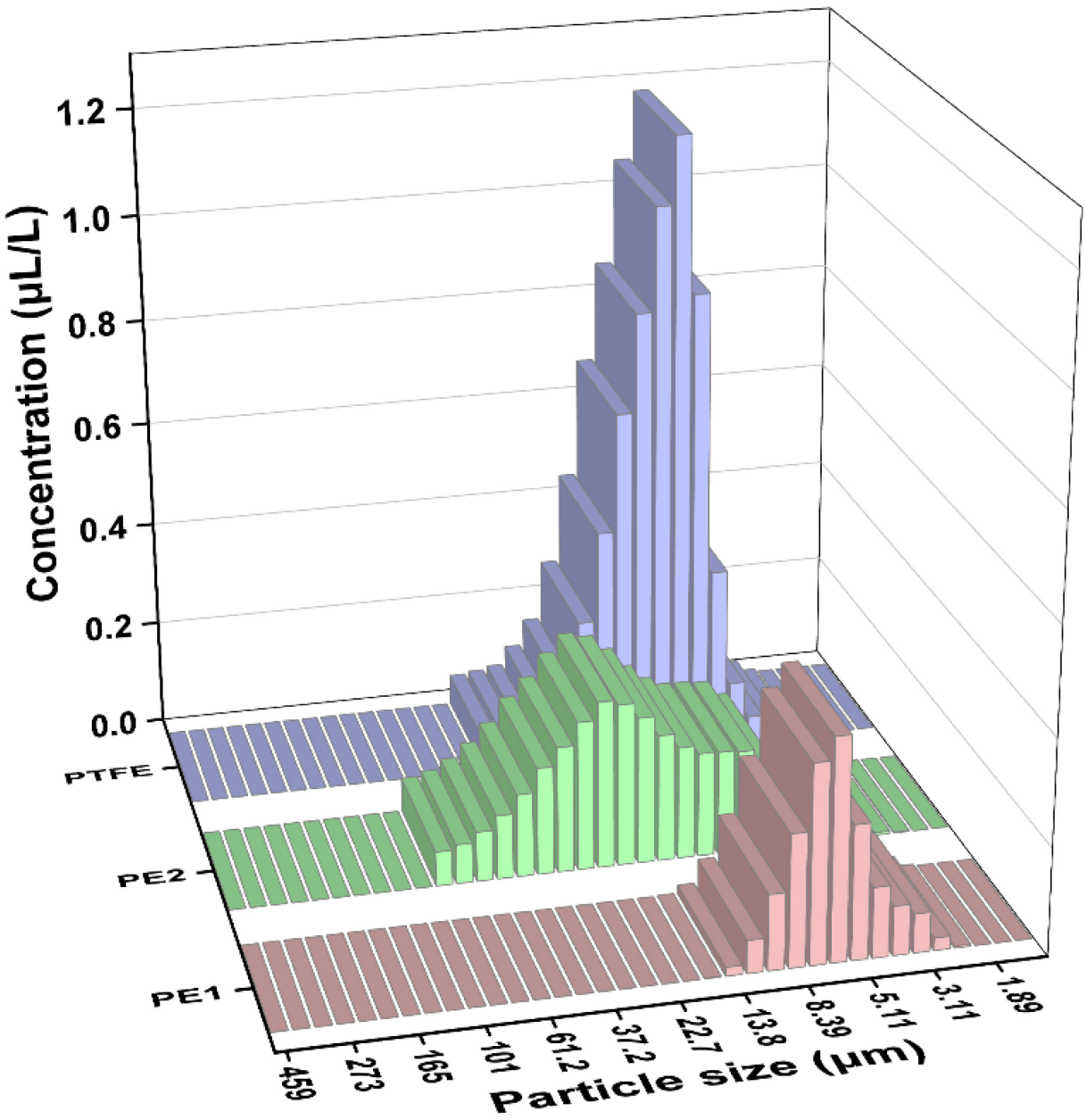


Figure 4.2 Particle size distributions of different types of MPs suspension.

The changes in the average size and in the concentration of MPs in suspensions over time were examined. The changes in the average size and concentration of PE1 are shown in Figure 4.3(a) and Figure 4.3(d). As can be seen at 15 min, the average particle sizes in the MPs–NBs and MPs–DI suspensions were found to be 7.40 ± 0.09 and 6.61 ± 0.17 μm, respectively. Similar to the change

in concentration, the average particle size in the MPs–NBs suspension gradually declined to 6.88 ± 0.24 and 6.71 ± 0.22 μm when standing for 30 and 60 min, respectively. In contrast, the average size in the MPs–DI suspension gradually rose to 6.61 ± 0.22 and 6.83 ± 0.19 μm after 30 and 60 min, respectively. After 90 and 120 min, the average particle sizes in the MPs–NBs suspension were 6.84 ± 0.18 and 6.27 ± 0.11 μm, respectively, while those in the MPs–DI suspension were 5.91 ± 0.13 and 6.37 ± 0.32 μm, respectively. For PE1 at 15 min, its concentration in the MPs–NBs suspension was 2.53 ± 0.19 μL/L—higher than that in the MPs–DI suspension (i.e., 2.07 ± 0.09 μL/L). When allowed to stand for 30 and 60 min, the concentration decreased to 2.29 ± 0.15 and 2.20 ± 0.13 μL/L, respectively, in the MPs–NBs suspension, while the concentration increased slightly to 2.09 ± 0.14 and 2.21 ± 0.09 μL/L, respectively, in the case of the MPs–DI suspension. The concentration difference between the two suspensions gradually decreased within 60 min, and the concentration of the MPs–DI suspension became slightly higher than that of the MPs–NBs suspension at 60 min. When allowed to stand for 90 and 120 min, the concentration in the MPs–NBs suspension continued to decrease (to 2.03 ± 0.05 and 1.83 ± 0.05 μL/L, respectively), while the corresponding concentrations in the MPs–DI suspension were 1.57 ± 0.05 and 1.80 ± 0.18 μL/L, respectively. It can be seen that, in the case of the MPs–NBs suspension, the average particle size and concentration generally decreased over time, particularly within the first 30 min, with this interval seeing the greatest reduction among the standing durations considered.

Figure 4.3(b) and Figure 4.3(e) show the respective variations in the average size and concentration of PE2 over time. As can be seen, the average size of PE2 in the MPs–NBs suspension was 15.07 ± 1.46, 13.51 ± 1.34 and 10.32 ± 0.46 μm at 15, 30, and 60 min, respectively. When allowing the preparation to stand for 90 min, meanwhile, the average size rose to 13.03 ± 1.72 μm, whereas it

once again decreased (to 10.08 ± 1.55 μm, i.e., close to what the concentration was at 60 min) during the period ending at 120 min. Similar to the case of the MPs–NBs suspension, the average particle size in the MPs–DI suspension decreased from 11.95 ± 0.86 to 9.18 ± 0.51 μm over 60 min, then remained essentially constant over the 60–120 min period. The trend of concentration in the MPs–NBs solution was similar to that in the MPs–DI solution. The concentrations of NB and DI decreased by 37.68% and 34.08%, respectively, within 60 min. During the 60–120 min period, the concentrations once again decreased, this time by 22.09% and 8.84%, respectively.

In the case of PTFE, the average particle sizes in the MPs–NBs and MPs–DI suspensions decreased from 10.60 ± 0.71 and 9.53 ± 0.34 μm, respectively, at 15 min to 7.32 ± 0.97 μm and 6.65 ± 0.92 μm, respectively. In clear contrast to the PE1 and PE2, in the case of PTFE the MPs–NBs and MPs–DI suspensions both showed a significant increase in concentration during the 60–120 min interval of standing time. At 120 min, the average particle sizes in the MPs–NBs and MPs–DI suspensions were 12.30 ± 0.47 and 9.78 ± 0.72 μm, respectively, i.e., 68.03% and 44.07% larger, respectively, than those at 60 min, and even larger than those at 15 min. Overall, the concentration of PTFE in the MPs–NB and MPs–DI suspensions decreased over the 120 min period, in contrast to the trend of average particle size. In addition, the decreases in NBs and DI were 66.14% and 85.28%, respectively, in the first 60 min period, and 27.65% and 27.59%, respectively, in the latter 60 min period.

In the case of the PE1–DI suspension, the average size and concentration increased slowly during the first 60 min and then decreased during the latter 60 min period. Compared to the MPs–NBs suspension, in the case of the MPs–DI suspension, the initial average particle size and concentration did not differ significantly from the final values, and these variables can be considered to have

remained relatively stable over the course of the 120 min period. For PE2, which has the same density as PE1 but a different particle size, the variations in average size and concentration in the suspension were different from those of PE1 in suspension. In the case of PE2, the average size and concentration decreased significantly within 60 min of standing time for both the MPs–NBs and MPs–DI suspensions and remained relatively stable for the next 60 min. At 120 min, the average particle size in the MPs–NBs and MPs–DI suspensions decreased by 33.11% and 21.51%, respectively, compared to those after 15 min of standing time. While for PE1, the reduction was only 15.27% and 3.63%, respectively. Despite the different magnitudes of variation, the average size and concentration showed similar trends for both PE1 and PE2. Meanwhile, PTFE showed completely different phenomena from PE, particularly in terms of average particle size. After allowing the suspension to stand for 60 min, the average size of PTFE increased markedly, but the concentration of PTFE dropped sharply and then continued to decrease during the latter 60 min period, indicating that there was very little PTFE suspended in the solution to begin with. It can be inferred that, when the concentration was very low, a small number of large-sized particles greatly inflated the average particle size reading, this being a notable limitation of the light scattering measurement method. Overall, when MPs were in contact with NBs, the average size increased, in turn leading to an increase in the concentration calculated based on particle volume. Meanwhile, the average size and concentration of suspended MPs basically decreased with the standing duration. The initial size and density of the MPs influenced their behavior in the suspension. The larger the particle size was, the lower the concentration of MPs in suspension was, and the smaller the average size of the particles left behind was. Similarly, denser MPs were less likely to become stably suspended in solutions.

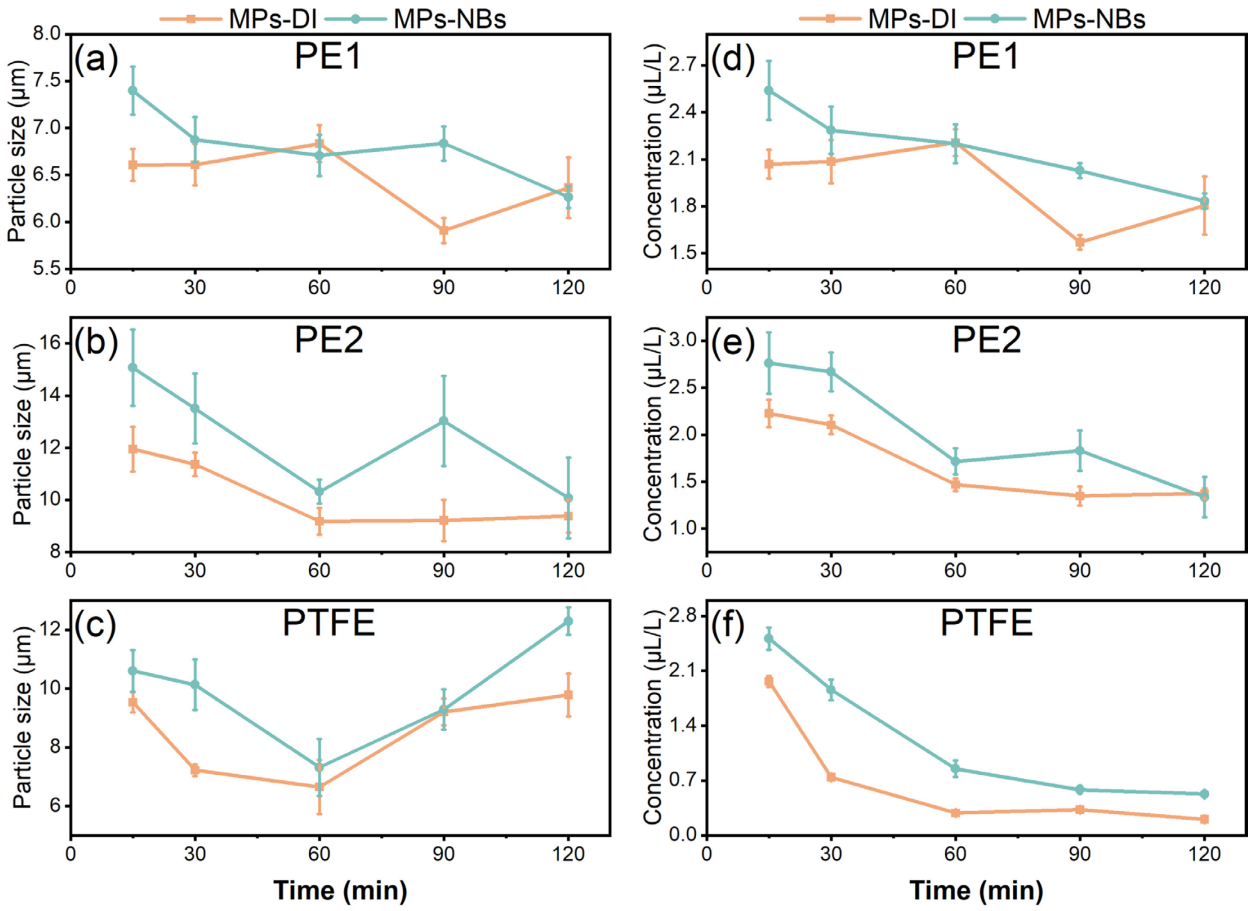


Figure 4.3 Changes in the average particle size and concentration of MPs suspensions. (a), (b), and (c) are average sizes of PE1, PE2, and PTFE, respectively. (d), (e) and (f) are concentrations of PE1, PE2 and PTFE, respectively.

An interesting phenomenon observed in the study was that aggregated MPs were found on both the surface and bottom of the suspension, regardless of whether the density of MPs was greater or less than the solution density. The settling/rising ratios of MPs in suspensions are shown in Figure 4.4. As can be seen, the PE2 of larger particle size had a higher settling/rising ratio compared to PE1, while the highly dense PTFE exhibited the highest settling rate. When NBs were present, the concentration of MPs suspended in the solution increased compared to that in the absence of NBs,

this being attributable to the fact that NBs reduced the aggregation between MPs, while the NBs present combined with MPs to make them more stable in solution.

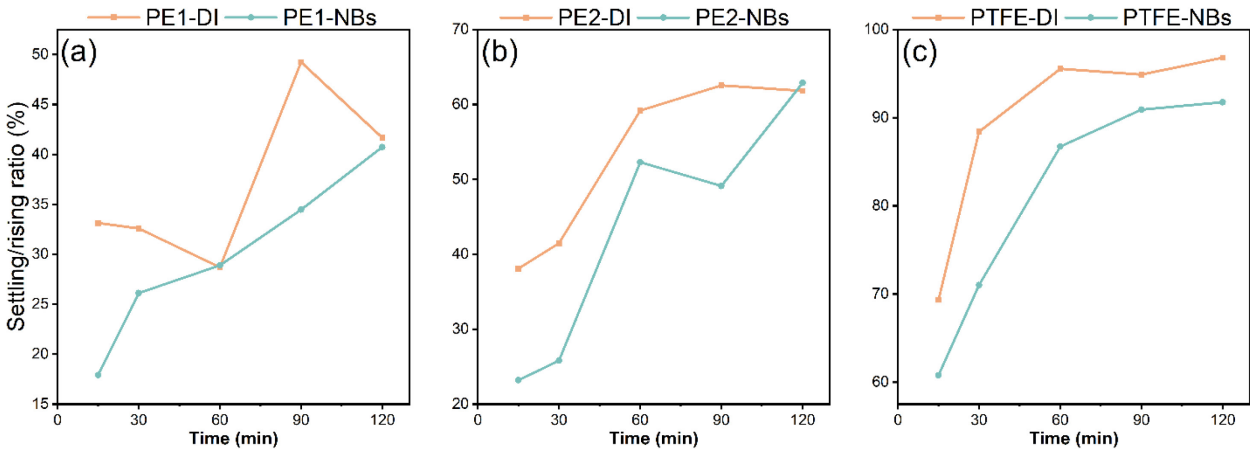


Figure 4.4 The settling/rising ratios of MPs over time. (a), (b), and (c) are PE1, PE2, and PTFE, respectively.

4.3.2 Effect of salinity on MPs motion

One of the distinctive features of seawater is the high content of sodium chloride and the considerable temporal and spatial variation in the concentration (Curry et al., 2003). Different concentrations of salinity can profoundly affect the fate and transport of pollutants such as MPs. Salinity is also a determining factor in the generation and stabilization of NBs solution (Uchida et al., 2016). Previous studies have shown that by adding NaCl to the solution, positive ions are attracted to the surface of the bubble. The accumulation of positive ions near the bubble surface triggers an ion shielding effect, which also changes the ζ potential of the system and thus affects the stability of the NBs (Uchida et al., 2016). Figure 4.5 shows the changes in average size and concentration of MPs over time under different salinities in the presence of NBs. For PE1, when the salinity was 10 psu, the initial average size of suspended MPs was significantly higher than in the

other salinity conditions—similar to the case in which there were no NBs present (see Figure 4.6). The average size of particles in the MPs–NBs suspension decreased by 8.73%, 12.12%, 18.24%, 23.62%, and 20.14% for 5, 10, 15, 25 and 35 psu, respectively, as the standing time was extended to 120 min, while, for the MPs–DI suspension, it decreased by 17.07%, 10.64%, 10.46%, 17.44%, and 15.56%, respectively. It can be seen that, with the exception of the case of a salinity 5 psu, the presence of NBs led to a larger initial average particle size that was more likely to decrease with standing time. The decrease in average particle size was accompanied by a decline in the concentration of MPs in the suspension. The concentrations at salinities of 5 and 10 psu were slightly higher than those under other high salinity conditions. The concentrations of measured particles in the PE1–NBs suspension decreased by 24.05%, 29.92%, 42.27%, 48.19%, and 44.80% at different salinities, respectively, after 120 min of standing time. Increasing salinity was found to result in a reduction in the concentration of PE1 in the suspension. In addition, the changes in average size and concentration of measured PE1 showed a fluctuating decrease in the presence of NBs at various salinities, in contrast to the continuous decrease observed when there were no NBs present.

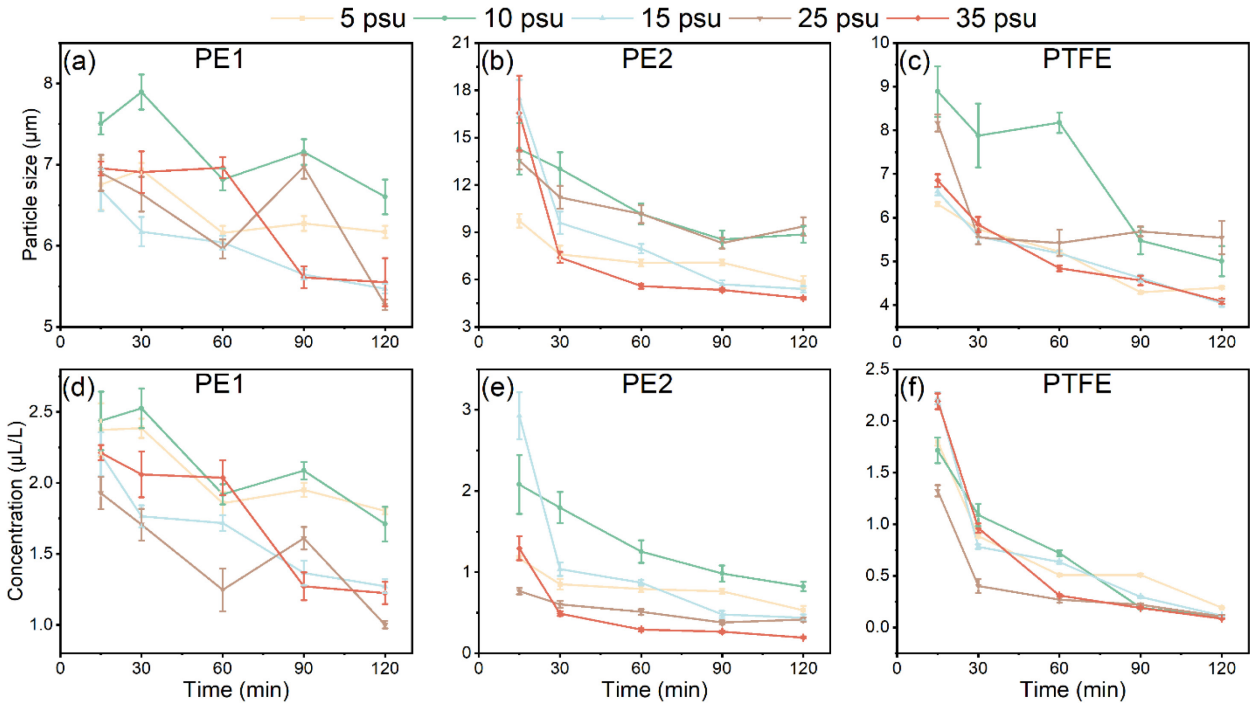


Figure 4.5 Changes in the average particle size and concentration of MPs over time under different salinities in the presence of NBs. (a), (b), and (c) are average sizes of PE1, PE2 and PTFE in suspensions, respectively. (d), (e) and (f) are concentrations of PE1, PE2 and PTFE, respectively.

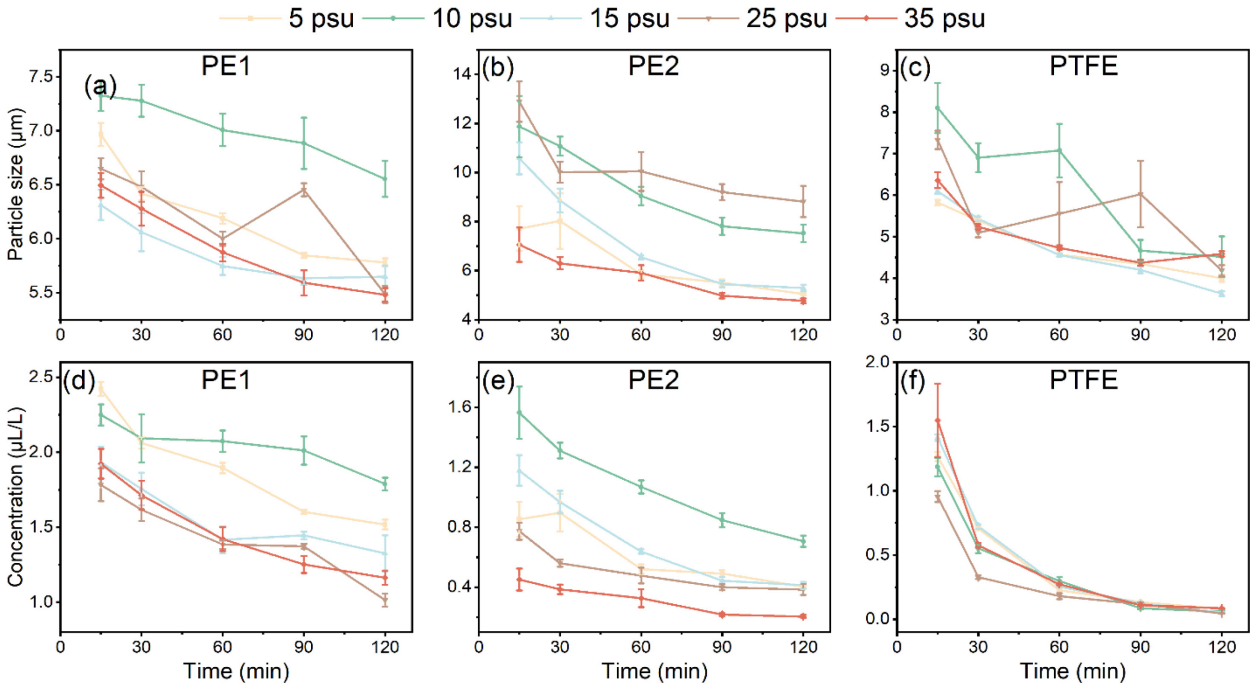


Figure 4.6 The changes of the average particle size and concentration of MPs over time under different salinities in the absence of NBs. (a), (b), and (c) are average particle size of PE1, PE2, and PTFE in MPs−DI solution, (d), (e), and (f) are concentrations of PE1, PE2, and PTFE in MPs−DI solution.

There was a continuous decrease in the average size and concentration of measured particles in PE2 suspension at different salinities, regardless of the presence/absence of NBs. The average sizes at 15 min were 14.28 ± 1.63, 17.48 ± 1.19, 13.55 ± 0.57 and 16.56 ± 2.37 μm for salinities of 10, 15, 25 and 35 psu, respectively (i.e., significantly higher than that at a salinity of 5 psu). In the presence of NBs and after allowing the solutions to stand for 120 min, the average particle size under each salinity condition decreased by 39.98%, 37.89%, 69.11%, 30.77%, and 70.95%, respectively (i.e., a more significant decrease compared to the 0 psu condition). A similar trend was observed when no NBs were present. Moreover, throughout the standing duration, the concentration of MPs in the suspension was lower under the various salinity levels than in the 0 psu condition, with this trend

being particular pronounced when there were NBs present. Similar to the case of PE1, the concentration of PE2 was markedly higher when the salinity was 10 psu than in the other salinity conditions.

The average particle size of measured particles in PTFE suspension also differed between the suspensions containing NaCl and those not containing NaCl. The average particle size of measured PTFE tended to decrease with standing time regardless of the presence/absence of NBs, rather than exhibiting a decreasing followed by an increasing pattern similar to that of PE. The average size of measured PTFE at a salinity of 10 psu was also slightly greater than that at other salinities. Another notable feature of the PTFE in suspension is that, regardless of the presence/absence of NBs, the average particle size and particularly the concentration saw little variation relative to salinity. Although the initial concentrations varied slightly, when the suspensions were allowed to stand for 120 min, the concentration of PTFE in suspension was almost identical for the different salinities.

Salinity altered the characteristics of MPs in suspension, and NBs played a non-negligible role as well, with different types and sizes of MPs being affected to different extents. As a representative of MPs with low density and small particle size, PE1 remained stable over the course of the 120 min of standing time in the suspension without NBs and without NaCl (Figure 4.3[a]) and Figure 4.3[d]). However, the average size and concentration of measured particles gradually decreased for the suspension containing NaCl, with the effect of salinity being moderated by the presence of NBs. Similar to the condition of zero salinity, the presence of NBs led to an initial increase in size of measured particles followed by a fluctuating decrease. Despite the dominant role of NBs, salinity also played a factor, with the concentration of PE1 in the suspensions with low salinity being higher than the concentration of PE1 in the suspensions with high salinity, this trend being particularly

pronounced in the case of salinity of 10 psu. This implies that high salinity destabilized the PE1, allowing it to either rise to the surface or sink to the bottom. The effect of salinity on MPs was further enhanced as the average particle size of the measured particles increased. It can be seen from Figure 4.7 that, when NaCl was present, the reduction percentage of both the average size and the concentration of PE2 increased compared to PE1. Nevertheless, the results demonstrated that there is an optimal salinity that will allow for the rapid aggregation, settlement, or rise of MPs. This is because salinity not only plays upon the nature of MPs themselves, but also affects the stability of NBs, which in turn affects the interactions between MPs and NBs. For PTFE, which has a higher density, the effect of salinity difference on the average size and concentration was found to be negligible. Although the average size of PTFE at 0 psu increased after 120 min of standing time, the change in concentration was more clearly identifiable, as almost all of the PTFE had either settled or floated to the surface. In other words, salinity, as an important parameter affecting water properties, also affected the behavior of the MPs in the water, with MPs of a lower density and smaller particle size being found to be more susceptible to the influence of salinity. Meanwhile, salinity was found to influence the generation and stability of NBs, thereby indirectly affecting the MPs.

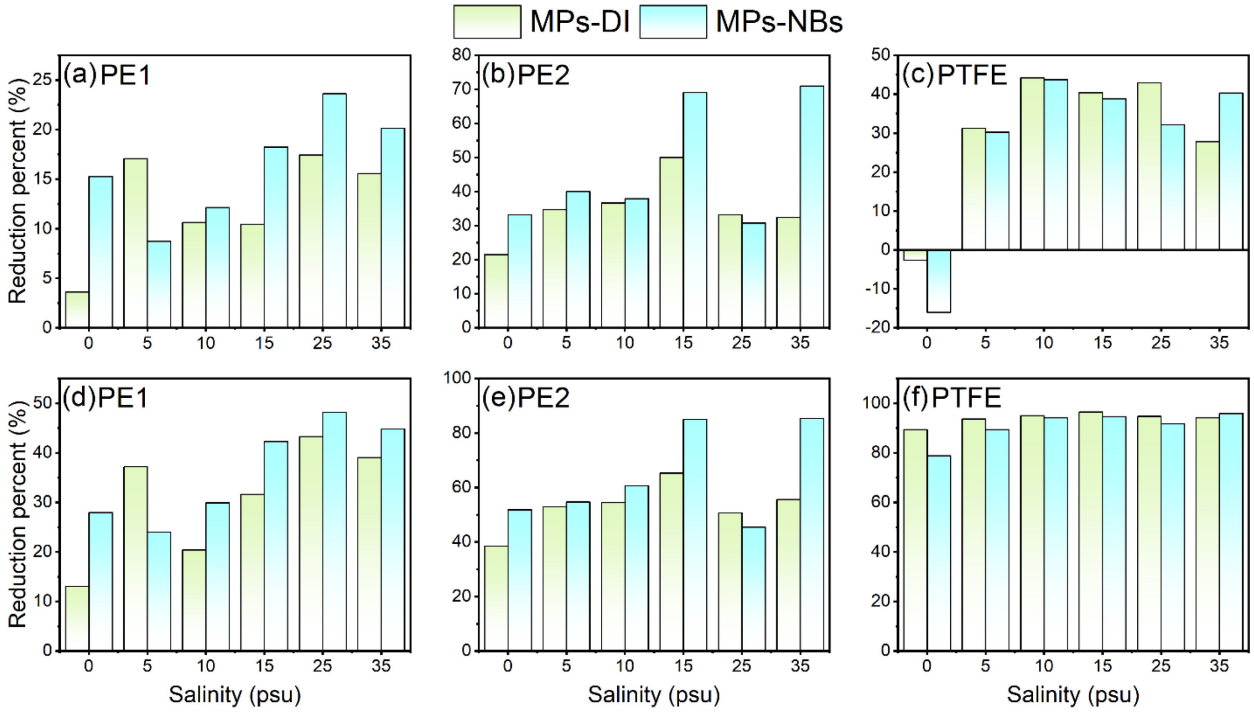


Figure 4.7 Reduction percent of the average size and concentration under different salinities. (a), (b), and (c) are average sizes, (d), (e), and (f) are concentrations.

4.3.3 Interaction of external energy on MPs and NBs

Variable coastal energy is one of the most distinctive features of the coastal environment. Energy conditions strongly influence the fate and transport of pollutants in the shoreline environment. More importantly, energy also affects the generation and stability of the NBs. In this study, the external energy provided by the shaking was used to imitate the wave energy in the actual environment. The average size and concentration of MPs in the suspension after shaking are shown in Figure 4.8. When the shaking time was just 0.5 h, a larger average particle size corresponded with an increase in shaking speed, and, as the shaking time increased, the average particle size of PE1 was large even at slower shaking speeds. Previous studies have suggested that NBs can also be produced under shaking/agitation conditions (Kyzas et al., 2020), and our most recent work also found that NBs are

more likely to bust with long-term and high-speed shaking (Wang et al., 2023b). We can thus hypothesize that short-term and high-speed shaking promoted the generation of NBs, in turn resulting in a higher rate of PE1 aggregating with NBs. Nevertheless, the dispersion of aggregates due to prolonged high-speed shaking was dominant. In addition, the PE1 aggregation phenomenon was more pronounced at a shaking time of 6 h than in other cases, and this tendency was particularly evident when NB was not present, regardless of the shaking speed. The behavior of PE1 in suspension was more clearly characterized by changes in concentration. It is evident from Figure 4.8 and Figure 4.9 that the concentration of PE1 in the suspension was significantly higher than the condition without external energy after 6 h of shaking. In addition, the higher the shaking speed was, the lower the PE1 concentration was observed to be. Due to its low density and small particle size, PE1 was found to be highly susceptible to external energy. When less energy was applied, PE1–PE1 and PE1–NBs aggregation was less obvious, with PE1 particles more likely to float to the surface of the suspension. As the energy increased, the average size of the measured PE1 due to aggregation of particles continued to increase, in turn inhibiting the buoyant force and resulting in PE1 being suspended in solution for a longer period. When the energy was further increased, this phenomenon became more pronounced. The effect of external energy on PE2 in suspension, on the other hand, was more clearly reflected in variations in the concentration. In general, when the shaking speed was high, the concentration of PE2 was low, except in the case of 24 h shaking time. However, it should be noted that the concentration of PE2 was still lower after 24 h in this case than under other conditions after 24 h shaking time, particularly under shaking speed conditions of 100 and 200 rpm. Similar to the case of PE1, in the case of PE2 the concentration was higher after shaking times of 6 and 12 h than under other conditions. Although the trend of average particle size was less apparent in the case of PE2, it can still be seen that the average size was slightly greater than in the other cases for shaking times of 6 and 12 h. The average size and concentration of PTFE in suspension also did

not differ significantly under various shaking conditions. The concentration of PTFE in suspension dropped by 60% to 90% compared to the case without shaking, regardless of the presence of NBs. This indicates that, after being subjected to shaking, most of the PTFE either settled or floated to the surface.

The effect of external energy varied for different kinds of MPs. Although the particle sizes of PE1 and PE2 were different, both of them were less dense than the solution, and they exhibited similar characteristics after shaking, especially in terms of concentration. Both high and low energy were beneficial for the settling or floating of low-density MPs, whereas medium energy kept MPs suspended in solution. Moreover, the average size of PE after shaking was generally larger than that when the suspension was not subjected to shaking. Although PTFE and PE1 have similar particle sizes, due to the higher density of PTFE, its behavior in suspension was less affected by changing energy. However, the decrease in the concentration of PTFE after shaking was greater than that of PE1 and PE2 compared to the case without external energy. Finally, the presence of NBs had a distinct influence on PE, whereas its influence on PTFE under shaking conditions was less obvious.

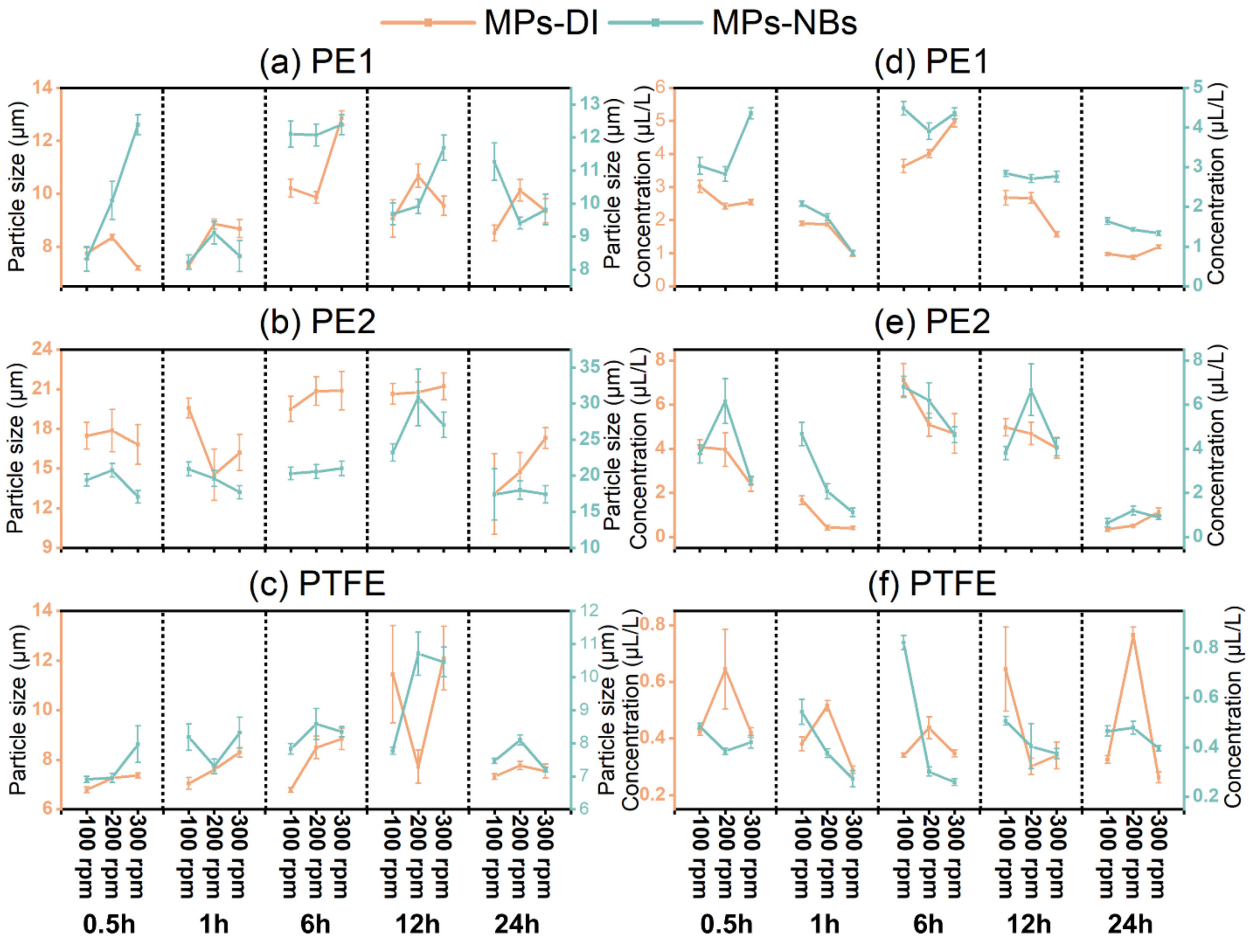


Figure 4.8 Effect of external energy on the average size and concentration of MPs suspension.

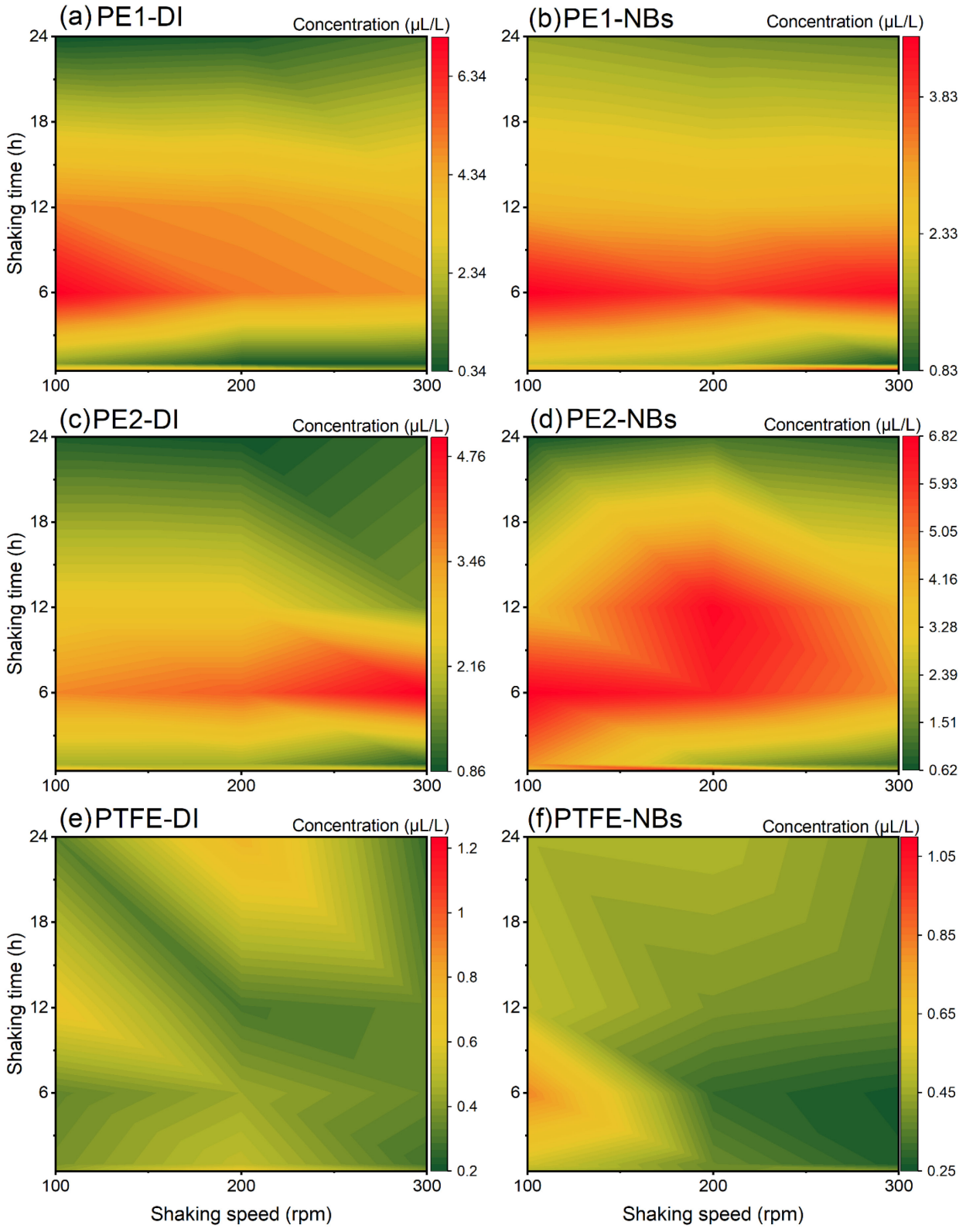


Figure 4.9 Effect of shaking conditions on the MPs concentration.

4.3.4 Analysis of the mechanism underlying behavior of MPs–NBs suspensions

The Péclet number (Pe) was calculated to determine the potential influences of Brownian motion and buoyant force on the vertical movement of MPs in suspension. Figure 4.10(a) shows that, for PE1, Brownian motion played a dominant role in the motion, regardless of the salinity. The Brownian motion inhibited the upward motion of PE1, resulting in more PE1 being suspended in the solution. This is consistent with the previous results that the concentration of PE1 in suspension decreased slowly. NBs as a non-negligible factor further enhanced the retention of PE1 in the suspension. Regarding the freshly generated PE2 suspensions, regardless of the presence of NBs, the average size of PE2 was greater than 15 μm, implying that the buoyant force was dominant at this juncture, and these large-sized PE2 particles floated to the surface of the suspension. However, after 15 min standing time, the average size of particles left in the PE2 suspension was below 10 μm, and Brownian motion played a leading role instead. The Péclet number of PTFE is shown in Figure 4.10(b). As can be seen, there was almost no change in Péclet number of PTFE under different salinity conditions. The Péclet number was 1 when the particle size was approximately 7 μm. Thus, for freshly generated PTFE suspensions, buoyancy was the dominant effect initially, and then Brownian motion became dominant as the standing time increased.

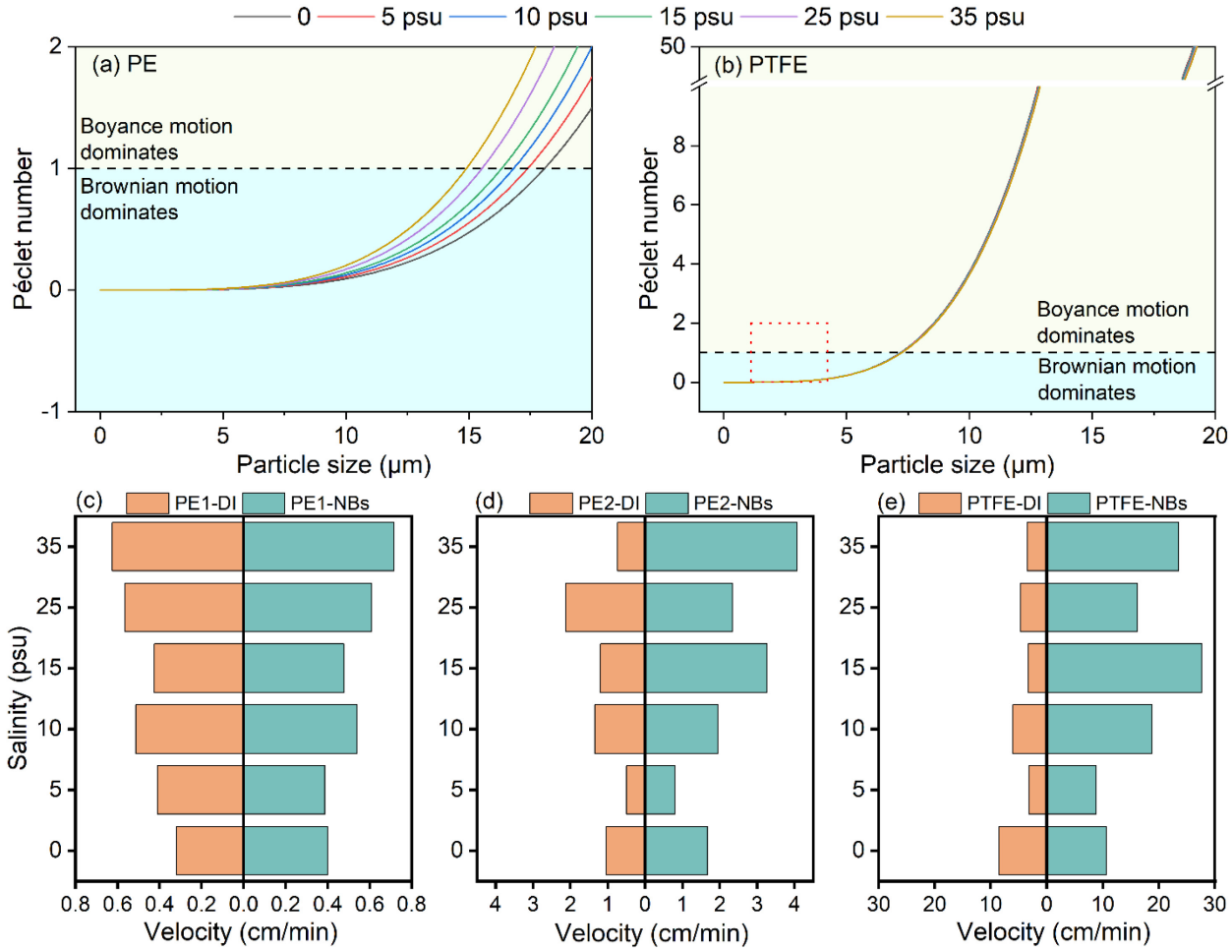


Figure 4.10 Péclet numbers and velocity of MPs under different conditions.

Since the vertical motion varied depending on the type of MPs, the settling/rising velocities could be obtained based on the average particle size of the MPs. Figure 4.10(c-e) shows the vertical velocity of MPs under different conditions. The effect of NBs was also considered. As can be seen, the behavior of PE1, which has a small particle size, was mainly influenced by Brownian motion, although this does not mean that PE1 would not settle or float to the surface of the solution. As the salinity increased, the difference in density between PE1 and the solution increased, causing PE1 to float to the surface more rapidly. The velocity increased slightly in the presence of NBs. PE2 rose faster in suspension than PE1, particularly in the presence of NBs. In addition, the rising velocity

increased with increasing salinity. The rising velocity of PTFE was higher than that of PE1 and PE2. An increase in salinity resulted in a decline in the difference in density between the PTFE and the suspension, in turn leading to a decrease in velocity. However, when NBs were present, the trend of the change in velocity was opposite. Similar to the case of PE2, in the case of PTFE the presence of NBs promoted an increase in velocity.

Increasing ionic strength can not only alter the motion of MPs, but also indirectly affect the properties of MPs by altering the performance of NBs. In our study, in keeping with DLVO theory, as the ionic strength increased, the double-layer repulsion between MPs gradually disappeared, and the attraction between them increased accordingly. Figure 4.11 shows that, when the salinity was less than 10 psu, PE1 was mainly subjected to electrostatic repulsion caused by the electric double layer. As the salinity increased, the excess electrolyte compressed the thickness of the double layer, thus reducing the potential barrier, and attraction, rather than repulsion, became the dominant force. The PE2–PE2 interaction was similar to the PE1–PE1 interaction observed in the PE1 suspensions, playing a dominant role when the salinity was greater than 10 psu, although the PE2–PE2 attraction was more pronounced compared to the PE1–PE1 attraction observed. Besides, PTFE particles need to overcome larger energy barrier over shorter distance than PE2 to aggregate. However, the energy the PTFE needs to overcome was similar to that of PE1 due to the close average particle size of both. When NBs were present, the energy barrier between NBs and MPs was significantly larger than that between MPs and MPs, so homogeneous aggregation between MPs was easy. On the contrary, it also shows that once NBs were attached to the surface of MPs, the binding of the two would be very strong.

In summary, the ionic strength did change the interaction energy between particles in solution. Regardless of the presence or absence of NBs, increasing ionic strength reduced the energy barriers between the particles and facilitated their aggregation. Although both PE and PTFE need to overcome a certain energy barrier in order to aggregate, the energy barrier differed depending on the type of MP. At low salinity, PTFE required the greatest energy, followed by PE1, and finally PE2. This means that PE2 was more likely to aggregate. In addition, the hydrophobicity of PTFE was greater than that of PE (Feng et al., 2022), and this contributed to the aggregation in the water phase. As hydrophobic substances, NBs can bind to MPs as well. The particle size of NBs was significantly smaller than that of MPs, so it can be inferred that MPs acted as the core particles with smaller NBs adsorbed on their surface, in turn leading to a larger particle size of MPs, as well as altering their behavior and physicochemical properties. Moreover, the inherent properties of MPs, such as particle size and density, as well as other factors in the external environment, also profoundly affect the behavior and motion of MPs in the shoreline environment.

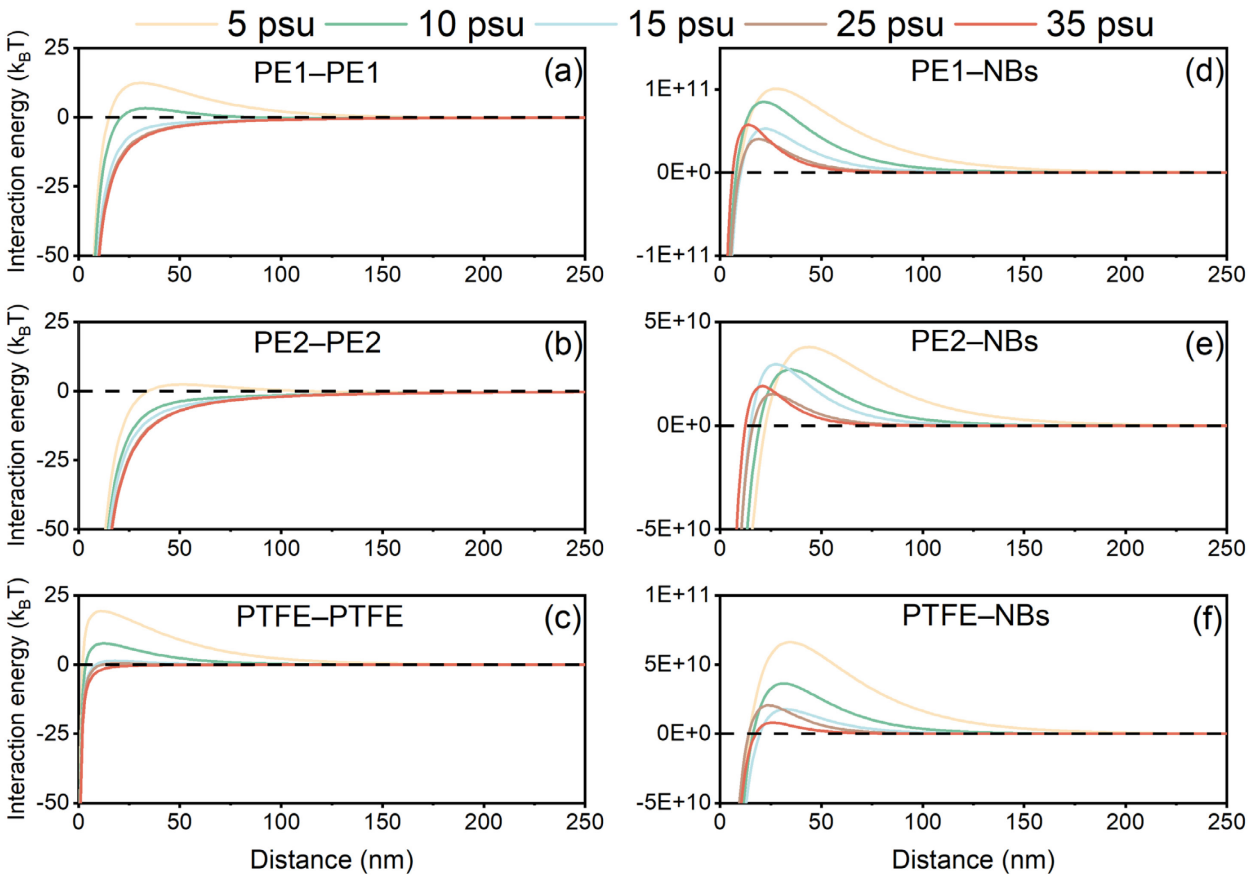


Figure 4.11 Interaction energy versus surface-to-surface separation distance for MPs and NBs at various salinities.

4.3.5 Environmental implications

The conventional view is that density is one of the control parameters affecting the vertical motion of MPs, where a greater difference in density between MPs and solution corresponds with an increased likelihood that the MPs will sink. However, we found in our study that the denser PTFE may partially float to the surface of the solution, the same finding having been obtained in other recent studies in the literature (Feng et al., 2022). This suggests that the motion of MPs is influenced by multiple factors—both the inherent properties of MPs and external environmental conditions. In this way, although even MPs of a high density, if they are hydrophobic, will tend to aggregate into

large ‘plastic films’ that are likely to float to the surface under the effect of surface tension. Salinity and external energy are also important factors influencing the behavior of MPs. Meanwhile, the impact of NBs, as small ‘particles’ widely present in the ocean, on the fate and transport of traditional and emerging pollutants has received relatively little attention in the literature. When considering the motion and behavior of MPs in the shoreline environment, the role of NBs, particularly at the microscopic level, cannot be ignored. NBs change the physicochemical parameters (e.g., dissolved oxygen, surface tension, pH, ζ potential) of the solution, and are also directly involved in the aggregation and settle of MPs. The feasibility of NBs in flotation for the removal of MPs in water treatment processes was also verified.

The increasing enrichment of MPs in the shoreline environment poses both ecological and social-economic risks. A systematic and in-depth understanding of the alteration and motion of MPs in the ocean environment is the basis and prerequisite for mitigation of these risks (Liu et al., 2022; Xiao et al., 2022). Previous studies have focused primarily on the characteristics of MPs under the influence of traditional factors, whereas less attention has been given to NBs in spite of the important role they play in the behavior and motion of MPs. In this study, behavior and motion of various MPs in the presence of NBs were evaluated, as well as the effect of salinity and external energy on the interaction of MPs and NBs. We found that, in the presence of NBs, the binding of MPs and NBs resulted in an increase in the measured average particle size and concentration. Meanwhile, the average size and concentration of suspended particles in MPs suspension decreased significantly with increasing standing time. Moreover, salinity not only directly altered the properties of MPs in suspensions, but also indirectly influenced the effect of NBs on the movement of MPs by affecting the generation and stability of NBs. The Péclet numbers obtained show that bulk NBs can influence the effects of Brownian motion and buoyancy on the vertical motion of MPs in suspension by

aggregation. In addition, it was found that the velocity of motion of MPs driven by NBs varies under different salinity conditions. The DLVO results show that salinity changes affected the energy barrier between MPs and NBs. When MPs and NBs bound, the high salinity limited the separation of the two, which in turn remained more stable and accelerated the movement in the water column. Moreover, various types of MPs were found to be affected distinctly by external energy. High and low energies promoted the vertical motion of low-density MPs, while medium energy tended to lead to the suspension of MPs in solution. High-density MPs were less affected by energy in the vertical motion. The presence of NBs, meanwhile, had a clear effect on PE under shaking conditions, whereas the effect on PTFE was less obvious. Given this, we can hypothesize that the presence of NBs in the shoreline environment not only affects the hydraulic parameters but also alters the microenvironment in which MPs are located. Future studies can further investigate the effects of NBs on the fate and transport of pollutants due to the altered physicochemical properties and biological microenvironment, as well as the application and optimization of MPs removal in water treatment processes.

Chapter 5. Effect of nanobubbles on the mobilization of microplastics in shorelines subject to seawater infiltration

5.1 Background

The widespread use of plastics has caused serious damage to the natural environment, living creatures, and even human society (Lau et al., 2020). Given the diversity of sources of MPs, including primary and secondary sources, MPs have emerged as a pressing environmental concern in recent decades (Lei et al., 2017; Naji et al., 2017; Wang et al., 2021c). MPs are now observed in the atmosphere (Zhang et al., 2020), soil (Corradini et al., 2019), and aquatic environments (Li et al., 2018), particularly ocean environments (Andrady, 2011). Bakaraki Turan et al. (2021) examined the distribution of MPs in the world's marine environments and noted that MPs are most abundant in the Pacific Ocean, followed by the Atlantic, Arctic, Indian, and Southern oceans. The widespread presence of MPs in the ocean has had an impact on the survival and generation of aquatic plants, zooplankton, fish, and mammals to varying degrees (Eltemsah and Bohn, 2019; Wang et al., 2020a; Yong et al., 2020). MPs can also act as carriers of other pollutants, leading to bioaccumulation and biomagnification in marine food chains, ultimately threatening human health (Huang et al., 2021b; Wang et al., 2019). The concentration and distribution of MPs in coastal areas have gained significant attention due to the dynamic interactions between marine and terrestrial systems (Chen et al., 2023; Zhang, 2017). Qualitative and quantitative analyses of MPs in the coastal environment and a comprehensive understanding of MPs occurrence and transport mechanisms are urgently needed.

Coastlines, typically defined as the intersection between land and sea, are pivotal in determining the environmental behavior of numerous pollutants, including MPs (Wang et al., 2021c; Wang et al., 2020c). The dynamic forces at play along coastlines, influenced by tides, waves, shoreline substrate, and human activities, contribute to the distribution of MPs (Zhang, 2017). Given the important roles of substrate, salinity, capillarity, and tidal cycle in this regard, a number of studies have been conducted on the infiltration, transport, and resuspension of MPs in shoreline environments employing such methods as column experiments (Feng et al., 2022), meso-scale tank simulation (Feng et al., 2023b), and modeling (Feng et al., 2023a). A fascinating aspect of the coastal environment, especially as it relates to pollutant transport, is the presence of vast vadose zones, also known as unsaturated zones, which are regions in the soil or substrate that are neither fully saturated with water nor fully air. The characteristics of vadose zones are directly influenced by waves and tidal force, and indirectly influenced by the groundwater table (Guo and Jiao, 2008; Jiao and Li, 2004). Previous studies have proved that the vadose zones are crucial in controlling the movement of pollutants. Russell et al. (2012) investigated the migration of enterococci from naturally contaminated unsaturated zones of beaches to the water table through seawater infiltration using a combination of field tests, lab experiments, and simulations. In study examining the transport and fate of benzene and toluene in tidally influenced beaches, meanwhile, various numerical models were used to calculate the center trajectory of the pollutant plume, the area of dispersion, and the percentage of biodegradation, with a key finding being that aerobic biodegradation was the main fate of the pollutants on beaches (Geng et al., 2017). In this regard, given that the coastal environment is an important sink for MPs, there is an urgent need to understand their fate and transport in this unique structure.

The existence and role of natural nanobubbles (NBs) is a relatively uncharted area of research when it comes to ocean environments. Although Johnson and Cooke (1981) found that stabilized NBs can be generated in seawater in the presence of surface-active substances and suggested that NBs are a common feature of near surface regions and many aquatic environments, little research has explored the effect of NBs in natural settings. NBs, it should be noted, are defined as tiny gas bubbles (diameter less than 1000 nm) that are surrounded by solution or attached to the surface of media (Alheshibri et al., 2016; Peng et al., 2015). Compared to macro bubbles, NBs have some unique properties due to their smaller size. Not only can NBs alter the pH and ζ potential of the solution, but they also have a high mass transfer efficiency and strong oxidation capacity (Bai et al., 2021; Takahashi et al., 2021; Wang et al., 2023b). Moreover, NBs in some environments have been noted for their role in processes such as flotation (Fan et al., 2010a; b), irrigation (Liu et al., 2015; Liu et al., 2019b), surface cleaning (Jin et al., 2022; Li et al., 2022), soil remediation (Kim and Han, 2020; Zhang et al., 2019a), and drug delivery (Batchelor et al., 2020; Wang et al., 2010). Our earlier research has shown the significance of bulk NBs in determining how pollutants transport in the marine environment (Wang et al., 2023a; Wang et al., 2023b). Due to their stability, large quantities of NBs are attached to the coastal substrate by means of wave circulation, further influencing the penetration and suspension of MPs. In addition, the gases produced by microorganisms and algae in the coastal substrate due to photosynthesis and respiration are also prone to form bubbles during seawater submergence of the coast, and this, in turn, affects the solute transport in the pores (Cheng et al., 2014; Mendoza-Lera and Mutz, 2013). Given this aspects, there is a pressing need to understand the presence and influence of NBs in coastal vadose zones, especially concerning the fate and transport of MPs. In this context, the study presented herein sought to gather insights into the role of natural NBs in influencing the vertical movement of MPs in coastal vadose zones under wave conditions. The infiltration of MPs under steady-state and transient conditions, as well as the

upward transport induced with high tide were considered. With the increasing environmental footprint of MPs, understanding such intricate interactions is essential for holistic coastal management and remedial strategies.

5.2 Methods

5.2.1 Materials and chemicals

Three different MPs were procured for the MP suspension. Among this, Polyethylene 1 (PE1) and Polyethylene 2 (PE2) have different particle sizes but the same density, while PE2 and Polymethylmethacrylate (PMMA) have similar particle sizes but different densities. Further details on the MPs used are given in Table 5.1. Artificial seawater samples of varying salinities were prepared using Sodium chloride (NaCl) from Sigma Aldrich (Ontario, Canada). Tween 20 was first diluted 10 times as a stock solution, and it was then added as a dispersant in the preparation of the MP suspensions, glass beads (GBs) with a particle diameter of 1 mm were procured from VWR (Ontario, Canada).

Table 5.1 Properties of different MPs particles

Types	**Density (g/cm^3)**	**Size (µm)**	**Contact angle (°)**	**Sources**
Polyethylene 1 (PE1)	0.98	20–25	139.9	Micro Powders Inc. (New York, NY, USA)
Polyethylene 2 (PE2)	0.98	4–6	139.9	Micro Powders Inc. (New York, NY, USA)
Polymethylmethacrylate (PMMA)	1.19	6	40.7	Goodfellow Cambridge Ltd. (Huntingdon, UK)

5.2.2 Samples preparation and characterization

The NBs solution was configured according to our established method employed in previous studies (Wang et al., 2023a; Wang et al., 2023b). Various properties of the freshly generated NBs solution were then examined of various properties. The pH was measured using a pH meter (AR15, Fisher Scientific, USA), and size distribution and ζ potential were analyzed by using a Zetasizer Nano ZS90 (Malvern Analytical, the UK). The suspension of uniformly distributed MPs was prepared by mixing 20 mg of MPs particles with 500 mL of DI water in a 1 L beaker. 100 μL of the Tween 20 stock solution was introduced to ensure the concentration of Tween 20 was only 0.001% v/v. The blend was then thoroughly mixed at a speed of 10,000 rpm for 10 min using a T25 digital Ultra–Turrax homogenizer (IKA, USA). The size distribution of MPs in the suspension was assessed using a LISST-200X laser scattering and transmissometry instrument (Sequoia Scientific, Bellevue, USA). Meanwhile, the pH and ζ potential of the MPs suspension were measured. The properties of the NBs solution and MPs suspension are presented in Table 5.2 and Figure 5.1. Water contact angle was the metric to assess the hydrophobicity of the MPs, with a contact angle goniometer (VCA Optima, AST Products, USA) being employed for this purpose. The results are shown in Table 5.2.

Table 5.2 Properties of NBs solution and MPs suspension

	ζ potential (mV)				**pH**			
Salinity (psu)	0	10	25	35	0	10	25	35
NBs	-18.1	-2.5	-2.3	-2.1	4.8	5.3	5.4	5.6
PE1	-42.4	-3.8	-2.7	-2.1	5.5	5.6	5.8	5.9
PE2	-48.3	-4.8	-4.4	-2.7	5.5	5.7	5.9	5.9
PMMA	-12.7	-2.0	-1.4	-1.5	5.5	5.7	5.8	5.9

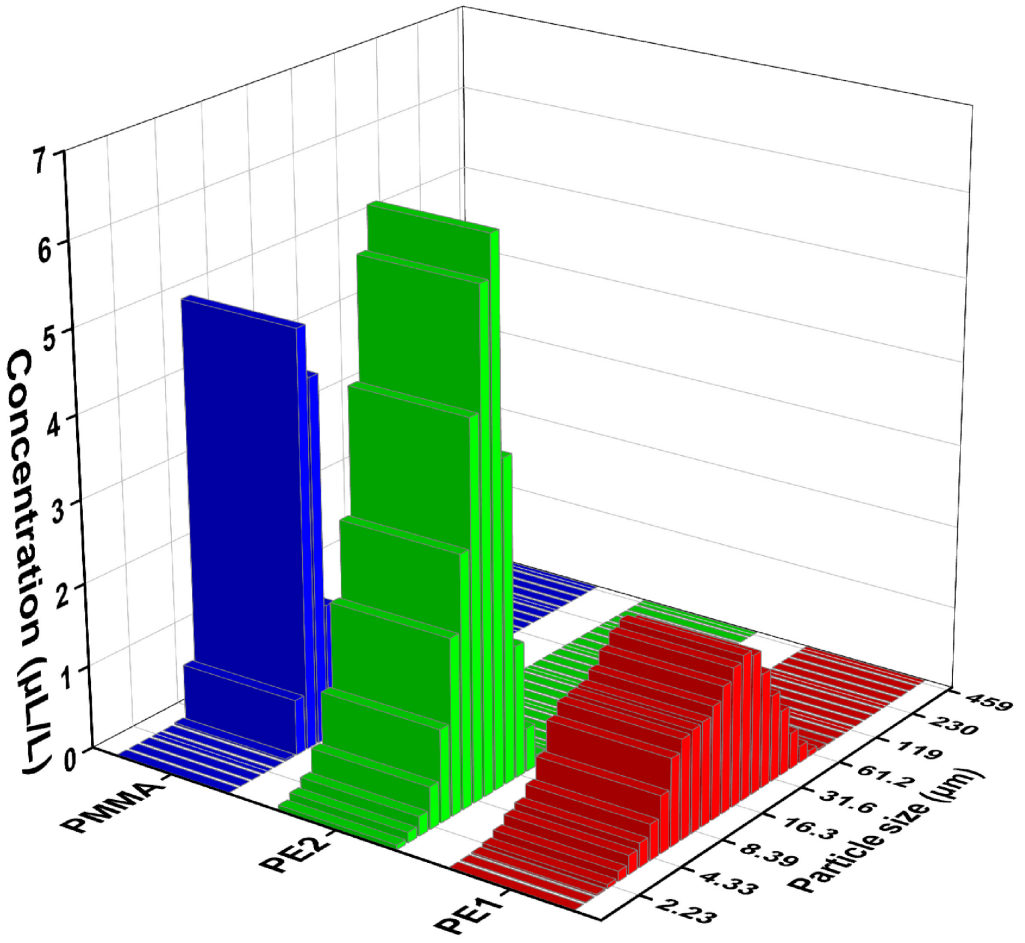


Figure 5.1 Particle size distribution of different MPs suspension

5.2.3 Experiment design

The column test was used to gain insights as to the extent to and manner in which NBs influence the vertical motion of MPs in coastal vadose substrates under various conditions. An acrylic column with a length of 15 cm and an inner diameter of 26 mm was employed in the column test. The column was loaded with GBs to a height of 10 cm to mimic the coastal matrix. A stainless-steel woven wire was used to seal the bottom of the column in order to secure the substrates in place.

Either NB solution or DI water was then pumped from the top of the column using a peristaltic pump (Masterflex L/S, Cole–Parmer, USA) set to a flow rate of 20 mL/min for 20 minutes in order to stabilize the column. The MPs suspension was evenly mixed using a disperser before being pumped into the column at a predetermined flow rate (Figure 5.2[a–b]). Effluent was gathered from the bottom of the column at 5 mL intervals until a cumulative total of 150 mL was reached. 5 mL of effluent and 3 mL of DI water were added to a turbidity sample cell, and the turbidity was examined via a turbidimeter (2100Q, Hach, USA). The calibration curve was used to determine the concentration of MPs in the suspension. The ratio (C/C_0) of MPs concentration (C) in the effluent to the original MPs suspension (C_0) was calculated.

To assess the influence of salinity on the movement of MPs through the substrate, NBs solutions and MPs suspensions at varying salinity levels (0.001M, 10, 25, and 35 psu) were prepared and tested. A salinity level of 0.001 M was used to represent the case of zero salinity; (the relevant portion of the experiment confirmed that there was no difference in the experimental results between 0 and 0.001 M, thereby justifying this experimental setting). Differences in flow rate (2.5, 5, and 10 mL/min) among the MPs suspensions within the column were also studied. Moreover, to simulate infiltration due to the effects of uninterrupted waves, after the first infiltration of 50 mL at a salinity of 0 and a flow rate of 5 mL/min, 50 mL was infiltrated at 10 min intervals, resulting in a total infiltration of 150 mL. In addition, appropriate modifications were made to the columns to simulate the upward transport of MPs through the column due high tide. Both the top and bottom of the column were sealed using rubber caps, and the tube was connected to the column system by means of quick connectors. The inlet was positioned at the bottom, while the outlet was located at the top (Figure 5.2[c–d]). Similar to the setup for the infiltration experiments, the upward transport of MPs in the column was simulated under different salinity and flow rate conditions once the column had

been pre-equilibrated using an NBs solution or DI water. Calibration curves of MPs suspensions of different concentrations versus turbidity were plotted in advance and applied to calculate the concentration of MPs in the effluent. An MPs suspension with a concentration of 100 mg/L was first prepared, and it was then diluted 2, 4, 6, 8, 12, 24, 48, and 96 times to determine the turbidity of the suspensions at different concentrations; finally, the standard curve was plotted (Figure 5.3).

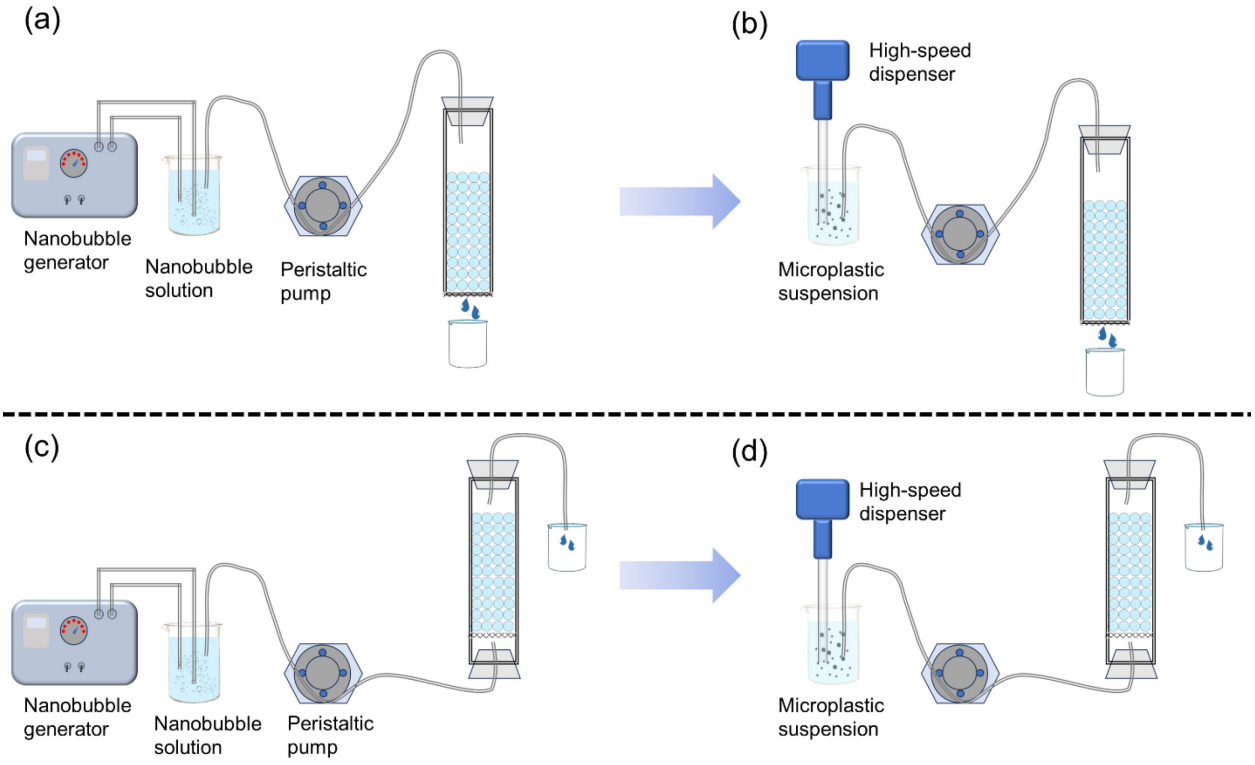


Figure 5.2 Apparatus of the column experiments. (a) and (b) are under ebb ride condition, (c) and (d) are under flood tide condition.

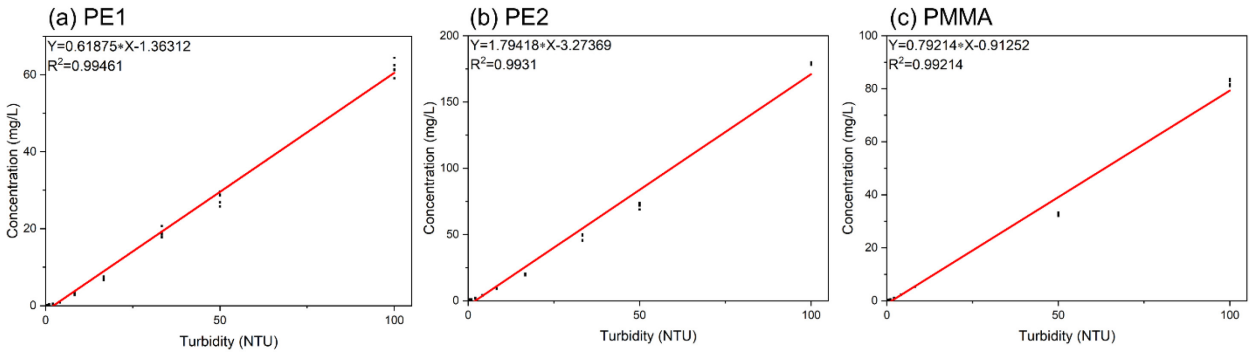


Figure 5.3 Standard curve of different MPs suspension

5.2.4 Theoretical considerations and model simulation

The interaction energies between MPs, NBs, and GBs were evaluated using the Derjaguin−Landau−Verwey−Overbeek (DLVO) theory (Feng et al., 2023a; Li et al., 2019; Wang et al., 2023a). The equation below was employed to determine the total interaction energy:

$$U_{total}=U_{vdw}+U_{el} \quad 5.1$$

where U_{total} is the total interaction energy; U_{vdw} is the Van der Waals interaction energy; U_{el} is the electrostatic interaction energy.

The interaction of MPs–MPs was treated as a particle–particle mode and was calculated as follows:

$$U_{vdw}=\frac{-Ar_1r_2}{6h(r_1+r_2)}\left(\frac{1}{1+\frac{11.12h}{\lambda_c}}\right) \quad 5.2$$

$$U_{el}=4\pi\varepsilon\varepsilon_0\frac{r_1r_2}{r_1+r_2}\left[\xi_1\xi_2e^{-\kappa h}-\frac{1}{4}(\xi_1^2+\xi_2^2)e^{-2\kappa h}\right] \quad 5.3$$

where A is the Hamaker constant; r_1 and r_2 are the radius of particle 1 and 2, respectively; h is the separation distance between two interacting particles; λ_c is the "characteristic wavelength" of the

interaction; ε is the dielectric constant of DI water; ε_0 is dielectric permittivity of a vacuum; κ is the inverse Debye length; and ξ_1 and ξ_2 are the ζ potentials of particle 1 and 2, respectively.

Since the size of MPs was greatly larger than the NBs, a particle–plate mode was employed in the DLVO calculation of MPs–NBs interactions:

$$U_{vdw}=\frac{-A}{6}\left(\frac{r_3}{h}+\frac{r_3}{h+2r_3}+\ln\frac{h}{h+2r_3}\right) \quad 5.4$$

$$U_{el}=\pi\varepsilon\varepsilon_0\left(\xi_1^2+\xi_2^2\right)\left[\frac{2\xi_1\xi_2}{\xi_1^2+\xi_2^2}\ln\frac{1+e^{-\kappa h}}{1-e^{-\kappa h}}+\ln\left(1-e^{-2\kappa h}\right)\right] \quad 5.5$$

where r_3 is the radius of the smaller one of the two particles.

The interactions of GB and MPs and GB and NBs were also obtained using the above equation based on the particle-plate mode. The ξ potential of glass beads was obtained by the following equations:

$$\xi=a+b\log C_f,\ C_f<0.4M \quad 5.6$$

$$\xi=c,\ C_f\geq 0.4M \quad 5.7$$

where ξ is the ξ potential, a is -9.67 mV, b is 19.02 mV, c is -17 mV, and C_f is the salinity.

To assess whether NBs were exerting a significant effect on MPs concentration in the effluent under different conditions, the paired *t*-test was used to verify the independence of the data obtained from the column study. (The normality and the dependency of the data were checked prior to conducting the paired *t*-test.)

HYDRUS-1D as a modeling software is capable of modeling water flow, as well as solute transport in matrices involved in successive first-order decay reactions. It can also deduce soil hydraulic parameters and solute transport parameters by analyzing specific measurements through reverse procedures. In the present work, the transport of MPs in the substrate was inversed based on the physicochemical parameters of the substrate in the column, flow rate, and concentration of MPs in the effluent by employing the van Genuchten model and Two Kinetic Sites Model built into the software. The first-order attachment coefficient (AttS1), the blocking function for the first sorption site (Smax1), the second-order attachment coefficient (AttS2), and the second-order detachment coefficient (DetS2) were combined with other parameters (including average size, pH, ζ potential, density of MPs suspension, pH of MPs suspension, flow rate, contact angle, salinity, and presence of NBs) in order to calculate the contribution of each to the diffusion coefficient.

5.3 Results and discussion

5.3.1 Mobilization of MPs under ebb tide in unsaturated substrate

Column tests were applied in order to study the infiltration of MPs in the substrate under various conditions. The change in concentration ratio of MPs over the pore volume (PV) as shown in Figure 5.4. When the flow rate was set to 2.5 mL/min, the concentration of MPs in the effluent became stable after 20 PV. Before reaching 20 PV, the concentration of MPs in the effluent did not show any correlation with the presence or absence of NBs. However, when the PV exceeded 20, the MPs concentration was marginally lower when NBs were present compared to when they were absent. Comparing the maximum concentration of MPs in the effluent under different flow rate conditions, it was observed that, at a PV of 20 to 30, the low flow rate of 2.5 mL/min promoted a higher concentration of PE1 in the effluent compared to at the higher flow rates of 5 mL/min and 10 mL/min.

When the flow rate was 5 mL/min or 10 mL/min and the PV was greater than 30, meanwhile, the concentration of MPs in the effluent ranged from 30% to 40% and was relatively stable. At a flow rate of 2.5 mL/min, the concentration of MPs in the effluent remained around 40% when the PV was greater than 60. In general, the infiltration of PE1 in the substrate differed significantly at a flow rate of 2.5 mL/min depending on whether the system had been pre-equilibrated with DI or with NBs ($p < 0.05$). However, after raising the flow rate to either 5 mL/min or 10 mL/min, the *p*-values exceeded 0.05, suggesting that the impact of NBs was not notable. For PE2, the MPs concentration in the effluent varied significantly depending on the flow rate. At a flow rate of 2.5 mL/min, the MPs concentration in the effluent increased rapidly in the interval between 15 PV and 25 PV and peaked in this range, then gradually decreased from 50 PV onwards. When NBs were absent, the concentration of MPs in infiltration was greater than that in the presence of NBs, even approaching 100%. When the PV exceeded 100, meanwhile, there was no difference in effluent MPs concentration between these two conditions (i.e., absence versus presence of NBs). When the flow rate was 5 mL/min, the PV was greater than 30, and there were no NBs, the concentration of MP in the effluent was stable at 80%, while it remained at 70% when under the same flow rate and PV but in the presence of NBs. The case with a flow rate of 10 mL/min was similar to that with a flow rate of 5 mL/min. When the PV exceeded 30, the effluent's MP concentration was higher in the absence of NBs than when NBs were present. This difference was even more pronounced than in situations with a flow rate of 5 mL/min. Importantly, the pattern of MP concentration in the effluent at a 2.5 mL/min flow rate was markedly different from that under the other two conditions. When the PV exceeded 30, the MPs concentration in the effluent gradually decreased, while, at other flow rates, the MPs concentration in the effluent remained stable. The *t*-test revealed that, in contrast to PE1, the PE2 concentration in the effluent was significantly influenced by the presence of NBs across all three flow rates. Meanwhile, PMMA showed completely different results from PE. At a flow rate

of 2.5 mL/min, the effluent MP concentration increased rapidly when the PV was less than 30, while the increasing trend slowed when the PV exceeded 30, and the concentration was lower in the presence of NBs than in the absence of NBs. As the flow rate was increased to 5 mL/min and 10 mL/min, the concentration of MPs in the effluent increased for the first 60 PV, then stabilized in the interval between 60 PV and 120 PV before decreasing when the PV exceeded 120. The *p*-values of the *t*-test results were less than 0.05 for different flow rates conditions, proving that the presence of NBs also significantly affected the concentration of PMMA in the effluent.

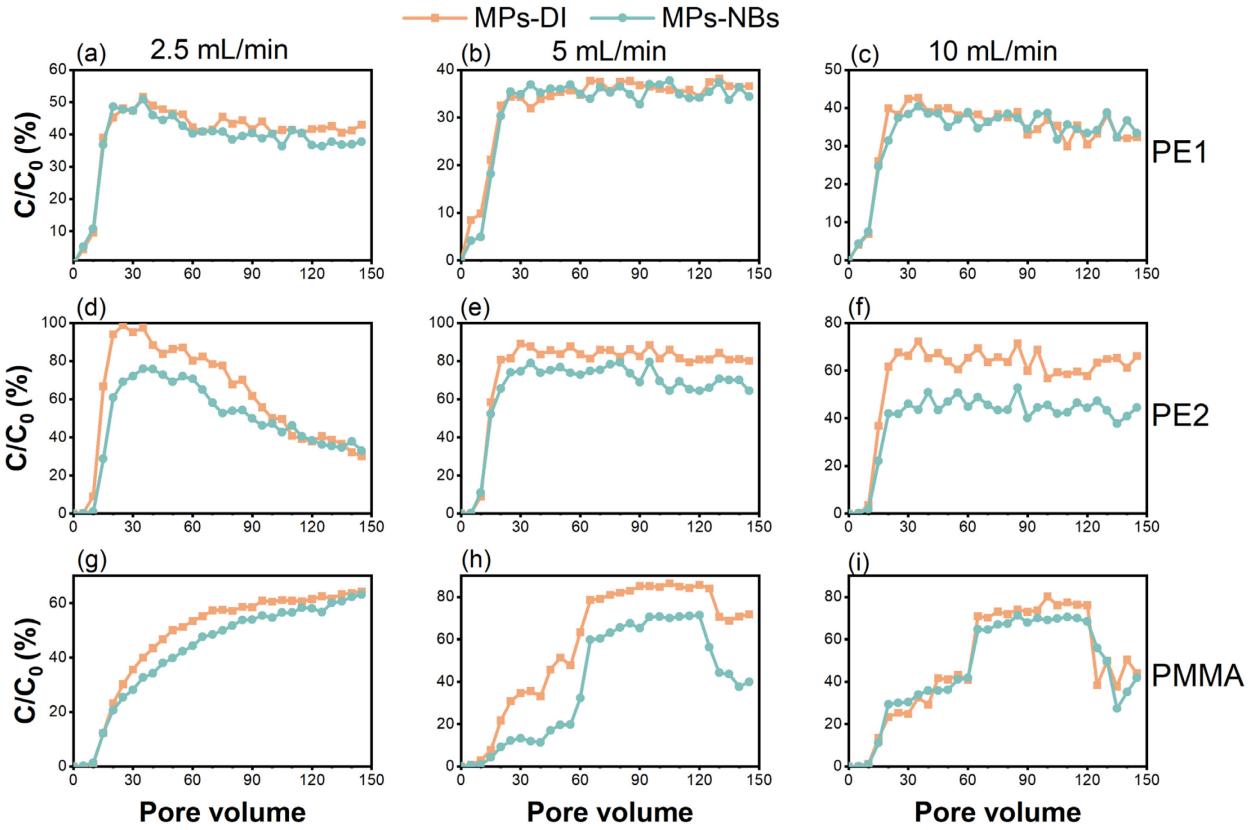


Figure 5.4 Mobilization of MPs under ebb tide in the unsaturated media

The effect of salinity on the infiltration of different MPs in the substrate when the flow rate was 5 mL/min is illustrated in Figure 5.5. Regarding PE1, at PVs less than 30, the concentration of MPs

in the effluent increased quickly and then remained stable. It can be seen that the presence of salinity led to a trend of decreasing MPs concentration in the effluent compared to the case of 0 salinity. When the PV was greater than 30, the MP concentration in the effluent stayed between 30% and 40% at a salinity of 0, regardless of the presence of NBs. However, the MPs concentration of the stabilized effluent was less than 30% when the salinity increased. Compared with the presence of NBs did not affect the concentration of MP in the effluent when the salinity was 0. At salinity levels of 10 psu, 25 psu, and 35 psu, the *p*-values were all below 0.05. This suggests that the NBs contributed to a reduction in the MP concentration in the effluent, with this difference being more pronounced at higher salinities. PE2 and PE1 showed similar trends in that the concentration of MPs in the effluent increased significantly when the PV was less than 30 and stabilized when the PV was greater than 30. Moreover, the introduction of salinity caused a decrease in the peak concentration of MPs in the effluent. When the salinity was 0, the MPs concentration in the effluent leveled off at 60%–90% for PVs exceeding 30, whereas, at salinities of 10, 25, and 35 psu, the maximum MPs concentration in the effluent was less than 50%, and it decreased slightly with the continuous increase of PV. In contrast to PE1, the influence of NBs on the concentration of PE2 in the effluent was less pronounced under saline conditions than under non-saline conditions. When the salinity was 35 psu, the change in the concentration of PE2 in the effluent was almost the same under the two conditions. The results of the *t*-test also verified this conclusion. The *p*-value was greater than 0.05 at a salinity of 35 psu, while, in all other conditions, the *p*-values were less than 0.05. Regarding PMMA, the distinguishing feature was that the concentration of MPs in the effluent greatly increased for PVs exceeding 60 and under salinity conditions, whereas this increase was smooth when the salinity was 0. Although the trend of changing concentration of PMMA in the effluent was different from those of PE1 and PE2, the salinity effect was similar between PMMA and PE2 in that the effect of NBs on the concentration of MPs in the effluent was diminished under high salinity conditions.

p-values were greater than 0.05 for salinities of both 25 and 35 psu and less than 0.05 for salinities of 10 psu and even 0 psu. Moreover, the concentrations of PMMA in the effluent were 80%–90% in the absence of NBs, while they ranged from 60% to 70% in the presence of NBs.

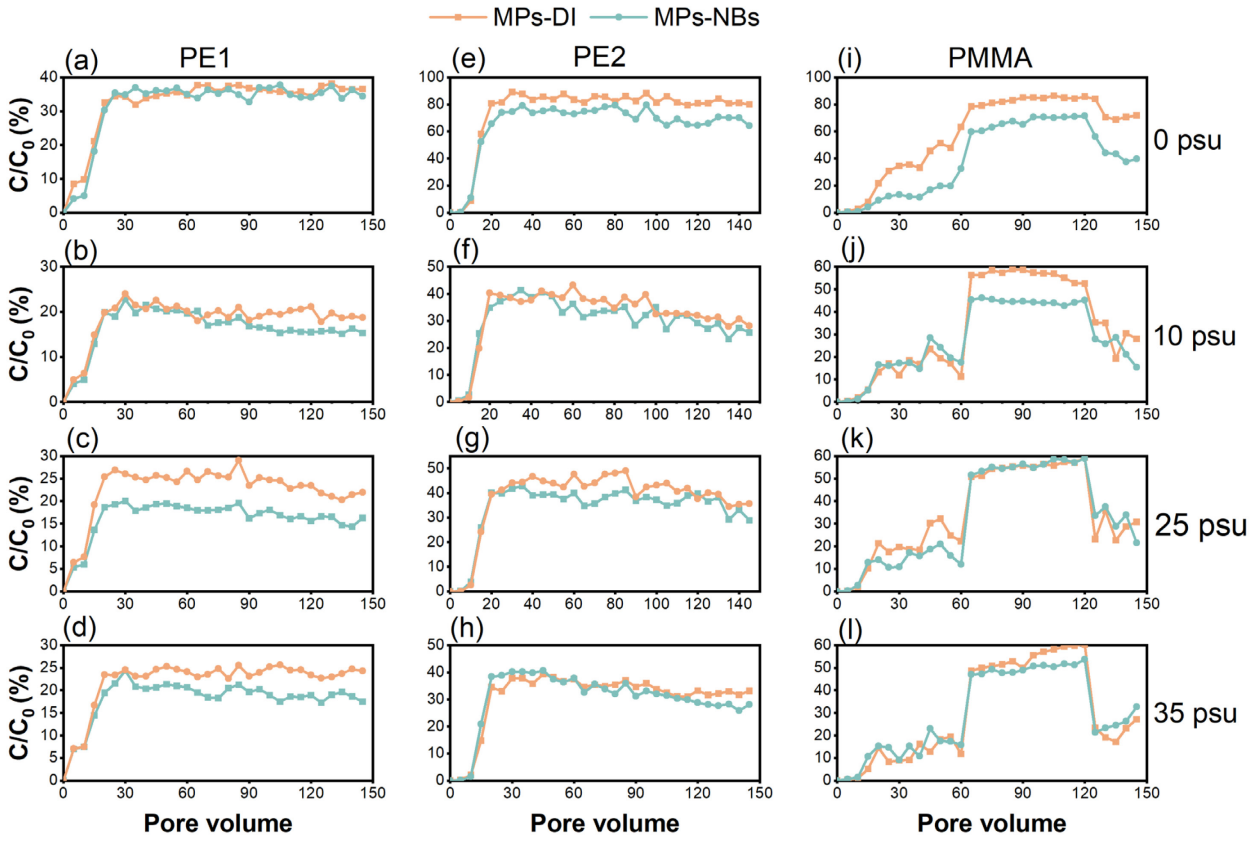


Figure 5.5 Effect of salinity on the mobilization of MPs under ebb tide in the unsaturated media

5.3.2 Mobilization of MPs at transient flow under ebb tide condition

Rising tides or waves washing up on the beach carry seawater containing MPs into the beach substrate, and from there in then seeps into the groundwater table through the vadose zone. This kind of infiltration is temporary since waves hit the beach periodically. The infiltration of three types of MPs solutions under these transient conditions was explored at a salinity of 0 and a flow rate of 5 mL/min. For PE1, the changes of MPs concentration were comparable under steady and transient

infiltration conditions. However, the presence of NBs affected the MPs concentration in the effluent under transient infiltration ($p < 0.05$), leading to a decrease in the PE1 concentration in the effluent. Another interesting phenomenon is that, in the case of transient infiltration, the concentration of MPs in the effluent stabilized between 40%–50% when the PV was greater than 30 (i.e., slightly greater than in the case of steady infiltration). However, the concentration of PE2 in the effluent did not differ significantly between the two infiltration conditions, and the presence of NBs had no additional effect.

In the case of transient infiltration, the concentration of PMMA in the effluent showed entirely different patterns compared to PE1 and PE2. Figure 5.6(c) and Figure 5.6(f) show that, when the PV was less than 50, the concentration of PMMA in the effluent increased in both steady and transient infiltration scenarios. When the PV exceeded 50, the PMMA concentration in the effluent surged for the steady infiltration scenario. In contrast, during the transient infiltration scenario, there was a noticeable decline between 50 PV and 55 PV, but this was followed by a swift rise starting at 55 PV. A similar phenomenon occurred when the PV was between 100 and 105. The concentration of PMMA in the effluent remained stable under steady infiltration, but there was also a significant decrease in PV from 100 to 105 under transient infiltration. In contrast to the previous trend of a decrease followed by a sharp increase at the PV of 55, the PMMA concentration in the effluent did not increase rapidly when the PV was greater than 105, but rather increased in a gradual and oscillating pattern. Moreover, in the steady infiltration scenario, the concentration of PMMA in the effluent decreased when the PV was greater than 120 and then increased when the PV exceeded 140. For transient infiltration, the concentration of PMMA in the effluent did not show a similar phenomenon at a PV of 120. Comparing the concentration of PMMA after the two interruptions, it can be seen that the concentration at PV 105 was greater than that at PV 55. Another interesting

phenomenon was the disappearance of the influence of NBs on the concentration of MPs under the transient infiltration condition ($p > 0.05$). The behavior and transport of various MP suspended in the substrate varied under the transient infiltration condition. Although PE1 and PE2 have different particle sizes, their transport within the substrate and the concentration patterns of MPs remained largely consistent between the two under both steady and transient infiltration conditions. The concentration of MPs in the effluent showed continuity before and after the interval. For PMMA, on the contrary, there was a clear break in the concentration of MPs in the effluent before versus after the interval.

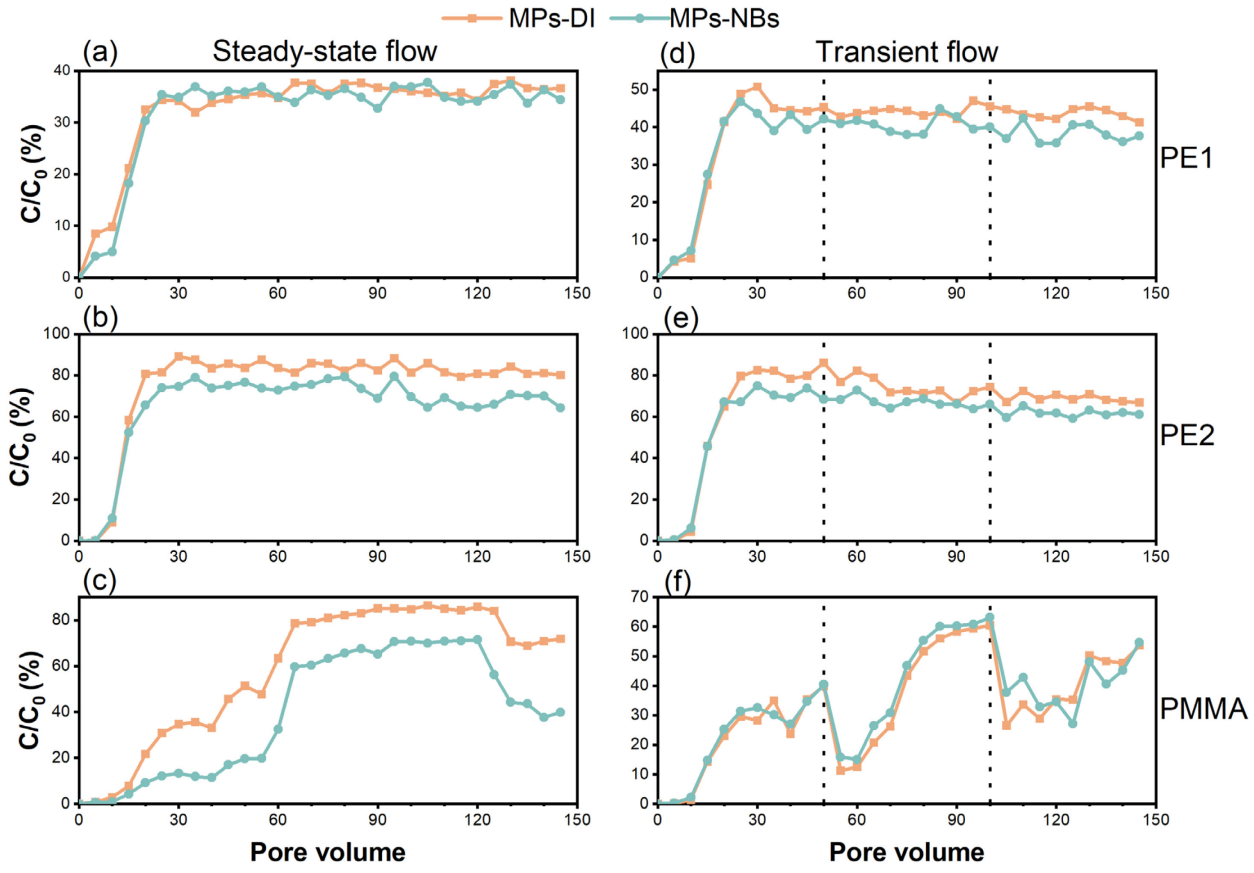


Figure 5.6 Mobilization of MPs at transient flow under ebb tide condition

5.3.3 Mobilization of MPs under flood tide in saturated substrate

Tide-induced upward transport of MPs within the coastal substrate was also studied. Because the transport of pollutants in this case is stable and continuous, only the behavior of MPs in the steady-state transport scenario was explored (i.e., the transient condition was not considered). Figure 5.7 demonstrates the relationship between MP concentration and PV at three different flow rates. For PE1, the concentration of MPs in the effluent was already high compared to the infiltration scenario when the PV was only 5, regardless of the flow rate. The concentration of PE1 in the effluent at the three flow rates was 33.7%, 20.8%, and 33.4% when NBs were present compared to 19.5%, 17.65, and 21.9% when NBs were not present. While the concentration of PE1 in the effluent in the presence of NBs was close to that in the absence of NBs when the PV was between 10 and 30, the overall trend showed that the presence of NBs contributed to an increase in the concentration of PE1 in the effluent. This observation was corroborated by *t*-test. The maximum concentrations of PE1 in the effluent were less at flow rates of 5 mL/min and 10 mL/min than that at a flow rate of 2.5 mL/min. However, the maximum concentration of PE1 in the effluent at a flow rate of 10 mL/min was slightly greater than that at a flow rate of 5 mL/min. In addition, the *p*-values of the *t*-test decreased with increasing flow rate, proving that the presence of NBs also enhances the effect of MPs concentration in the effluent. Compared to PE1, where the concentration of MPs in the effluent was essentially stable when the PV was less than 30, the concentration of MPs in the effluent of PE2 stabilized when the PV was greater than 30, i.e., similar to the infiltration scenario. Changes in flow rate did not significantly affect the trend of MPs concentration in effluent with PV. The concentration of PE2 in the effluent remained roughly within the range 70%–90% when the PV was greater than 30 for all of the flow rates observed. In addition, NBs significantly affected the MP concentration in the effluent at all flow rates except at a flow rate 5 mL/min, in which case the effect of NB was negligible for the PE2 concentration in the effluent ($p > 0.05$). Regarding the PMMA, the pattern of

concentration of MPs in effluent varied depending on the flow rate. When the flow rate was 2.5 mL/min, the concentration of PMMA in the effluent showed a pattern of continuous growth coinciding with the increase of PV. The maximum concentration of PMMA in the effluent in the absence of NBs was 40.7%, while, in the presence of NBs, it was only 32.7%. The presence of NBs resulted in a smaller concentration of PMMA in the effluent than in the absence of NBs, and the difference between the two conditions intensified with increasing PV ($p < 0.05$). The most striking feature of the trend in PMMA concentration in the effluent when the flow rate was 5 mL/min was that it was clearly influenced by the presence of NBs. The maximum concentration of PMMA in the effluent was 48.4% when NBs were absent, compared to 24.8% when NBs were present. In the absence of NBs, the concentration of PMMA in the effluent rose slowly when the PV was between 5 and 60, while there was a rapid increase for PVs in the range of 60–65, and then the concentration was basically stable at 40%–50% when the PV exceeded 65. In the presence of NBs, the overall trend of PMMA concentration in the effluent maintained a pattern of slow growth as the PV increased, although there was a small decrease during the PV ranged of 50–55. At a flow rate of 10 mL/min, the respective maximum concentrations of PMMA in the effluent under the absence and presence of NBs were 81.0% and 53.2% greater than under the other two flow-rate scenarios, regardless of the presence or absence of NBs. Similar to the case with a flow rate of 5 mL/min, the concentration of PMMA in the effluent showed an increasing trend when the PV was less than 60, whereas the concentration remained stable when the PV exceeded 60. In addition, as the flow rate increased, the *p*-value became smaller, implying that the effect of the presence of NBs on the concentration of PMMA in the effluent was also enhanced.

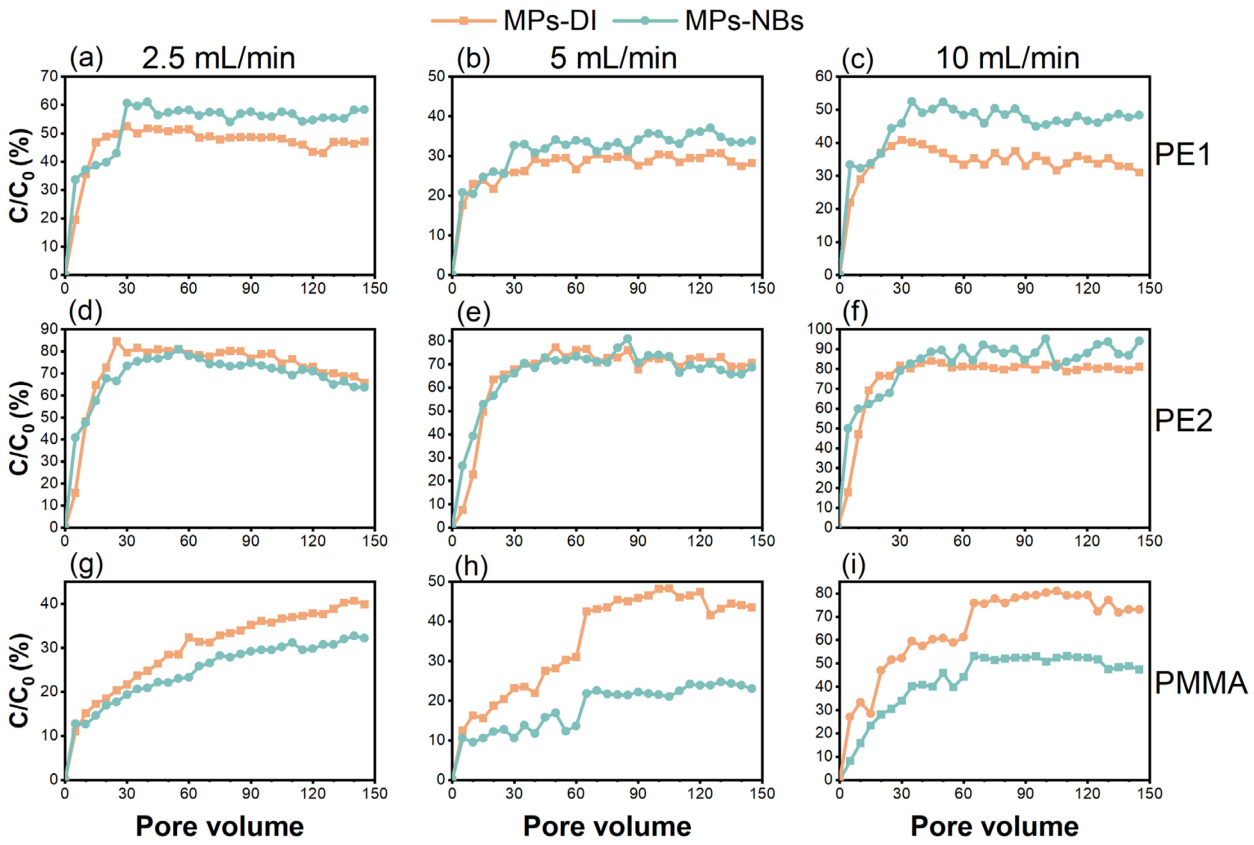


Figure 5.7 Mobilization of MPs under flood tide in saturated media

The impact of salinity on the upward movement of MPs within the substrate is depicted in Figure 5.8. As in the infiltration study, all flow rates were set to 5 mL/min and four different salinity gradients were compared. For PE1, the concentrations of MPs in the initial effluent (PV of 5) when no NBs were present were 17.6%, 20.6%, 17.8%, and 18.9% at salinities of 0, 10, 25 and 35 psu, respectively; when there were NBs present, meanwhile, the concentrations were, respectively, 20.8%, 30.5%, 30.3%, and 27.3%. Irrespective of whether NBs were present or not, the concentration of MPs in the initial effluent at a salinity of 0 was less than under the other conditions. The concentration of PE1 in the effluent increased when the PV was less than 30, while, when the PV was greater than 30, the concentration continued to increase in the case of 0 salinity but decreased in the other salinity conditions. Moreover, in the presence of NBs, the concentration of MPs in the

effluent decreased with increasing salinity compared to in the absence of NBs. Even at a salinity of 35 psu, the concentration in the effluent was lower than that in the absence of NBs. For PE2, which has a much smaller particle size, the trend of MP concentration in the effluent had similar characteristics to that of PE1. When the PV was below 30, the MPs concentration in the effluent surged across various salinity levels. Nonetheless, it is important to highlight that the MP concentration in the effluent was higher during this time when NBs were present compared to when they were absent. With a PV greater than 30, the concentration of MPs in the effluent remained stable at a salinity of 0 and showed a slight downward trend in the presence of salinity. The difference in MPs concentration in the effluent due to the presence of NBs was progressively significant with increasing salinity. The *p*-value was less than 0.05 under both 25 psu and 35 psu conditions, in contrast to the almost overlapping pattern of curves under salinity conditions of 0 psu and 10 psu salinity ($p > 0.05$). Regarding the PMMA, the presence of salinity modified the effect of NBs on the concentration of MPs in the effluent. Compared to the salinity condition of 0, where the maximum concentration of MPs in the effluent was less than 25%, the maximum concentrations of MPs in the effluent at salinities of 10, 25, and 35 psu were 53.8%, 55.2%, and 64.0%, respectively. The same phenomenon was observed when NBs were absent. The maximum concentrations of MPs in the effluent were 47.5%, 54.7%, 52.1%, and 54.8% for salinities of 0, 10, 25, and 35 psu, respectively. Also of note is that the nodes at which the MPs in the effluent remained stable varied with and without salinity. At salinity 0, the concentration of MPs in the effluent increased and then stabilized when the PV reached 60, whereas, under other salinity conditions, the concentration increased rapidly for PVs less than 30 but stabilized for PVs greater than 30.

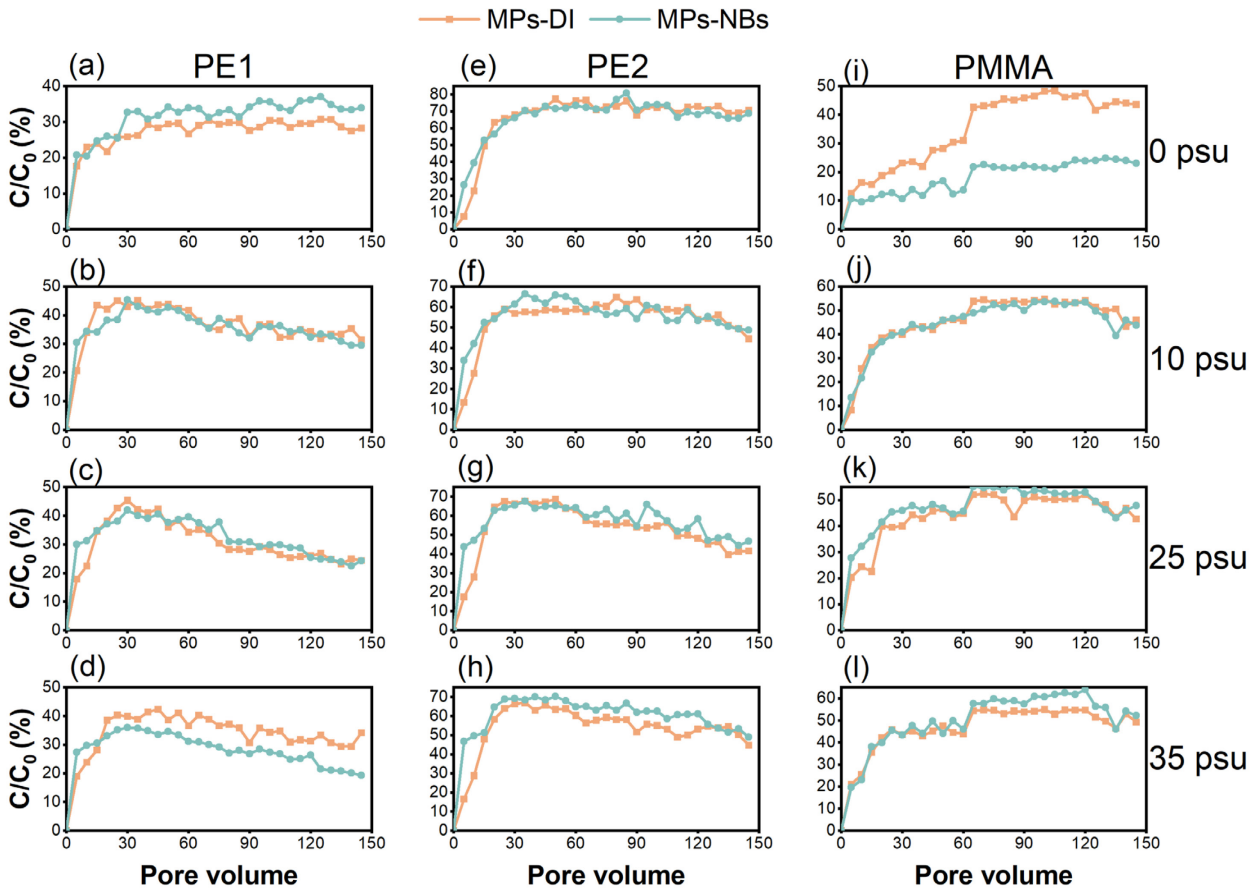


Figure 5.8 Effect of salinity on the mobilization of MPs under flood tide in saturated media

5.3.4 Theoretical analysis of MPs motion in the substrate

Ionic strength can both modify the movement of MPs in the porous matrix and indirectly affect solute transport by altering the properties of the NBs solution. Figure 5.9 demonstrates the variations in MPs–NBs interaction energy and MPs-–GB interaction energy with interparticle distance. As explained above, in order to calculate the interaction energy between particles at a salinity of 0, the salinity of 0.001M was used to represent the case of 0 salinity. It was observed that changes in salinity altered the interaction energy between PE1 and GBs. It was assumed that, with a salinity of 0, a large repulsive force would be maintained between PE1 and GBs. When the salinities were 10, 25 and 35 psu, the force between PE1 and the GBs shifted from attractive to repulsive as the distance

increased, and the higher the salinity was, the lower the energy barrier was. The PE1–NB interaction energy also shifted from attractive to repulsive as the distance increased when the salinity was 0. However, for salinities of 10, 25 and 35 psu, there was always a repulsive force between PE1 and NBs as distance increased, and this repulsive force gradually decreased. Furthermore, the rise in salinity lowered the energy barriers between PE1 particles. Even at a salinity of 35 psu, there was a prevailing attractive force among the PE1 particles, suggesting that they are more likely to cluster together under high salinity conditions. This also suggests that, as the MPs moved downward in the column, the increased salinity led to easier aggregation between the PE1 particles, and that this, in turn, contributed to the formation of larger particle sizes. Due to the increase in particle size, meanwhile, the spatial site resistance caused PE1 to become less easily transported downward and therefore more likely to be retained in the substrate. At the same time, increasing salinity lowered the energy barrier between PE1 and GBs. This made some PE1 bond with GBs, reducing PE1 concentration in the effluent. Higher salinity also diminished the energy barrier between PE1 and NBs, causing them to combine. The energy barrier between NBs and GBs was so small, in fact, that NBs became tightly attached to GBs, further contributing to partial retention of PE1 on the substrate. On the contrary, at a salinity of 0, the high repulsive force between PE1 and NBs as well as GBs, together with the lack of aggregation between PE1 particles, resulted in a high concentration of PE1 in the effluent and a lack of retention of NBs on PE1. For the case of upward transport, when the salinity was 0, MPs were subjected to more surface tension in the saturated environment, and this promoted their upward movement (since the MPs did not easily attach to GBs or NBs under these conditions). However, with increasing salinity and longer residence time, more PE1 tended to remain within the substrate, and thus the PE1 concentration in the effluent showed a decreasing trend with increasing PV. The interaction energy between PE2 particles, between PE2 and GBs, and between PE2 and NBs was similar to that of the interactions involving PE1. Salinity lowered the

energy barrier between particulate matter, resulting in more PE2 being retained within the substrate. Because PE2 has smaller particles, when the salinity is at 0, the repulsion between the particles makes the PE more prone to being carried away by water. As a result, the amount of PE2 in the discharge was notably greater compared to under other salinity conditions.

Unlike with PE, in the case of PMMA, when the salinity was 0, the interaction between PMMA and GBs was dominated by the force of attraction, whereas when the salinity increased from 10 to 35 psu, the attraction between PMMA and GBs came to be dominated by the repulsive force with the increased distance, and the energy barrier gradually decreased as well. PMMA–NB interactions, on the other hand, were characterized by repulsive forces that decreased with increasing salinity. Similarly, the energy barrier between PMMA particles was larger at salinity 0 than under other salinity conditions, but it was still smaller than the energy barrier between PE particles at salinity 0. With increasing salinity, PMMA particles were more likely to aggregate with each other. However, it is worth noting that PE is hydrophobic, whereas PMMA is extremely hydrophilic, so even when the salinity was 0, PMMA was attractive to GBs, and there was still a high concentration of PMMA in the effluent. The presence of NBs reduced the affinity between PMMA and DI water, leading to a weakening of the downward transport in water. In addition, for all three MP types, the concentration trends at 2.5 mL/min were different from those at both 5 mL/min and 10 mL/min, presumably because the saturation of the substrate at low flow rates was different from that at high flow rates, with this indirectly affecting the attachment and detachment capacity of GBs for both NBs and MPs.

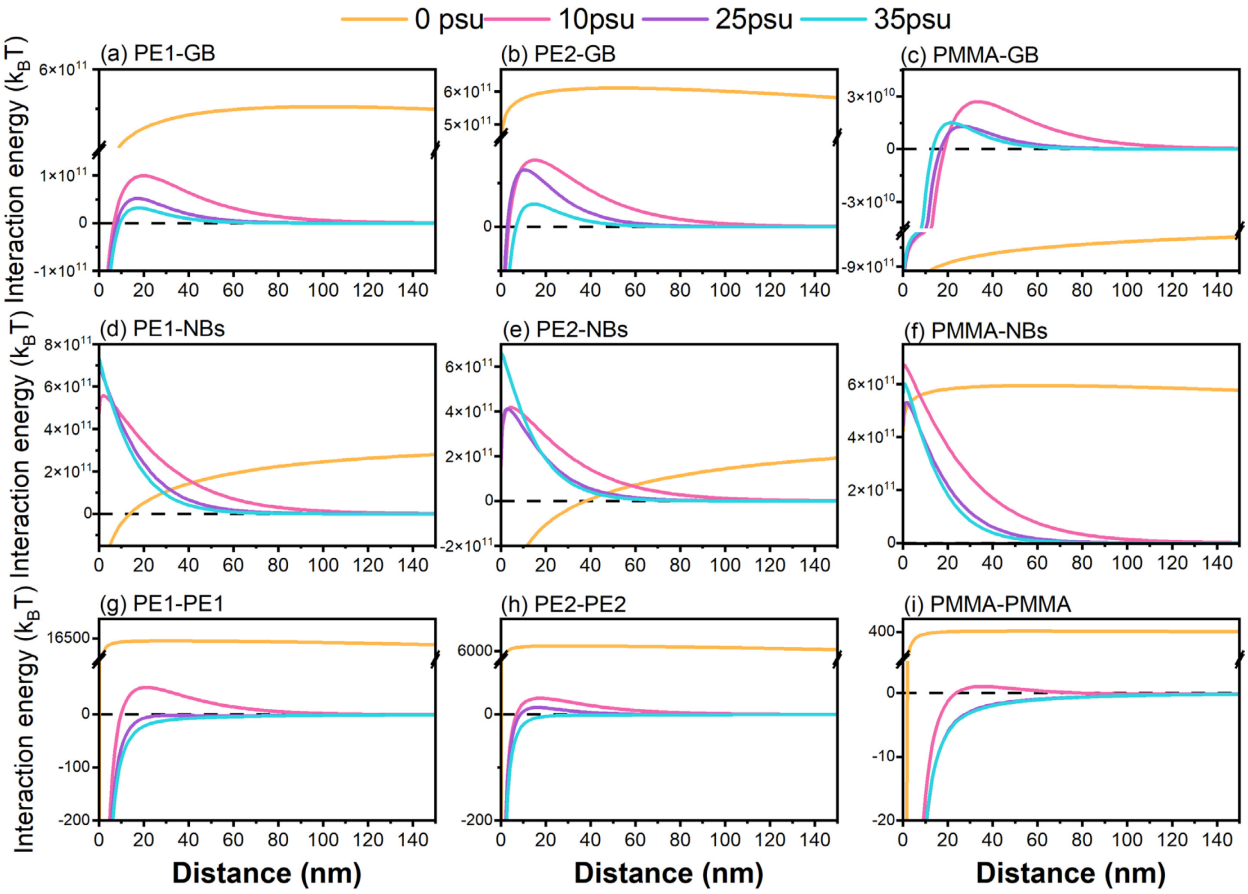


Figure 5.9 Interaction energy between particles under different salinity conditions

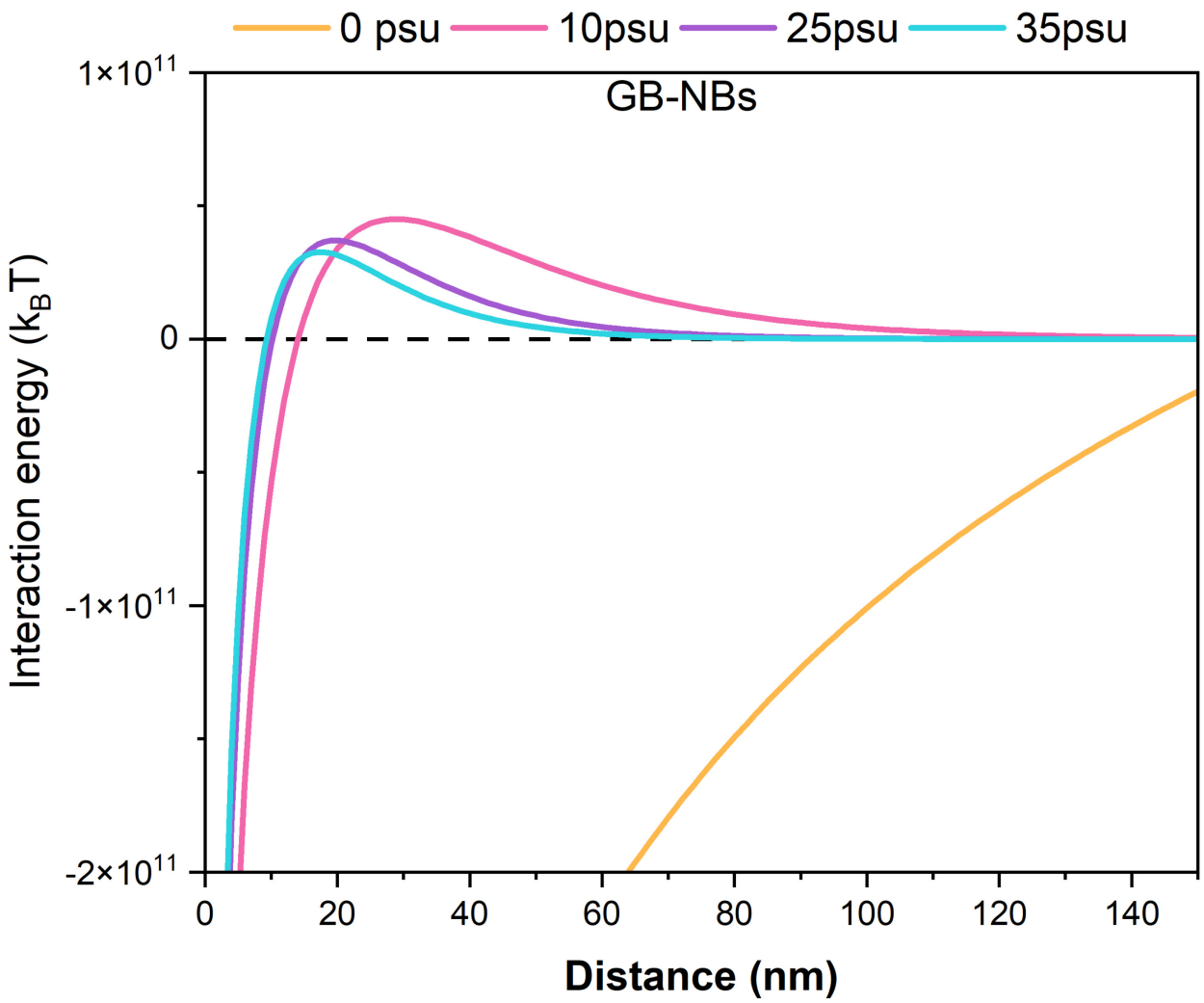


Figure 5.10 The interaction energy between NBs and GB

Based on the experimental data, the inverse simulation of each transport process was performed using HYDRUS–1D, and the coefficients of dispersion, attachment, and detachment parameters for two kinds of sorption sites were obtained. Figure 5.11 illustrates the contribution of each parameter to the diffusion coefficient. As can be seen, the most significant influence on diffusion was the attachment coefficient at the second sorption site, followed by the detachment coefficient at the second sorption site and the attachment coefficient at the first sorption site. This indicates that the introduction of the second sorption site can better explain the transport of MPs in the substrate, an

inference consistent with the findings of previous studies. In the present study, NBs as a newly introduced substance altered the adsorption capacity of GBs after being attached to the surface of GBs. The difference between the two kinds of sorption sites may be attributable to the presence of NBs in the substrate. Although the contribution of NBs was less than 0.1 in the regression analysis, they affected the physicochemical properties of the substrate and acted on the dispersion of MPs through other parameters. Moreover, salinity was a key parameter affecting the diffusion. Contact angle, finally, had a negative effect on the diffusion coefficient, confirming that hydrophilic MPs are more likely to transport.

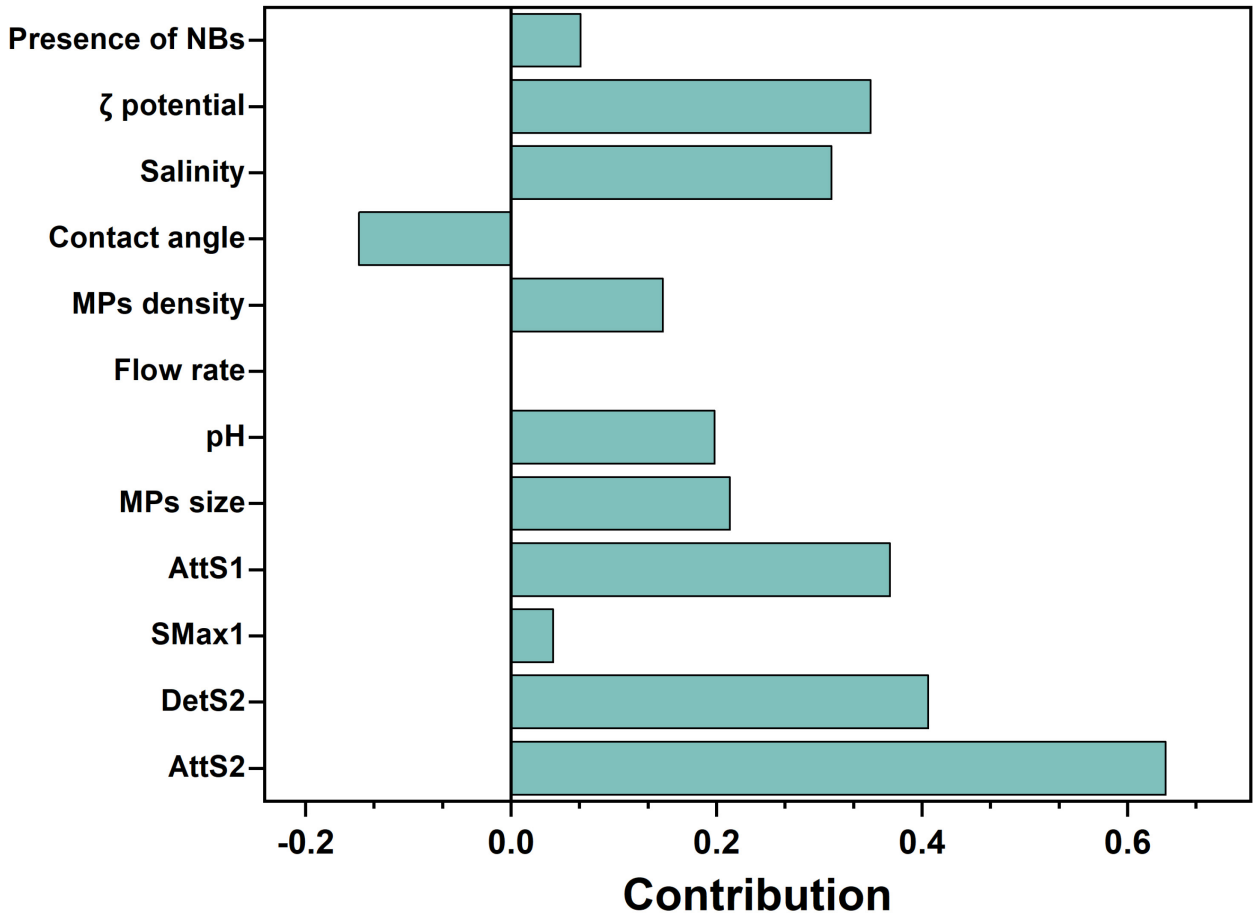


Figure 5.11 The contributions of each parameter to the diffusion coefficient based on inversion simulation

5.3.5 Environmental implications

The transport and fate of MPs in the natural environment have received extensive attention within the research community, but most studies have focused on either their environmental behavior under conventional conditions or their co-transport with other pollutants. In the present study, NBs were found to play a significant role in MPs movement within the substrate under various conditions. The MPs concentration in the effluent was found to vary depending on the flow rate, and NBs were found to limit the vertical motion of MPs within the substrate. Attraction between NBs and GBs was also observed, meaning that, once a solution containing NBs flows through the substrate, NBs are highly susceptible to attaching to GBs, and this, in turn, alters the surface properties of GB, in particular their ability to attach to and detach from other substances. For PE1 and PE2, the HYDRUS–1D inversion simulation aligned well with the experimental results, suggesting the feasibility of using the Two Kinetic Sites Model to analyze the movement of MPs within the substrate. This also verified that NBs indeed changes the surface properties of GBs, forming two sorption sites with different attachment and detachment properties. However, for PMMA, the results of the inversion simulation did not align as well with the experimental data as in the case of PE, especially for flow rates of 5 mL/min and 10 mL/min, where the R^2 was less than 0.9. The experimental results show that, as the PV increased, the concentration of PMMA in the effluent increased abruptly at a certain point, followed by a 'plateau' period during which the concentration remained almost constant, and then a subsequent drop in concentration. However, the model struggled to capture this pattern. The characteristic of PMMA that clearly distinguishes it from PE is its better hydrophilicity. Since PE is hydrophobic, the interaction of PE with GBs and NBs was a key parameter in determining PE transport in the present study, particularly considering that the formation of different sorption sites due to the presence of NBs could explain the vertical movement

in the substrate. For PMMA, however, the ‘sorption’ of water was apparent, suggesting that there are unknown sorption sites with different properties than the two currently known sorption sites. Given this consideration, one proposed avenue of future research would be to develop applicable models or methods for substances with different physicochemical properties.

The transport of MPs in in coastal vadose zones is highly complex in terms of both the constraints of the natural environment and the physicochemical properties of the MPs themselves. Meanwhile, there are unknown factors that can have a direct or indirect effect on the fate and transport of MPs. NBs, as a ubiquitous but poorly understood substance in oceans, especially prevalent in near-surface regions, has received very little attention in terms of its effect on the natural environment and even on the transport and transformation of pollutants. The persistence of NBs is one of its most notable characteristics. After invading the beach with the waves or tides, it not only adheres to the substrate, but may also be free in the aqueous phase of the pores within the substrate. However, it should not be overlooked that, unlike other effects of co-transport of multiple pollutants in a given environment, the effect of NBs on the transport of other pollutants within the substrate is dynamic due to the properties of NBs themselves. The intricate nature of the natural environment results in the creation of NBs with varying sizes, lifespans, and traits. Moreover, due to the constraints of existing analytical methods, it is difficult to directly study NBs in their natural setting through field research. As such, the laboratory production of NBs with the same physicochemical properties as those found in their natural setting and the subsequent simulation of the corresponding natural environment provide effective means of studying the role of NBs in natural environments.

In contrast to the transport of conventional pollutants such as organics and metals, the transport of MPs in the natural environment is often accompanied by physical, chemical, and biological

processes, and the stability of the plastic properties limits the chemical and other changes. As such, only the effects of NBs on the diffusion and transport of the MPs in the substrate were considered in this study, whereas it was not examined whether chemical changes had occurred. In fact, NBs could enhance the oxidizing ability of the solution and degrade organic pollutants such as spilled oil in shorelines. Our previous studies found that some low weight *n*-alkanes in oil spills can be degraded by NBs (Wang et al., 2023b). Investigation of the changes to the physicochemical properties of MPs brought about by the presence of NBs over an extended period of time, especially changes to the surface structure in terms of functional groups—as well as the interactions between MPs and other substances in the natural environment—can yield useful insights concerning the migration and transport of MPs in substrates. Moreover, air NBs can enhance the level of dissolved oxygen in solutions, and this change can influence micro-ecosystems, notably microbial growth. Such effects are crucial in understanding the development and characteristics of biofilm on the surface of the MPs over an extended duration. Our future research will explore MPs prevention and remediation strategies centered on NBs, building on the emerging body of knowledge in this domain.

Chapter 6. Disposable masks release microplastics to the aqueous environment with exacerbation by natural weathering[5]

6.1 Background

With the spread of the coronavirus (SARS-CoV-2), as of March 2021, a total of more than 115 million cases have been diagnosed around the world (Johns Hopkins University Coronavirus Resources Cenrer, 2021). Based on emerging evidence early in the pandemic, the World Health Organization (WHO) recommended wearing surgical masks or other face covering to prevent airborne transmission of the virus (World Health Organization, 2020), leading to a dramatic increase in the demand for disposable face masks (Gereffi, 2020). Due to the shortage of disposable mask stock and the increase in prices, the public was encouraged to use alternative face coverings in the early stage of the pandemic. However, with increasing production capacity, the supply and use of disposable masks have gradually increased to unprecedented levels. For example, the daily production of disposable masks in China increased from 20 million in January, 2020, to 200 million in March, 2020 (Organisation for Economic Co-operation and Development, 2020). It is estimated that more than 129 billion face masks are consumed globally every month (Prata et al., 2020).

However, the explosive growth in the use of masks has introduced numerous issues related to the disposal and management of waste masks (Patricio Silva et al., 2021; Prata et al., 2020). A large amount of mask waste is discarded without any treatment, as a result of inappropriate waste

[5] This work has been published as Wang, Z; An, C; Lee, K; Zhang, B; Feng, Q. 2021. Disposable masks release microplastics to the aqueous environment with exacerbation by natural weathering. Journal of Hazardous Materials, 417, 126036.

management and the lack of environmental awareness (Cordova et al., 2021; Haque et al., 2021). Various types of masks have been widely observed on shorelines, rivers, lakes and in the aqueous environment (Aragaw, 2020; Canning-Clode et al., 2020; Fadare and Okoffo, 2020). The masks themselves pose a direct threat to marine life (Guzzetti et al., 2018). Moreover, the plastic fragments or MPs derived from masks can further cause many other environmental problems. MPs even nano-size plastic particles (less than 100 nm) are widely present in marine (Andrady, 2011), sediments (Lin et al., 2020), soil (Corradini et al., 2019; Yin et al., 2015), freshwater (Li et al., 2018), the atmosphere (Zhang et al., 2020), and other environmental matrices (Geilfus et al., 2019; Kanhai et al., 2019). Recent studies have revealed that MPs can also be released from teabags (Hernandez et al., 2019), cigarette butts (Belzagui et al., 2020), food containers (Du et al., 2020; Fadare et al., 2020), disposable paper cups (Ranjan et al., 2020), personal care products (Hernandez et al., 2017b), and other household and industrial products (Dibke et al., 2021; Hernandez et al., 2017a). Not surprisingly, evidences of MPs in living organisms is now being discovered. MPs can accumulate and transfer within plankton, fish, and birds through the food chain (de Sa et al., 2018). What is more shocking is that MPs have been found in the human colon (Ibrahim et al., 2021), and even in the human placenta (Ragusa et al., 2021). Therefore, it is necessary to investigate the potential release of MPs from disposable face masks to determine the pollution risk and improve waste mask management.

The commonly used disposable masks are made from polymeric materials, especially polypropylene. A standard disposable mask typically consists of 3 layers: the outer hydrophobic spun bond layer, a middle melt-blown layer, and an inner non-woven layer. The plastic can be weathered when it is subjected to UV irradiation, mechanical abrasion, oxidation, and biodegradation, leading to changes in physical and chemical properties. On the one hand, the surface of the virgin polymer will become

rougher after weathering, making the plastic more friable and prone to form small fragments, even MPs and NPs (Cai et al., 2018; Song et al., 2017). On the other hand, the adsorption ability of weathered plastic to organic matter or other pollutants will increase after disposal and introduced to the environment (Liu et al., 2020b; Liu et al., 2020c). As large numbers of improperly disposed masks enter the ocean, the risk disposed plastics pose to the marine ecological system is exacerbated, particularly in shoreline environments (De-la-Torre et al., 2021). The coast, it should be noted, is a complex environment that comprises seawater, underwater, soil, atmosphere, and other environmental factors (Bi et al., 2021; Chen et al., 2019). Discarded disposable masks on beaches will be further weathered when exposed to natural factors such as sunlight (including UV irradiation), sand abrasion, and sea waves (De-la-Torre and Aragaw, 2021; Kotek et al., 2004; Song et al., 2017). With the increasing presence of waste masks on shorelines, it is critical that the environmental effect of disposable masks on the shoreline environment be evaluated in a timely manner. In this context, the main objective of the study described in this paper was to explore the changing characteristics and environmental behaviors of disposable masks when exposed to the shoreline environment. Disposable masks were subjected to weathering, followed by the characterization through various methods. The phenomenon of MPs being released from disposable masks to the aqueous environment, compounded by natural weathering, was then explored.

6.2 Methods

6.2.1 Materials and chemicals

Ecoparksg disposable masks were purchased from Fisher Scientific (Canada). The elastic earloop and nose bridge were first removed, and the rest of the mask was then cut into strips (1.5 cm × 14 cm). Some virgin mask strips were placed in glass Petri dishes uncovered, then exposed to UV light

(254 nm, 20 mW/cm^2) for 1 to 48 h in a UV chamber (CX-2000 Crosslinker, Analytik Jena, USA). Control samples were placed in glass Petri dishes and wrapped in aluminum foil before exposure in the UV chamber under the same conditions as the exposed samples. The mask strips (outer layer, middle layer, and inner layer) with different irradiation times and 50 mL of deionized (DI) water were added into the Erlenmeyer flask in the absence and presence of sand (20 g). The flasks were placed in a New Brunswick Innova 42R incubator shaker (Eppendorf, USA) with 300 rpm and 25 ℃ for 24 h. The calcinated quartz standard sand was obtained from MilliporeSigma (Canada), and the particle size of the solid sand is 0.2-0.8 mm. Before the formal experiments, the sand was washed with DI water and dried in an oven under 60 ℃ for 24 hours to remove the impurities. Since the solid sand was settled in the bottle of the flask, the sand had no effect on the results when the particle size of MPs in the aqueous phase was analyzed. The potential effect of remaining micro or nano particles released from sand was also considered. The sand and DI water were added to the flask and shaken in a shaker for 24 hours prior to experiment. The particle size of remaining substances from sand in water samples was analyzed by two different particle analyzers (LISST-200X, size range: 1-500 μm; Zetasizer ZS, Malvern, size range: 0.3 nm-10 μm). Then, we poured out the water and added fresh DI water to the flask. We repeated the previous step until the particle size in the water was smaller than the range we concerned. Finally, we poured out all the water and dried the sand for later use. The final particle size distribution in the water with only sand obtained by different particle size analyzers is shown in the Figure 6.1. It can be found that the particle size of remaining substances from sand in the aqueous phase was mostly in the nano scale. Although some particle size fractions were larger than 1 um, most of them were smaller than the range we concerned, that is 5-500 um. At the same time, the concentration of MPs was obtained by subtracting the sand concentration from the total concentration. Therefore, the sand had no effect on the results in this study. The same procedure was applied to observe the particles released from each of the mask

layers. Triplicate slices of mask layer were added to the Erlenmeyer flask. Control experiments without masks were conducted following the same procedure to explore the potential effect of sand (Figure 6.2).

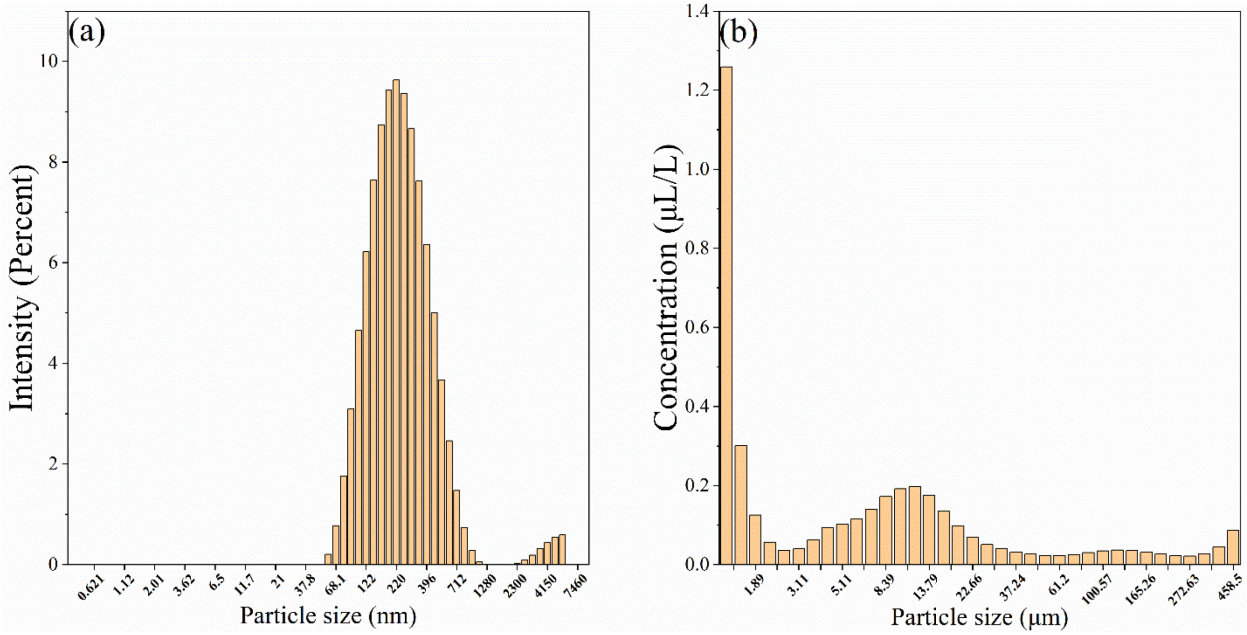


Figure 6.1 The particle size distribution in the water with only sand using different particle size analyzers. (a) Zetasizer ZS; (b) LISST-200X.

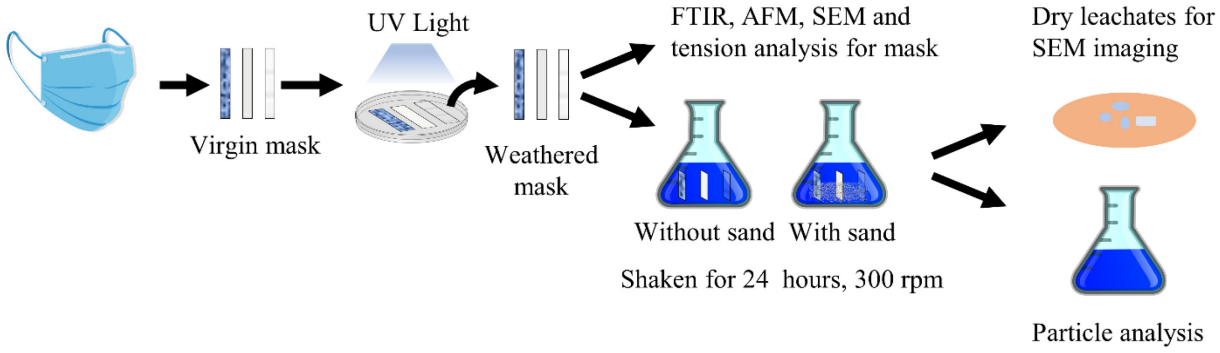


Figure 6.2 Experimental procedure for studying the release of particles from masks

6.2.2 Characterization of physicochemical properties of disposable masks

The virgin and UV weathered mask strips were analyzed using Attenuated Total Reflection–Fourier Transform Infrared Spectroscopy (ATR–FTIR, Tensor 27, Bruker, USA). Spectra were acquired in wavenumber ranges of 4000–400 cm^{-1} with 32 scans. The background spectrum was obtained for each sample. Four measurements were taken for each sample on the surface. The FTIR spectra were compared with a set of reference data in order to identify the peaks. The mechanical properties of the mask strips before and after UV irradiation were measured using the Model 42 Material Test System (MTS Criterion, USA). Each measurement was repeated three times, and the average values were calculated. An Innova atomic force microscope (AFM, Bruker, USA) with RTESPA-150 silicon probes was used to analyze single fiber of the mask surface in tapping mode. The probe had a spring constant of 6 N/m and a resonance frequency of 150 kHz. The AFM images obtained were analyzed using Nanoscope Analysis v1.8 (Bruker, USA). Physical damage and structural changes on the mask surface were examined using an S-3400N scanning electron microscope (SEM, Hitachi, Japan) with 5 kV electron accelerating voltage. The mask strip was cut into small squares (0.5 cm × 0.5 cm) and placed on the carbon tape that affixed on the surface of the sample holder. The sample holder was then coated with a 2 nm layer of gold for SEM imaging. The mask samples were viewed under different magnifications ranging from 100 to 5000. In addition, the hydrophobicity of the weathered mask surface was evaluated by the water contact angle, which was measured by a contact angle goniometer (VCA Optima, AST Products, UAS).

6.2.3 Particle size analysis for mask leachates

The particle size distribution (PSD) in the water sample was analyzed using a laser in-situ scattering and transmissometry analyzer (LISST-200X, Sequoia, USA). The detection range of the analyzer was 1-500 μm, and the concentration of particulate matter (μL/L) was obtained by calculating the

equivalent volume of the irregular spheres. Samples of 20 mL were added to the small chamber of the LISST, and live data collecting mode was used to scan the samples. Each sample was scanned for 1 minute, and a total of 60 data points were collected (Serra et al., 2020; Yang et al., 2021b). Control samples containing only sand were also tested. The DI water in the control samples was applied as the background for each test. To view the shape of particles released in the leachates, 20 μL of water was carefully drop onto the sample holder and dried for SEM observation. After drying, the sample holders were coated with a 2 nm layer of gold for imaging.

6.3 Results and discussion

6.3.1 Changes in the chemical composition of the masks under UV weathering

ATR–FTIR analysis was performed in order to analyze structural changes of the mask strips after weathering. Figure 6.3 presents the FTIR spectra of three layers of both virgin and weathered mask strips. The three layers of the mask displayed indistinguishable spectra, with four large peaks in the wavenumber ranging from 3000 to 2800 cm^{-1} and two large peaks in the range from 1540 to 1300 cm^{-1}. The peaks at 2918 and 2835 cm^{-1} were attributable to asymmetric and symmetric stretching vibrations of CH_2 groups, while the peaks at 2950 and 2870 cm^{-1} were due to the asymmetric and symmetric stretching vibrations of CH_3 groups (Morent et al., 2008; Ullah et al., 2020). This results also indicates that the CH_3 asymmetric vibrations or CH_2 scissor vibrations led to the peak at 1456 cm^{-1}, while the peak at 1375 cm^{-1} was the result of CH_3 symmetric deformation. In addition, the small peaks between 1200 and 700 cm^{-1} were identified as the characteristic bands of the polypropylene crystal structure, including C–C asymmetric and symmetric stretching, C–H wagging vibrations, CH_3 asymmetric rocking, and CH_2 asymmetric rocking vibrations. The formation of C=C

and C=O structures contributed to the peaks in the 1750 to 1600 cm^{-1} range (Morent et al., 2008; Ullah et al., 2020).

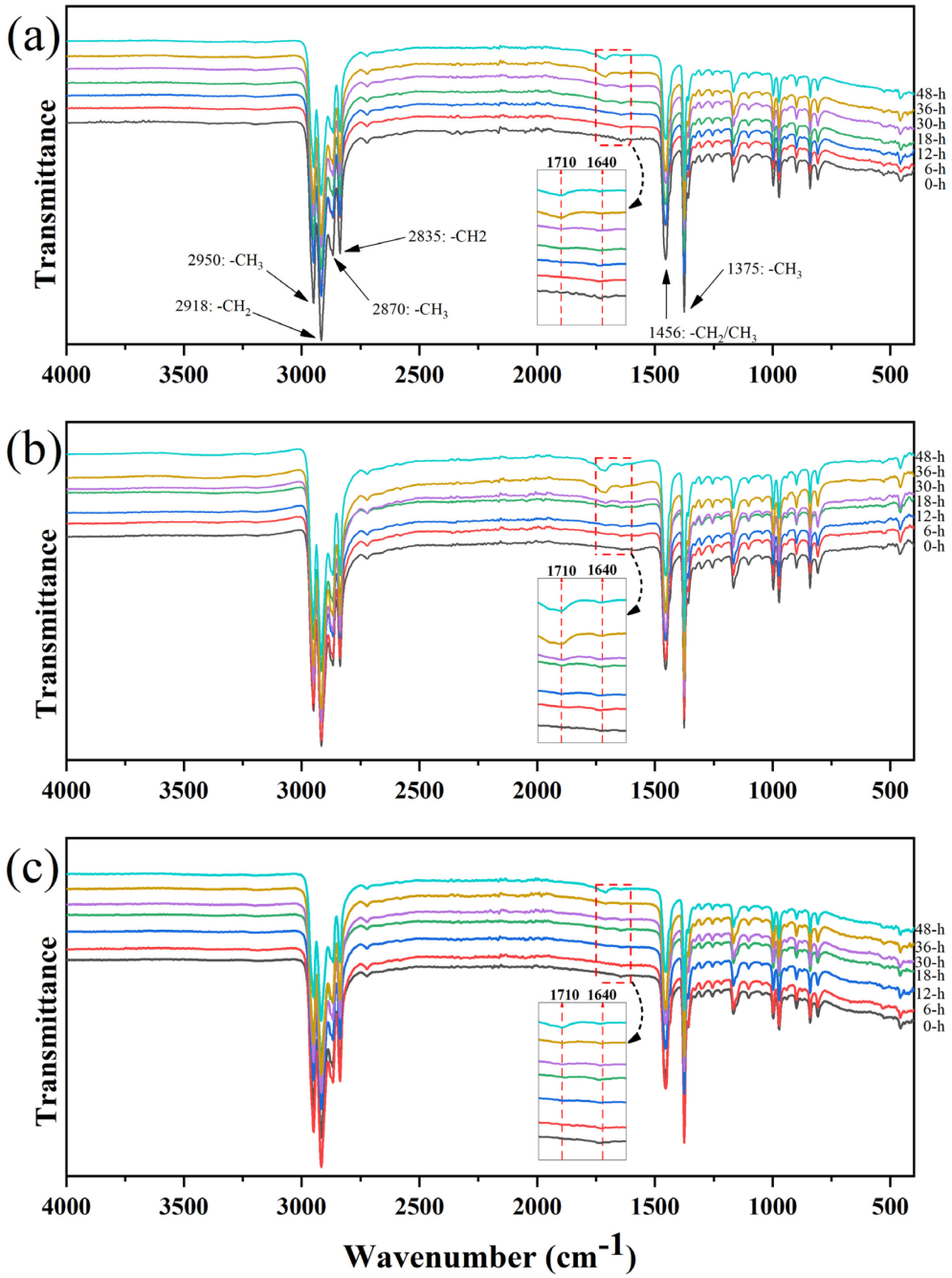


Figure 6.3 FTIR spectra of masks with different UV weathering durations. (a) The outer layer. (b) The middle layer. (c) The inner layer.

The FTIR spectra of the virgin masks indicated that all three mask layers were made from polypropylene. The obvious peaks caused by the vibration of CH_3 and CH_2, meanwhile, indicated that these functional groups were the main components of the mask. Comparing the spectra of masks under different durations of UV weathering, it was found that the intensity of all peaks gradually decreased as the UV weathering duration increased, with some small peaks appeared between 1750 and 1600 cm^{-1} simultaneously. These minor changes imply that some C–H bonds were broken and double bond structures were formed (Aslanzadeh and Haghighat Kish, 2010; Aslanzadeh and Kish, 2005). Moreover, it is worth noting that the resistance to UV weathering varied depending on the layer. The inner layer exhibited strong resistance, followed by the outer layer, while the middle layer was the most vulnerable to UV weathering. With respect to the middle layer, after 18 hours of weathering, a tiny peak appeared in the range of 1750–1600 cm^{-1}, and after 36 hours of weathering, a more pronounced peak appeared at 1710 cm^{-1}. These peaks can be attributed to the formation of C=C and C=O structures. After 36 hours of weathering, a peak at 1710 cm^{-1} was found in the spectrum of the outer layer, while, for the inner layer, a more obvious peak resulting from the formation of double bond structures did not appear until 48 hours of weathering. The weathering of masks is due to photo-oxidation, resulting from free-radical chain reactions (Cai et al., 2018). In the present case, the UV radiation provided sufficient energy for the C–C and C–H bonds to be broken, generating alkoxy radicals and peroxyl radicals. This, in turn, led to chain scission or crosslinking. Meanwhile, some double bond groups, such as carbonyl groups were also formed.

6.3.2 Physicochemical characteristics of masks impacted by UV weathering

To explore the surface characteristics of masks, AFM and SEM were applied to observe the micro changes in the mask fibers before and after UV weathering. It can be seen from SEM images (Figure

6.4) that the majority of fibers were intact and had a smooth surface before weathering. Only a small part of the surface was accidented or attached with tiny particles. It also can be seen that the diameter of individual fibers in the outer and inner layers was about 30 μm, while the fibers in the middle layer were roughly 5 μm in diameter. After 18 hours of weathering, the outer and inner layers showed a similar change in fiber surface, i.e., obvious deformation or even damage on the surface. This was caused by irradiation at the intersections of fibers, which were easy to bend. At the same time, some small particles and fiber fragments formed where the damage occurred. The middle layer showed signs of more severe weathering. Not only did the surface of the fiber became abrasive, but some fractures of fiber occurred. When weathered for 36 hours, most of the fibers in all three layers became fractured, forming fiber fragments of varying lengths. Meanwhile, as the weathering duration increased, small particles attached to the mask fibers began to appear. The surface roughness of mask fiber could also be observed using AFM. Comparing the AFM images of the virgin fibers with those of the fibers subjected to weathering for 24 hours, it can be seen that the surface of the virgin fiber was relatively smoother. After UV weathering, some protrusions and depressions, resulting in increased roughness, could be observed. The roughness of the mask fibers before and after UV weathering is summarized in Table 6.1. As can be seen in the table, regardless of the arithmetic roughness average of the surface (Ra) or the root mean square of the surface roughness (Rq), the virgin roughness of the outer and inner layers was similar. After weathering for 24 hours, the increase in roughness of the inner layer was significantly greater than that of the outer layer. Although the fiber of the middle layer was too thin to be analyzed using AFM, the roughness of the middle can be described by SEM imaging (Figure 6.4 and Figure 6.5). It can be seen that the fiber surface of virgin middle layer was smooth, and there were few particles attached. After 18 hours of weathering, cracks, flakes, grooves or pits appeared on the surface. Compared with the outer and inner layers, the fibers of the middle layer were rougher, and some of the fibers were

completely broken. When subjected to weathering for 36 hours, all the fibers of middle layer were broken into small fragments.

Table 6.1 Changes in the surface fiber roughness of the mask after UV weathering

	Roughness of outer layer (nm)		**Roughness of inner layer (nm)**	
	Ra	Rq	Ra	Rq
Virgin	12.4	6.04	13.2	8.15
Weathered 24h	20.1	16	47.1	35.4
Increment (%)	62.1	163.2	256.8	330.7

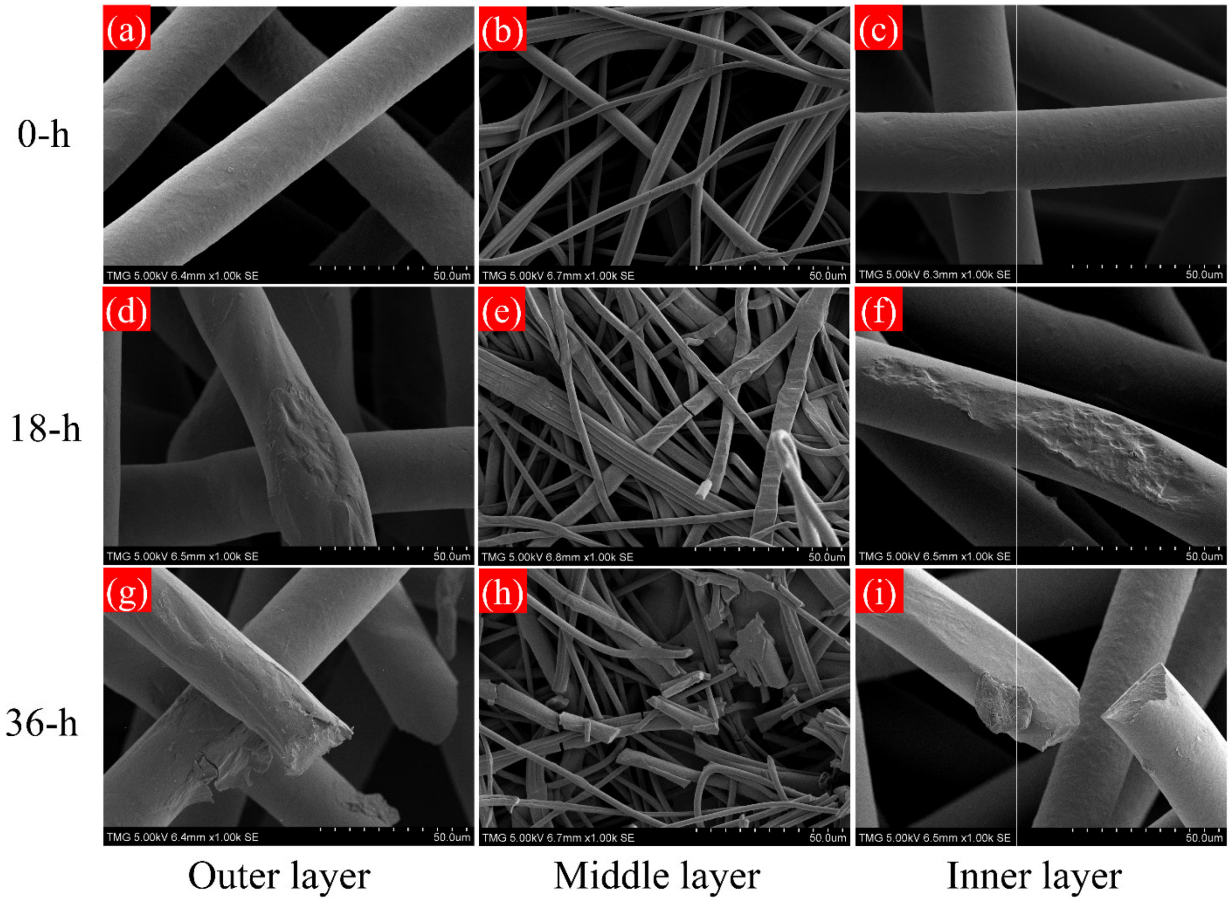


Figure 6.4 SEM images for the three layers of masks with different UV weathering durations: (a, d, g) Images at 1000 magnification of the outer layer of mask with UV irradiation for 0, 18 and 36 hours. (b, d, h) Images at 1000 magnification of the middle layer of mask with UV irradiation for 0, 18 and 36 hours. (c, f, i) Images at 1000 magnification of the inner layer of mask with UV irradiation for 0, 18 and 36 hours.

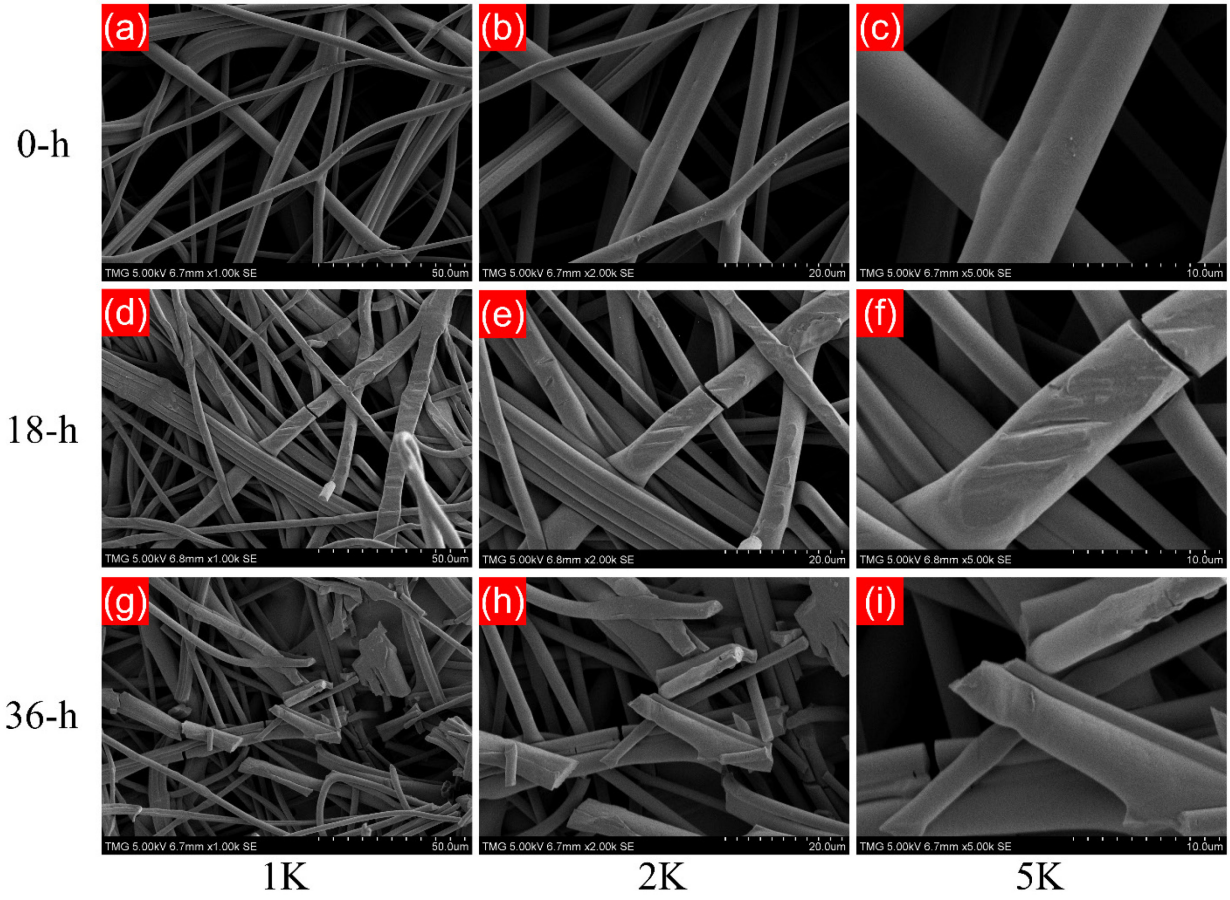


Figure 6.5 SEM images for the middle layer of masks with different UV weathering durations: (a, d, g) Images at 1000 magnification of the middle layer of mask with UV irradiation for 0, 18 and 36 hours. (b, d, h) Images at 2000 magnification of the middle layer of mask with UV irradiation for 0, 18 and 36 hours. (c, f, i) Images at 5000 magnification of the middle layer of mask with UV irradiation for 0, 18 and 36 hours.

Figure 6.6 shows the changes in the maximum load force of different mask layers with UV weathering. As can be seen, the general tendency for all layers was that, as the weathering duration increased, the maximum load force decreased. The initial maximum load force for the outer and inner layers was in the range of 7 to 8 N. Within 15 hours of UV weathering, the maximum load force changed little. However, the maximum load force was markedly reduced when subjected to

weathering for more than 15 hours. The force of the outer and inner layers decreased by 87.2% and 59.5%, respectively, compared with initial load after 36 hours of weathering, while, if weathered for more than 36 hours, the outer and inner layers became very brittle and difficult to test on the instrument. The outer and inner layers exhibited a similar change when subjected to weathering, while changes observed in the middle layer differed. The initial maximum load force of the middle layer was about 3.5 N, lower than of the outer and the inner layers. When weathered for more than 9 hours, the maximum load force decreased considerably, and it was lower than the instrument detection limit when weathered more than 15 hours. This result matched well the FTIR spectra, in which the middle layer was the layer most sensitive to UV weathering.

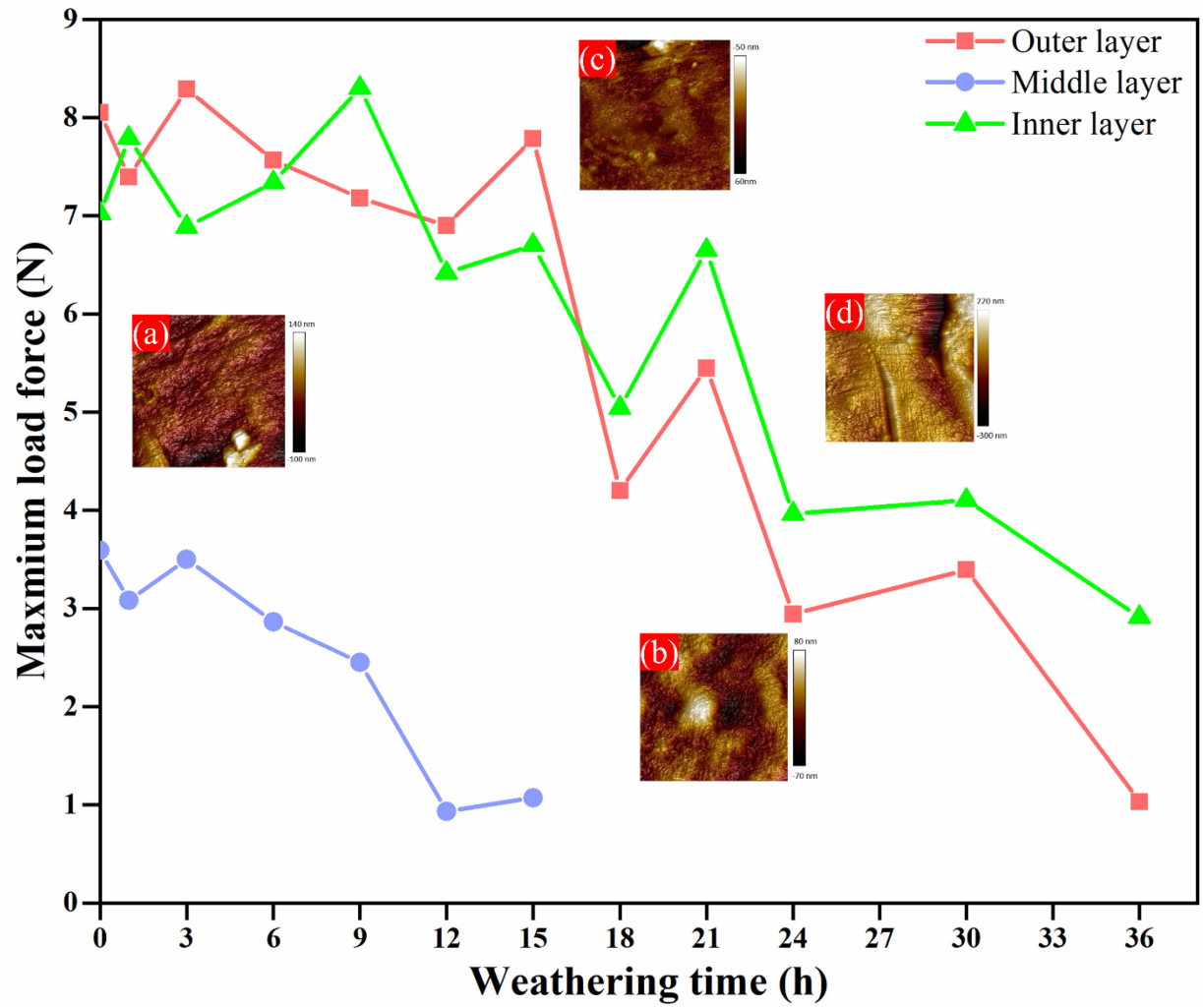


Figure 6.6 Mechanical tension and AFM images for different mask layers. (a) The AFM image of the virgin outer layer. (b) The AFM image of the outer layer when weathered for 24 hours. (c) The AFM image of the virgin inner layer. (d) The AFM image of the inner layer when weathered for 24 hours.

The hydrophilicity of masks can also change during weathering. The contact angles of different layers affected by weathering are shown in Figure 6.7 For the virgin mask, the water droplet cannot be absorbed on the surface regardless of which layer is tested. After subjected to weathering for 24 hours, the water droplets adhered to the outer and inner layers, with contact angles of 123.7° and

127.8°, respectively. Meanwhile, the contact angle decreased to 100° and 92° for the outer and inner layers, respectively, when subjected to weathering for 48 hours. On the contrary, water droplet still cannot be absorbed on the middle layer after weathering. Nevertheless, some small particles or fiber fragments were adsorbed on the surface of the water droplets when the water droplets left the surface of the middle layer. This phenomenon was more evident for the middle layer after weathered for 48 hours.

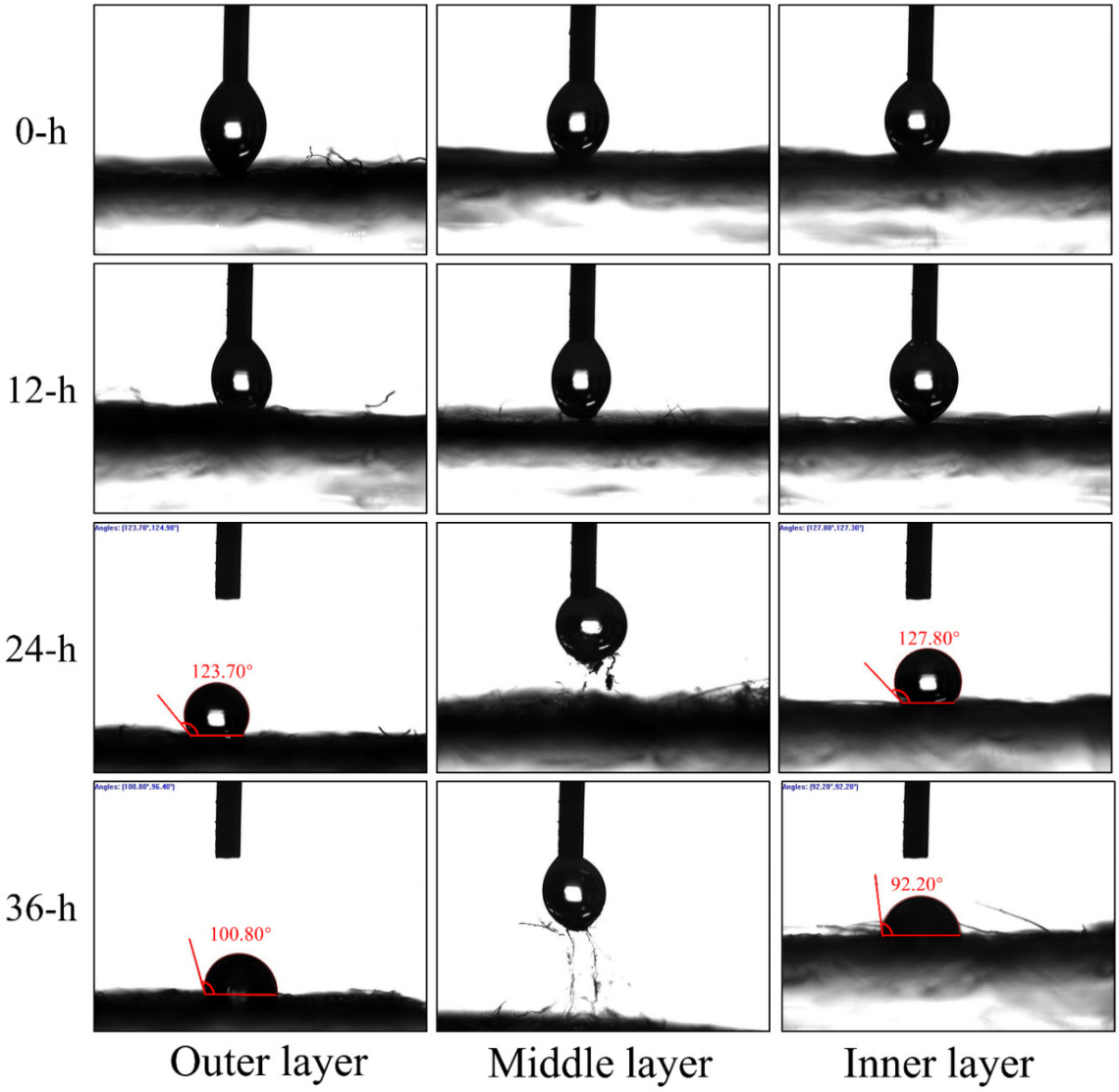


Figure 6.7 Contact angels for mask layers with different UV weathering durations

With different weathering durations, the surface and mechanical properties of the mask exhibited various aging characteristics. In general, the outer and inner layers of the mask showed a comparable weathering trend under UV weathering, while weathering in the middle layer was different. For the virgin mask, the outer and inner layers had consistent properties in terms of chemical inertness, hydrophobic performance, and mechanical performance. If the UV weathering duration was less than 12 hours, little changes was observed in the mechanical performance and chemical structure of these two layers. When weathered for 12 hours, however, and even more so weathered for 12 to 18 hours, the physical properties of the outer and inner layers changed significantly. Due to damage to or tearing of the mask fibers, the maximum load force decreased sharply. The chemical composition of the mask, however, changed little according to the results of FTIR. Although the intensity of the peak representing the C–H bond decreased, no obvious new peaks appeared. It can be inferred that the main chain was broken and the molecular weight was reduced, resulting in decreased mechanical strength (Gewert et al., 2018; Shi et al., 2021). When weathered for more than 36 hours, most of the fibers became fractured, resulting in a very low maximum load force that was in fact too low to be measured by the instrument. Meanwhile, based on the FTIR spectra, some C–H bonds changed to C=C or C=O bonds. Moreover, the decrease in contact angle also indicates that some hydrophilic double bond groups, such as carbonyl groups, were formed on the surface of the mask.

As those observations indicate, the middle layer of the mask was found to be more sensitive to UV weathering compared with the outer and inner layers. This is attributable to the fact that the middle layer of masks is composed of melt-blown fabric, which has a smaller fiber diameter than non-woven fabrics. In this regard, some studies have found that the filtration performance of the middle layer is significantly reduced after chemical treatment (Ullah et al., 2020). With respect to the virgin

mask, except for the difference in maximum load force, the middle layer had the same characteristics as the other two layers. However, after weathering for just 12 hours, the maximum load force decreased to an undetectable level, while the chain-like chemical structure changed, causing the fibers to become brittle. Figure 6.7 also proves that most fibers of the middle layer broken into small fragments, causing the layer to lose its basic mechanical features.

6.3.3 Plastic particles released from weathered masks in aqueous environment

The particle release from masks under different conditions was further investigated. Figure 6.8(a, b, c) show the morphology of particles in leachates of masks after different durations of weathering. It was found that the number of particles in the leachate of the virgin mask was low and the particle size was small, with the exception of a small number of particles having a particle size in the tens of microns, most of these being distributed at the nanometer range. In reference to the SEM image of the mask (Figure 6.4), it can be seen that most of the virgin mask fibers had good mechanical features and a smooth surface, with only a small fraction of the fibers having small particles or impurities. This suggests that few particles from the masks entered the water phase as a result of subjection to shaking conditions. After 18 h of UV weathering, however, the number of particles released to the water increased, including a significant increase in the number of particles of micro size being released. Interestingly, due to the accumulation of nano-size particles during water evaporation, a film formed on the surface of the sample holder. The middle layer of the masks not only released a large quantity of small particles, but also produced larger fiber fragments. Moreover, the outer and inner layers were important sources of MPs released under shaking conditions, corresponding with a decrease in mechanical features after 18 h of weathering. When weathered for 36 h, the mask fibers could easily enter the water since most of them have been broken down, while irregular fiber fragments were observed in the water phase, readily agglomerating to form flocs. In

addition, most of the fibers were observed to be tens to hundreds of microns in length, even visible to the naked eye. In addition to large fiber fragments, there were individual nano-size particles were difficult to observe, while a more distinct film was observed on the surface of the sample holder, this film having been formed by millions of small particles.

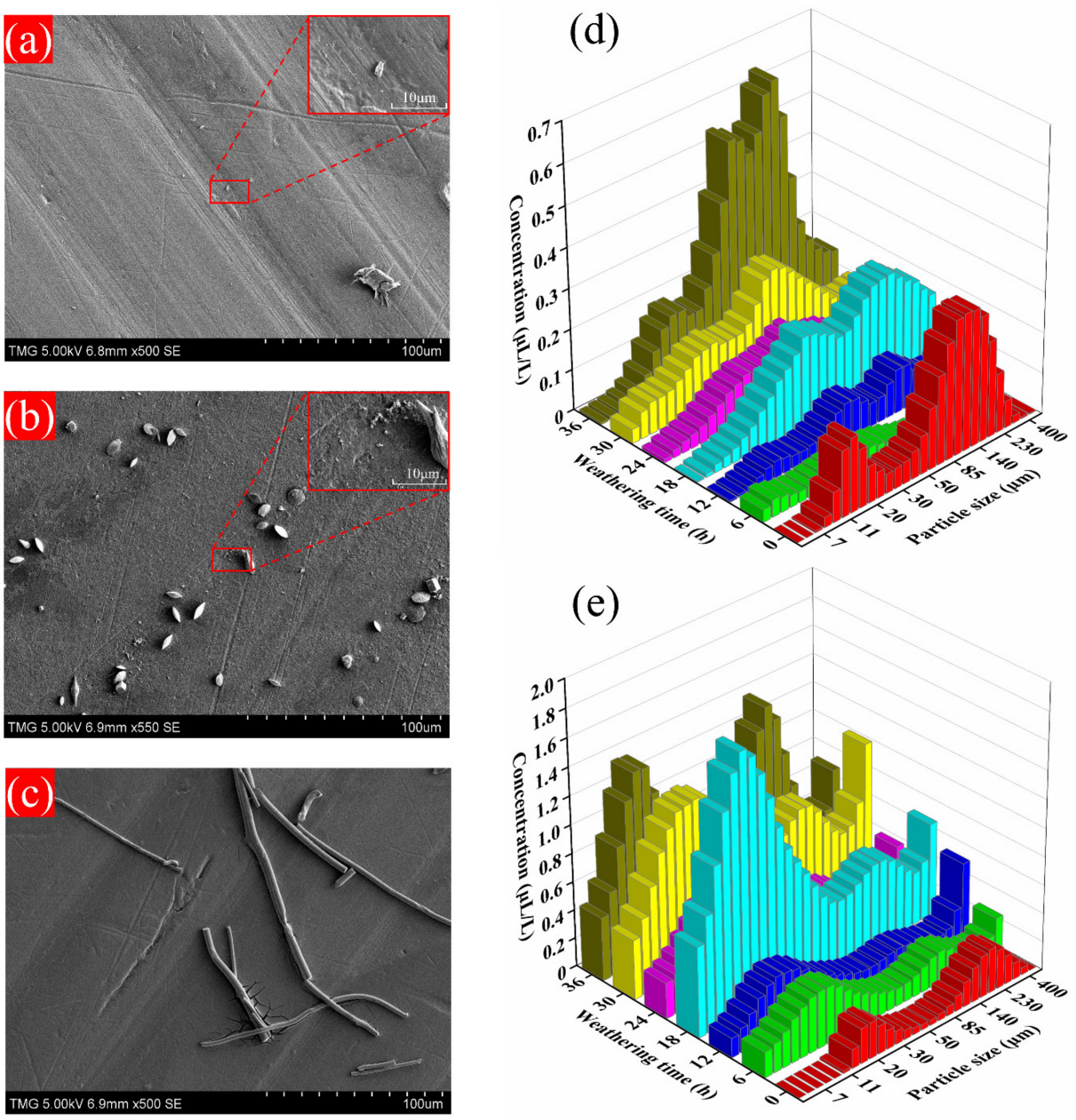


Figure 6.8 Analysis of particles entering the water from masks. (a) The SEM image of particles released from the virgin mask. (b) The SEM image of particles released from the mask weathered for 18 h. (c) The SEM image of particles released from the mask weathered for 36 h. (d) The particle size distribution in the absence of sand. (e) The particle size distribution in the presence of sand.

Figure 6.8(d) shows the distribution of particles released to the water from masks after different weathering durations. Regarding to virgin mask leachates, two main particle size distribution ranges were observed, which were 10 – 20 μm and 50 – 250 μm. The total concentration of MPs in the virgin mask was 3.49 μL/L. After 6 hours of UV weathering, the concentration of MPs in the solution was only 0.61 μL/L, and more than 90% of particles were less than 100 μm in diameter. When weathered for 12 hours, the total concentration of MPs in the solution was 1.52 μL/L, and about 80% of the particles had a size greater than 30 μm. It should be noting that the release of MPs significantly decreased after UV weathering for 6 h and 12 h. Previous studies validated that the polymers (e.g., polyethylene, polypropylene, and polystyrene) and some monomer or functional groups can be crosslinked under short term UV irradiation, leading to the maintenance or even enhancement of mechanical properties (Bendjaouahdou and Bensaad, 2018; Liao et al., 2019; Shyichuk et al., 2001). Chemical additives, such as stabilizers, may accelerate or slow down the photolysis process, and further affect the crosslinking or scission caused by UV irradiation (White and Shyichuk, 2007; White et al., 2006). Although the molecular weight decreases under UV irradiation, the scission and crosslinking may exist simultaneously (Cui et al., 2013; Guan and Xu, 2001). According to the results of the tension test and FTIR, we hypothesize that short-time UV weathering caused self-crosslinking in the main chain, thereby increasing the density and maintaining the mechanical strength of the mask, inhibiting the release of MPs. For masks weathered for 18 hours, the size of the MPs released increased overall, and only 2% of the particle size was less than 10 μm. Compared to the concentrations after 6 and 12 h of weathering, the concentration of particles released after 18 hours of weathering increased dramatically to 4.35 μL/L. This phenomenon demonstrated that, once again, the most marked changes in mask characteristics occurred in the weathering duration range of 12–18 h. As the weathering duration extended to 24, 30 and 36 h, the concentration of MPs released from the masks showed an overall increasing trend, with respective concentrations of 2.59,

3.82 and 7.10 μL/L observed. In addition, the respective concentrations of MPs with a diameter greater than 10 μm after these weathering durations were 95.0%, 91.1% and 98.9%. Comparing and analyzing the size distribution of the MPs released after different weathering durations, it was found that, for short UV weathering durations, most of the particles released fell within the size distribution of less than 200 μm. As the weathering duration increased, the size of MPs increased correspondingly, a result aligned with the SEM images of the mask leachates.

The characteristics of the MPs released from different mask layers were also explored, with the results shown in Figure 6.9(a-c). For the virgin mask, the concentrations of MPs released from the outer, middle, and inner layers were 4.47, 1.52 and 0.80 μL/L, respectively. The MPs released from the outer layer was mainly distributed in two size ranges, which were 15–50 μm and 200–500 μm, accounting for 24.2% and 44.3%, respectively, of the total concentration, while the MPs released from the middle and inner layers mostly ranged between 10 and 200 μm in diameter, contributing 76.2% and 83.6% to the total concentration, respectively. After 24 h of UV weathering, the concentrations of MPs released from the outer, middle, and inner layers were 6.19, 27.81 and 4.27 μL/L, representing increases by 0.39, 17.30 and 4.33 times, respectively, compared with the virgin masks leachates. The concentration of MPs released from the middle layer was much higher than those form the outer and inner layers. This was due damage to the mechanical structure of the middle layer, resulting in a mass of small particles and fiber fragments being formed that could readily enter the water phase.

Most of the particles released were less than 200 μm in size for all three mask layers, with this trend being particularly pronounced for the middle layer, where this size distribution accounted for 91.2% of the total concentration. When weathered for 36 hours, the respective concentrations of MPs

released from the outer, middle, and inner mask layers increased to 70.73, 60.36 and 11.44 μL/L. Since the inner layer was the most resistant to weathering among the three layers, the concentration of particles released from the inner layer was significantly less than that from the other two layers. The particle size distribution of the MPs released from the different layers, meanwhile, exhibited different modes. Regarding the leachates of the outer and inner layers, the particle size distributions presented a bimodal pattern, while the middle layer showed a unimodal pattern. Specifically, the particle from the outer layer was mainly distributed in the range of 20–100 μm and 100–500 μm, accounting for 51.3% and 38.1%, respectively, of the total concentration. The particle size of the inner layer was mainly distributed between 30–100 μm and 100–500 μm, contributing 56.8% and 35.9%, respectively. For the middle layer, the particle size of the MPs released was mainly distributed between 50–200 μm, accounting for 56.9% of the total concentration.

6.3.4 Effect of sand on MPs release from masks in aqueous environment

To assess the behavior of the masks in the shoreline environment, the changes in the properties of particles released from the mask after physical abrasion were evaluated. The analysis of the particle size of the sand showed that the presence of sand had no effect on the measurement of plastic particles released from masks (Supplementary Material). Figure 6.7(e) shows the distribution of particles released from the masks to the water in the presence of sand. For the virgin mask, a total of 3.13 μL/L particles were released, with the particle size mainly distributed within the ranges 15–30 μm and 100–250 μm, accounting for 33.9% and 44.4% of total concentrations, respectively. When the masks were subjected to weathering for 6 h, 6.08 μL/L of MPs were released, and their particle size was mainly distributed in two ranges, 5–50 μm and 100–250 μm, accounting for 66.7% and 17.9%, respectively, of the total concentration. For masks weathered for 18 h, the MPs released sharply increased to 23.78 μL/L. Similarly, most of the particles after this weathering duration were

less than 50 μm in diameter, with this size distribution accounting for 72.8% of total concentration. When the masks were weathered for 30 and 36 hours, the MPs released were 21.9 and 20.8 μL/L, respectively. In addition, the particles showed a bimodal mode particle size distribution, with size distributed between 5–50 μm and 50–250 μm. However, it is worth noting that there was an increasing trend when the particle size was higher than 400 μm. Compared with the case where there was no sand, the presence of sand in the aqueous environment promoted the release of MPs from masks. In addition to the virgin mask, the concentration of particles released increased 4.5 times on average for the weathered masks in the presence of sand. Moreover, the particles released from the mask after 18 hours of weathering increased sharply compared to the mask subjected to weathering for 12 hh. It was found that, after 24 h of shaking, masks that have been weathered for more than 30 h broken down into small fragments, with this phenomenon being particularly pronounced when sand was present in flasks. It should be noted in this regard that particles with a size greater than 500 μm or less than 1 μm were not calculated by the size analyzer, leading to the underestimation of concentration.

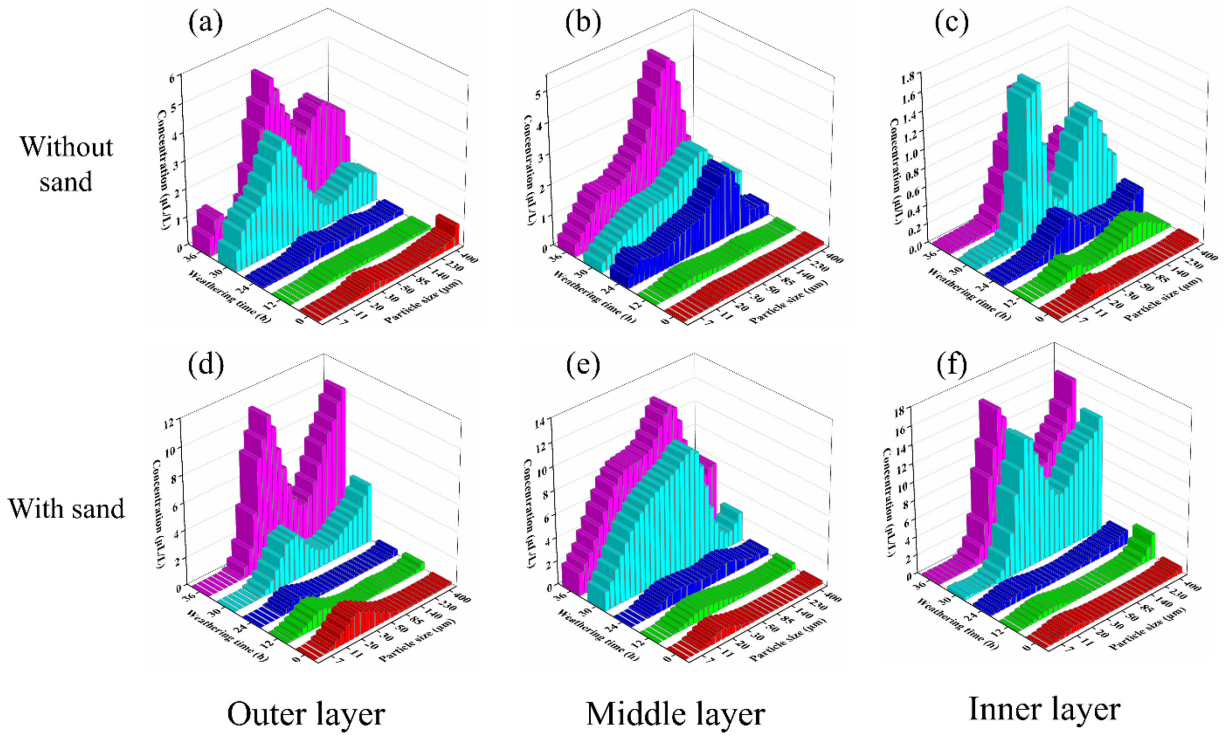


Figure 6.9 Size distributions for particles released from three mask layers under different weathering conditions

The effect of sand on particle release from different mask layers was also investigated, with the results shown in Figure 6.9(d-f). For the virgin mask, the concentrations of particles released from the outer, middle, and inner mask layers were 14.6, 6.2 and 7.0 μL/L, respectively, when shaken in water for 24 h in the presence of sand. The particle size distribution of the MPs released was observed to be unimodal for all layers under these conditions, with most of the particles falling within the size range of of 10–50 μm. The proportions in the outer, middle, and inner layers were found to be 84.9%, 84.1% and 54.6%, respectively. The concentrations of MPs released from the three mask layers weathered for 12 h were 10.2, 10.7 and 11.4 μL/L, respectively. For the outer and middle layers, most of the particles released were less than 50 μm in diameter, with this size distribution accounting for 76.9% and 71.5% of the total concentration for the outer and middle

layers, respectively. For the inner layer, however, the particles were distributed in two ranges, 5–50 μm and 300–500 μm, which contributed to 43.2% and 44.7%, respectively, of total concentrations. With regard to the mask weathered for 24 h, the respective concentrations of MPs released from the outer, middle and inner layers were 5.41, 20.52 and 17.49 μL/L. Different particle size distributions were observed among the different mask layers. Most of the particles released from the outer layer were small in diameter, (i.e., less than 50 μm), with this size distribution accounting for 76.0% of the total concentration. The particles released from the middle layer were mainly distributed between 10–200 μm, with this distribution accounting for 87.4% of the total concentration. For the inner layer, the particle size of the MPs released was mainly distributed in two ranges, 5–50 μm and 100–500 μm, accounting for 48.0% and 47.4%, respectively, of the total concentrations. When the masks weathered for 36 h were shaken in the water with sand, the respective concentrations of particles released from the outer, middle, and inner layers were found to be 132.52, 210.23 and 186.94 μL/L. The particles released from the outer and inner layers had the same size distribution, mainly distributed in the two ranges of 20–100 μm and 200–500 μm. However, the particles released from the middle layer was more evenly distributed, with most of the particles distributed between 10–200 μm, this range accounting for 68.65% of the total concentration. When UV weathering exceeded 30 h, the particle size distribution of the MPs released from the mask was similar regardless of whether or not sand was present.

6.3.5 Environmental implications

Masks have been proven to be effective in preventing the spread of COVID-19 (Eikenberry et al., 2020; Okuku et al., 2021), and it can be expected that they will be a normal part of everyday life both during and after the pandemic (Rab et al., 2020; Xu and Ren, 2021). However, this preventive measure puts tremendous pressure on plastic waste management (Ammendolia et al., 2021).

Shorelines already suffer from the large quantities of plastic debris, and the discarded masks pose a new challenge for the shoreline environment around the world. The environmental conditions on shoreline are complex and discarded masks on shorelines may undergo a series of changes (Li et al., 2020b). The present study has shown that the physicochemical features of disposable masks can change dramatically under UV weathering. After being exposed to weathering conditions, the transformation of chain structure and chemical composition and decreased mechanical strength were observed. These changes caused the masks to be broken into small fragments, triggering the release of a large quantity of MPs to the aqueous environment. Around 483,888 plastic particles can be released from one virgin disposable mask, and 1,566,560 particles form the weathered mask. Although shortwave UV in particular was applied in this study, the findings serve to demonstrate that photo-oxidation plays a crucial role in the release of MPs from discarded masks. The middle layer of the mask is found to be the most sensitive part to UV irradiation and is the easiest to break, releasing a large number of MPs to water. Moreover, in a shoreline environment (i.e., in the presence of both water and sand), the physical abrasion caused by sand can further exacerbate the release of MPs from masks. In this regard, we found that as many as 16,001,943 particles can be released from one weathered mask in the presence of sand. The cumulative amount of MPs produced during the 24 h breathing simulation of the disposable mask was ranged from 4678 to 24,643, and even the cumulative amount after 720 h was less than 2 million (Li et al., 2020a). Our findings indicate that the quantity of MPs released from the mask to the water is significantly larger than that released through inhalation during normal mask use. Shorelines are not only the main receptor of discarded masks from oceans and lands, but also play host to further transformation of masks to plastic particles under weathering conditions. Given these considerations, appropriate strategies need to be developed to better assess and mitigate the risks posed by discarded masks in order to protect coastal

ecosystem. In addition, the release of chemical compounds from masks under different conditions can also be studied in future research.

Chapter 7 Physicochemical change and microparticle release from disposable gloves in the aqueous environment impacted by accelerated weathering[6]

7.1 Background

Since early 2020, the spread of the pandemic has exerted a profound influence on normal production and life in cities around the world (Cai et al., 2021; Tian et al., 2021). To prevent the transmission of the coronavirus (SARS-CoV-2), the public is encouraged to wear personal protective equipment (PPE), according to recommendations from the World Health Organization (WHO) (World Health Organization, 2020). As one of the most convenient and effective means of protection, disposable gloves are widely used in various scenarios, especially for shopping and other contact activities (Anedda et al., 2020; Jedruchniewicz et al., 2021). More importantly, the growth in the number of people diagnosed and a corresponding increase in surgical procedures have also posed a challenge in the demand for disposable gloves (Powell-Jackson et al., 2020). It is estimated that more than 65 billion gloves are consumed globally every month (Prata et al., 2020). This increased demand for disposable gloves has prompted an expansion of the glove market. The market for procedural gloves is expected to reach USD 18.56 billion by 2026, at a compound annual growth rate of 11.64% (Research and Markets, 2021).

[6] This work has been published as Wang, Z; An, C; Lee, K; Chen, X; Zhang, B; Yin, J; Feng, Q. 2022. Physicochemical change and microparticle release from disposable gloves in the aqueous environment impacted by accelerated weathering. Science of the Total Environment, 823, 154986.

The materials used and the performance of disposable gloves used vary widely for different applications. Three main types of disposable gloves used during the pandemic are latex, nitrile, and folic, accounting for almost 94.6% of all gloves (Jedruchniewicz et al., 2021). Latex or nitrile gloves are typically used in medical, manufacturing, laboratories, and domestic environments. Specifically, latex gloves are mainly made of natural rubber (cis-1,4-polyisoprene), which has good physical properties (Yew et al., 2019). However, natural rubber also contains small amounts of protein, fatty acids, wax, phospholipids, steroids, and other impurities (Rolere et al., 2015), indicating that natural rubber can trigger allergic reactions among a small number of people. Nitrile gloves are widely used as a better alternative to latex gloves in a variety of environments. Nitrile rubber is produced with butadiene and acetonitrile, and it is also called nitrile-butadiene rubber (NBR) (Yew et al., 2020). Varying the relative content of components such as carboxylic acid, acrylonitrile and acetonitrile can affect glove physical properties, such as solvent resistivity, mechanical strength, and stiffness (Yew et al., 2020). Metal ion crosslinkers, including Zn, Fe, and Al, can promote chain bonding of the polymer and enhance the dexterity of gloves (Yew et al., 2020; Zhang et al., 2019b). In comparison to latex and nitrile gloves, vinyl gloves have been used less during the Covid-19 pandemic. The main component of vinyl gloves is polyvinyl chloride (PVC), which can release chlorinated substances in degradation, leading to a high level of environmental risk (Chao et al., 2015; Jedruchniewicz et al., 2021; Yan et al., 2021).

As one of the most commonly used PPEs, the increase of glove waste has posed a considerable risk to municipal solid management and disposal. First, the sharp growth in glove waste from the medical sector exceeds the capacity of existing waste facilities (Yang et al., 2021a). It has been estimated that during the pandemic, the amount of medical waste has increased 6-fold, from 40 tons per day to 240 tons per day in Wuhan, China. Similarly, the US could generate a full year's growth of

medical waste within two months (Cutler, 2020). Second, the disposable gloves is the main laboratory contribution to landfill waste, accounting for around a quarter of all waste (Eizagirre, 2019). Although some of the contaminated PPEs are sorted into hazardous waste, most of the uncontaminated PPEs are mixed with regular garbage and go into municipal waste management systems (Ammendolia et al., 2021; Wang et al., 2021d).

PPE wastes have been widely observed in urban waste system (Ammendolia et al., 2021; Xu and Ren, 2021). The lack of the public's environmental awareness leads to glove wastes being discarded randomly and ending up in the soil and/or the aquatic ecosystem through urban runoff (Akhbarizadeh et al., 2021b; Ardusso et al., 2021; De-la-Torre et al., 2021). When exposed to the natural environment, PPE wastes can weather and form fragments or even MPs or NPs (Cai et al., 2018; Sullivan et al., 2021). As emerging pollutants, MPs and NPs are widely found in the atmosphere (Akhbarizadeh et al., 2021a), soil (Dobaradaran et al., 2018), various aqueous environments, and even in fish and humans (Akhbarizadeh et al., 2020; Ragusa et al., 2021). To improve the glove performance, such as stretch, modulus of elasticity and sensitivity and tactility upon wearing, various additives are added during the manufacturing process (Aalto-Korte et al., 2007; Olson et al., 2019; Reichel, 2012). Along with weathering, these chemical additives can be released into the environment, which not only harms terrestrial and marine animals, but also ultimately affects humans via the food chain (Takdastan et al., 2021; Taylor et al., 2019). Additionally, glove wastes are also the source and carrier of pathogens and chemical contaminants. Existing evidence shows that viruses can survive on the media surface for 72 hours or longer (Doremalen et al., 2020). The adsorption capacity of weathered PPE to other pollutants in the surrounding environment will increase after weathering (Feng et al., 2021b; Liu et al., 2020b; Maderuelo-Sanz et al., 2021). These processes can be exacerbated by natural conditions, such as

ultraviolet (UV) irradiation, physical abrasion, and microorganisms (Ding et al., 2020b; Ganesh Kumar A. et al., 2020; Shrestha and Wang, 2020; Song et al., 2017; Wang et al., 2021c). As the mediator between the land and ocean, shorelines play a key role in the transport and transformation of pollutants (Gaylarde et al., 2020; Huang et al., 2021a; Kalogerakis et al., 2017). When subjected to the shoreline environment, the physicochemical characteristics of glove wastes are altered by the effects of sun light, waves, and sand abrasion, and this, in turn, affects the surrounding environment. Therefore, it is necessary to evaluate the environmental effects of glove wastes on such complicated environment in a timely manner. The objective of this study is to explore the physicochemical changes and environmental behaviors of disposable glove wastes in the aqueous environment.

7.2 Methods

7.2.1 Sample preparation

Three types of disposable powder-free examination gloves (latex, nitrile, and vinyl) and glass beads (GB) with a particle diameter of 1 mm were purchased from VWR (Canada). The palm of the gloves was chosen as the experimental material for this research. The palm of the gloves was then cut into small strips measuring 2 cm × 2 cm, and a portion of the pristine glove strip was put into a glass Petri dish and subjected to UV light (254 nm, 20 mW/cm^2) for 1 to 48 h in a UV chamber (CX-2000 Crosslinker, Analytik Jena, Germany). Other samples were left untreated and served as the control group. 1-g glove strips subjected to different UV irradiation durations were added to 50 mL of deionized (DI) water in Erlenmeyer flasks. The DI water was generated by a water-purification system (Milli Q, Merck, German). Some groups also had 20 g of glass beads added to study the effect of physical abrasion on the release of particles. The flasks were sealed with aluminum foil and placed in an incubator shaker (New Brunswick Innova 42R, Eppendorf, Germany) at 300 rpm

and 20°C for 24 h. Prior to usage, 20 g of glass beads were first added to a flask with 50 mL of DI water and then placed in a shaker for 24 h. This step was repeated three times by adding water. Finally, the glass beads were dried in an oven at 60°C for 24 h and stored for future use. Control experiments without gloves were conducted following the same procedure to explore the potential effects of glass beads. Blank tests were performed to eliminate system errors. All batches were tested in triplicate and average values were used. All glass containers used in this study had been specially cleaned beforehand, rinsed three times with DI water, and dried in the oven.

7.2.2 Characterization of physical and chemical properties

The glove strips with different UV irradiation durations were examined using Attenuated Total Reflection–Fourier Transform Infrared Spectroscopy (ATR–FTIR; INVENIO, Bruker, USA). The scanning range was 4000–400 cm^{-1} with a resolution of 4 cm^{-1}. Data were measured at three different points on the surface of samples and the average values were used. The FTIR imaging of glove strips was captured at the Canadian Light Source in Saskatoon, Canada. The spectroscopic images were collected at a resolution of 4 cm^{-1}.

The surface microscopic changes of gloves with different UV weathering durations were visualized using a scanning electron microscope (SEM; S-3400N, Hitachi, Japan). The glove strips were cropped into squares measuring 0.5 cm × 0.5 cm and fixed on carbon strips glued to the SEM sample holder. Three layers of gold were then coated on the sample holder for imaging at magnifications of 100, 500, 1000 and 2000. The mechanical strength of the glove strips was measured using a material test system (MTS; Model 42, MTS Criterion, USA), and the average of three parallel samples were applied. An atomic force microscope (AFM; Innova, Bruker, USA) with an RTESPA-150 silicon probe was used to characterize the roughness of the glove surface using tapping mode with a spring

constant of 6 N/m and a resonance frequency of 150 kHz. The hydrophilicity was evaluated by the water contact angle, which was measured by a contact angle goniometer (VCA Optima, AST Products, USA).

7.2.3 Analysis of leachable components

The particle size distributions of glove leachates were measured using laser in-situ scattering and transmissometry analyzer (LISST-200X, Sequoia, USA). The analyzer has a detection range of 1–500 μm, and the particle concentration (μL/L) is obtained by calculating the equivalent volume of irregular spheres. Sample of 18 mL was added to the chamber of the LISST, and the sample was scanned in live data acquisition mode once per second for 1 min per sample. The mean data of three parallel samples were analyzed in this study.

A 6-mL sample of the glove leachate was filtered with a 0.2 μm nylon membrane for elemental analysis by an inductively coupled plasma mass spectrometry (ICP-MS; 7700x, Agilent Technologies, USA) to measure Al, Cr, Mn, Co, Ni, Cu, Zn, As, Sr, Ag, Cd, Sb, Ba, and Pb concentrations. In addition, a gas chromatography mass spectrometry system (GC-MS; 7890/5977, Agilent Technologies, USA) with an HP-5MS capillary column was employed to identify the organic compounds of the glove leachates. The samples were solid-phase extracted with cartridges (Supelclean, ENVI C18, USA) prior to GC-MS analysis. First, the cartridges were conditioned with 10 mL dichloromethane, 10 mL methanol, and 10 mL DI water, in turn. Next, 12 mL glove leachates were filtered at a flow rate of 10 mL/min, and air dried for 1 h with the auxiliary of a pump. The retained compounds were eluted with 4 mL of methanol at a flow rate of 2 mL /min (Bonansea et al., 2013; Guart et al., 2011). The helium carrier gas flow was 1 mL/min, and the injection volume was 2 μL. The injector temperature was 270°C, and the initial oven temperature was 90°C, raised to

132°C at 3°C/min, then to 166°C at 10°C/min, to 175°C at 1°C/min and held for 2 min, then to 232°C at 2°C/min, and finally to 300°C at 25°C/min and held for 5 min (Bonansea et al., 2013; Fauvelle et al., 2018; Xie et al., 2021).

7.3 Results and discussion

7.3.1 Characteristics of gloves impacted by weathering

The chemical structures of the pristine glove strips analyzed by ATR–FTIR are shown in Figure 7.1. For the latex glove samples, the wavenumber within the 3700 to 3200 cm^{-1} regions can be attributed to modes of OH stretching (Agrebi et al., 2018). As is common with many hydrocarbons, the strong peak within the 3000 to 2800 cm^{-1} spectrum, including 2958, 2918, and 2851 cm^{-1}, were due to the C-H stretching. The structure of C=O led to the peak at 1730 cm^{-1} (Agostini et al., 2008). Peaks between 1650 and 1500 cm^{-1} were most likely attributable to amides I and II, which are specific to peptide bonds and are linked to the protein content of NR (Rolere et al., 2015). The characteristic peak at 823 cm^{-1} was due to the $-CCH_3=CH$, which is the main structure of natural rubber (Rolere et al., 2015; Sornsanee et al., 2018). The peak at 700 cm^{-1} was identified as =C-H (Sornsanee et al., 2018). Similar to the latex glove map, the peaks at 3418 cm^{-1} in the nitrile glove spectrum represented OH stretching, 3000–2800 cm^{-1} represented C-H stretching and 1732 cm^{-1} was due to the C=O stretching vibration. The characteristic nitrile structure (C≡N stretching vibration) was observed at 2235 cm^{-1} (Tan et al., 2021). The methylene group also produced two characteristic peaks at 1435 and 1353 cm^{-1}. The peaks at 1641, 1542, 1177, and 1089 cm^{-1} belonged to C=C, N-H bending, ester, and C-N stretching. The strong peak at 966 cm^{-1} was due to the C=H out-of-plane bending of the trans-butadiene double bond (Celina et al., 1998; Esmizadeh et al., 2020; Saviello et al., 2014). For vinyl gloves, the characteristic bands were found at 1719, 1267, 1102 and 730 cm^{-1},

which corresponded to the C=O carbonyl group, C(=O)-O group, O-CH_2 group, C-Cl group, and C=C bending. Similarly, the C-H stretching was observed at peaks of 2959, 2928, and 2860 cm^{-1} (Esmizadeh et al., 2020; Zhang et al., 2013). The FTIR mapping was further obtained to clarify the spatial chemical changes of the glove strips after UV weathering (Figure 7.1[d–o]). Regardless of the glove type, the C-H single bond strength in the range of 3000–2800 cm^{-1} dropped after the sample was subjected to 48 h of UV irradiation. Meanwhile, the strength of the C=O double groups in the range of 1780–1700 cm^{-1} increased. Although the C-H bond strength of latex gloves was significantly reduced, the C=O bond strength increased slowly, which indicated that the transition of C-H to C=O was not a linear relationship.

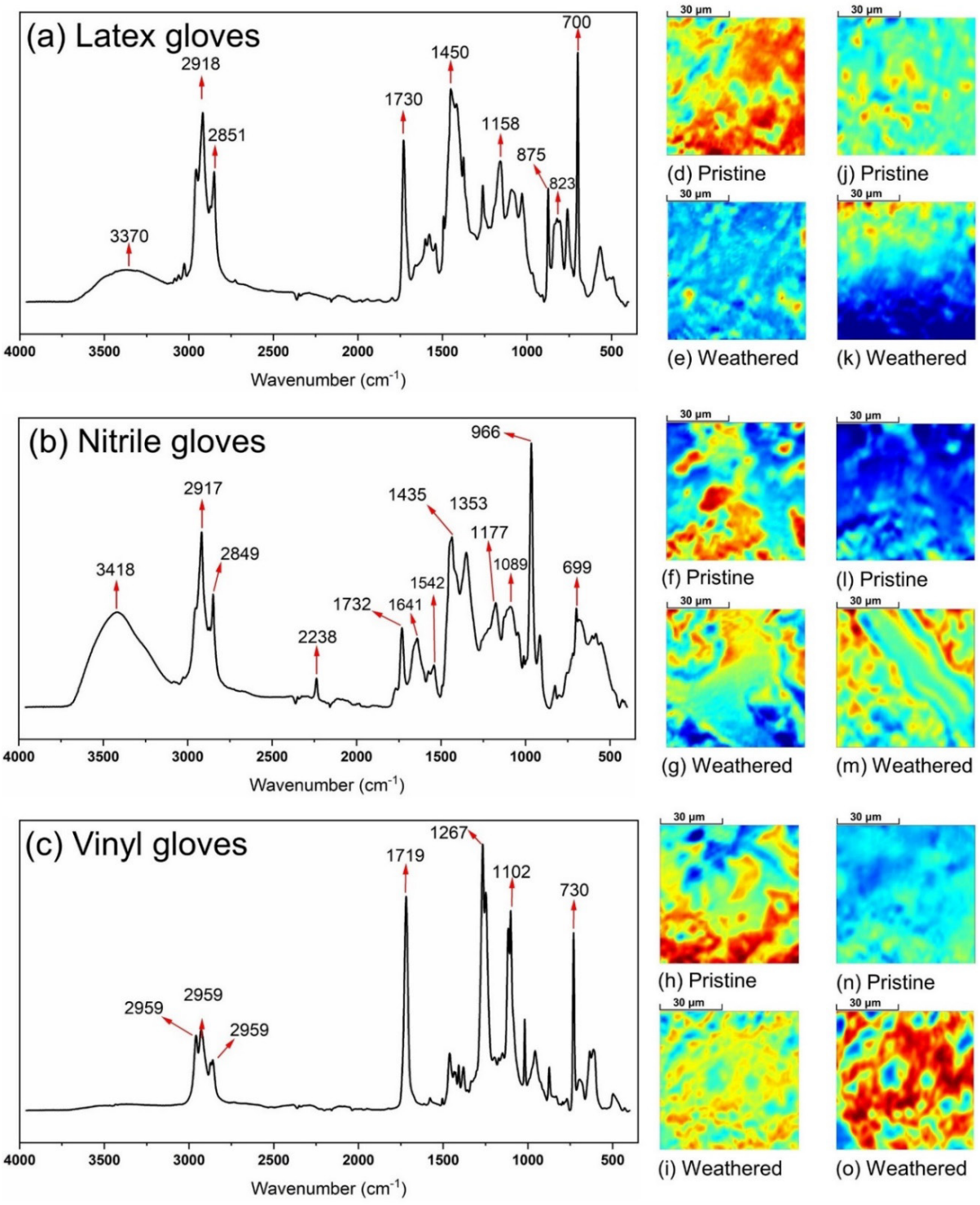


Figure 7.1 FTIR spectra of disposable gloves (a–c). FTIR mapping of the C-H functional groups (3000–2800 cm^{-1}) of pristine gloves (d–i). FTIR mapping of the C=O functional groups (1780–1700 cm^{-1}) of gloves after 48 h of UV weathering (j–o).

To further investigate the surface morphological characteristics of the glove strips, SEM was applied to visualize the microphysical changes before and after UV irradiation. As shown in Figure 7.2, the most significant feature was that, after UV weathering, the surface of the gloves appeared damaged or cracked in different manners. For latex gloves, the number of cracks increased with the prolonged UV weathering, and the degrees of breakage varied. Vinyl gloves exhibited a feature that a high number of cracks but a low degree of cracking after 48 h of UV irradiation. Apart from that, the surface of the nitrite gloves had not only a small amount of severe cracking degrees, but also many tiny fissures when subjected to 48 h of UV weathering. In addition to cracks, the surface roughness of these three types of gloves differed. For pristine latex gloves, there were many small particles attached to the surface, leading to a greater surface roughness compared to the other gloves. As the UV irradiation duration extended, these particles gradually coalesced and formed flakes that stuck to the glove surface. When weathered for 48 h, these flakes covered the original surface of the gloves and became the new surface layer, resulting in lower surface roughness. Vinyl gloves showed the opposite trend in surface roughness, and the surface of the pristine vinyl glove was the smoothest among the three types of gloves. When UV weathered for 24 h, many tiny cracks appeared on the glove surfaces, and after 48 h of weathering, the number of cracks increased further and the rest of the surface appeared as grooves or pits, resulting in a constant increase in surface roughness. Initially, the surface of the nitrile gloves had only a few pits, which did not change significantly as the weathering proceeded. AFM was employed to quantitatively characterize the variation in surface roughness (Figure 7.3). Obviously, before being exposed to UV irradiation, regardless of the arithmetic roughness average of the surface (Ra) or the root mean square of the surface roughness (Rq), the surface of the latex gloves was the roughest, followed by nitrile, and vinyl was the smoothest. After weathering for 24 h, the surface roughness of the latex gloves was reduced

remarkably, while the other two changed little. When weathered for 48 h, the roughness of the latex gloves gradually increased, as did the vinyl gloves, while the nitrile remained constant. This phenomenon coincided with the results of the SEM analysis. In general, the surface roughness of the latex gloves showed a trend of decreasing and then increasing, while vinyl gradually increased, and nitrile remained stable.

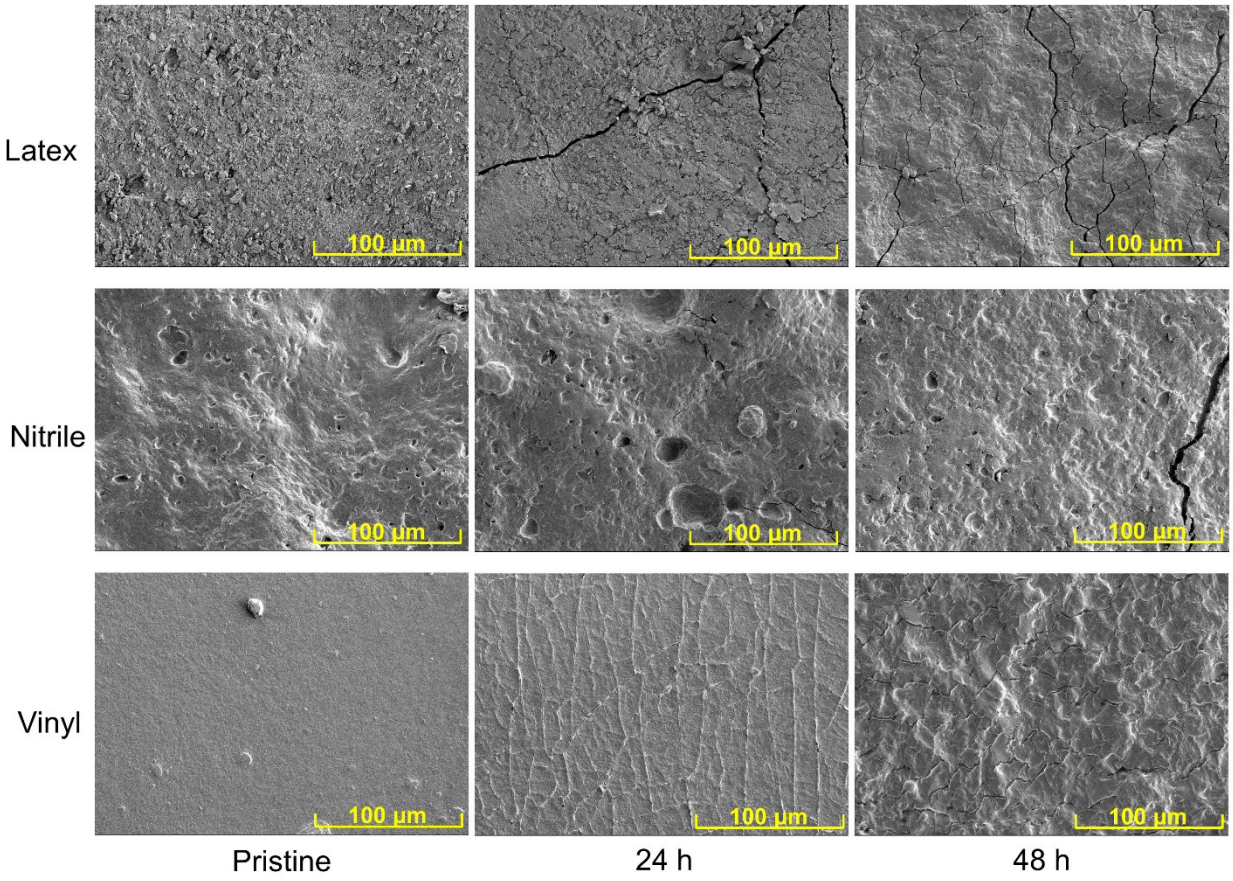
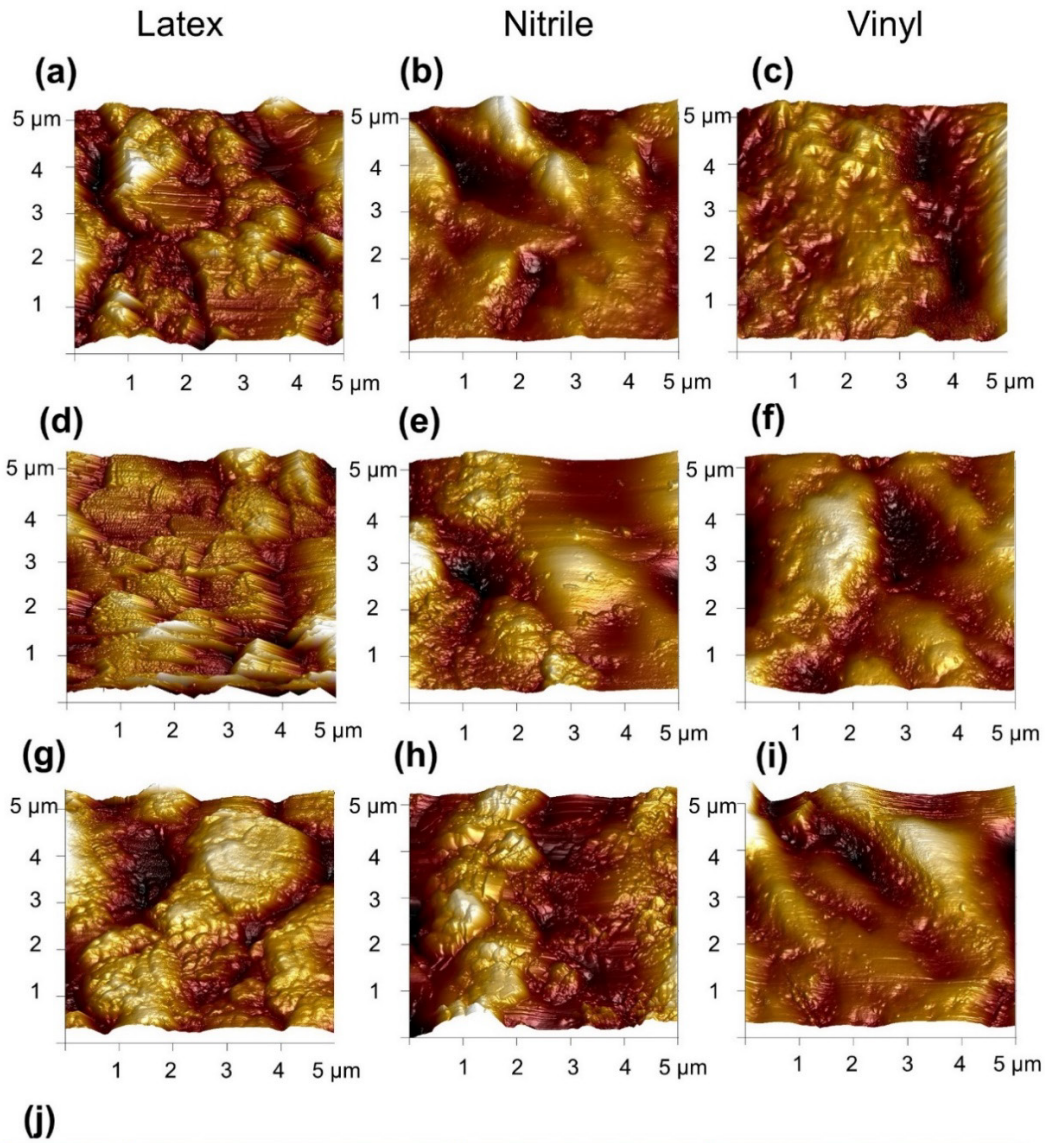


Figure 7.2 SEM images for the disposable glove with different UV weathering durations. Images are at 500X magnification.



(j)

	Latex		Nitrile		Vinyl	
	Ra (nm)	Rq (nm)	Ra (nm)	Rq (nm)	Ra (nm)	Rq (nm)
Pristine	157±12.9	118.5±7.6	78.6±4.5	59.5±2.7	62.3±1.1	47.8±1.0
24 h	101.2±12.9	78.8±9.4	64.1±7.7	50.5±6.0	64.7±8.9	53.8±4.5
48 h	160.3±21.7	129.7±15.1	69.8±9.6	54.9±6.6	100.2±19.8	77.7±18.6

Figure 7.3 (a–i): The AFM image of the surface of disposable gloves after UV weathering. (a), (d) and (g) are pristine, weathered 24 and 48 h of latex gloves, respectively. (b), (e) and (h) are pristine, weathered 24 and 48 h of nitrile gloves, respectively. (c), (f) and (i) are pristine, weathered 24 and 48 h of vinyl gloves, respectively. (j) is the surface roughness of the gloves after UV weathering.

The variations in the peak load of different glove strips after exposure to UV irradiation are demonstrated in Figure 7.4. Initially, the peak load of the nitrile glove strips was 32.5±0.7 N, which was considerably greater than that of the latex and vinyl gloves. However, after weathering for 12 h, the peak load decreased pointedly to 5.3±0.6 N and was less than the other two gloves. After more than 12 h, the peak load rarely altered. With 42 h of weathering, the peak load of latex gloves showed a downward trend, but in the first 6 h, the average hourly load decreased about 1 N, and between 6 h and 42 h, the rate of decline was around 0.2 N/h. As weathering continued, the peak load increased notably, from 3.6±1.5 N to 7±2 N. The vinyl gloves presented a completely different pattern, with peak loads fluctuating around 15 N with weathering duration, but they can be considered to have remained stable.

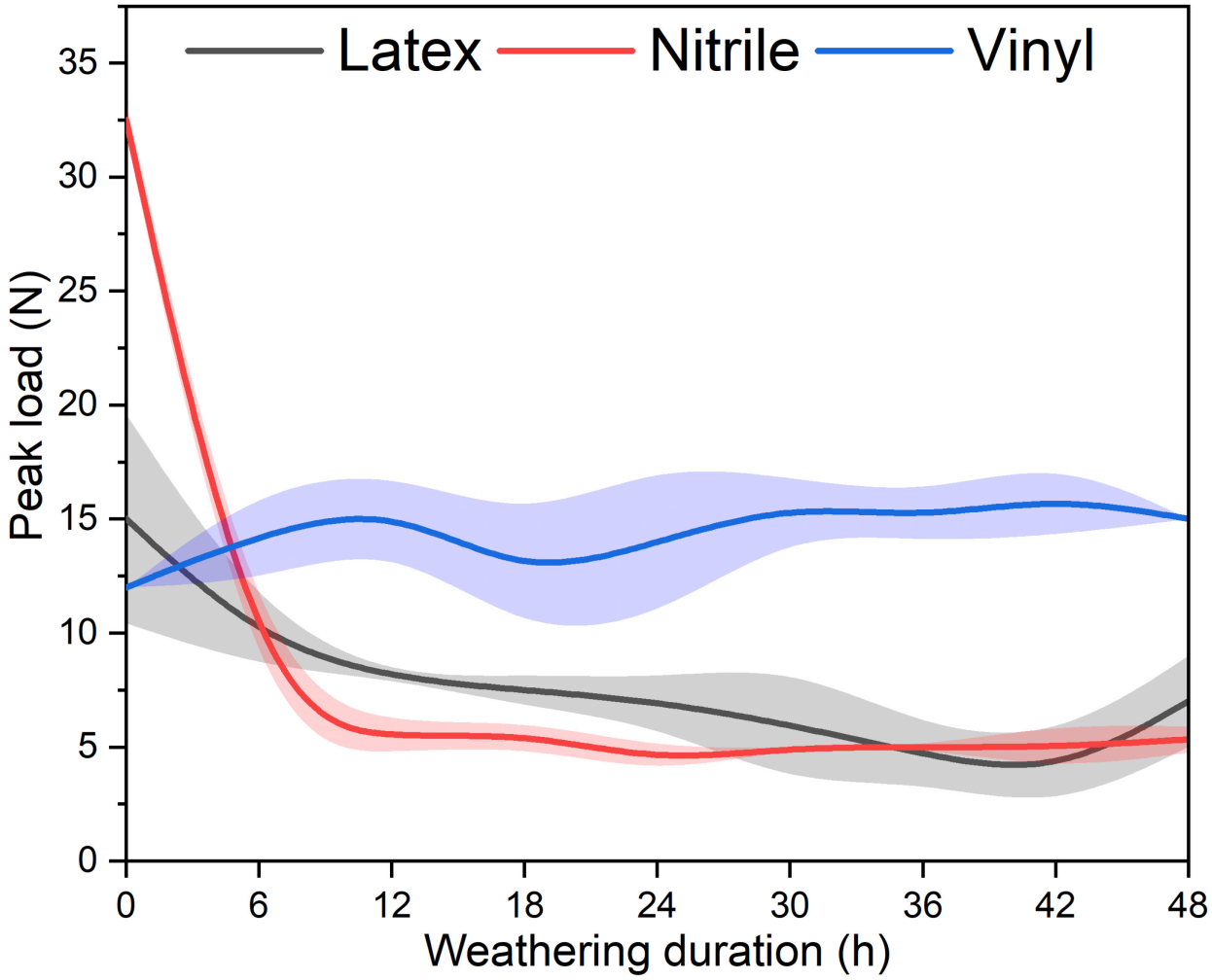


Figure 7.4 Mechanical strength of disposable gloves with different UV weathering durations

The hydrophilicity of the glove surface changed after UV irradiation, as shown by the changes in the contact angle (Figure 7.5). Concerning pristine latex gloves, the water droplet can adhere to the surface with a contact angle of 115.70°. After being subjected to weathering for 24 and 48 h, the contact angle decreased to 85.70° and 63.60°, respectively. The contact angle for the pristine nitrile gloves was 108.6°, which was similar to that of pristine latex gloves, and dropped to 83.30° and 65.80° when subjected to weathering for 24 and 48 h, respectively. The vinyl gloves displayed a different trend than the latex and nitrile gloves. The contact angle of the pristine vinyl glove was

84.50°, which slightly increased to 93.10° after 24 h of UV weathering. When weathered for 48 h, the contact angle declined to 44.90°. This phenomenon indicates that the hydrophilicity of latex and nitrile gloves was enhanced with increased weathering durations. The pristine vinyl gloves were more hydrophilic than the latex and nitrile gloves. When exposed to short periods of UV irradiation, the hydrophobic properties of the vinyl gloves increased marginally. However, as the weathering duration extended further, the hydrophilicity raised again.

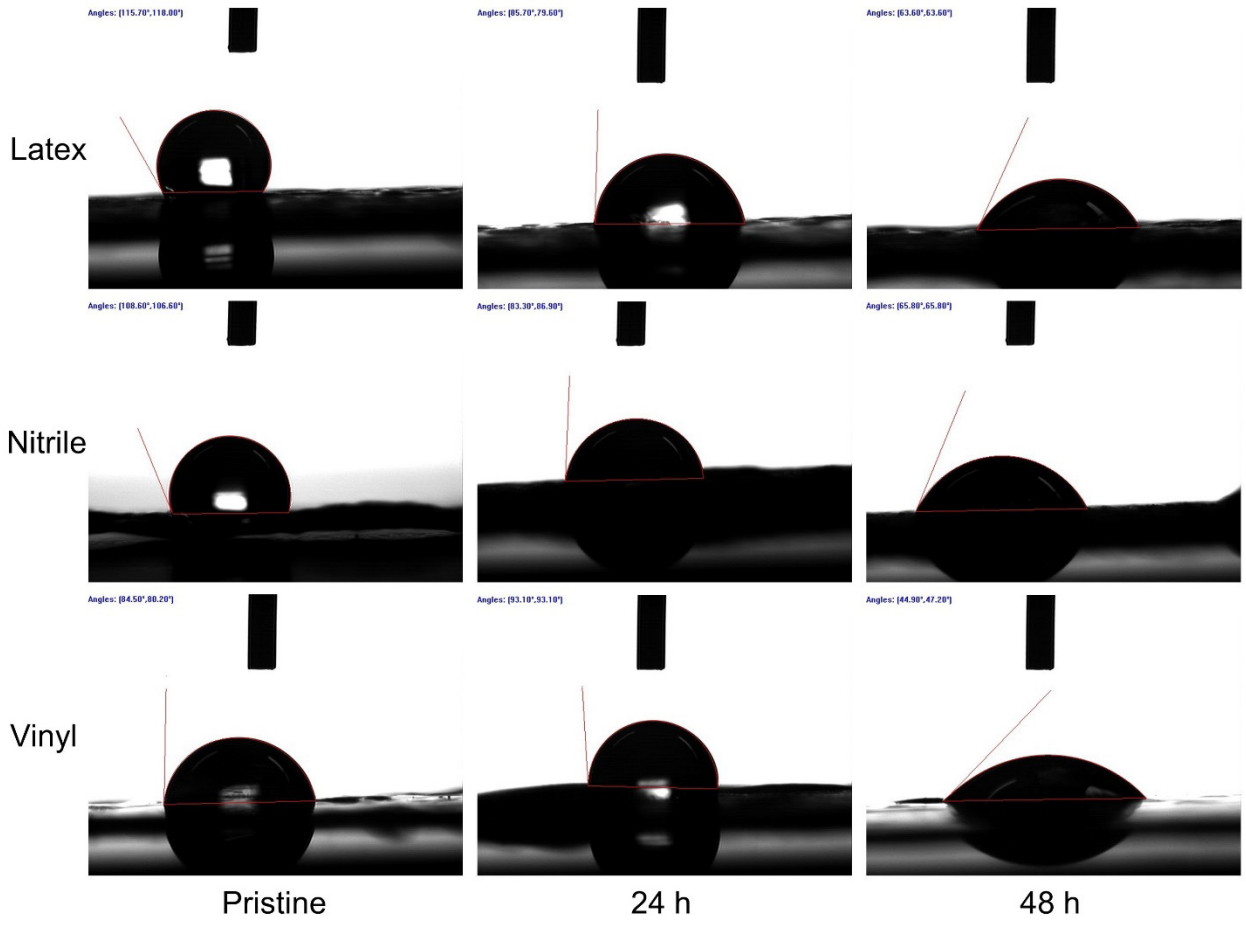


Figure 7.5 The changes of contact angle of disposable gloves with different UV weathering durations

7.3.2 MPs release from gloves into the aqueous environment

The patterns of pollutant releasing may very under different environmental conditions (Sundar et al., 2021; Wei et al., 2021; Zhao et al., 2015). The MPs released from the gloves into water under different conditions were further evaluated. Figure 7.6(a-c) shows the distribution of MPs released from the glove strips into the water after different UV irradiation durations. For the latex gloves, the concentration of MPs released gradually rose with increasing weathering durations. The concentration of MPs released from pristine latex gloves was 5.9±1.3 μL/L, and 96% of the particles were less than 25 μm in size. The concentration of particles released from the latex gloves irradiated with 12 h of weathering was 377.7±74.9 μL/L, an increase of about 63 times compared to the pristine state. Despite the distinct increase in concentration, the particle size distribution was consistent with the pristine gloves, with more than 89% of the particle size still less than 20 μm. When weathered for 24 h, the particles released from the latex gloves further increased by around 2.3 times to a concentration of 1264.3±366.7 μL/L, while the particle size distribution changed from a unimodal pattern to a trimodal pattern. Particles in the size ranges of 1–5, 5–25 and 25–250 μm accounted for 17%, 36% and 43% of the total concentration, respectively. After weathering for 36 h, the concentration of particles released by the latex gloves was 1689.6±135.9 μL/L, and the particle sizes were 1–5, 5–25 and 25–250 μm accounting for 15%, 32% and 44% of the total concentration, respectively. At 48 hours of UV weathering, the concentration of released particles was 2044.1±78.1 μL/L, and more than 53% of the particles had a size distribution between 25–200 μm, followed by particles in the range of 5–25 μm accounting for 23%. The size distributions of the particles released from nitrile gloves with weathering time are shown in Figure 7.6(b). The pristine nitrile glove strips released 0.5±0.2 μL/L MPs into water under shaking conditions, and more than 93% of the particles were less than 25 μm. The concentration of particles reached 5.5±2.6 μL/L after 12 h of weathering, and the concentration of particles with size distributions of 5–50 μm and 50–200 μm accounted for

60% and 31% of the total concentration, respectively. After 24, 36, and 48 h of UV weathering, the concentrations of particle released were 9.6±6.5, 22.4±2.4 and 46.4±10.1 μL/L, respectively. Additionally, regarding the increase in concentration, the particle size distributions all showed a unimodal pattern, with the percentage of particle sizes in the range of 5-25 μm being about 60%, 54% and 60%, respectively. Figure 7.6(c) exhibits the particle size distribution of the microparticles released by vinyl gloves. Initially, the concentration of MPs released from pristine vinyl gloves was 1.4±0.4 μL/L, and the particle size was largely located in the range of 50–100 and 100–400 μm. After 12 h of UV weathering, the concentration of particles released increased significantly to 15.1±3.2 μL/L, but as the weathering time extended, the concentration remained almost unchanged. While weathering for 48 h, the concentration once again increased fairly to 26.7±0.7 μL/L. The particle size distribution of the MPs released by the vinyl gloves was markedly different from that of the other two gloves. As seen in Figure 7.6(c), the concentration of particles smaller than 5 μm accounted for a high percentage, especially when the UV weathering duration exceeded 24 h.

These results show that latex gloves released far greater concentrations of MPs than nitrile and vinyl gloves, especially after UV irradiation. Weathering greatly increased the capacity for particle release from latex gloves. A latex glove weathered for 48 h released 340 times more particles than the pristine latex gloves. With the extension of weathering time, not only did the concentration of released particles increase, but the particle size distribution was also altered (Figure 7.6[g–i]). When the weathering time was less than 12 h, the particle sizes released by the latex gloves were mostly less than 25 μm. If the weathering time was greater than 24 h, the concentration of particles in the 25–250 μm range steadily increased. Combined with the SEM image, it was found that the pristine latex gloves had a large amount of particles less than 20 μm attached to the surface, and these particles separated from the glove surface and entered the water under shaking conditions. Prolonged

weathering time caused the particles on the surface to aggregate together, resulting in an increase in the sizes of the particles entering the water. Nitrile gloves were significantly less capable of releasing MPs than latex gloves, but the concentration of particles released after 48 h of UV weathering was still 93 times higher than that released by the pristine ones. In contrast to the latex gloves, the particle size distribution of particles released from the nitrile gloves was relatively stable. It can also be seen in the SEM image that there were no particles attached to the surface of the nitrile gloves, and after weathering, there was little change in surface roughness, except for cracks appearing. Furthermore, after 12 h of weathering, the concentration of released particles increased by a factor of 10 compared to the pristine state, while from 12 h to 24, 36, and 48 h, the concentration increased by factors of 0.7, 1.3, and 1.1, respectively. This was also consistent with the mechanical strength analysis, which showed that the peak load of nitrile gloves decreased the most in the first 12 h and then remained stable. The concentration of particles released by the vinyl gloves was also clearly smaller than that of the latex gloves. Because the detection range of the LISST is 1–500 μm, particles smaller than 1 μm were counted as 1 μm particles, which indicated that many nano-sized particles were released from the vinyl gloves. It was observed that with the increase in weathering time, the colors of the latex gloves and vinyl gloves' leachates turned yellow and creamy, respectively. This showed that during the shaking process, the weathered gloves not only released a large amount of MPs, but also many other leachable substances, such as stearates, fatty acids and inorganic salts (Witzig et al., 2020). Nevertheless, there was no distinctive color change for the leachate of the nitrile gloves.

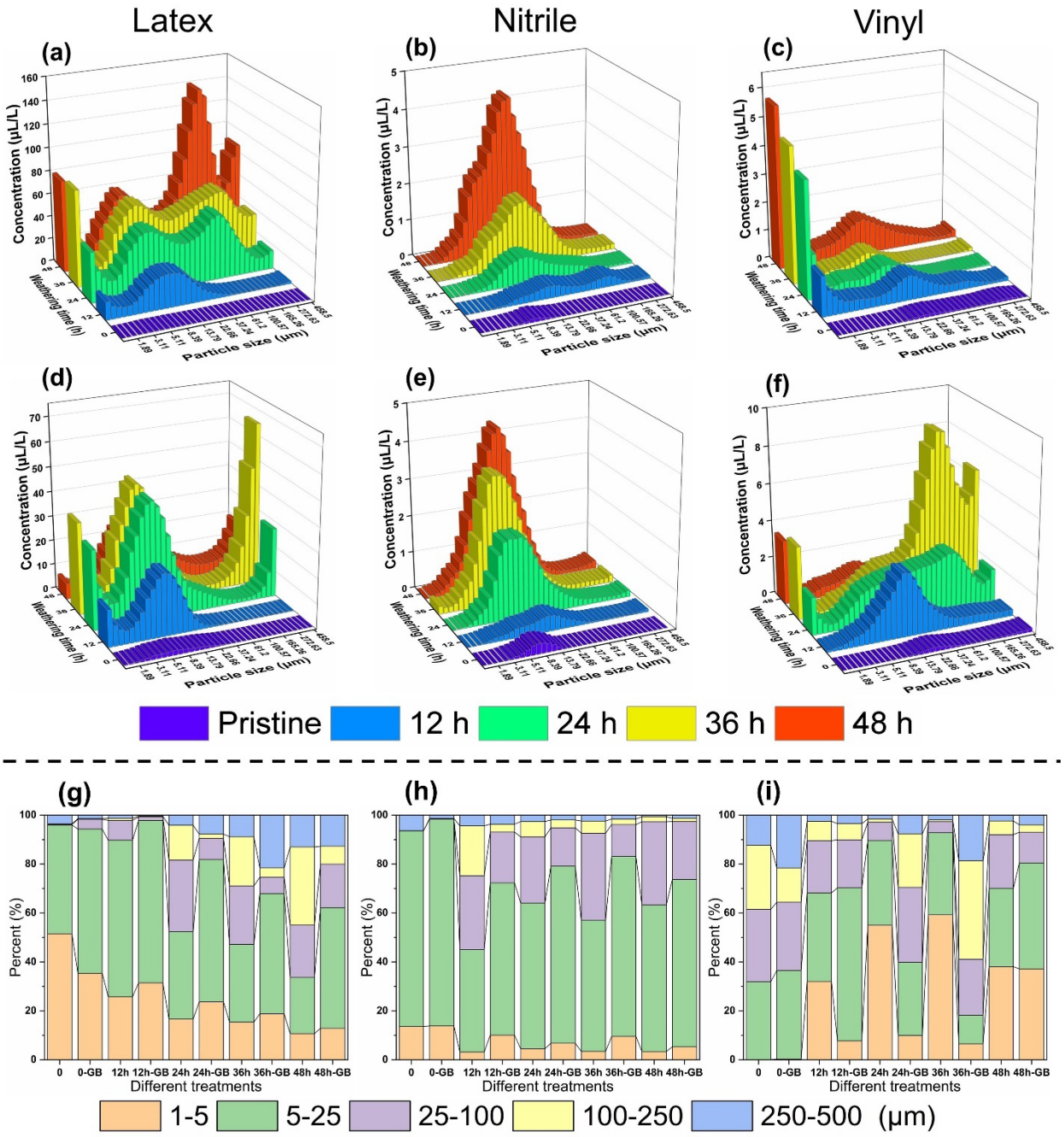


Figure 7.6 (a–c): The particle size distribution of MPs released from latex, nitrile, and vinyl gloves in the absence of sand. (d–i): The particle size distribution of MPs released from latex, nitrile, and vinyl gloves in the presence of sand. (g–i): The volume percent of particle size of MPs.

7.3.3 Release of MPs from gloves with exacerbation by physical abrasion

The features of particles released from the gloves after physical abrasion were analyzed to estimate the behavior of gloves in a shoreline environment. The background values of the glass bead leachates were first evaluated to show that the glass beads had no effect on the measurement of the MPs released from the gloves (Figure 7.7). The distribution of particles released from gloves into the water in the presence of glass beads is shown in Figure 7.6(d–f). Concerning pristine latex gloves, the concentration of MPs in the presence of glass beads was 22.5±3.9 μL/L, which was about a 3-fold increase compared to the absence of glass beads. Similar to the case without glass beads, more than 94% of the particles were less than 25 μm in size. When weathered for 12, 24, and 36 h, the concentrations of MPs in the presence of glass beads were 241.3±37.1, 584.7±14.6 and 729.7±269.7 μL/L, respectively. Conversely, the glass beads reduced the release of microparticles when the gloves were UV irradiated. In comparison with MPs released in the absence of glass beads, the concentrations were reduced by 36%, 54%, and 57%, respectively. Additionally, the particle size distribution of MPs also altered with weathering durations. When subjected to 12 h of weathering, or in cases with and without glass beads, most of the particle sizes that were distributed were below 100 μm, accounting for 98% and 99% of the total concentrations with beads and without, respectively. When weathered for 24 h, nearly 89% of the particle sizes were less than 50 μm in contrast to the multimodal distribution without glass beads. After 36 h of weathering, 73% of the particles were less than 50 μm, while 22% of the particles were distributed between 250 and 500 μm in size. Distinctly, the concentration of MPs released from latex gloves weathered for 48 h was only 387.8±141.8 μL/L, 81% lower than when there were no glass beads. Furthermore, considering only the presence of glass beads, the latex gloves weathered for 48 h released fewer MPs than gloves weathered for 36 h. Even so, 80% of the particles were less than 100 μm in size, and 20% of the

particles were between 100 and 500 μm, which is a pattern that is comparable to the gloves weathered 24 or 36 h.

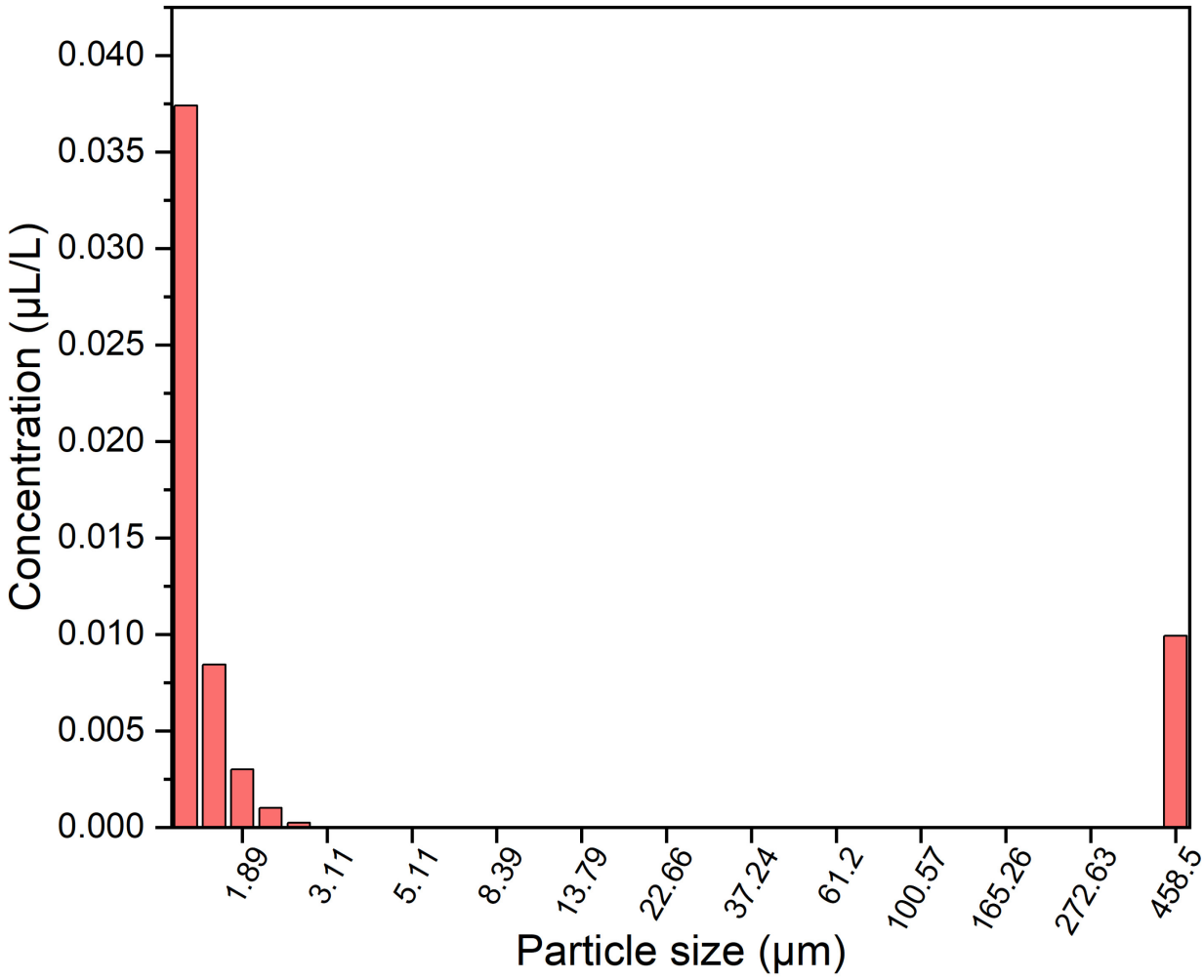


Figure 7.7 The size distribution of particles released from glass beads

In terms of nitrile gloves, the distributions of the particles released in the presence of glass beads are displayed in Figure 7.6(e). When glass beads were present, the concentration of MPs released by pristine nitrile gloves was 1.8±0.1 μL/L, a 2.6-fold increase compared to the absence of glass beads, and more than 98% of the particles were less than 25 μm. After 12 h of weathering, the concentration of released particles was 5.1±1.3 μL/L, which was identical to the concentration without glass beads.

Nevertheless, the particle size distributions were different. In contrast to the bimodal pattern when the glass beads were present, a unimodal pattern was exhibited when glass beads existed, and particles less than 100 μm in size accounted for more than 93% of the total. When weathered for 24 and 36 h, the concentrations of particles released were 24.9±10.2 and 37.6±11.5 μL/L, respectively. Compared to the absence of glass beads, the concentrations increased by 1.6 and 0.7, respectively. In addition, although most particles were less than 100 μm, the average particle size was reduced. After weathering for 48 h, the concentration and size distribution of particles released were consistent, regardless of the presence of glass beads.

With respect to the pristine vinyl gloves, the concentration of particles released was 2.7±0.3 μL/L, an increase of 90% over the absence of glass beads. The increase in the concentration had little effect on the particle size distribution. Particles that measured 2–100 μm and 100–500 μm accounted for 64% and 36% of the total distributed particles, respectively. If weathered for 12 h and with glass beads, the concentration of particles released was 38.0±16.1 μL/L, and more than 82% of the particles distributed were between 5 and 100 μm, displaying a unimodal pattern. The concentration of particles released from vinyl gloves weathered for 24 h increased to 67.7±2.6 μL/L. In particular, the particle size distribution at this time was distinct from the other conditions. It was found that the particles were evenly distributed between 5–500 μm without dominant peaks. For 36 h of weathering, the concentration of particles released was 114.47±75.1 μL/L, and more than 74% of the particles were located in the 50–500 μm size range. In contrast to the absence of glass beads, the size of the particles released from vinyl gloves weathered for 24 and 36 h increased significantly in the presence of glass beads. The situation was quite different with 48 h of weathering of the vinyl gloves, when the concentration of particles released was 19.8±3.3 μL/L in the presence of glass beads, which was slightly less than when the glass beads were absent, yet the particle size distributions were similar.

In general, the effect of glass beads on the release of MPs varied for gloves with different weathering durations and materials. For latex gloves, glass beads prevented weathered gloves from releasing MPs into the water phase. Furthermore, this hindering effect increased with the extension of weathering durations. The results showed that the concentrations of released particles in the presence of glass beads were reduced by 36%, 54%, 57%, and 81% when compared to those in the absence of glass beads for 12, 24, 36, and 48 h of weathering, respectively. Not only did the concentration decrease, but the average size of the particles released also reduced. According to the color change of the leachates, it is speculated that other substances in the latex gloves occupied a larger proportion, and these substances adsorbed to the surface of the glass beads, resulting in a decrease in the concentration of particles in the aqueous phase. In addition, these substances were more likely to be deposited at the bottom during testing, resulting in an underestimation of the results. The concentration of particles released by nitrile gloves was significantly lower than that of latex gloves, regardless of the presence of glass beads. The presence of glass beads facilitated the release of microparticles from the nitrile gloves, unlike other chemical crystals or other substances, which is consistent with the fact that the color of leachates changed little with increasing weathering durations. In addition, the physical abrasion of glass beads also reduced the size of the particles released, to some extent. The presence of glass beads not only increased the concentration of particles released by the vinyl gloves but also considerably changed the particle size distribution, except with gloves weathered for 48 h. With weathering durations from 1 h to 36 h, the concentrations of particle released by gloves when glass beads were present increased by 0.9, 1.5, 3.4, and 7.8 times, respectively, compared to those without glass beads. In addition, in the presence of glass beads, the average size of particles also became larger. In the absence of glass beads, particles were mainly distributed in the range of less than 50 μm, particularly less than 1 μm.

7.3.4 Leachable hazardous components released from gloves

Additives (including metal and metalloid elements) are widely used in plastics production. In this study, Al, Cr, Mn, Co, Ni, Cu, Zn, As, Sr, Ag, Cd, Sb, Ba, and Pb released from the gloves were measured using ICP-MS. Regarding the pristine, 24-h and 48-h weathering latex gloves, the total concentrations of specific elements released was 216.3, 8219.5 and 9338.5 ppb. Figure 7.8(a–c) reveal that Zn had the highest concentration (from 8200 to 9089 ppb) of heavy metals released from weathered latex gloves, which was more than 70 times higher than that released from the pristine gloves. In addition to Zn, the weathered latex gloves also released Al at a concentration of more than 100 ppb. The levels of Fe, Cu, Sr, and Sb released from the weathered latex gloves to the aqueous phase were above 20 ppb, while the Cr, Mn, Co, Ni, As, Ag, Cd, Ba, and Pb released were less than 10 ppb, especially the Cr, Co, Ag, Cd, and Pb, which were below 1 ppb. Figure 7.8(d) shows that Zn and Mn were the main metals released from pristine latex gloves, accounting for 54% and 33% of the total concentration, respectively. When weathered for 24 and 48 h, Zn became the predominant leachable, accounting for 96% and 97% of the total concentrations, respectively. The total concentration of elements released by the pristine nitrile gloves was 130.0 ppb, in which Zn, Cu, Sb and Al accounted for 39%, 24%, 17% and 12%, respectively. After 24 and 48 h of UV irradiation, the total concentrations of elements released were 1810.5 and 1658.1 ppb, respectively. Similar to latex gloves, Zn was also the dominant heavy metal released from the weathered nitrile gloves, at a concentration greater than 1400 ppb, a 28-fold increase compared with pristine nitrile gloves. The release of Al from nitrile gloves was exacerbated by UV weathering, with an increase of 15.3 to 144.6 ppb concentration. Along with Al, the concentration of Fe released increased from 0.9 to 43.2 ppb, a 47-fold increase. The concentrations of Cu, Sr, and Sb released from the pristine nitrile gloves were greater than 5 ppb, and weathering slightly facilitated the release. Nevertheless,

regardless of weathering, the concentrations of Cr, Co, Ni, As, Ag, Cd, and Pb released from the nitrile gloves was less than 1 ppb. The total concentrations of elements released from the pristine, weathered 24 and 48 h vinyl gloves were 122.3, 1086.1 and 1122.1 ppb, respectively. However, the types and percentages of elements released differed from those of latex and nitrile gloves. Concerning the pristine vinyl gloves, the main metal released was Zn, accounting for 51% of the total concentration, followed by Cu, Sb, and Al, accounting for 18%, 18% and 8% of the total concentration, respectively. After 24 h of weathering, the concentrations of Zn and Al were 42% and 40%, and when weathering was extended to 48 h, the values became 38% and 45%, respectively. Furthermore, weathered vinyl gloves released concentrations of Fe and Cu in excess of 60 ppb, and the concentrations of Cr, Co, As, Cd, and Pb were below 1 ppb. Ag was not detected in the leachates of the vinyl gloves.

In addition to the element release, the organic compounds released in the leachates of the gloves were also identified. Alkanes and aliphatic compounds, both chain and cyclic, were found in the leachates of all three types of gloves. It can be seen in Table 7.1 that benzo[h]quinoline, furan/furanone, and pyridine were detected in all three glove leachates. In addition, latex gloves released heterocyclic aromatic organic compounds into the water, including benzo[β]pyran, benzocycloheptene, and benzofurazan. Formamide, as a component of nitrile gloves, was also detected in the leachates. In addition, two kinds of phthalic acid were detected in the leachates of nitrile gloves weathered for 48 h. These were 3,5-difluorophenyl neopentyl ester phthalic acid and 5-methoxy-3-methylpent-2-yl octyl ester phthalic acid. Different from the other two types of gloves, vinyl gloves released a variety of phthalic acids. Overall, as a commonly used chelating agent, zinc is widely used in rubber, plastic, and other production processes. UV weathering promoted the release of Zn from gloves into the aqueous phase. Previous studies have also proved that the heavy

metal with the highest rates of glove release is Zn (Garçon et al., 2017; Jedruchniewicz et al., 2021). Concurrently, other chelating agents, such as Fe, Al, and Cu, were also released into the water. In addition, the risk of other heavy metals, including Pb, Cd, and Cr, cannot be ignored due to their high toxicity, even at small doses. The results of organic matter analysis showed that vinyl gloves released phthalic acid more easily, which can pose a potential risk to human health.

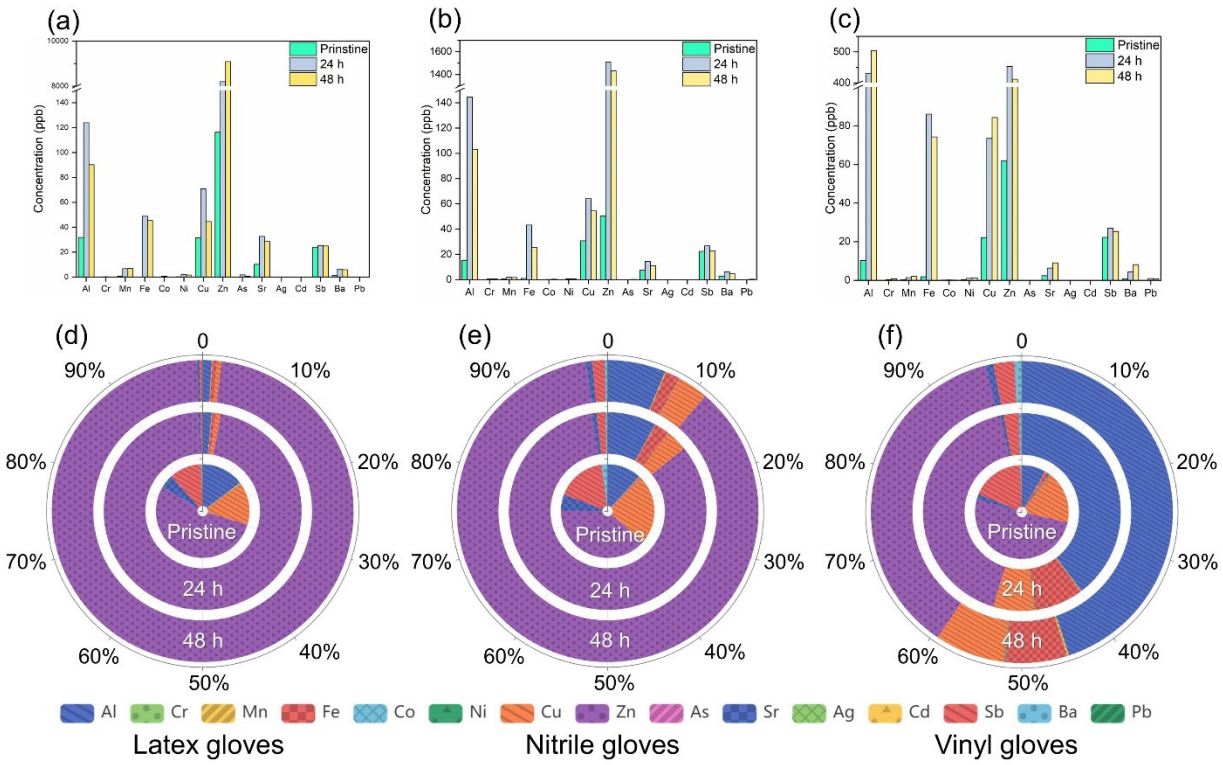


Figure 7.8 (a–c): Concentrations of elements released from disposable gloves before and after UV weathering. (d–f): The concentration percent of leachable elements by different gloves before and after UV weathering.

Table 7.1 The organic matters released from disposable gloves

Compounds	L 0	L 24	L 48	N 0	N 24	N 48	V 0	V 24	V 48
Benzo[h]quinoline	+			+	+	+	+		+
Benzocycloheptene	+	+							
benzofurazan	+	+				+			
Benzo[b]pyran	+	+							
Furan/Furanone	+	+			+		+	+	
Pyridine	+		+	+	+	+	+	+	
Formamide				+	+		+		
Benzenediol				+	+	+			
Phthalic acid, 3,5-difluorophenyl neopentyl ester						+			
Phthalic acid, 5-methoxy-3-methylpent-2-yl octyl ester						+			
Phthalic acid, 4-bromophenyl 2-ethylhexyl ester							+	+	+
Phthalic acid, 3,5-difluorophenyl 2-ethylhexyl ester							+	+	+
Phthalic acid, hexyl 2-methylallyl ester							+	+	+

*Continuous

Compounds	L 0	L 24	L 48	N 0	N 24	N 48	V 0	V 24	V 48
Phthalic acid, neopentyl nonyl ester							+	+	+
Phthalic acid, 3,5-difluorophenyl octyl ester							+	+	
Phthalic acid, cyclohexylmethyl octyl ester								+	
Phthalic acid, 4-chloro-3-methylphenyl 2-ethylhexyl ester								+	+
Phthalic acid, 2-ethylhexyl non-5-yn-3-yl ester								+	
Phthalic acid, monoamide, N-isopropyl-, isobutyl ester								+	+
Phthalic acid, 3,4-dichlorophenyl 2-ethylhexyl ester								+	+
Phthalic acid, 2-ethylhexyl 3-methylphenyl ester							+	+	
Phthalic acid, 2-ethylhexyl 4-methoxyphenyl ester							+		+

*Continuous

Compounds	L 0	L 24	L 48	N 0	N 24	N 48	V 0	V 24	V 48
Phthalic acid, isohexyl isoporpyl ester							+		
Phthalic acid, 2-cyclohexylethyl ethyl ester							+		+
Phthalic acid, isobutyl 3-methylbut-2-en-1-yl ester							+		
Phthalic acid, ethyl pentadecyl ester							+		
Phthalic acid, 3-chlorophenyl 2-ethylhexyl ester							+		
Phthalic acid, 2-cyclohexylethyl dodecyl ester								+	+
Phthalic acid, 2-cyclohexylethyl propyl ester							+		
Phthalic acid, ethyl pentyl ester									+
Phthalic acid, 4-chlorophenyl 2-ethylhexyl ester							+		
Phthalic acid, 4-cyanophenyl heptyl ester									+

+: The substance was detected. L means latex gloves, N means nitrile gloves, V means vinyl gloves. 0, 24 and 48 represent pristine, 24 h of weathering and 48 h of weathering, respectively.

7.3.5 Environmental implications

Disposable gloves are essential in medical, catering, production, and other industries, and the pandemic has resulted in a significant increase in glove consumption among the public. The environmental impact of disposable masks has been given attention (Li et al., 2020a; Sullivan et al., 2021; Wang et al., 2021c). However, few studies have concentrated on the environmental effects of disposable gloves discarded into the water system. Surface water (rivers, lakes and ocean) is important sink for pollutants, while the shoreline plays a key role in the transport and transformation of pollutants (Wang et al., 2021c; Wang et al., 2022c; Xie et al., 2020). This study showed that the physicochemical characteristics of disposable gloves made of different materials were altered to different degrees by UV weathering. Nitrile gloves were more stable than latex and vinyl gloves after being exposed to weathering conditions. Although the chemical structures were not clearly demonstrated through FTIR after 48 h of weathering, the SEM results showed significant microscopic changes on the surfaces of the gloves. Compared to disposable masks, which were completely weathered after 48 h of UV radiation, disposable gloves exhibited better performance in mechanical properties (Wang et al., 2021c). Analysis of the leachate results showed that UV weathered gloves released leachable substances, including MPs, organic matter, and heavy metals. Due to the stability of the nitrile gloves, the concentration of particles released was lower than that of the other two types of gloves. Latex gloves were more likely to release microparticles and other substances into the water after UV weathering. In addition, the impact of physical abrasion triggered by glass beads on the release of microparticles was shown to vary. Overall, nitrile and vinyl gloves released more microparticles when glass beads were present, while latex gloves did the opposite.

This study indicates that, given the variety of materials and ingredients, the environmental risk of gloves is more uncertain than that with disposable masks. This uncertainty is exacerbated by the role of various environmental factors in aqueous environments. Besides, glove wastes should also be well managed in cities to reduce the amount getting into the natural environment. However, there are some limitations for this study. For example, the particles less than 1 μm were not measured and discussed in the present study. In order to simulate a more realistic natural environment, the impact of other environmental factors such as temperature and water salinity can be further considered. In order to further explore the impact of gloves on urban and natural aquatic ecosystems, it is expected to (i) know the type, quantity, and spatial and temporal distribution of disposable gloves for an integrated socio-environmental impact assessment; (ii) evaluate the behavior and toxicology of the gloves and glove-derived chemicals in the natural environment, as well as their effects on the surrounding microenvironment; (ii) establish a more robust management system for glove waste collection and disposal. Given these considerations, uniform standards for the production, transport, use and disposal of disposable gloves are vital. To achieve this, a multidisciplinary approach and the collaborative efforts of researchers, governments, industries, and the public are required.

Chapter 8. Contributions and significance of thesis research, and suggestions for future work

8.1 Contributions and significance of thesis research

- NBs significantly increased the concentration of dissolved oxygen as well as changed the pH, ζ potential, and surface tension of the water. Surface active materials and salinity affected the properties of NBs. Bulk NBs in the ocean contributed to the oil detachment from sand surface, and Surface nanobubbles in the substrate obstructed the downward transport of oil colloids.
- Natural NBs can influence the motion and aggregation of MPs in the ocean. In the presence of NBs, the binding of MPs and NBs resulted in an increase in the measured average particle size and concentration. The increase in ionic strength reduced the energy barrier between particles and promoted their aggregation.
- NBs attached to the substrate of the coastal vadose zone, altering the vertical movement of MPs within the substrate, that was subject to mutual forces between the substrate, MPs, and NBs. Increased salinity reinforced the retention of NBs for MPs during the transport. Transient penetration induced by wave wash had a significant effect on the motion of hydrophilic MPs.
- The transformation of chain structure and chemical composition of masks as well as the decreased mechanical strength of PPE waste after UV weathering were observed. The physical abrasion caused by sand further exacerbated the release of MPs particles from PPE

wastes. Shorelines are not only the main receptor of PPE waste from oceans and lands, but also play host to further transformation of PPE waste to plastic particles.

8.2 Suggestions for future work

- The complex environment represented by the coastline is not only a sink for pollutants, but also play host for further transport and transformation of pollutants. The identification of key parameters of complex environments is essential for determining the fate of pollutants and assessing their environmental risks.
- Pollutants represented by PPE wastes pose new pressures on the environment. Identifying the fate and transport of these pollutants in the environment, as well as the environmental hazards, is a prerequisite for the formulation of sound policies.
- NBs can change the physicochemical parameters of aqueous solutions, which in turn affects the transformations and transport of pollutants in multiphase media. Biodegradation of pollutants is an important pathway for pollutant degradation. Since natural NBs enhance dissolved oxygen, explore the role of NBs for the growth of microbial populations can deepen our understanding of biodegradation processes.
- NBs can influence the fate and transport of pollutants in both aqueous and solid phases, but this process is still not understood well. A multifaceted exploration of the role played by NBs in the fate and transport of different pollutants at the micro-scale is necessary. This is also a prerequisite for the application of NBs to pollutant treatment.

Publications

Peer-reviewed journal articles

[1] **Zheng Wang**, Chunjiang An, Kenneth Lee, Qi Feng. 2023. Overlooked role of bulk nanobubbles in the alteration and motion of microplastics in the ocean environment. ***Environmental Science & Technology***, 57(30), 11289-11299.

[2] **Zheng Wang**, Chunjiang An, Kenneth Lee, Qi Feng, Baiyu Zhang. 2023. Exploring the role of nanobubbles in the fate and transport of spilled oil on shorelines. ***ACS EST Water***, 3 (1), 30-40.

[3] **Zheng Wang**, Chunjiang An, Kenneth Lee, Xiujuan Chen, Baiyu Zhang, Jianan Yin, Qi Feng. 2022. Physicochemical change and microparticle release from disposable gloves in the aqueous environment impacted by accelerated weathering. ***Science of the Total Environment***, 823, 154986.

[4] **Zheng Wang**, Chunjiang An, Kenneth Lee, Edward Owens, Michel Boufadel, Qi Feng. 2021. Dispersion modeling of particulate matter from the in-situ burning of spilled oil in the northwest Arctic area of Canada. ***Journal of Environmental Management***, 301, 113913.

[5] **Zheng Wang**, Chunjiang An, Kenneth Lee, Baiyu Zhang, Qi Feng. 2021. Disposable masks release microplastics to the aqueous environment with exacerbation by natural weathering. ***Journal of Hazardous Materials***, 417, 126036.

[6] **Zheng Wang**, Christophe Guy, Kelvin Tsun Wai Ng, Chunjiang An. 2021. A new challenge for the management and disposal of personal protective equipment waste during the COVID-19 pandemic. ***Sustainability***, 13, 7034.

[7] **Zheng Wang**, Chunjiang An, Kenneth Lee, Edward Owens, Zhi Chen, Michel Boufadel, Elliott Taylor, Qi Feng. 2020. Factors influencing the fate of oil spilled on shorelines: a

review. ***Environmental Chemistry Letters***, 19, 1611–1628.

[8] Qi Feng, Chunjiang An, Zhi Chen, Kenneth Lee, **Zheng Wang**. 2023. Identification of the driving factors of microplastic load and morphology in estuaries for improving monitoring and management strategies: A global meta-analysis. ***Environmental Pollution***, 333, 122014.

[9] Qi Feng; Zhi Chen; Chunjiang An; Xiaohan Yang; **Zheng Wang**. Tide-induced Infiltration and Resuspension of Microplastics in Shorelines: Insights from Tidal Tank Experiments. ***Water Research***, 236, 119970.

[10] Mengfan Cai, Zhiming Qi, Christophe Guy, Chunjiang An, Xiujuan Chen, **Zheng Wang**, Qi Feng. Insights into the Abiotic Fragmentation of Biodegradable Mulches under Accelerated Weathering Conditions. ***Journal of Hazardous Materials***, 454, 131477.

[11] Qi Feng, Chunjiang An, Zhi Chen, **Zheng Wang**. 2023. New Perspective on the Mobilization of Microplastics through Capillary Fringe Fluctuation in a Tidal Aquifer Environment. ***Environmental Science & Technology***, 57 (2), 929-938.

[12] Linxiang Lyu, **Zheng Wang**, Monisha Bagchi, Zhibin Ye, Ahmed Soliman, Ashutosh Bagchi, Nektaria Markoglou, Jianan Yin, Chunjiang An, Xiaohan Yang, Huifang Bi, Mengfan Cai. 2023. An investigation into the aging of disposable face masks in landfill leachate. ***Journal of Hazardous Materials***, 446, 130671.

[13] Mohammadmehdi Raznahan, S. Samuel Li, **Zheng Wang**, Michel Boufadel, Xiaolong Geng, Chunjiang An. 2022. Numerical simulation of multiphase oil behaviors in ice-covered nearshore water. ***Journal of Contaminant Hydrology***, 251, 104069.

[14] Qi Feng, Zhi Chen, Charles W. Greer, Chunjiang An, **Zheng Wang**. 2022. Transport of microplastics in shore substrates over tidal cycles: roles of polymer characteristics and environmental factors. ***Environmental Science & Technology***, 56 (12), 8187-8196.

[15] Qi Feng, Chunjiang An, Zhi Chen, Jianan Yin, Baiyu Zhang, Kenneth Lee, **Zheng Wang**.

2022. Investigation into the impact of aged microplastics on oil behavior in shoreline environments. ***Journal of Hazardous Materials***, 421, 126711.

[16] Qi Feng, Chunjiang An, Zhi Chen, Yingchun Zhang, Edward Owens, Kenneth Lee, Biao Li, Elliott Taylor, **Zheng Wang**. 2022. Exploring the effects of substrate mineral fines on oil translocation in the shoreline environment: Experimental analysis, numerical simulation, and implications for spill response. ***Journal of Hazardous Materials***, 437, 129341.

[17] Huifang Bi, Chunjiang An, Catherine N. Mulligan, **Zheng Wang**, Baiyu Zhang, Kenneth Lee. 2021. Exploring the use of alginate hydrogel coating as a new initiative for emergent shoreline oiling prevention. ***Science of The Total Environment***, 797, 149234.

[18] Qi Feng, Chunjiang An, Zhi Chen, Edward Owens, Haibo Niu, **Zheng Wang**. 2021. Assessing the coastal sensitivity to oil spills from the perspective of ecosystem services: A case study for Canada's Pacific coast. ***Journal of Environmental Management***, 296, 113240.

[19] Qi Feng, Chunjiang An, Yitian Cao, Zhi Chen, Edward Owens, Elliott Taylor, **Zheng Wang**, El Azzaoui Saad. 2021. An analysis of selected oil spill case studies on the shorelines of Canada. ***Journal of Environmental Informatics Letters***, 5 (1), 39-47.

[20] Qi Feng, Chunjiang An, Zhi Chen, **Zheng Wang**. 2020. Can deep tillage enhance carbon sequestration in soils? A meta-analysis towards GHG mitigation and sustainable agricultural management. ***Renewable and Sustainable Energy Reviews***, 133, 110293.

[21] Xinghua Zhang, **Zheng Wang**, Peng Huo, Lijia Zhang, Qingcai Chen, Yang Zhang. Pollution characteristics of environmental persistent free radicals and coexisting health risk substances in $PM_{2.5}$ in Huairou, Beijing. ***Environmental Chemistry***, 2022, 41 (3), 813-822. (In Chinese).

[22] **Zheng Wang**, Xinghua Zhang, Lijia Zhang, Peng Huo, Yuanxun Zhang, Yang Zhang. Detection of environmentally persistent free radicals in atmospheric particulate matter by electron paramagnetic resonance, ***Environmental Chemistry***, (2), 317-325. (In Chinese).

Conference presentations & abstracts

[1] Zheng Wang et al. The role of bulk nanobubbles in the motion of microplastics on shorelines. *PEOPLE 2023*, Montreal, Canada, 2023.

[2] Zheng Wang et al. Effect of nanobubbles on the fate and transport of oil spill. *International oil spill science conference 2022*, Halifax, Canada, 2022.

[3] Zheng Wang et al. Microplastic Release from Weathered Disposable Gloves in the Shoreline Environment. *International Conference on Persistent, Emerging, and Organic Pollution in the Environment – Challenges and Solutions under Climate Change*, Charlottetown, Canada, 2022.

[4] Zheng Wang et al. Dispersion of Particulate Matter from Oil Spill Response in Cold Regions. Cold Regions Specialty, Computer Science, *Computer Engineering, & Applied Computing (CSCE 2022)*, Whistler, Canada, 2022.

[5] Zheng Wang et al. Disposable face masks: a new source of microplastics in aqueous environment. *LEADERS & PEOPLE 2021 Virtual Symposium: Environmental Research and Career Training*, Virtual, Canada, 2021.

[6] Zheng Wang, et al. Study on the concentration of free radicals in atmospheric $PM_{2.5}$ in Beijing. *The 23rd China conference on atmospheric environmental science and technology*, Beijing, China, 2017. (In Chinese)

References

Aalto-Korte, K., Ackermann, L., Henriks-Eckerman, M.-L., Valimaa, J., Reinikka-Railo, H., Nen, E.L. and Jolanki, R. 2007. 1,2-benzisothiazolin-3-one in disposable polyvinyl chloride gloves for medical use. Contact Derm, 57, 365-370.

Abou-Khalil, C., Prince, R.C., Greer, C.W., Lee, K. and Boufadel, M.C. 2022. Bioremediation of petroleum hydrocarbons in the upper parts of sandy beaches. Environ Sci Technol, 56(12), 8124-8131.

Aeppli, C., Mitchell, D.A., Keyes, P., Beirne, E.C., McFarlin, K.M., Roman-Hubers, A.T., Rusyn, I., Prince, R.C., Zhao, L., Parkerton, T.F. and Nedwed, T. 2022. Oil irradiation experiments document changes in oil properties, molecular composition, and dispersant effectiveness associated with oil photo-oxidation. Environ Sci Technol, 56(12), 7789-7799.

Agarwal, A., Ng, W.J. and Liu, Y. 2011. Principle and applications of microbubble and nanobubble technology for water treatment. Chemosphere, 84(9), 1175-1180.

Agostini, D.L.S., Constantino, C.J.L. and Job, A.E. 2008. Thermal degradation of both latex and latex cast films forming membranes. J Therm Anal Calorim, 91(3), 703-707.

Agrebi, F., Ghorbel, N., Bresson, S., Abbas, O. and Kallel, A. 2018. Study of nanocomposites based on cellulose nanoparticles and natural rubber latex by ATR/FTIR spectroscopy: the impact of reinforcement. Polym Compos, 40(5), 2076-2087.

Agyei-Tuffour, B., Gbogbo, S., Dodoo-Arhin, D., Damoah, L.N.W., Efavi, J.K., Yaya, A., Nyankson, E. and Arellano-Garcia, H. 2020. Photocatalytic degradation of fractionated crude oil: potential application in oil spill remediation. Cogent Eng, 7(1), 1744944.

Ahn, S., Haas, K.A. and Neary, V.S. 2019. Wave energy resource classification system for US coastal waters. Renew Sust Energ Rev, 104, 54-68.

Akhbarizadeh, R., Dobaradaran, S., Amouei Torkmahalleh, M., Saeedi, R., Aibaghi, R. and Faraji Ghasemi, F. 2021a. Suspended fine particulate matter ($PM_{2.5}$), microplastics (MPs), and polycyclic aromatic hydrocarbons (PAHs) in air: their possible relationships and health implications. Environ Res, 192, 110339.

Akhbarizadeh, R., Dobaradaran, S., Nabipour, I., Tajbakhsh, S., Darabi, A.H. and Spitz, J. 2020. Abundance, composition, and potential intake of microplastics in canned fish. Mar Pollut Bull, 160, 111633.

Akhbarizadeh, R., Dobaradaran, S., Nabipour, I., Tangestani, M., Abedi, D., Javanfekr, F., Jeddi, F. and Zendehboodi, A. 2021b. Abandoned Covid-19 personal protective equipment along the Bushehr shores, the Persian Gulf: an emerging source of secondary microplastics in coastlines. Mar Pollut Bull, 168, 112386.

Alheshibri, M., Qian, J., Jehannin, M. and Craig, V.S. 2016. A history of nanobubbles. Langmuir, 32(43), 11086-11100.

Allen, D., Allen, S., Abbasi, S., Baker, A., Bergmann, M., Brahney, J., Butler, T., Duce, R.A., Eckhardt, S., Evangeliou, N., Jickells, T., Kanakidou, M., Kershaw, P., Laj, P., Levermore, J., Li, D., Liss, P., Liu, K., Mahowald, N., Masque, P., Materić, D., Mayes, A.G., McGinnity, P., Osvath, I., Prather, K.A., Prospero, J.M., Revell, L.E., Sander, S.G., Shim, W.J., Slade, J., Stein, A., Tarasova, O. and Wright, S. 2022. Microplastics and nanoplastics in the marine-atmosphere environment. Nat Rev Earth Environ, 3(6), 393-405.

Allen, S., Allen, D., Moss, K., Le Roux, G., Phoenix, V.R. and Sonke, J.E. 2020. Examination of the ocean as a source for atmospheric microplastics. PLoS One, 15(5), e0232746.

Ammendolia, J., Saturno, J., Brooks, A.L., Jacobs, S. and Jambeck, J.R. 2021. An emerging source of plastic pollution: environmental presence of plastic personal protective equipment (PPE) debris related to COVID-19 in a metropolitan city. Environ Pollut, 269, 116160.

Andrady, A.L. 2011. Microplastics in the marine environment. Mar Pollut Bull, 62(8), 1596-1605.

Andrady, A.L. 2017. The plastic in microplastics: a review. Mar Pollut Bull, 119(1), 12-22.

Anedda, J., Ferreli, C., Rongioletti, F. and Atzori, L. 2020. Changing gears: medical gloves in the era of coronavirus disease 2019 pandemic. Clin Dermatol, 38(6), 734-736.

Aragaw, T.A. 2020. Surgical face masks as a potential source for microplastic pollution in the COVID-19 scenario. Mar Pollut Bull, 159, 111517.

Ardusso, M., Forero-Lopez, A.D., Buzzi, N.S., Spetter, C.V. and Fernandez-Severini, M.D. 2021. COVID-19 pandemic repercussions on plastic and antiviral polymeric textile causing pollution on beaches and coasts of South America. Sci Total Environ, 763, 144365.

Asif, Z. and Chen, Z. 2016. Multimedia environmental analysis of PCBs fate and transport mechanism through a case study of transformer oil leakage. Int J Environ Sci Technol (Tehran), 13(3), 793-802.

Aslanzadeh, S. and Haghighat Kish, M. 2010. Photo-oxidation of polypropylene fibers exposed to short wavelength UV radiations. Fibers and Polymers, 11(5), 710-718.

Aslanzadeh, S. and Kish, M.H. 2005. Photodegradation of polypropylene thermal bonded non-woven fabric. Polym Degrad Stab, 90(3), 461-470.

Atkinson, A.J., Apul, O.G., Schneider, O., Garcia-Segura, S. and Westerhoff, P. 2019. Nanobubble technologies offer opportunities to improve water treatment. Acc Chem Res, 52(5), 1196-1205.

Avio, C.G., Cardelli, L.R., Gorbi, S., Pellegrini, D. and Regoli, F. 2017. Microplastics pollution after the removal of the Costa Concordia wreck: first evidences from a biomonitoring case study. Environ Pollut, 227, 207-214.

Badiozamani, M.M., Ben-Awuah, E. and Askari-Nasab, H. 2019. Mixed integer linear programming for oil sands production planning and tailings management. J Environ Inform, 33(2), 96-104.

Bai, M., Liu, Z., Zhang, J. and Lu, L. 2021. Prediction and experimental study of mass transfer properties of micronanobubbles. Ind Eng Chem Res, 60(22), 8291-8300.

Bakaraki Turan, N., Sari Erkan, H. and Onkal Engin, G. 2021. Current status of studies on microplastics in the world's marine environments. J Clean Prod, 327, 129394.

Bao, Q., Chen, J., Xiang, Y., Zhang, K., Li, S., Jiang, X., Xu, Q.-H., Loh, K.P. and Venkatesan, T. 2015. Graphene nanobubbles: a new optical nonlinear material. Adv Opt Mater, 3(6), 744-749.

Batchelor, D.V.B., Abou-Saleh, R.H., Coletta, P.L., McLaughlan, J.R., Peyman, S.A. and Evans, S.D. 2020. Nested nanobubbles for ultrasound-triggered drug release. ACS Appl Mater Interfaces, 12(26), 29085-29093.

Bejarano, A.C. and Michel, J. 2010. Large-scale risk assessment of polycyclic aromatic hydrocarbons in shoreline sediments from Saudi Arabia: environmental legacy after twelve years of the Gulf war oil spill. Environ Pollut, 158(5), 1561-1569.

Belzagui, F., Buscio, V., Gutierrez-Bouzan, C. and Vilaseca, M. 2020. Cigarette butts as a microfiber source with a microplastic level of concern. Sci Total Environ, 762, 144165.

Bendjaouahdou, C. and Bensaad, S. 2018. Aging studies of a polypropylene and natural rubber blend. International Journal of Industrial Chemistry, 9(4), 345-352.

Bera, A., Mandal, A. and Guha, B.B. 2013. Synergistic effect of surfactant and salt mixture on interfacial tension reduction between crude oil and water in enhanced oil recovery. J Chem Eng Data, 59(1), 89-96.

Bernabeu, A.M., Fernandez-Fernandez, S. and Rey, D. 2016. A theoretical model to estimate the oil burial depth on sandy beaches: a new oil spill management tool. Mar Pollut Bull, 109(1), 361-372.

Bernabeu, A.M., Nuez de la Fuente, M., Rey, D., Rubio, B., Vilas, F., Medina, R. and Gonzalez, M.E. 2006. Beach morphodynamics forcements in oiled shorelines: coupled physical and chemical processes during and after fuel burial. Mar Pollut Bull, 52(10), 1156-1168.

Beyer, J., Trannum, H.C., Bakke, T., Hodson, P.V. and Collier, T.K. 2016. Environmental effects of the Deepwater Horizon oil spill: a review. Mar Pollut Bull, 110(1), 28-51.

Bi, H., An, C., Chen, X., Owens, E. and Lee, K. 2020. Investigation into the oil removal from sand using a surface washing agent under different environmental conditions. J Environ Manage, 275, 111232.

Bi, H., An, C., Owens, E., Lee, K., Chen, Z., Mulligan, C., Taylor, E. and Boufadel, M. 2021. A framework for the evaluation and selection of shoreline surface washing agents in oil spill response. J Environ Manage, 287, 112346.

Blair, R.M., Waldron, S. and Gauchotte-Lindsay, C. 2019. Average daily flow of microplastics through a tertiary wastewater treatment plant over a ten-month period. Water Res, 163, 114909.

Boehm, P.D., Page, D.S., Brown, J.S., Neff, J.M., Bragg, J.R. and Atlas, R.M. 2008. Distribution and weathering of crude oil residues on shorelines 18 years after the Exxon Valdez spill. Environ Sci Technol, 42(24), 9210-9216.

Boehm, P.D., Page, D.S., Brown, J.S., Neff, J.M. and Gundlach4, E. 2014. Long-term fate and persistence of oil from the Exxon Valdez oil spill: lessons learned or history repeated? Proceedings: International Oil Spil Conference, 63-79.

Bonansea, R.I., Ame, M.V. and Wunderlin, D.A. 2013. Determination of priority pesticides in water samples combining SPE and SPME coupled to GC-MS. a case study: Suquia River basin (Argentina). Chemosphere, 90(6), 1860-1869.

Borchers, A. and Pieler, T. 2010. Programming pluripotent precursor cells derived from Xenopus embryos to generate specific tissues and organs. Genes (Basel), 1(3), 413-426.

Botello, A.V., Soto, L.A., Ponce-Vélez, G. and Villanueva F, S. 2015. Baseline for PAHs and metals in NW Gulf of Mexico related to the Deepwater Horizon oil spill. Estuar Coast Shelf Sci, 156, 124-133.

Boufadel, M., Geng, X., An, C., Owens, E., Chen, Z., Lee, K., Taylor, E. and Prince, R.C. 2019. A review on the factors affecting the deposition, retention, and biodegradation of oil stranded on beaches and guidelines for designing laboratory rxperiments. Curr Pollut Rep, 5, 407-423.

Boufadel, M.C., Sharifi, Y., Aken, B.V., Wrenn, B.A. and Lee, K. 2010. Nutrient and oxygen concentrations within the sediments of an Alaskan beach polluted with the Exxon Valdez oil spill. Environ Sci Technol, 44(19), 7418-7424.

Buch, V., Milet, A., cha, R.V., Jungwirth, P. and Devlin, J.P. 2007. Water surface is acidic. Proc Natl Acad Sci, 104(18), 7342-7347.

Bui, T.T., Nguyen, D.C. and Han, M. 2019. Average size and zeta potential of nanobubbles in different reagent solutions. J Nanopart Res, 21(8), 173.

Bunkin, N.F., Kochergin, A.V., Lobeyev, A.V., Ninham, B.W. and Vinogradova, O.I. 1996. Existence of charged submicrobubble clusters in polar liquids as revealed by correlation between optical cavitation and electrical conductivity. Colloids Surf A Physicochem Eng Asp, 110, 207-212.

Cai, L., Wang, J., Peng, J., Wu, Z. and Tan, X. 2018. Observation of the degradation of three types of plastic pellets exposed to UV irradiation in three different environments. Sci Total Environ, 628-629, 740-747.

Cai, M., Guy, C., Heroux, M., Lichtfouse, E. and An, C. 2021. The impact of successive COVID-19 lockdowns on people mobility, lockdown efficiency, and municipal solid waste. Environ Chem Lett, 19(6), 3959-3965.

Canning-Clode, J., Sepúlveda, P., Almeida, S. and Monteiro, J. 2020. Will COVID-19 containment and treatment measures drive shifts in marine litter pollution? Front mar sci, 7, Article 361.

Cao, Y., Kang, Q., Zhang, B., Zhu, Z., Dong, G., Cai, Q., Lee, K. and Chen, B. 2022. Machine learning-aided causal inference for unraveling chemical dispersant and salinity effects on crude oil biodegradation. Bioresour Technol, 345, 126468.

Cao, Y., Zhang, B., Zhu, Z., Song, X., Cai, Q., Chen, B., Dong, G. and Ye, X. 2020. Microbial eco-physiological strategies for salinity-mediated crude oil biodegradation. Sci Total Environ, 727, 138723.

Carbery, M., Herb, F., Reynes, J., Pham, C.K., Fong, W.-K. and Lehner, R. 2022. How small is the big problem? Small microplastics <300 μm abundant in marine surface waters of the Great Barrier Reef Marine Park. Mar Pollut Bull, 184, 114179.

Carlin, J., Craig, C., Little, S., Donnelly, M., Fox, D., Zhai, L. and Walters, L. 2020. Microplastic accumulation in the gastrointestinal tracts in birds of prey in central Florida, USA. Environ Pollut, 264, 114633.

Celina, M., Wise, J., Otteseqb, D.K., Gillen, K.T. and Clough, R.L. 1998. Oxidation profiles of thermally aged nitrile rubber. Polym Degrad Stab, 60, 493-504.

Chao, K.P., Huang, C.S. and Wei, C.Y. 2015. Health risk assessments of DEHP released from chemical protective gloves. J Hazard Mater, 283, 53-59.

Chen, H.L., Selvam, S.B., Ting, K.N., Tshai, K.Y. and Gibbins, C.N. 2022. Relative contributions of different local sources to riverborne microplastic in a mixed landuse area within a tropical catchment. Environ Res, 210, 112972.

Chen, Z., An, C., Boufadel, M., Owens, E., Chen, Z., Lee, K., Cao, Y. and Cai, M. 2019. Use of surface-washing agents for the treatment of oiled shorelines: research advancements, technical applications and future challenges. Chem Eng J, 123565.

Chen, Z., An, C., Yin, J., Owens, E., Lee, K., Zhang, K. and Tian, X. 2021. Exploring the use of cellulose nanocrystal as surface-washing agent for oiled shoreline cleanup. J Hazard Mater, 402, 123464.

Chen, Z., Elektorowicz, M., An, C. and Tian, X. 2023. Entrainment and enrichment of microplastics in ice formation processes: implications for the transport of microplastics in cold regions. Environ Sci Technol, 57(8), 3176-3186.

Cheng, C.H., Huettel, M. and Wildman, R.A. 2014. Ebullition-enhanced solute transport in coarse-grained sediments. Limnol Oceanogr, 59(5), 1733-1748.

Chu, L.B., Xing, X.H., Yu, A.F., Zhou, Y.N., Sun, X.L. and Jurcik, B. 2007. Enhanced ozonation of simulated dyestuff wastewater by microbubbles. Chemosphere, 68(10), 1854-1860.

Chubarenko, I. and Stepanova, N. 2017. Microplastics in sea coastal zone: lessons learned from the Baltic amber. Environ Pollut, 224, 243-254.

Cole, M., Lindeque, P., Halsband, C. and Galloway, T.S. 2011. Microplastics as contaminants in the marine environment: a review. Mar Pollut Bull, 62(12), 2588-2597.

Cordova, M.R., Nurhati, I.S., Riani, E., Nurhasanah and Iswari, M.Y. 2021. Unprecedented plastic-made personal protective equipment (PPE) debris in river outlets into Jakarta Bay during COVID-19 pandemic. Chemosphere, 268, 129360.

Corradini, F., Bartholomeus, H., Huerta Lwanga, E., Gertsen, H. and Geissen, V. 2019. Predicting soil microplastic concentration using vis-NIR spectroscopy. Sci Total Environ, 650(Pt 1), 922-932.

Cui, H., Hanus, R. and Kessler, M.R. 2013. Degradation of ROMP-based bio-renewable polymers by UV radiation. Polym Degrad Stab, 98(11), 2357-2365.

Curry, R., Dickson, B. and Yashayaev, I. 2003. A change in the freshwater balance of the Atlantic Ocean over the past four decades. Nature, 426, 826-829.

Curtis, D., Elango, V., Collins, A.W., Rodrigue, M. and Pardue, J.H. 2018. Transport of crude oil and associated microbial populations by washover events on coastal headland beaches. Mar Pollut Bull, 130, 229-239.

Cutler, S. 2020. Mounting medical waste from COVID-19 emphasizes the need for a sustainable waste management strategy. https://www.frost.com/frost-perspectives/managing-the-growing-threat-of-covid-19-generated-medical-waste/.

Dai, Z., Zhang, H., Zhou, Q., Tian, Y., Chen, T., Tu, C., Fu, C. and Luo, Y. 2018. Occurrence of microplastics in the water column and sediment in an inland sea affected by intensive anthropogenic activities. Environ Pollut, 242, 1557-1565.

De-la-Torre, G.E. and Aragaw, T.A. 2021. What we need to know about PPE associated with the COVID-19 pandemic in the marine environment. Mar Pollut Bull, 163, 111879.

De-la-Torre, G.E., Rakib, M.R.J., Pizarro-Ortega, C.I. and Dioses-Salinas, D.C. 2021. Occurrence of personal protective equipment (PPE) associated with the COVID-19 pandemic along the coast of Lima, Peru. Sci Total Environ, 774, 145774.

De Leo, A., Cutroneo, L., Sous, D. and Stocchino, A. 2021. Settling velocity of microplastics exposed to wave action. J Mar Sci Eng, 9(2), 142.

de Sa, L.C., Oliveira, M., Ribeiro, F., Rocha, T.L. and Futter, M.N. 2018. Studies of the effects of microplastics on aquatic organisms: what do we know and where should we focus our efforts in the future? Sci Total Environ, 645, 1029-1039.

Dibke, C., Fischer, M. and Scholz-Bottcher, B.M. 2021. Microplastic mass concentrations and distribution in German Bight Waters by pyrolysis-gas chromatography-mass

spectrometry/thermochemolysis reveal potential impact of marine coatings: do ships leave skid marks? Environ Sci Technol, 55, 2285-2295.

Dietrich, W.E. 1982. Settling velocity of natural particles. Water Resour Res, 18(6), 1615-1626.

Ding, J., Li, J., Sun, C., Jiang, F., He, C., Zhang, M., Ju, P. and Ding, N.X. 2020a. An examination of the occurrence and potential risks of microplastics across various shellfish. Sci Total Environ, 739, 139887.

Ding, L., Mao, R., Ma, S., Guo, X. and Zhu, L. 2020b. High temperature depended on the ageing mechanism of microplastics under different environmental conditions and its effect on the distribution of organic pollutants. Water Res, 174, 115634.

Dobaradaran, S., Schmidt, T.C., Nabipour, I., Khajeahmadi, N., Tajbakhsh, S., Saeedi, R., Javad Mohammadi, M., Keshtkar, M., Khorsand, M. and Faraji Ghasemi, F. 2018. Characterization of plastic debris and association of metals with microplastics in coastline sediment along the Persian Gulf. Waste Manag, 78, 649-658.

Doremalen, N.v., Bushmaker, T., Morris, D.H., Holbrook, M.G., Gamble, A., Williamson, B.N., Tamin, A., Harcourt, J.L., Thornburg, N.J., Gerber, S.I., Lloyd-Smith, J.O., Wit, E.d. and Munster, V.J. 2020. Aerosol and surface stability of SARS-CoV-2 as compared with SARS-CoV-1. N Engl J Med, 382(16), 1564-1657.

Doustmohammadi, N. and Babazadeh, R. 2020. Design of closed loop supply chain of wood plastic composite (WPC) Industry. J Environ Inform, 35(2), 94-102.

Dris, R., Gasperi, J., Rocher, V., Saad, M., Renault, N. and Tassin, B. 2015. Microplastic contamination in an urban area: a case study in Greater Paris. Environ Chem, 12(5), 592-599.

Du, F., Cai, H., Zhang, Q., Chen, Q. and Shi, H. 2020. Microplastics in take-out food containers. J Hazard Mater, 399, 122969.

Du, M. and Kessler, J.D. 2012. Assessment of the spatial and temporal variability of bulk hydrocarbon respiration following the Deepwater Horizon oil spill. Environ Sci Technol, 46(19), 10499-10507.

Duan, J., Liu, W., Zhao, X., Han, Y., O'Reilly, S.E. and Zhao, D. 2018. Study of residual oil in Bay Jimmy sediment 5 years after the Deepwater Horizon oil spill: persistence of sediment retained oil hydrocarbons and effect of dispersants on desorption. Sci Total Environ, 618, 1244-1253.

Eikenberry, S.E., Mancuso, M., Iboi, E., Phan, T., Eikenberry, K., Kuang, Y., Kostelich, E. and Gumel, A.B. 2020. To mask or not to mask: modeling the potential for face mask use by the general public to curtail the COVID-19 pandemic. Infect Dis Model, 5, 293-308.

Eizagirre, S. 2019. Science has a garbage problem. why aren't recycling schemes more popular? https://massivesci.com/articles/research-labs-generate-plastic-waste-recycling-sustainability-gloves/.

Eltemsah, Y.S. and Bohn, T. 2019. Acute and chronic effects of polystyrene microplastics on juvenile and adult Daphnia magna. Environ Pollut, 254(Pt A), 112919.

Epstein, P.S. and Plesset, M.S. 1950. On the stability of gas bubbles in liquid-gas solutions. J Chem Phys, 18(11), 1505-1509.

Esmizadeh, E., Chang, B.P., Jubinville, D., Ojogbo, E., Seto, C., Tzoganakis, C. and Mekonnen, T.H. 2020. Can medical-grade gloves provide protection after repeated disinfection? ACS Appl Polym Mater, 3(1), 445-454.

Esquinas, N., Rodriguez-Valdes, E., Marquez, G. and Gallego, J.L.R. 2017. Diagnostic ratios for the rapid evaluation of natural attenuation of heavy fuel oil pollution along shores. Chemosphere, 184, 1089-1098.

Etkin, D.S., Michel, J., McCay, D.F., Boufadel, M. and Li, H. 2008. Intergating state-of-the-art shoreline interaction konowledge into spill mdeling. Proceedings: International Oil Spil Conference, 915-922.

Evangeliou, N., Grythe, H., Klimont, Z., Heyes, C., Eckhardt, S., Lopez-Aparicio, S. and Stohl, A. 2020. Atmospheric transport is a major pathway of microplastics to remote regions. Nat Commun, 11(1), 3381.

Evans, M., Liu, J., Bacosa, H., Rosenheim, B.E. and Liu, Z. 2017. Petroleum hydrocarbon persistence following the Deepwater Horizon oil spill as a function of shoreline energy. Mar Pollut Bull, 115(1-2), 47-56.

Fadare, O.O. and Okoffo, E.D. 2020. Covid-19 face masks: a potential source of microplastic fibers in the environment. Sci Total Environ, 737, 140279.

Fadare, O.O., Wan, B., Guo, L.H. and Zhao, L. 2020. Microplastics from consumer plastic food containers: are we consuming it? Chemosphere, 253, 126787.

Fan, M., Tao, D., Honaker, R. and Luo, Z. 2010a. Nanobubble generation and its application in froth flotation (part I): nanobubble generation and its effects on properties of microbubble and millimeter scale bubble solutions. Min Sci Technol, 20(1), 1-19.

Fan, M., Tao, D., Honaker, R. and Luo, Z. 2010b. Nanobubble generation and its applications in froth flotation (part II): fundamental study and theoretical analysis. Min Sci Technol, 20(2), 159-177.

Fan, W., An, W., Huo, M., Xiao, D., Lyu, T. and Cui, J. 2021. An integrated approach using ozone nanobubble and cyclodextrin inclusion complexation to enhance the removal of micropollutants. Water Res, 196, 117039.

Fang, R., Littke, R., Zieger, L., Baniasad, A., Li, M. and Schwarzbauer, J. 2019. Changes of composition and content of tricyclic terpane, hopane, sterane, and aromatic biomarkers throughout the oil window: a detailed study on maturity parameters of Lower Toarcian Posidonia Shale of the Hils Syncline, NW Germany. Org Geochem, 138, 103928.

Fang, Z., Wang, X., Zhou, L., Zhang, L. and Hu, J. 2020. Formation and stability of bulk nanobubbles by vibration. Langmuir, 36(9), 2264-2270.

Fauvelle, V., Castro-Jiménez, J., Schmidt, N., Carlez, B., Panagiotopoulos, C. and Sempéré, R. 2018. One-single extraction procedure for the simultaneous determination of a wide range of polar and nonpolar organic contaminants in seawater. Front Mar Sci, 5, Article295.

Feizi, F., Sarmah, A.K. and Rangsivek, R. 2021. Adsorption of pharmaceuticals in a fixed-bed column using tyre-based activated carbon: experimental investigations and numerical modelling. J Hazard Mater, 417, 126010.

Feng, Q., An, C., Chen, Z., Owens, E., Niu, H. and Wang, Z. 2021a. Assessing the coastal sensitivity to oil spills from the perspective of ecosystem services: a case study for Canada's pacific coast. J Environ Manage, 296, 113240.

Feng, Q., An, C., Chen, Z. and Wang, Z. 2023a. New perspective on the mobilization of microplastics through capillary fringe fluctuation in a tidal aquifer environment. Environ Sci Technol, 57(2), 929-938.

Feng, Q., An, C., Chen, Z., Yin, J., Zhang, B., Lee, K. and Wang, Z. 2021b. Investigation into the impact of aged microplastics on oil behavior in shoreline environments. J Hazard Mater, 421, 126711.

Feng, Q., Chen, Z., An, C., Yang, X. and Wang, Z. 2023b. Tide-induced infiltration and resuspension of microplastics in shorelines: insights from tidal tank experiments. Water Res, 236, 119970.

Feng, Q., Chen, Z., Greer, C.W., An, C. and Wang, Z. 2022. Transport of microplastics in shore substrates over tidal cycles: roles of polymer characteristics and environmental factors. Environ Sci Technol, 56(12), 8187-8196.

Fernandez-Fernandez, S., Bernabeu, A.M., Rey, D., Mucha, A.P., Almeida, C.M.R. and Bouchette, F. 2014. The effect of sand composition on the degradation of buried oil. Mar Pollut Bull, 86(1-2), 391-401.

Gallego, J.R., González-Rojas, E., Peláez, A.I., Sánchez, J., García-Martínez, M.J., Ortiz, J.E., Torres, T. and Llamas, J.F. 2006. Natural attenuation and bioremediation of Prestige fuel oil along the Atlantic coast of Galicia (Spain). Org Geochem, 37(12), 1869-1884.

Galloway, T.S., Cole, M. and Lewis, C. 2017. Interactions of microplastic debris throughout the marine ecosystem. Nat Ecol Evol, 1(5), 0116.

Ganesh Kumar A., Anjana K., Hinduja M., Sujitha K. and Dharani G. 2020. Review on plastic wastes in marine environment - biodegradation and biotechnological solutions. Mar Pollut Bull, 150, 110733.

Garçon, M., Sauzéat, L., Carlson, R.W., Shirey, S.B., Simon, M., Balter, V. and Boyet, M. 2017. Nitrile, latex, neoprene and vinyl gloves: a primary source of contamination for trace element and Zn isotopic analyses in geological and biological samples. Geostand Geoanal Res, 41(3), 367-380.

Garrett, R.M., Pickering, I.J., Haith, C.E. and Prince, R.C. 1998. Photooxidation of crude oils. Environ Sci Technol, 32(23), 3719-3723.

Gaylarde, C.C., Baptista Neto, J.A. and da Fonseca, E.M. 2020. Nanoplastics in aquatic systems - are they more hazardous than microplastics? Environ Pollut, 115950.

Geilfus, N.X., Munson, K.M., Sousa, J., Germanov, Y., Bhugaloo, S., Babb, D. and Wang, F. 2019. Distribution and impacts of microplastic incorporation within sea ice. Mar Pollut Bull, 145, 463-473.

Geng, X. and Boufadel, M.C. 2015. Numerical study of solute transport in shallow beach aquifers subjected to waves and tides. J Geophys Res Oceans, 120, 1409-1428.

Geng, X., Boufadel, M.C. and Cui, F. 2017. Numerical modeling of subsurface release and fate of benzene and toluene in coastal aquifers subjected to tides. J Hydrol, 551, 793-803.

Gereffi, G. 2020. What does the COVID-19 pandemic teach us about global value chains? The case of medical supplies. J Int Bus Stud, 3(3), 287-301.

Gewert, B., Plassmann, M., Sandblom, O. and MacLeod, M. 2018. Identification of chain scission products released to water by plastic exposed to ultraviolet light. Environ Sci Technol Lett, 5(5), 272-276.

Gies, E.A., LeNoble, J.L., Noël, M., Etemadifar, A., Bishay, F., Hall, E.R. and Ross, P.S. 2018. Retention of microplastics in a major secondary wastewater treatment plant in Vancouver, Canada. Mar Pollut Bull, 133, 553-561.

Gong, Y., Zhao, X., Cai, Z., O'Reilly, S.E., Hao, X. and Zhao, D. 2014. A review of oil, dispersed oil and sediment interactions in the aquatic environment: influence on the fate, transport and remediation of oil spills. Mar Pollut Bull, 79(1-2), 16-33.

Grbić, J., Helm, P., Athey, S. and Rochman, C.M. 2020. Microplastics entering northwestern Lake Ontario are diverse and linked to urban sources. Water Res, 174, 115623.

Guan, R. and Xu, X. 2001. Structure and properties of isotactic polypropylene functionalized by ultraviolet irradiation. J Appl Polym Sci, 79(8), 1456-1466.

Guart, A., Bono-Blay, F., Borrell, A. and Lacorte, S. 2011. Migration of plasticizers phthalates, bisphenol A and alkylphenols from plastic containers and evaluation of risk. Food Addit Contam Part A Chem Anal Control Expo Risk Assess, 28(5), 676-685.

Guo, H.-P. and Jiao, J.J. 2008. Numerical study of airflow in the unsaturated zone induced by sea tides. Water Resour Res, 44(6), W06402.

Guo, Q., Li, H., Boufadel, M.C. and Sharifi, Y. 2010. Hydrodynamics in a gravel beach and its impact on the Exxon Valdezoil. J. Geophys Res, 115(C12).

Guo, Z., Li, P., Yang, X., Wang, Z., Lu, B., Chen, W., Wu, Y., Li, G., Zhao, Z., Liu, G., Ritsema, C., Geissen, V. and Xue, S. 2022. Soil texture is an important factor determining how microplastics affect soil hydraulic characteristics. Environ Int, 165, 107293.

Gustitus, S.A. and Clement, T.P. 2017. Formation, fate, and impacts of microscopic and macroscopic oil-sediment residues in nearshore marine environments: a critical review. Rev Geophys, 55(4), 1130-1157.

Guzzetti, E., Sureda, A., Tejada, S. and Faggio, C. 2018. Microplastic in marine organism: environmental and toxicological effects. Environ Toxicol Pharmacol, 64, 164-171.

Hagemann, L., Buchty-Lemke, M., Maaß, A.-L., Schüttrumpf, H., Lehmkuhl, F. and Schwarzbauer, J. 2019. Potential hotspots of persistent organic pollutants in alluvial sediments of the meandering Wurm River, Germany. J Soils Sed, 20(2), 1034-1045.

Hajiouni, S., Mohammadi, A., Ramavandi, B., Arfaeinia, H., De-la-Torre, G.E., Tekle-Röttering, A. and Dobaradaran, S. 2022. Occurrence of microplastics and phthalate esters in urban runoff: a focus on the Persian Gulf coastline. Sci Total Environ, 806, 150559.

Hajji, S., Ben-Haddad, M., Abelouah, M.R., De-la-Torre, G.E. and Alla, A.A. 2023. Occurrence, characteristics, and removal of microplastics in wastewater treatment plants located on the Moroccan Atlantic: The case of Agadir metropolis. Sci Total Environ, 862, 160815.

Haque, M.S., Uddin, S., Sayem, S.M. and Mohib, K.M. 2021. Coronavirus disease 2019 (COVID-19) induced waste scenario: a short overview. J Environ Chem Eng, 9(1), 104660.

Hernandez, E., Nowack, B. and Mitrano, D.M. 2017a. Polyester textiles as a source of microplastics from households: a mechanistic study to understand microfiber release during washing. Environ Sci Technol, 51(12), 7036-7046.

Hernandez, L.M., Xu, E.G., Larsson, H.C.E., Tahara, R., Maisuria, V.B. and Tufenkji, N. 2019. Plastic teabags release billions of microparticles and nanoparticles into tea. Environ Sci Technol, 53(21), 12300-12310.

Hernandez, L.M., Yousefi, N. and Tufenkji, N. 2017b. Are there nanoplastics in your personal care products? Environ Sci Technol Lett, 4(7), 280-285.

Hongprasith, N., Kittimethawong, C., Lertluksanaporn, R., Eamchotchawalit, T., Kittipongvises, S. and Lohwacharin, J. 2020. IR microspectroscopic identification of microplastics in municipal wastewater treatment plants. Environ Sci Pollut Res Int, 27(15), 18557-18564.

Hu, L. and Xia, Z. 2018. Application of ozone micro-nano-bubbles to groundwater remediation. J Hazard Mater, 342, 446-453.

Huang, J., Chen, H., Zheng, Y., Yang, Y., Zhang, Y. and Gao, B. 2021a. Microplastic pollution in soils and groundwater: characteristics, analytical methods and impacts. Chem Eng J, 425, 131870.

Huang, W., Song, B., Liang, J., Niu, Q., Zeng, G., Shen, M., Deng, J., Luo, Y., Wen, X. and Zhang, Y. 2021b. Microplastics and associated contaminants in the aquatic environment: a review

on their ecotoxicological effects, trophic transfer, and potential impacts to human health. J Hazard Mater, 405, 124187.

Huba, A.K. and Gardinali, P.R. 2016. Characterization of a crude oil weathering series by ultrahigh-resolution mass spectrometry using multiple ionization modes. Sci Total Environ, 563-564, 600-610.

Humphrey, B., Owens, E. and Sergy, G. 1993. Development of a stranded oil In coarse sediment(SOCS) model Proceedings: International Oil Spil Conference, 575-582.

Ibrahim, Y.S., Tuan Anuar, S., Azmi, A.A., Wan Mohd Khalik, W.M.A., Lehata, S., Hamzah, S.R., Ismail, D., Ma, Z.F., Dzulkarnaen, A., Zakaria, Z., Mustaffa, N., Tuan Sharif, S.E. and Lee, Y.Y. 2021. Detection of microplastics in human colectomy specimens. JGH Open, 5(1), 116-121.

Irvine, G.V., Mann, D.H. and Short, J.W. 2006. Persistence of 10-year old Exxon Valdez oil on Gulf of Alaska beaches: the importance of boulder-armoring. Mar Pollut Bull, 52(9), 1011-1022.

Iwasaki, S., Isobe, A., Kako, S.i., Uchida, K. and Tokai, T. 2017. Fate of microplastics and mesoplastics carried by surface currents and wind waves: a numerical model approach in the Sea of Japan. Mar Pollut Bull, 121(1), 85-96.

Jalon-Rojas, I., Romero-Ramirez, A., Fauquembergue, K., Rossignol, L., Cachot, J., Sous, D. and Morin, B. 2022. Effects of biofilms and particle physical properties on the rising and settling velocities of microplastic fibers and sheets. Environ Sci Technol, 56(12), 8114-8123.

Jedruchniewicz, K., Ok, Y.S. and Oleszczuk, P. 2021. COVID-19 discarded disposable gloves as a source and a vector of pollutants in the environment. J Hazard Mater, 417(5), 125938.

Ji, W., Boufadel, M., Zhao, L., Robinson, B., King, T., An, C., Zhang, B.H. and Lee, K. 2021. Formation of oil-particle aggregates: impacts of mixing energy and duration. Sci Total Environ, 795, 148781.

Jiao, J.J. and Li, H. 2004. Breathing of coastal vadose zone induced by sea level fluctuations. Geophys Res Lett, 31(11), L11502.

Jin, N., Zhang, F., Cui, Y., Sun, L., Gao, H., Pu, Z. and Yang, W. 2022. Environment-friendly surface cleaning using micro-nano bubbles. Particuology, 66, 1-9.

Johns Hopkins University Coronavirus Resources Cenrer 2021. COVID-19 dashboard by the Center for Systems Science and Engineering (CSSE) at Johns Hopkins Univesity. 2021. https://coronavirus.jhu.edu/map.html.

Johnson, B.D. and Cooke, R.C. 1981. Generation of stabilized microbubbles in seawater. Science, 213(4504), 209-211.

Jones, S. 2020. Waste management in Australia Is an environmental crisis: what needs to change so adaptive governance can help? Sustainability, 12(21), 9212.

Juahir, H., Ismail, A., Mohamed, S.B., Toriman, M.E., Kassim, A.M., Zain, S.M., Ahmad, W.K.W., Wah, W.K., Zali, M.A., Retnam, A., Taib, M.Z.M. and Mokhtar, M. 2017. Improving oil classification quality from oil spill fingerprint beyond six sigma approach. Mar Pollut Bull, 120(1-2), 322-332.

Jungwirth, P. 2009. Spiers memorial lecture. ions at aqueous interfaces. Faraday Discuss, 141, 31-39.

Kaiser, D., Estelmann, A., Kowalski, N., Glockzin, M. and Waniek, J.J. 2019. Sinking velocity of sub-millimeter microplastic. Mar Pollut Bull, 139, 214-220.

Kalogerakis, N., Karkanorachaki, K., Kalogerakis, G.C., Triantafyllidi, E.I., Gotsis, A.D., Partsinevelos, P. and Fava, F. 2017. Microplastics generation: onset of fragmentation of polyethylene films in marine environment mesocosms. Front Mar Sci, 4, Article84.

Kanhai, L.D.K., Johansson, C., Frias, J.P.G.L., Gardfeldt, K., Thompson, R.C. and O'Connor, I. 2019. Deep sea sediments of the Arctic Central Basin: a potential sink for microplastics. Deep Sea Res 1 Oceanogr Res Pap, 145, 137-142.

Kawahara, A., Sadatomi, M., Matsuyama, F., Matsuura, H., Tominaga, M. and Noguchi, M. 2009. Prediction of micro-bubble dissolution characteristics in water and seawater. Exp Therm Fluid Sci, 33(5), 883-894.

Ke, S., Xiao, W., Quan, N., Dong, Y., Zhang, L. and Hu, J. 2019. Formation and stability of bulk nanobubbles in different solutions. Langmuir, 35(15), 5250-5256.

Khadanga, M.K., Mishra, R.K. and Sahu, B.K. 2022. Assessment of pollution and ecological risk index of heavy metals in the durface sediment of estuary and the coastal environment of Bay of Bengal. J Environ Inform, 39(1), 35-48.

Khaled Abdella Ahmed, A., Sun, C., Hua, L., Zhang, Z., Zhang, Y., Marhaba, T. and Zhang, W. 2018. Colloidal properties of air, oxygen, and nitrogen nanobubbles in water: effects of ionic strength, natural organic matters, and surfactants. Environ Eng Sci, 35(7), 720-727.

Khoo, K.S., Ho, L.Y., Lim, H.R., Leong, H.Y. and Chew, K.W. 2021. Plastic waste associated with the COVID-19 pandemic: crisis or opportunity? J Hazard Mater, 417, 126108.

Kim, D. and Han, J. 2020. Remediation of copper contaminated soils using water containing hydrogen nanobubbles. Appl Sci, 10(6), 2185.

Kooi, M., Nes, E.H.V., Scheffer, M. and Koelmans, A.A. 2017. Ups and downs in the ocean: effects of biofouling on vertical transport of microplastics. Environ Sci Technol, 51(14), 7963-7971.

Kotek, J., Kelnar, I., Baldrian, J. and Raab, M. 2004. Structural transformations of isotactic polypropylene induced by heating and UV light. Eur Polym J, 40(12), 2731-2738.

Kowalski, N., Reichardt, A.M. and Waniek, J.J. 2016. Sinking rates of microplastics and potential implications of their alteration by physical, biological, and chemical factors. Mar Pollut Bull, 109(1), 310-319.

Kyzas, G.Z., Favvas, E.P., Kostoglou, M. and Mitropoulos, A.C. 2020. Effect of agitation on batch adsorption process facilitated by using nanobubbles. Colloids Surf A Physicochem Eng Asp, 607, 125440.

Lau, W.W.Y., Shiran, Y., Bailey, R.M., Cook, E., Stuchtey, M.R., Koskella, J., Velis, C.A., Godfrey, L., Boucher, J., Murphy, M.B., Thompson, R.C., Jankowska, E., Castillo, A.C., Pilditch, T.D., Dixon, B., Koerselman, L., Kosior, E., Favoino, E., Gutberlet, J., Baulch, S., Atreya, M.E., Fischer, D., He, K.K., Petit, M.M., Sumaila, U.R., Neil, E., Bernhofen, M.V., Lawrence, K. and Palardy, J.E. 2020. Evaluating scenarios toward zero plastic pollution. Science, 369, 1455-1461.

Law, k.L. and Thompson, R.C. 2014. Microplastics in the seas. Science, 345, 144-145.

Le Bihanic, F., Clerandeau, C., Cormier, B., Crebassa, J.C., Keiter, S.H., Beiras, R., Morin, B., Begout, M.L., Cousin, X. and Cachot, J. 2020. Organic contaminants sorbed to microplastics affect marine medaka fish early life stages development. Mar Pollut Bull, 154, 111059.

Lee, K., Boufadel, M., Chen, B., Foght, J., Hodson, P., Swanson, S. and Venosa, A. (2015) Behaviour and environmental impacts of crude oil released into aqueous environments.

Lee, K., Stoffyn-Egli, P. and Owens, E.H. 2002. The OSSA II pipeline oil spill: natural mitigation of a riverine oil spill by oil–mineral aggregate formation. Spill Sci Technol Bull, 7(3-4), 149-154.

Lei, K., Qiao, F., Liu, Q., Wei, Z., Qi, H., Cui, S., Yue, X., Deng, Y. and An, L. 2017. Microplastics releasing from personal care and cosmetic products in China. Mar Pollut Bull, 123(1-2), 122-126.

Li, H. and Boufadel, M.C. 2010. Long-term persistence of oil from the Exxon Valdez spill in two-layer beaches. Nat Geosci, 3(2), 96-99.

Li, H., Hu, L. and Xia, Z. 2013. Impact of groundwater salinity on bioremediation enhanced by micro-nano bubbles. Materials, 6(9), 3676-3687.

Li, J., Guo, K., Cao, Y., Wang, S., Song, Y. and Zhang, H. 2021. Enhance in mobility of oxytetracycline in a sandy loamy soil caused by the presence of microplastics. Environ Pollut, 269, 116151.

Li, J., Liu, H. and Paul Chen, J. 2018. Microplastics in freshwater systems: a review on occurrence, environmental effects, and methods for microplastics detection. Water Res, 137, 362-374.

Li, J., Shan, E., Zhao, J., Teng, J. and Wang, Q. 2023. The factors influencing the vertical transport of microplastics in marine environment: a review. Sci Total Environ, 870, 161893.

Li, L., Zhao, X., Li, Z. and Song, K. 2020a. COVID-19: performance study of microplastic inhalation risk posed by wearing masks. J Hazard Mater, 411, 124955.

Li, P., Takahashi, M. and Chiba, K. 2009. Enhanced free-radical generation by shrinking microbubbles using a copper catalyst. Chemosphere, 77(8), 1157-1160.

Li, P., Wang, J., Liao, Z., Ueda, Y., Yoshikawa, K. and Zhang, G. 2022. Microbubbles for effective cleaning of metal surfaces without chemical agents. Langmuir, 38(2), 769-776.

Li, R., Lu, Y., Hu, X., Guo, D., Zhao, P., Wang, N., Lee, K. and Zhang, B. 2020b. Space–time variations of sea ice in Bohai Sea in the winter of 2009–2010 simulated with a coupled ocean and ice model. J Oceanogr, 77(2), 243-258.

Li, Y., Wang, X., Fu, W., Xia, X., Liu, C., Min, J., Zhang, W. and Crittenden, J.C. 2019. Interactions between nano/micro plastics and suspended sediment in water: implications on aggregation and settling. Water Res, 161, 486-495.

Liao, J., Brosse, N., Pizzi, A. and Hoppe, S. 2019. Dynamically cross-linked tannin as a reinforcement of polypropylene and UV protection properties. Polymers (Basel), 11, 102.

Lin, J., Xu, X.P., Yue, B.Y., Li, Y., Zhou, Q.Z., Xu, X.M., Liu, J.Z., Wang, Q.Q. and Wang, J.H. 2020. A novel thermoanalytical method for quantifying microplastics in marine sediments. Sci Total Environ, 760, 144316.

Lin, L., Li, H., Hong, H., Yuan, B., Sun, X., He, L., Xue, C., Lu, H., Liu, J. and Yan, C. 2022. Enhanced heavy metal adsorption on microplastics by incorporating flame retardant hexabromocyclododecanes: mechanisms and potential migration risks. Water Res, 225, 119144.

Lindeberg, M.R., Maselko, J., Heintz, R.A., Fugate, C.J. and Holland, L. 2018. Conditions of persistent oil on beaches in Prince William Sound 26 years after the Exxon Valdez spill. Deep Sea Res Part II Top Stud Oceanogr, 147, 9-19.

Liu, K., Courtene-Jones, W., Wang, X., Song, Z., Wei, N. and Li, D. 2020a. Elucidating the vertical transport of microplastics in the water column: a review of sampling methodologies and distributions. Water Res, 186, 116403.

Liu, P., Zhan, X., Wu, X., Li, J., Wang, H. and Gao, S. 2020b. Effect of weathering on environmental behavior of microplastics: properties, sorption and potential risks. Chemosphere, 242, 125193.

Liu, S., Kawagoe, Y., Makino, Y. and Oshita, S. 2013. Effects of nanobubbles on the physicochemical properties of water: the basis for peculiar properties of water containing nanobubbles. Chem Eng Sci, 93, 250-256.

Liu, S., Oshita, S., Makino, Y., Wang, Q., Kawagoe, Y. and Uchida, T. 2015. Oxidative capacity of nanobubbles and its effect on seed germination. ACS Sustain Chem Eng, 4(3), 1347-1353.

Liu, W., Zhang, J., Liu, H., Guo, X., Zhang, X., Yao, X., Cao, Z. and Zhang, T. 2021. A review of the removal of microplastics in global wastewater treatment plants: characteristics and mechanisms. Environ Int, 146, 106277.

Liu, X., Sun, P., Qu, G., Jing, J., Zhang, T., Shi, H. and Zhao, Y. 2020c. Insight into the characteristics and sorption behaviors of aged polystyrene microplastics through three type of accelerated oxidation processes. J Hazard Mater, 407, 124836.

Liu, X., Yuan, W., Di, M., Li, Z. and Wang, J. 2019a. Transfer and fate of microplastics during the conventional activated sludge process in one wastewater treatment plant of China. Chem Eng J, 362, 176-182.

Liu, Y., Zhou, Y., Wang, T., Pan, J., Zhou, B., Muhammad, T., Zhou, C. and Li, Y. 2019b. Micro-nano bubble water oxygation: synergistically improving irrigation water use efficiency, crop yield and quality. J Clean Prod, 222, 835-843.

Liu, Y.L., Du, J.Z., Wang, Q., Yang, W. and Cui, B.S. 2022. Toward an assessment of runoff and thermal connectivity in a river-lake system within an urban environment. J Environ Inform, 40(2), 125-140.

Liu, Z., Liu, J., Zhu, Q. and Wu, W. 2012. The weathering of oil after theDeepwater Horizonoil spill: insights from the chemical composition of the oil from the sea surface, salt marshes and sediments. Environ Res Lett, 7(3), 035302.

Maderuelo-Sanz, R., Acedo-Fuentes, P., Garcia-Cobos, F.J., Sanchez-Delgado, F.J., Mota-Lopez, M.I. and Meneses-Rodriguez, J.M. 2021. The recycling of surgical face masks as sound porous absorbers: preliminary evaluation. Sci Total Environ, 786, 147461.

Maduar, S.R., Belyaev, A.V., Lobaskin, V. and Vinogradova, O.I. 2015. Electrohydrodynamics near hydrophobic surfaces. Phys Rev Lett, 114(11), 118301.

Magni, S., Binelli, A., Pittura, L., Avio, C.G., Della Torre, C., Parenti, C.C., Gorbi, S. and Regoli, F. 2019. The fate of microplastics in an Italian Wastewater Treatment Plant. Sci Total Environ, 652, 602-610.

McGinnis, D.F., Kirillin, G., Tang, K.W., Flury, S., Bodmer, P., Engelhardt, C., Casper, P. and Grossart, H.P. 2015. Enhancing surface methane fluxes from an oligotrophic lake: exploring the microbubble hypothesis. Environ Sci Technol, 49(2), 873-880.

Mekala, C. and Nambi, I.M. 2016. Experimental and simulation studies on nitrogen dynamics in unsaturated and saturated soil using HYDRUS-2D. Proc Technol, 25, 122-129.

Mendoza-Lera, C. and Mutz, M. 2013. Microbial activity and sediment disturbance modulate the vertical water flux in sandy sediments. Freshw Sci, 32(1), 26-38.

Michielssen, M.R., Michielssen, E.R., Ni, J. and Duhaime, M.B. 2016. Fate of microplastics and other small anthropogenic litter (SAL) in wastewater treatment plants depends on unit processes employed. Environ Sci Water Res Technol, 2(6), 1064-1073.

Mohamed Nor, N.H., Kooi, M., Diepens, N.J. and Koelmans, A.A. 2021. Lifetime accumulation of microplastic in children and adults. Environ Sci Technol, 55(8), 5084-5096.

Morent, R., De Geyter, N., Leys, C., Gengembre, L. and Payen, E. 2008. Comparison between XPS- and FTIR-analysis of plasma-treated polypropylene film surfaces. Surf Interface Anal, 40(3-4), 597-600.

Mountford, A.S. and Morales Maqueda, M.A. 2019. Eulerian modeling of the three-dimensional distribution of seven popular microplastic types in the global ocean. J Geophys Res Oceans, 124(12), 8558-8573.

Mulabagal, V., Yin, F., John, G.F., Hayworth, J.S. and Clement, T.P. 2013. Chemical fingerprinting of petroleum biomarkers in Deepwater Horizon oil spill samples collected from Alabama shoreline. Mar Pollut Bull, 70(1-2), 147-154.

Murphy, F., Ewins, C., Carbonnier, F. and Quinn, B. 2016. Wastewater treatment works (WwTW) as a source of microplastics in the aquatic environment. Environ Sci Technol, 50(11), 5800-5808.

Naji, A., Esmaili, Z. and Khan, F.R. 2017. Plastic debris and microplastics along the beaches of the Strait of Hormuz, Persian Gulf. Mar Pollut Bull, 114(2), 1057-1062.

Napper, I.E., Wright, L.S., Barrett, A.C., Parker-Jurd, F.N.F. and Thompson, R.C. 2022. Potential microplastic release from the maritime industry: abrasion of rope. Sci Total Environ, 804, 150155.

Ngo, P.L., Pramanik, B.K., Shah, K. and Roychand, R. 2019. Pathway, classification and removal efficiency of microplastics in wastewater treatment plants. Environ Pollut, 255, 113326.

Nguyen Hai Le, N., Sugai, Y., Nguele, R. and Sreu, T. 2021. Bubble size distribution and stability of CO_2 microbubbles for enhanced oil recovery: effect of polymer, surfactant and salt concentrations. J Dispersion Sci Technol, 1-11.

Nirmalkar, N., Pacek, A.W. and Barigou, M. 2018a. Interpreting the interfacial and colloidal stability of bulk nanobubbles. Soft Matter, 14(47), 9643-9656.

Nirmalkar, N., Pacek, A.W. and Barigou, M. 2018b. On the existence and stability of bulk nanobubbles. Langmuir, 34(37), 10964-10973.

Nixon, Z. and Michel, J. 2018. A Review of distribution and quantity of lingering subsurface oil from the Exxon Valdez Oil Spill. Deep Sea Res Part II Top Stud Oceanogr, 147, 20-26.

Obbard, R.W. 2018. Microplastics in Polar regions: the role of long range transport. Curr Opin Environ Sci Health, 1, 24-29.

Okuku, E., Kiteresi, L., Owato, G., Otieno, K., Mwalugha, C., Mbuche, M., Gwada, B., Nelson, A., Chepkemboi, P., Achieng, Q., Wanjeri, V., Ndwiga, J., Mulupi, L. and Omire, J. 2021. The impacts of COVID-19 pandemic on marine litter pollution along the Kenyan Coast: a synthesis after 100 days following the first reported case in Kenya. Mar. Pollut. Bull., 162, 111840.

Olson, L., Miller, G.Z. and Belliveau, M. 2019. Taking off the toxic gloves: an Investigation of phthalates and other chemicals of concern in food-handling gloves. https://drive.google.com/file/d/1NbWOETSCoSd-PXT_4eTHgi7sTx8aOQgY/view.

Operational Science Advisory Team (2011) Summary reports for fate and effects of remnant oil in the beach environment

Organisation for Economic Co-operation and Development 2020. The face mask global value chain in the COVID-19 outbreak: Evidence and policy lessons. 2020. http://www.oecd.org/coronavirus/policy-responses/the-face-mask-global-value-chain-in-the-covid-19-outbreak-evidence-and-policy-lessons-a4df866d/#endnotea0z14.

Ostle, C., Thompson, R.C., Broughton, D., Gregory, L., Wootton, M. and Johns, D.G. 2019. The rise in ocean plastics evidenced from a 60-year time series. Nat Commun, 10(1), 1622.

Owens, E.H. 1978. Mechanical dispersal of oil stranded in the littoral zone. J, Fish. Res. Board Can, 35, 563-572.

Owens, E.H. 1985. Factors affecting the persistence of stranded oil on low energy coasts. Proceedings: International Oil Spil Conference, 359-365.

Owens, E.H., Haselwimmer, C.E. and Palandro, D.A. 2018. Recent lessons learned from UAS field activities for shoreline oiling survey applications. Interspill, 4.

Owens, E.H. and Lee, K. 2003. Interaction of oil and mineral fines on shorelines: review and assessment. Mar Pollut Bull, 47(9-12), 397-405.

Page, D.S., Boehm, P.D. and Neff, J.M. 2008. Shoreline type and subsurface oil persistence in the Exxon Valdez spill zone of Prince William Sound, Alaska. AMOP Technical Seminar on Environmental Contamination and Response, Environment Canada, 545-564.

Pang, L., Close, M.E., Watt, J.P.C. and Vincent, K.W. 2000. Simulation of picloram, atrazine, and simazine leaching through two New Zealand soils and into groundwater using HYDRUS-2D. J Contam Hydrol, 44(1), 19-46.

Parameswarappa Jayalakshmamma, M., Na Nagara, V., Borgaonkar, A., Sarkar, D., Sadik, O. and Boufadel, M. 2023. Characterizing microplastics in urban runoff: A multi-land use assessment with a focus on 1–125 μm size particles. Sci Total Environ, 904, 166685.

Pardue, J.H., Lemelle, K.R., Urbano, M. and Elango, V. 2014. Distribution and biodegradation potential of buried oil on a coastal headland beach. Proceedings: International Oil Spil Conference, 300129, 1073-1086.

Park, H.-J., Oh, M.-J., Kim, P.-G., Kim, G., Jeong, D.-H., Ju, B.-K., Lee, W.-S., Chung, H.-M., Kang, H.-J. and Kwon, J.-H. 2020. National reconnaissance survey of microplastics in municipal wastewater treatment plants in Korea. Environ Sci Technol, 54(3), 1503-1512.

Parmar, R. and Majumder, S.K. 2013. Microbubble generation and microbubble-aided transport process intensification—a state-of-the-art report. Chem Eng Process, 64, 79-97.

Patricio Silva, A.L., Prata, J.C., Walker, T.R., Duarte, A.C., Ouyang, W., Barcelo, D. and Rocha-Santos, T. 2021. Increased plastic pollution due to COVID-19 pandemic: challenges and recommendations. Chem Eng J, 405, 126683.

Pedrotti, M.L., Petit, S., Elineau, A., Bruzaud, S., Crebassa, J.-C., Dumontet, B., Martí, E., Gorsky, G. and Cózar, A. 2016. Changes in the floating plastic pollution of the Mediterranean Sea in relation to the distance to land. PLoS One, 11(8), e0161581.

Peng, H., Birkett, G.R. and Nguyen, A.V. 2015. Progress on the surface nanobubble story: what is in the bubble? why does it exist? Adv Colloid Interface Sci, 222, 573-580.

Pete, A.J., Brahana, P.J., Bello, M., Benton, M.G. and Bharti, B. 2022. Biofilm formation influences the wettability and settling of microplastics. Environ Sci Technol Lett, 10(2), 159-164.

Peterson, C.H., Rice, S.D., Short, J.W., Esler, D., Bodkin, J.L., Ballachey, B.E. and Irons, D. 2003. Long-term ecosystem response to the Exxon Valdez oil spill. Science, 302, 2082-2086.

Pi, Y., Chen, B., Bao, M., Fan, F., Cai, Q., Ze, L. and Zhang, B. 2017. Microbial degradation of four crude oil by biosurfactant producing strain Rhodococcus sp. Bioresour Technol, 232, 263-269.

Pinheiro, L.M., Britz, L.M.K., Agostini, V.O., Perez-Parada, A., Garcia-Rodriguez, F., Galloway, T.S. and Pinho, G.L.L. 2022. Salt marshes as the final watershed fate for meso- and microplastic contamination: a case study from Southern Brazil. Sci Total Environ, 838(Pt 2), 156077.

Piñon-Colin, T.d.J., Rodriguez-Jimenez, R., Rogel-Hernandez, E., Alvarez-Andrade, A. and Wakida, F.T. 2020. Microplastics in stormwater runoff in a semiarid region, Tijuana, Mexico. Sci Total Environ, 704, 135411.

Powell-Jackson, T., King, J.J.C., Makungu, C., Spieker, N., Woodd, S., Risha, P. and Goodman, C. 2020. Infection prevention and control compliance in Tanzanian outpatient facilities: a cross-sectional study with implications for the control of COVID-19. Lancet Glob Health, 8(6), e780-e789.

Prata, J.C., Silva, A.L.P., Walker, T.R., Duarte, A.C. and Rocha-Santos, T. 2020. COVID-19 pandemic repercussions on the use and management of plastics. Environ Sci Technol, 54(13), 7760-7765.

Prince, R.C., Garrett, R.M., Bare, R.E., Grossman, M.J., Townsend, T., Suflita, J.M., Lee, K., Owens, E.H., Sergy, G.A., Braddock, J.F., Lindstrom, J.E. and Lessard, R.R. 2003. The roles of photooxidation and biodegradation in long-term weathering of crude and heavy fuel oils. Spill Sci Technol Bull, 8(2), 145-156.

Prince, R.C., Owens, E.H. and Sergy, G.A. 2002. Weathering of an Arctic oil spill over 20 years: the BIOS experiment revisited. Mar Pollut Bull, 44, 1236-1242.

Qiu, J., Zou, Z., Wang, S., Wang, X., Wang, L., Dong, Y., Zhao, H., Zhang, L. and Hu, J. 2017. Formation and stability of bulk nanobubbles generated by ethanol-water exchange. Chemphyschem, 18(10), 1345-1350.

Rab, S., Javaid, M., Haleem, A. and Vaishya, R. 2020. Face masks are new normal after COVID-19 pandemic. Diabetes Metab Syndr, 14(6), 1617-1619.

Radovic, J.R., Aeppli, C., Nelson, R.K., Jimenez, N., Reddy, C.M., Bayona, J.M. and Albaiges, J. 2014. Assessment of photochemical processes in marine oil spill fingerprinting. Mar Pollut Bull, 79(1-2), 268-277.

Ragusa, A., Svelato, A., Santacroce, C., Catalano, P., Notarstefano, V., Carnevali, O., Papa, F., Rongioletti, M.C.A., Baiocco, F., Draghi, S., D'Amore, E., Rinaldo, D., Matta, M. and Giorgini, E. 2021. Plasticenta: first evidence of microplastics in human placenta. Environ Int, 146, 106274.

Raju, S., Carbery, M., Kuttykattil, A., Senthirajah, K., Lundmark, A., Rogers, Z., Scb, S., Evans, G. and Palanisami, T. 2020. Improved methodology to determine the fate and transport of microplastics in a secondary wastewater treatment plant. Water Res, 173, 115549.

Ranjan, V.P., Joseph, A. and Goel, S. 2020. Microplastics and other harmful substances released from disposable paper cups into hot water. J Hazard Mater, 404(Pt B), 124118.

Reddy, C.M., Arey, J.S., Seewald, J.S., Sylva, S.P., Lemkau, K.L., Nelson, R.K., Carmichael, C.A., McIntyre, C.P., Fenwick, J., Ventura, G.T., Van Mooy, B.A.S. and Camilli, R. 2012. Composition and fate of gas and oil released to the water column during the Deepwater Horizon oil spill. Proc Natl Acad Sci, 109(50), 20229-20234.

Reichel, C. 2012. Mass spectrometric analysis of EPO IEF-PAGE interfering substances in nitrile examination gloves. Drug Test Anal, 4(10), 761-774.

Reisser, J., Slat, B., Noble, K., du Plessis, K., Epp, M., Proietti, M., de Sonneville, J., Becker, T. and Pattiaratchi, C. 2015. The vertical distribution of buoyant plastics at sea: an observational study in the North Atlantic Gyre. Biogeosciences, 12(4), 1249-1256.

Research and Markets 2021. Global medical gloves market outlook report 2021-2026 featuring prominent vendors - Top Glove, Ansell, Kossan Rubber Industries, Hartalega, Supermax, Mercator. https://www.globenewswire.com/en/news-release/2021/08/20/2284047/28124/en/Global-Medical-Gloves-Market-Outlook-Report-2021-2026-Featuring-Prominent-Vendors-Top-Glove-Ansell-Kossan-Rubber-Industries-Hartalega-Supermax-Mercator.html.

Richter, A., Ng, K.T.W., Vu, H.L. and Kabir, G. 2021a. Identification of behaviour patterns in waste collection and disposal during the first wave of COVID-19 in Regina, Saskatchewan, Canada. J. Environ. Manage., 290, 112663.

Richter, A., Ng, K.T.W., Vu, H.L. and Kabir, G. 2021b. Waste disposal characteristics and data variability in a mid-sized Canadian city during COVID-19. Waste. Manag., 122, 49-54.

Ríos, S.M., Barquín, M. and Nudelman, N. 2009. Hydrocarbons characterization in coastal sediments of the Argentine Patagonia using the nuclear magnetic resonance (NMR) spectroscopy. Environ Chem Lett, 8(3), 223-229.

Rolere, S., Liengprayoon, S., Vaysse, L., Sainte-Beuve, J. and Bonfils, F. 2015. Investigating natural rubber composition with Fourier Transform Infrared (FT-IR) spectroscopy: a rapid and non-destructive method to determine both protein and lipid contents simultaneously. Polym Test, 43, 83-93.

Russell, T.L., Yamahara, K.M. and Boehm, A.B. 2012. Mobilization and transport of naturally occurring enterococci in beach sands subject to transient infiltration of seawater. Environ Sci Technol, 46(11), 5988-5996.

Saviello, D., Pouyet, E., Toniolo, L., Cotte, M. and Nevin, A. 2014. Synchrotron-based FTIR microspectroscopy for the mapping of photo-oxidation and additives in acrylonitrile-butadiene-styrene model samples and historical objects. Anal Chim Acta, 843, 59-72.

Serra, T., Barcelona, A., Pous, N., Salvado, V. and Colomer, J. 2020. Synergistic effects of water temperature, microplastics and ammonium as second and third order stressors on Daphnia magna. Environ Pollut, 267, 115439.

Shi, W., Pan, G., Chen, Q., Song, L., Zhu, L. and Ji, X. 2018. Hypoxia remediation and methane emission manipulation using surface oxygen nanobubbles. Environ Sci Technol, 52(15), 8712-8717.

Shi, Y., Liu, P., Wu, X., Shi, H., Huang, H., Wang, H. and Gao, S. 2021. Insight into chain scission and release profiles from photodegradation of polycarbonate microplastics. Water Res, 116980.

Short, J.W., Irvine, G.V., Mann, D.H., Maselko, J.M., Pella, J.J., Lindeberg, M.R., Payne, J.R., Driskell, W.B. and Rice, S.D. 2007. Slightly weathered Exxon Valdez oil persists in Gulf of Alaska beach sediments after 16 years. Environ Sci Technol, 41(4), 1245-1250.

Short, J.W., Lindeberg, M.R., Harris, P.M., Maselko, J.M., Pella, J.J. and Rice, S.D. 2004. Estimate of oil persisting on the beaches of Prince William Sound 12 years after the Exxon Valdez oil spill. Environ Sci Technol, 38(4), 19-25.

Short, J.W., Maselko, J.M., Lindeberg, M.R., Harris, P.M. and Rice, S.D. 2006. Vertical distribution and probability of encountering intertidal Exxon Valdez oil on shorelines of three embayments within Prince William Sound, Alaska. Environ Sci Technol, 40(12), 3723-3729.

Shrestha, N.K. and Wang, J. 2020. Water quality management of a cold climate region watershed in changing climate. J Environ Inform, 35(1), 56-80.

Shyichuk, A.V., Stavychna, D.Y. and White, J.R. 2001. Effect of tensile stress on chain scission and crosslinking during photo-oxidation of polypropylene. Polymer Degradation and Stability, 72, 279-285.

Skaare, B.B., Schaanning, M. and Mørkved, P.T. 2008. Source identification for oil-based drill cuttings on the seabed based on stable carbon isotopes. Environ Chem Lett, 7(2), 183-189.

Soliman, Y.S., Alansari, E.M.A., Sericano, J.L. and Wade, T.L. 2019. Spatio-temporal distribution and sources identifications of polycyclic aromatic hydrocarbons and their alkyl homolog in surface sediments in the central Arabian Gulf. Sci Total Environ, 658, 787-797.

Song, J., Rezaee, S., Guo, W., Hernandez, B., Puerto, M., Vargas, F.M., Hirasaki, G.J. and Biswal, S.L. 2020. Evaluating physicochemical properties of crude oil as indicators of low-salinity-induced wettability alteration in carbonate minerals. Sci Rep, 10(1), 3762.

Song, Y.K., Hong, S.H., Eo, S., Jang, M., Han, G.M., Isobe, A. and Shim, W.J. 2018. Horizontal and vertical distribution of microplastics in Korean coastal waters. Environ Sci Technol, 52(21), 12188-12197.

Song, Y.K., Hong, S.H., Jang, M., Han, G.M., Jung, S.W. and Shim, W.J. 2017. Combined effects of UV exposure duration and mechanical abrasion on microplastic fragmentation by polymer type. Environ Sci Technol, 51(8), 4368-4376.

Sornsanee, P., Jitprarop, V. and Tangboriboon, N. 2018. Preparation polyisoprene (NR) and polyacrylonitrile rubber latex glove films by dipping ceramic hand molds process and their properties. Defect Diffus Forum, 382, 21-25.

Srogi, K. 2007. Monitoring of environmental exposure to polycyclic aromatic hydrocarbons: a review. Environ Chem Lett, 5(4), 169-195.

Stout, S.A. and Payne, J.R. 2016. Chemical composition of floating and sunken in-situ burn residues from the Deepwater Horizon oil spill. Mar Pollut Bull, 108(1-2), 186-202.

Stout, S.A., Payne, J.R., Emsbo-Mattingly, S.D. and Baker, G. 2016. Weathering of field-collected floating and stranded Macondo oils during and shortly after the Deepwater Horizon oil spill. Mar Pollut Bull, 105(1), 7-22.

Sugiura, M., Takada, H., Takada, N., Mizukawa, K., Tsuyuki, S. and Furumai, H. 2021. Microplastics in urban wastewater and estuarine water: importance of street runoff. Environ Monit Contam Res, 1, 54-65.

Sullivan, G.L., Delgado-Gallardo, J., Watson, T.M. and Sarp, S. 2021. An investigation into the leaching of micro and nano particles and chemical pollutants from disposable face masks - linked to the COVID-19 pandemic. Water Res, 196, 117033.

Sun, L., Chiu, M.-H., Xu, C., Lin, P., Schwehr, K.A., Bacosa, H., Kamalanathan, M., Quigg, A., Chin, W.-C. and Santschi, P.H. 2018. The effects of sunlight on the composition of exopolymeric substances and subsequent aggregate formation during oil spills. Mar Chem, 203, 49-54.

Sun, L., Zhang, F., Guo, X., Qiao, Z., Zhu, Y., Jin, N., Cui, Y. and Yang, W. 2022. Research progress on bulk nanobubbles. Particuology, 60, 99-106.

Sun, Y., Ren, X., Rene, E.R., Wang, Z., Zhou, L., Zhang, Z. and Wang, Q. 2021. The degradation performance of different microplastics and their effect on microbial community during composting process. Bioresour Technol, 332, 125133.

Sun, Y., Yuan, J., Zhou, T., Zhao, Y., Yu, F. and Ma, J. 2020. Laboratory simulation of microplastics weathering and its adsorption behaviors in an aqueous environment: a systematic review. Environ Pollut, 265(Pt B), 114864.

Sundar, S., Mishra, A.K. and Shukla, J.B. 2021. Effects of mitigation options on the control of methane emissions caused by rice paddies and livestock populations to reduce global warming: a modeling study and comparison with environmental data. J Environ Inform, 38(2), 106-115.

Suneel, V., Rao, V.T., Suresh, G., Chaudhary, A., Vethamony, P. and Ratheesh, R. 2019. Oil pollution in the Eastern Arabian Sea from invisible sources: a multi-technique approach. Mar Pollut Bull, 146, 683-695.

Szewc, K., Graca, B. and Dołęga, A. 2021. Atmospheric deposition of microplastics in the coastal zone: characteristics and relationship with meteorological factors. Sci Total Environ, 761, 143272.

Takahashi, M., Shirai, Y. and Sugawa, S. 2021. Free-radical generation from bulk nanobubbles in aqueous electrolyte solutions: ESR spin-trap observation of microbubble-treated water. Langmuir, 37(16), 5005-5011.

Takdastan, A., Niari, M.H., Babaei, A., Dobaradaran, S., Jorfi, S. and Ahmadi, M. 2021. Occurrence and distribution of microplastic particles and the concentration of Di 2-ethyl hexyl phthalate (DEHP) in microplastics and wastewater in the wastewater treatment plant. J Environ Manage, 280, 111851.

Tan, J., Chen, C., Wu, J., He, R., Jiang, L. and Liu, Y. 2021. Influence of ultraviolet aging on the structure, mechanical and gas permeability properties of hydrogenated nitrile butadiene rubber. J Appl Polym Sci, 138(23), 50543.

Tarr, M., Zito, P., Overton, E., Olson, G., Adkikari, P. and Reddy, C. 2016. Weathering of oil spilled in the marine environment. Oceanography, 29(3), 126-135.

Taylor, A.R., Wang, J., Liao, C., Schlenk, D. and Gan, J. 2019. Effect of aging on bioaccessibility of DDTs and PCBs in marine sediment. Environ Pollut, 245, 582-589.

Temesgen, T., Bui, T.T., Han, M., Kim, T.I. and Park, H. 2017. Micro and nanobubble technologies as a new horizon for water-treatment techniques: a review. Adv Colloid Interface Sci, 246, 40-51.

Thorpe, S.A., Stubbs, A.R. and Hall, A.J. 1982. Wave-produced bubbles observed by side-scan sonar. Nature, 296(15), 636-638.

Tian, X., An, C., Chen, Z. and Tian, Z. 2021. Assessing the impact of COVID-19 pandemic on urban transportation and air quality in Canada. Sci Total Environ, 765, 144270.

Treilles, R., Gasperi, J., Gallard, A., Saad, M., Dris, R., Partibane, C., Breton, J. and Tassin, B. 2021. Microplastics and microfibers in urban runoff from a suburban catchment of Greater Paris. Environ Pollut, 287, 117352.

Turner, R.E., Overton, E.B., Meyer, B.M., Miles, M.S., McClenachan, G., Hooper-Bui, L., Engel, A.S., Swenson, E.M., Lee, J.M., Milan, C.S. and Gao, H. 2014. Distribution and recovery trajectory of Macondo (Mississippi Canyon 252) oil in Louisiana coastal wetlands. Mar Pollut Bull, 87(1-2), 57-67.

Uchida, T., Liu, S., Enari, M., Oshita, S., Yamazaki, K. and Gohara, K. 2016. Effect of NaCl on the lifetime of micro- and nanobubbles. Nanomaterials, 6(2), 31.

Ulatowski, K. and Sobieszuk, P. 2020. Gas nanobubble dispersions as the important agent in environmental processes – generation methods review. Water Environ J, 34(S1), 772-790.

Ullah, S., Ullah, A., Lee, J., Jeong, Y., Hashmi, M., Zhu, C., Joo, K.I., Cha, H.J. and Kim, I.S. 2020. Reusability comparison of melt-blown vs nanofiber face mask filters for use in the coronavirus pandemic. ACS Appl Nano Mater, 3(7), 7231-7241.

Ushikubo, F.Y., Furukawa, T., Nakagawa, R., Enari, M., Makino, Y., Kawagoe, Y., Shiina, T. and Oshita, S. 2010. Evidence of the existence and the stability of nano-bubbles in water. Colloids Surf A Physicochem Eng Asp, 361(1-3), 31-37.

Uurasjärvi, E., Pääkkönen, M., Setälä, O., Koistinen, A. and Lehtiniemi, M. 2021. Microplastics accumulate to thin layers in the stratified Baltic Sea. Environ Pollut, 268, 115700.

Van Melkebeke, M., Janssen, C. and De Meester, S. 2020. Characteristics and sinking behavior of typical microplastics including the potential effect of biofouling: implications for remediation. Environ Sci Technol, 54(14), 8668-8680.

Vergeynst, L., Greer, C.W., Mosbech, A., Gustavson, K., Meire, L., Poulsen, K.G. and Christensen, J.H. 2019. Biodegradation, photo-oxidation, and dissolution of petroleum compounds in an Arctic fjord during summer. Environ Sci Technol, 53(21), 12197–12206.

Vermaire, J.C., Pomeroy, C., Herczegh, S.M., Haggart, O. and Murphy, M. 2017. Microplastic abundance and distribution in the open water and sediment of the Ottawa River, Canada, and its tributaries. FACETS, 2, 301-314.

Vermeiren, P., Munoz, C.C. and Ikejima, K. 2016. Sources and sinks of plastic debris in estuaries: a conceptual model integrating biological, physical and chemical distribution mechanisms. Mar Pollut Bull, 113(1-2), 7-16.

Vethaak, A.D. and Legler, J. 2021. Microplastics and human health. Science, 371(6530), 672-674.

Vikas, M. and Dwarakish, G.S. 2015. Coastal pollution: a review. Aquatic Procedia, 4, 381-388.

Vu, H.L., Ng, K.T.W., Richter, A., Karimi, N. and Kabir, G. 2021. Modeling of municipal waste disposal rates during COVID-19 using separated waste fraction models. Sci. Total. Environ., 789, 148024.

Waldschlager, K. and Schuttrumpf, H. 2019. Effects of particle properties on the settling and rise velocities of microplastics in freshwater under laboratory conditions. Environ Sci Technol, 53(4), 1958-1966.

Walter, A.V., Jimenez, L.N., Dinic, J., Sharma, V. and Erk, K.A. 2019. Effect of salt valency and concentration on shear and extensional rheology of aqueous polyelectrolyte solutions for enhanced oil recovery. Rheol Acta, 58(3-4), 145-157.

Wang, C., Du, J., Gao, X., Duan, Y. and Sheng, Y. 2011. Chemical characterization of naturally weathered oil residues in the sediment from Yellow River Delta, China. Mar Pollut Bull, 62(11), 2469-2475.

Wang, C., O'Connor, D., Wang, L., Wu, W.-M., Luo, J. and Hou, D. 2022a. Microplastics in urban runoff: global occurrence and fate. Water Res, 225, 119129.

Wang, C., Zhao, J. and Xing, B. 2021a. Environmental source, fate, and toxicity of microplastics. J Hazard Mater, 407, 124357.

Wang, P. and Roberts, T.M. 2013. Distribution of surficial and buried oil contaminants across sandy beaches along NW Florida and Alabama coasts following the Deepwater Horizon oil spill in 2010. J Coast Res, 291, 144-155.

Wang, W., Gao, H., Jin, S., Li, R. and Na, G. 2019. The ecotoxicological effects of microplastics on aquatic food web, from primary producer to human: a review. Ecotoxicol Environ Saf, 173, 110-117.

Wang, W., Ge, J. and Yu, X. 2020a. Bioavailability and toxicity of microplastics to fish species: a review. Ecotoxicol Environ Saf, 189, 109913.

Wang, Y., Lee, K., Liu, D., Guo, J., Han, Q., Liu, X. and Zhang, J. 2020b. Environmental impact and recovery of the Bohai Sea following the 2011 oil spill. Environ Pollut, 263(Pt B), 114343.

Wang, Y., Li, X., Zhou, Y., Huang, P. and Xu, Y. 2010. Preparation of nanobubbles for ultrasound imaging and intracelluar drug delivery. Int J Pharm, 384(1-2), 148-153.

Wang, Y., Yang, Y., Liu, X., Zhao, J., Liu, R. and Xing, B. 2021b. Interaction of microplastics with antibiotics in aquatic environment: distribution, adsorption, and toxicity. Environ Sci Technol, 55(23), 15579-15595.

Wang, Z., An, C., Chen, X., Lee, K., Zhang, B. and Feng, Q. 2021c. Disposable masks release microplastics to the aqueous environment with exacerbation by natural weathering. J Hazard Mater, 417, 126036.

Wang, Z., An, C., Lee, K., Chen, X., Zhang, B., Yin, J. and Feng, Q. 2022b. Physicochemical change and microparticle release from disposable gloves in the aqueous environment impacted by accelerated weathering. Sci Total Environ, 832, 154986.

Wang, Z., An, C., Lee, K. and Feng, Q. 2023a. Overlooked role of bulk nanobubbles in the alteration and motion of microplastics in the ocean environment. Environ Sci Technol, 57(30), 11289-11299.

Wang, Z., An, C., Lee, K., Feng, Q. and Zhang, B. 2023b. Exploring the role of nanobubbles in the fate and transport of spilled oil on shorelines. ACS ES&T Water, 3(1), 30-40.

Wang, Z., An, C., Lee, K., Owens, E., Boufadel, M. and Feng, Q. 2022c. Dispersion modeling of particulate matter from the in-situ burning of spilled oil in the northwest Arctic area of Canada. J Environ Manage, 301, 113913.

Wang, Z., An, C., Lee, K., Owens, E., Chen, Z., Boufadel, M., Taylor, E. and Feng, Q. 2020c. Factors influencing the fate of oil spilled on shorelines: a review. Environ Chem Lett, 19(2), 1611-1628.

Wang, Z., Guy, C., Ng, K.T.W. and An, C. 2021d. A new challenge for the management and disposal of personal protective equipment waste during the COVID-19 pandemic. Sustainability, 13(13), 7034.

Wei, H.W., Hassan, M., Che, Y., Peng, Q.K., Su, Y.L. and Xie, B. 2021. Spatio-temporal characteristics and source apportionment of water pollutants in upper reaches of Maotiao River, southwest of China, from 2003 to 2015. J Environ Inform, 37(2), 93-106.

Wei, X.F., Capezza, A.J., Cui, Y., Li, L., Hakonen, A., Liu, B. and Hedenqvist, M.S. 2022. Millions of microplastics released from a biodegradable polymer during biodegradation/enzymatic hydrolysis. Water Res, 211, 118068.

Werbowski, L.M., Gilbreath, A.N., Munno, K., Zhu, X., Grbic, J., Wu, T., Sutton, R., Sedlak, M.D., Deshpande, A.D. and Rochman, C.M. 2021. Urban stormwater runoff: a major pathway for anthropogenic particles, black rubbery fragments, and other types of microplastics to urban receiving waters. ACS ES&T Water, 1(6), 1420-1428.

White, J.R. and Shyichuk, A.V. 2007. Effect of stabilizer on scission and crosslinking rate changes during photo-oxidation of polypropylene. Polymer Degradation and Stability, 92(11), 2095-2101.

White, J.R., Shyichuk, A.V., Turton, T.J. and Syrotynska, I.D. 2006. Effect of stabilizer and pigment on photodegradation of polypropylene as revealed by macromolecule scission and crosslinking measurements. Polymer Degradation and Stability, 91(8), 1755-1760.

Witzig, C.S., Foldi, C., Worle, K., Habermehl, P., Pittroff, M., Muller, Y.K., Lauschke, T., Fiener, P., Dierkes, G., Freier, K.P. and Zumbulte, N. 2020. When good intentions go bad-false positive microplastic detection caused by disposable gloves. Environ Sci Technol, 54(19), 12164-12172.

World Health Organization 2020. Rational use of personal protective equipment for coronavirus disease (COVID-19) and considerations during severe shortages. https://apps.who.int/iris/handle/10665/331695.

Xia, Y. and Boufadel, M.C. 2011. Beach geomorphic factors for the persistence of subsurface oil from the Exxon Valdez spill in Alaska. Environ Monit Assess, 183(1-4), 5-21.

Xia, Y., Li, H., Boufadel, M.C. and Sharifi, Y. 2010. Hydrodynamic factors affecting the persistence of the Exxon Valdezoil in a shallow bedrock beach. Water Resour Res, (10), W10528.

Xiao, Z., Du, J.Y., Guo, Y., Li, X. and Guo, L. 2022. Time variant interval linear programming for environmental management systems. J Environ Inform, 39(1), 22-34.

Xie, H., Han, W., Xie, Q., Xu, T., Zhu, M. and Chen, J. 2021. Face mask-a potential source of phthalate exposure for human. J Hazard Mater, 422, 126848.

Xie, W.P., Yang, J.S., Yao, R.J. and Wang, X.P. 2020. Impact study of impoundment of the three gorges reservoir on salt-water dynamics and soil salinity in the Yangtze River estuary. J Environ Inform, 36(1), 11-23.

Xu, B., Liu, F., Cryder, Z., Huang, D., Lu, Z., He, Y., Wang, H., Lu, Z., Brookes, P.C., Tang, C., Gan, J. and Xu, J. 2019. Microplastics in the soil environment: occurrence, risks, interactions and fate – a review. Crit Rev Environ Sci Technol, 50(21), 2175-2222.

Xu, E.G. and Ren, Z.J. 2021. Preventing masks from becoming the next plastic problem. Front Environ Sci Eng, 15(6), 125.

Xue, S., Zhang, Y., Marhaba, T. and Zhang, W. 2022. Aeration and dissolution behavior of oxygen nanobubbles in water. J Colloid Interface Sci, 609, 584-591.

Yakushev, E., Gebruk, A., Osadchiev, A., Pakhomova, S., Lusher, A., Berezina, A., van Bavel, B., Vorozheikina, E., Chernykh, D., Kolbasova, G., Razgon, I. and Semiletov, I. 2021. Microplastics distribution in the Eurasian Arctic is affected by Atlantic waters and Siberian rivers. Commun Earth Environ, 2(1), 23.

Yan, Y., Zhu, F., Zhu, C., Chen, Z., Liu, S., Wang, C. and Gu, C. 2021. Dibutyl phthalate release from polyvinyl chloride microplastics: Influence of plastic properties and environmental factors. Water Res, 204, 117597.

Yang, L., Yu, X., Wu, X., Wang, J., Yan, X., Jiang, S. and Chen, Z. 2021a. Emergency response to the explosive growth of health care wastes during COVID-19 pandemic in Wuhan, China. Resour Conserv Recycl, 164, 105074.

Yang, M., Chen, B., Xin, X., Song, X., Liu, J., Dong, G., Lee, K. and Zhang, B. 2021b. Interactions between microplastics and oil dispersion in the marine environment. J Hazard Mater, 403, 123944.

Yang, M., Zhang, B., Xin, X., Liu, B., Zhu, Z., Dong, G., Zhao, Y., Lee, K. and Chen, B. 2022a. Microplastic-oil-dispersant agglomerates in the marine environment: formation mechanism and impact on oil dispersion. J Hazard Mater, 426, 127825.

Yang, X., An, C., Feng, Q., Boufadel, M. and Ji, W. 2022b. Aggregation of microplastics and clay particles in the nearshore environment: characteristics, influencing factors, and implications. Water Res, 224, 119077.

Yang, Y., Xie, E., Du, Z., Peng, Z., Han, Z., Li, L., Zhao, R., Qin, Y., Xue, M., Li, F., Hua, K. and Yang, X. 2023. Detection of various microplastics in patients undergoing cardiac surgery. Environ Sci Technol, 57(30), 10911-10918.

Yang, Z., Shah, K., Laforest, S., Hollebone, B.P., Lambert, P., Brown, C.E., Yang, C. and Goldthorp, M. 2018. A study of the 46-year-old Arrow oil spill: persistence of oil residues and variability in oil contamination along Chedabucto Bay, Nova Scotia, Canada. J Clean Prod, 198, 1459-1473.

Yew, G.Y., Tham, T.C., Law, C.L., Chu, D.-T., Ogino, C. and Show, P.L. 2019. Emerging crosslinking techniques for glove manufacturers with improved nitrile glove properties and reduced allergic risks. Mater Today Commun, 19, 39-50.

Yew, G.Y., Tham, T.C., Show, P.L., Ho, Y.C., Ong, S.K., Law, C.L., Song, C. and Chang, J.S. 2020. Unlocking the secret of bio-additive components in rubber compounding in processing quality nitrile glove. Appl Biochem Biotechnol, 191(1), 1-28.

Yim, U.H., Ha, S.Y., An, J.G., Won, J.H., Han, G.M., Hong, S.H., Kim, M., Jung, J.H. and Shim, W.J. 2011. Fingerprint and weathering characteristics of stranded oils after the Hebei Spirit oil spill. J Hazard Mater, 197, 60-69.

Yin, F., John, G.F., Hayworth, J.S. and Clement, T.P. 2015. Long-term monitoring data to describe the fate of polycyclic aromatic hydrocarbons in Deepwater Horizon oil submerged off Alabama's beaches. Sci Total Environ, 508, 46-56.

Yong, C.Q.Y., Valiyaveettil, S. and Tang, B.L. 2020. Toxicity of microplastics and nanoplastics in mammalian systems. Int J Environ Res Public Health, 17(5), 1509.

Yoo, Y., Park, H., Choi, Y., Jung, J., Song, H., Kim, J. and Cho, H. 2021. Method for determining optimum operational conditions of microbubble scrubber using image processing. J Environ Inform, 38(2), 83-92.

Yoshida, A., Takahashi, O., Ishii, Y., Sekimoto, Y. and Kurate, Y. 2008. Water purification using the adsorption characteristics of microbubbles. J Appl Phys, 47(8), 6574-6577.

Yuan, L., Han, L., Bo, W., Chen, H., Gao, W. and Chen, B. 2017. Simulated oil release from oil-contaminated marine sediment in the Bohai Sea, China. Mar Pollut Bull, 118(1-2), 79-84.

Zakaria, M.P., Bong, C.-W. and Vaezzadeh, V. (2018) Fingerprinting of petroleum hydrocarbons in Malaysia using environmental forensic techniques: a 20-year field data review in the Book of Oil spill environmental forensics case studies. Stout, S.A. and Wang, Z. (eds), pp. 345-372, Elsevier, Kuala Lumpur.

Zhang, H. 2017. Transport of microplastics in coastal seas. Estuar Coast Shelf Sci, 199, 74-86.

Zhang, J., Ding, W., Zou, G., Wang, X., Zhao, M., Guo, S. and Chen, Y. 2023. Urban pipeline rainwater runoff is an important pathway for land-based microplastics transport to inland surface water: a case study in Beijing. Sci Total Environ, 861, 160619.

Zhang, J., Zhan, S., Zhong, L.B., Wang, X., Qiu, Z. and Zheng, Y.M. 2022. Adsorption of typical natural organic matter on microplastics in aqueous solution: kinetics, isotherm, influence factors and mechanism. J Hazard Mater, 443(Pt A), 130130.

Zhang, M., Feng, Y., Zhang, D., Dong, L. and Pan, X. 2019a. Ozone-encapsulated colloidal gas aphrons for in situ and targeting remediation of phenanthrene-contaminated sediment-aquifer. Water Res, 160, 29-38.

Zhang, Q., Liu, T., Liu, L., Fan, Y., Rao, W., Zheng, J. and Qian, X. 2021. Distribution and sedimentation of microplastics in Taihu Lake. Sci Total Environ, 795, 148745.

Zhang, W., Zhang, S., Wang, J., Wang, Y., Mu, J., Wang, P., Lin, X. and Ma, D. 2017. Microplastic pollution in the surface waters of the Bohai Sea, China. Environ Pollut, 231, 541-548.

Zhang, Y., Kang, S., Allen, S., Allen, D., Gao, T. and Sillanpää, M. 2020. Atmospheric microplastics: a review on current status and perspectives. Earth-Sci Rev, 203, 103118.

Zhang, Y., Xu, Y., Song, Y. and Zheng, Q. 2013. Study of poly(vinyl chloride)/acrylonitrile-styrene-acrylate blends for compatibility, toughness, thermal stability and UV irradiation resistance. J Appl Polym Sci, 130(3), 2143-2151.

Zhang, Z.F., Liu, X.T., Yang, K. and Zhao, S.G. 2019b. Design of coordination-crosslinked nitrile rubber with self-healing and reprocessing ability. Macromol Res, 27(8), 803-810.

Zhao, S., Huang, G., An, C., Wei, J. and Yao, Y. 2015. Enhancement of soil retention for phenanthrene in binary cationic gemini and nonionic surfactant mixtures: characterizing

two-step adsorption and partition processes through experimental and modeling approaches. J Hazard Mater, 286, 144-151.

Zhao, S., Huang, W.W., Wang, X.Q., Fan, Y.R. and An, C.J. 2019. Sorption of phenanthrene onto diatomite under the influences of solution chemistry: a study of linear sorption based on maximal information coefficient. J Environ Inform, 34(1), 35-44.

Zhou, Q., Zhang, H., Fu, C., Zhou, Y., Dai, Z., Li, Y., Tu, C. and Luo, Y. 2018. The distribution and morphology of microplastics in coastal soils adjacent to the Bohai Sea and the Yellow Sea. Geoderma, 322, 201-208.

Zhou, Y., Han, Z., He, C., Feng, Q., Wang, K., Wang, Y., Luo, N., Dodbiba, G., Wei, Y., Otsuki, A. and Fujita, T. 2021. Long-term stability of different kinds of gas nanobubbles in deionized and salt water. Materials, 14(7), 1808.

Zhu, Z., Zhang, B., Chen, B., Cai, Q. and Lin, W. 2016. Biosurfactant production by marine-originated bacteria bacillus subtilis and its application for crude oil removal. Wat Ari Soil Poll, 227(9), 328.

Zobkov, M.B., Esiukova, E.E., Zyubin, A.Y. and Samusev, I.G. 2019. Microplastic content variation in water column: the observations employing a novel sampling tool in stratified Baltic Sea. Mar Pollut Bull, 138, 193-205.